Institut für Geologie, Geotechnik und Baubetrieb

Technische Universität München

Measurements on the Structural Contribution to Friction in Granular Media

Wolfgang Eber

Vollständiger Abdruck der von der Fakultät für Bauingenieur- und Vermessungswesen der Technischen Universität München zur Erlangung des akademischen Grades eines

Doktors der Naturwissenschaften (Dr. rer. nat.)

genehmigten Dissertation.

Vorsitzender:	Univ.-Prof. Dr.-Ing. J. Zimmermann
Prüfer der Dissertation:	1. Univ.-Prof. Dr.-Ing. N. Vogt
	2. Univ.-Prof. Dr. rer. nat. H. Herrmann, Eidgenössische Technische Hochschule Zürich/Schweiz

Die Dissertation wurde am 06.12.2006 bei der Technischen Universität eingereicht und durch die Fakultät für Bauingenieur- und Vermessungswesen am 12.03.2007 angenommen.

Abstract

In this paper, some experimental results are presented, estimating the lateral stress response to a longitudinal stress applied to an ideal granular system as a function of friction parameters. Structural effects are taken into account through the use of angle of contact distributions. The two-dimensional model, based on mainly equally sized cylinder granules allows to derive a dependency of the friction between single granules and the overall angle of friction, which is commonly used to describe the macroscopic behaviour of granular material.

This approach is valid for materials that have been subjected to some unidirectional deformation, which enables shearing joints to establish. Such behaviour is compatible with classic theories derived from the basic Rankine concept.

In contrast to this, stochastically mixed materials with no deformation history exhibit somewhat different characteristics since the deformation is not concentrated to shearing joints. They can be described with good success by a purely statistical approach. For this case the importance of small irregularities on the surface of the model grains is pointed out.

Concerning the impact of the inner structure of a granular system, a scale can be determined, where three classes are defined. At the first level single particles are described, while the building of a network of force bearing chains is addressed at the second level. A rough estimation of the mesh size is given and confirmed by experimental results. At the third level the granular structure of a medium can be neglected and continuous theories work well.

Table of Contents

1 Introduction

The behaviour of granular material has been studied previously by many scientists [1,2]. In particular, the state of static and slowly sheared systems has been the subject of several investigations [11-13,18-22,25-27]. The current availability of affordable computing power has given rise to simulations [14-15], since the indefinite position of a single granule within the lot prohibits analytical approaches to detailed characterisations.

However, civil engineers know, that granular media behave very well according to phenomenological laws [8,9,28-33]. Several attempts have been made to describe them from a more theoretical point of view [30,31,33,63,65,66,68,69], yet always comprising some phenomenological elements.

Restricting models to dry, cohesionless materials, where the intrinsic properties of the single granules contribute only negligible impact on its macroscopic behaviour we find two fundamental issues:

Besides the characterisation as a conglomerate, consisting of a large number of granules, where position and orientation of single contacts are not defined, the contact itself is determined mainly through friction, which introduces another indefinite property of the lot [17,25]. Hence, the behaviour of a sample concerning redirection of forces and stress is dominated by two different aspects: the inherent particle friction and the structural contribution.

Civil engineers describe the shear strength of granular soil mainly through macroscopic properties like the angle of friction φ and cohesion c. Previous famous investigators like Coulomb [3,4] and later Rankine [5,6] have built up very basic and well-founded theories on just these values. Some more recent developments can be found in references [7-10,16,23,24,28-33].

Nevertheless, a very fundamental problem in understanding granular media turned out to be the pure structural contribution to the overall stress transmission behaviour in contrast to the true grain to grain friction-induced share. This has often been addressed theoretically, e.g. in Ref. [68,69], but hardly tackled by experiments directly.

Experimental results concerning friction are not easy to obtain in a reproducible manner. Nevertheless, the important role that friction plays within the context of stochastic structures motivated us to perform the most basic experiment of soil mechanics: we established an

elementary two-dimensional model of granular soil, consisting of well defined granules both in shape and friction parameters and measured the transversal stress σ_3 in response to longitudinal compression stress σ_1, as a dimensionless averaged factor $\overline{K} = \sigma_3/\sigma_1$.

The correspondence of the measurement results depending on coefficients of particle friction and structure to the conventional macroscopic description is investigated and presented in this dissertation.

2 Granular Parameters in Soil Mechanics

Natural soil is a very complex conglomerate of several constituents, each contributing its particular properties to the whole.

Very roughly, cohesionless soil always comprises a set of granules, where the distribution of size plays an important role. In particular, the broadness of the size distribution and the density characterize the mechanical behaviour of the sample. Beyond this, each granule contributes its local properties of shape, roughness, elasticity and strength to the lot. Furthermore, the presence of water in natural soil leads to cohesion, buoyant volume force and hydrostatic pressure. Finally, due to the mainly frictional character of the particle interaction, the deformation history of a sample highly influences the response of the sample to stress.

2. 1 General Remarks on Approaches to Soil Mechanics

Civil engineers need to describe the mechanical behaviour of natural soil in dependance of strain and stress and to survey the limits of strength in order to provide a save loading capacity, e.g. see Drucker, Greenberg, Prager [61,62,70]. Several sets of constitutive equations and the appropriate macroscopic parameters summarize the results of this effort and are commonly used in soil mechanics. As a typical detail, the relation of shear stress *versus* strain according to de Borst and Vermeer [63] is plotted in the following graph:
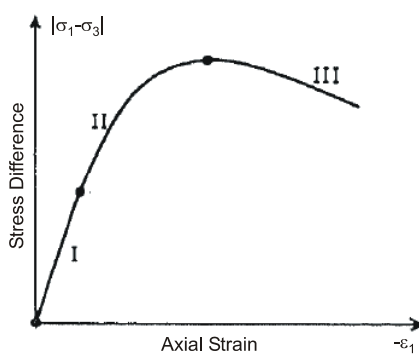
FIG. 1. Typical dependency of shear stress vs. strain.   FIG. 2. Measured dependency of shear stress vs. strain
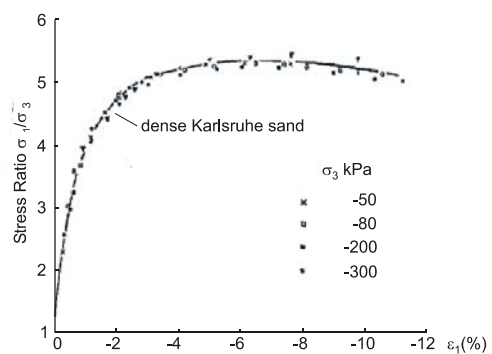
In this graph, section I denotes elastic behaviour, followed by hardening in section II, and the softening regime in section III.

One first approach to an appropriate description is gained through ***theories of elasticity,*** where all strain induced by applied stress is completely reversible. Linear elasticity defined by the law of Hooke $\varepsilon_k = E^{-1}(\sigma_k - v\sigma_j)$ and $\gamma_{kj} = E^{-1}2(1 + v)\tau_{kj}$ is the first order approximation valid for very small deformations while nonlinear but mainly still reversible effects - besides e.g. the non reversible influence of porosity - occur with increasing strain. This is well established in linear and nonlinear elastic theory, e.g. in Timoshenko [64]. (ε_k, σ_k are the strain and the stress in direction k, γ_{kj} and τ_{kj} is the shear strain and stress, E, v the modulus of Young and the Coefficient of Poisson).

With further increasing stress, the resulting strain is no more reversible and ***plasticity*** begins to dominate the behaviour of soil. Constitutive equations reproduce plastic strain resulting from a given stress state. Since the mechanism triggering the yielding process of the material is very complex and dependant on the material and the type of stress (dynamic, static, impulsive), the particularly used criteria σ_V is specified by different authors (assuming $\sigma_1 \geq \sigma_2 \geq \sigma_3$) [see e.g. 70] of which some examples are listed here:

- Hypothesis 1: Largest principal stress $\sigma_V = \sigma_1$ (Rankine) [5,6],

- Hypothesis 2: Largest shear stress $\sigma_V = \sigma_1 - \sigma_3 = 2\tau_{max}$ (Coulomb [3,4], St.Venant, Tresca, Guest)

- Hypothesis 3: Maximum strain $\sigma_V = \sigma_1 - v(\sigma_2 + \sigma_3)$ (Bach),

- Hypothesis 4: Maximum distortion energy

  $\sigma_V = \sqrt{\frac{1}{2}\left[(\sigma_1 - \sigma_2)^2 + (\sigma_2 - \sigma_3)^2 + (\sigma_3 - \sigma_1)^2\right]}$ (Huber, Hencky, Mises).

- Hypothesis 5: Maximum distortion energy under the influence of hydrostatic stress

  $\sigma_V = a(\sigma_1 + \sigma_2 + \sigma_3) + \beta\sqrt{\frac{1}{2}\left[(\sigma_1 - \sigma_2)^2 + (\sigma_2 - \sigma_3)^2 + (\sigma_3 - \sigma_1)^2\right]}$ (Drucker-Prager)

Decomposed natural soil comprises distinct elements of finite size. Thus, all descriptions derived from continuous theories cover the average behaviour and in particular the average particle-induced character of granular material. Some typical characteristics like e.g. dilatancy need to have additional considerations. In a continuous description of natural material, a central parameter of the plastic potential which governs the plastic strain rate is the angle of dilatancy. The choice of its value determines the variation of the specimen volume with the shearing deformation, and hence the character of the sample. Vermeer and

de Borst present a very comprehensive view of the theoretical background and give appropriate measurement results concerning this subject in Ref. [63].

Further investigations dealing with dilatancy on the basis of averaged geometrical considerations of noncontinuous material were carried out by Goddard [68,69] in order to derive appropriate predictions for the dilatancy characteristics of granular media. This extends the fundamental approach of Reynolds [7].

Another theory is the ***Cosserat-Continuum***, well described by de Borst in [65]. The effect of finite size elements is taken into account by additionally introducing torque moments at the points of contact. At the transition to a continuous theory, lengths are assumed to be small enough to ensure infinitesimal volumes but still large enough to keep these torque moments finite.

A well founded example of another continuous theory covering the behaviour of granular material is the ***hypoplasticity model family*** of Kolymbas, Gudehus, Herle et al [30] which uses seven macroscopic parameters obtained from experiments on natural soil.

Many approaches are necessarily phenomenological in character since it is indispensable to meet engineering requirements to describe real natural soil, especially regarding the prediction of stability and deformation. On this basis, the physical task is to reconstruct the behaviour of a sample through microscopic mechanisms by creating simple comprehensible models. This requires the modelling of the transition from properties of the particles to the behaviour of the complex granular sample. Based on what we know about the underlying processes, microscopic parameters can be developed which are in accordance with the macroscopic parameters required by engineers.

As the perception of 'friction' is used both in macroscopic and in microscopic systems, it is necessary to investigate its different meaning and its influence on the redirection of local forces and average stresses. Yet, redirection of local forces and average stress is defined by frictional properties in co-action with the finite structure of the granular system, so that the question of the contributing rates arises.

Hence, this paper deals with the very fundamental problem in granular material physics, which is the difficulty to distinguish between effects of grain to grain friction and effects of packing organization in the description of stress transmission. In order to obtain results, which are comparable to the known macroscopic characteristics of granular material, we

chose an experimental approach and will discuss the measurement readings on the basis of some appropriate plausibility computations.

Because the measurements described in this paper were carried out on a largely simplified model of granular material, they need to be viewed on the background of real soil. For this reason, some classical methods of characterising dry granular soil are shortly presented here. Furthermore, typical ranges of parameters for natural soil are presented in order to provide a more realistic picture of the situation.

2. 2 Angle of Friction and Cohesion of Natural Soil

Two types of experiments are used to determine the plastic parameters of natural granular material like the Angle of Friction φ and the cohesion c, where the shear joint is predetermined or may develop freely:

2. 2. 1 Experiments with an undefined shear joint

Some experimental setups allow a shear joint to establish freely under a well defined stress situation. They are classified by the different handling of the third principal stress σ_3. This may vary in the range from zero, which equals a plain two dimensional experiment, to a free value controlled by a fixed position, inhibiting lateral expansion, which is typical for problems which can be modelled in two dimensions.

In a **Triaxial Compression Cell** the lateral stresses σ_2, σ_3 are kept equal on a cylindrical sample by submerging it in a tank filled with water under pressure. The longitudinal stress σ_1 is applied by a hydraulic cylinder until the sample yields. The minimum diameter of the probe is required to be at least ten times the maximum diameter of the granules. Several tests conducted with different lateral stresses result in points on the yielding limit which can be described quite well with a linear function. The gradient and offset of this approximation are φ and c.

A **True Triaxial Apparatus** where all stresses or alternatively strains can be controlled individually is complicated and expensive and hence is used only in scientific experiments. Since only a few, well defined states of stress are required in soil mechanics in order to

provide comparable parameters, a freely variable third principal stress is not necessary but would be useful however very expensive. Thus, such tests are not common in soil mechanics.

In the **Uniaxial Compression Test** both lateral stresses σ_2, σ_3 are zero. Besides some information about the elastic behaviour, this apparatus only provides the compressive strength. After all, a rough estimation of the angle of friction in correspondence to the cohesion can be obtained from the uniaxial compression strength.

Triaxial Compression Cell   True Triaxial Apparatus   Uniaxial Compression Cell
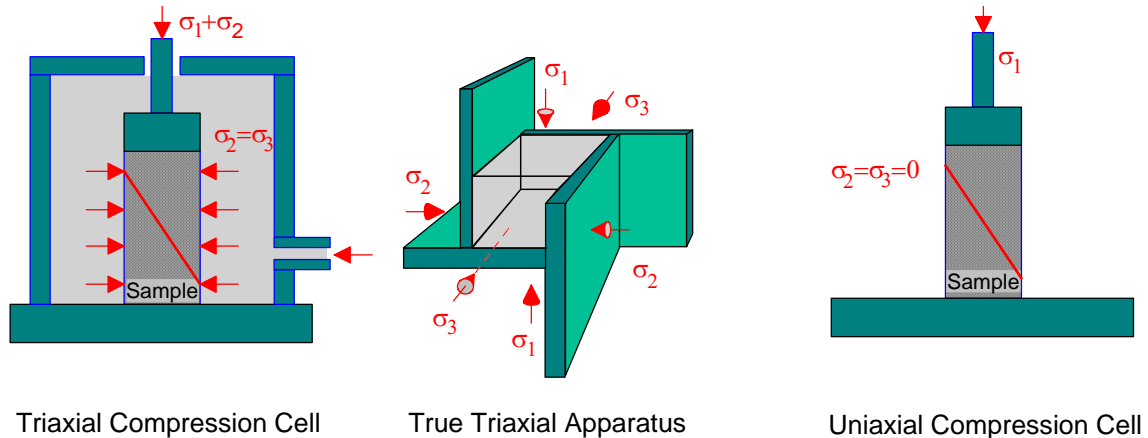
FIG. 3. Experiments allowing for free development of a shear joint

2. 2. 2 Experiments with a fixed shear joint

Other setups enforce a given shear joint, like the Frame Shearing Test or the Simple Shear Method:

In a **Frame Shearing Test** two frames filled with the sample material are shifted against each other while the normal load and the shear stress are measured. This is especially useful for measuring the residual shearing strength. Also the angle of friction φ and the cohesion c can be derived easily.

The **Simple Shear Method** is still more basic as a volume of the sample material is deformed rhomboidically while the vertical load and deforming stress are recorded. With this setup the angle of dilatancy ψ_D can be obtained directly from the displacement parameters. (However this is also possible with the Triaxial Compression Cell)

The main difference between these two methods is derived from the much better homogeneity of the stress situation of the Simple Shear Test which is not given by a Frame Shearing Test.
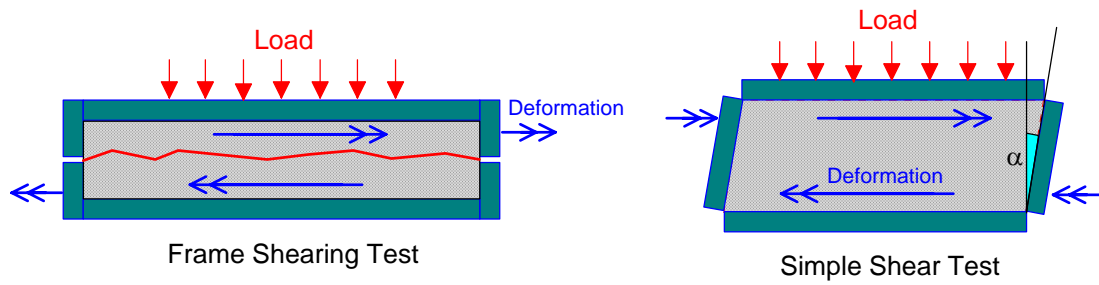
FIG. 4. Experiments enforcing a given shear joint

In all cases the content of water in the tested soil plays an important role. Therefore, the test instructions include directives of how the sample is to be dried or saturated prior to the measurement. Thus, restricting a model to dry granular material is of extreme importance for studying basic properties but at the same time denotes a significant discrepancy in comparison with real soil.

2. 3 Porosity/Packing Fraction

In soil mechanics, the value of porosity rsp. packing fraction and overconsolidation are a very important parameters, defining essential consequences of the history of the material. In particular, it subsumes parameters of shape, angularity, ability to keep a certain water content and compaction.

Packing fractions κ are defined in a different way compared to the physics of granular matter, where κ is the fraction of massive volume with respect to the total volume: $\kappa = \dfrac{V_{massiv}}{V_{total}}$.

Instead, the ***porosity*** $n = \dfrac{V_{total} - V_{massiv}}{V_{total}} = 1 - \kappa$ is determined as the fraction of the total volume which is not filled by material.

Alternatively, the commonly used ***void ratio*** $e = \dfrac{n}{1-n}$ is the ratio of empty volume to massive volume.

Since the compaction process is mirrored to the porosity, many different values are presented by several sources, each referring to a different situation and history of natural soil. Herle et al. [30] uses a set of three void ratio values e_i, e_d, e_c to enter in the hypoplastic constitutive equation. e_i represents the maximum void ratio, achieved by compressing isotropically from an initial suspension. e_d is the void ratio at the most dense state, and e_c the void ratio of the

critical state. All three parameters are known to be dependent on the pressure and reach their maximum at zero pressure.
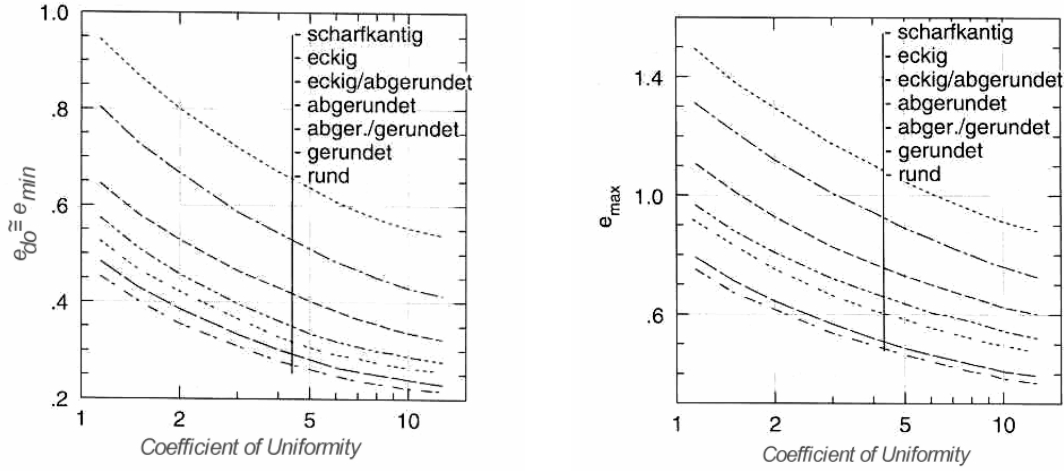
FIG. 5. Minimum and maximum void ratio dependent on uniformity and shape of granules (according to [30])

Some numerical values are presented in the following table (according [30]):

Material	$e_{d0} \simeq e_{\min}$	$e_{c0} \simeq e_{\max}$	$n_{\min}^{(3d)}$	$n_{\max}^{(3d)}$	$n_{\min}^{(2d)}$	$n_{\max}^{(2d)}$
Toyoura-Sand (angular/rounded)	0,61	0,98	0,38	0,49	0,27	0,37
Hochstetten-Sand (rounded)	0,55	0,95	0,35	0,49	0,25	0,36
Schlabendorf-Sand (rounded)	0,44	0,85	0,31	0,46	0,22	0,34
Hostun-Sand (angular/rounded)	0,61	0,91	0,38	0,48	0,27	0,35
Karlsruhe-Sand (rounded)	0,53	0,84	0,35	0,46	0,25	0,33
Zbraslav-Sand (angular/rounded)	0,52	0,82	0,34	0,45	0,24	0,33
Ottawa-Sand (round/rounded)	0,49	0,76	0,33	0,43	0,23	0,31
Ticino-Sand (angular/rounded)	0,60	0,93	0,38	0,48	0,27	0,35
Silver-Leighton-Buzzard-Sand (rounded)	0,49	0,79	0,33	0,44	0,23	0,32
Hochstetten-Gravel (rounded)	0,26	0,45	0,21	0,31	0,14	0,22
Polymer Granulate (elliptic cylinders $l = 4mm$, $d_1 = 3mm$, $d_2 = 4.5mm$)	0,53	0,73	0,35	0,42	0,25	0,31
Dry wheat (elliptic cylinders $l \simeq 6.6mm$, $d \simeq 3.7mm$)	0,57	0,84	0,36	0,46	0,26	0,33

The quoted porosity values $n_{\min}^{(3d)}$ and $n_{\max}^{(3d)}$ have been recalculated from the measured void ratios by: $n^{(3d)} = e/(e+1)$. Additionally, a corresponding porosity value $n^{(2d)}$ for a two-dimensional equivalent is specified by the relation $n^{(2d)} \simeq 1 - (1 - n^{(3d)})^{\frac{2}{3}}$, just converting volumes to areas, which provides at least a rough estimation.
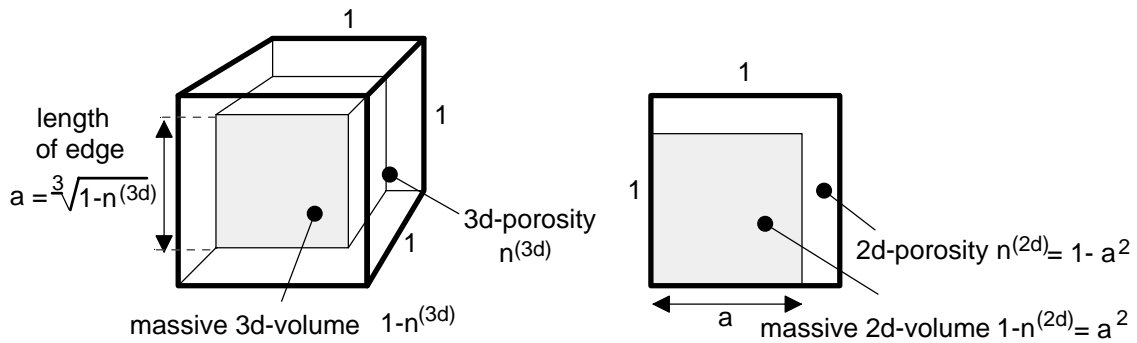
FIG. 6. Estimation of 2d-porosity from 3d measurements

2. 4 Particle Properties and Distribution in Natural Soils

In order to position the simplified granular model used in our measurements within the wide range of natural soil, we need to compare it by some of the commonly used parameters.

The **distribution of particle sizes** of soil is usually given as aggregate grading curves $S(r) = \int_0^d h(d')dd'$, where $h(d')dd'$ is the normalized relative frequency of occurrence of a granule with radius d in the interval dd'. This definition is identical to the throughput of a set of sieves with increasing mesh width.
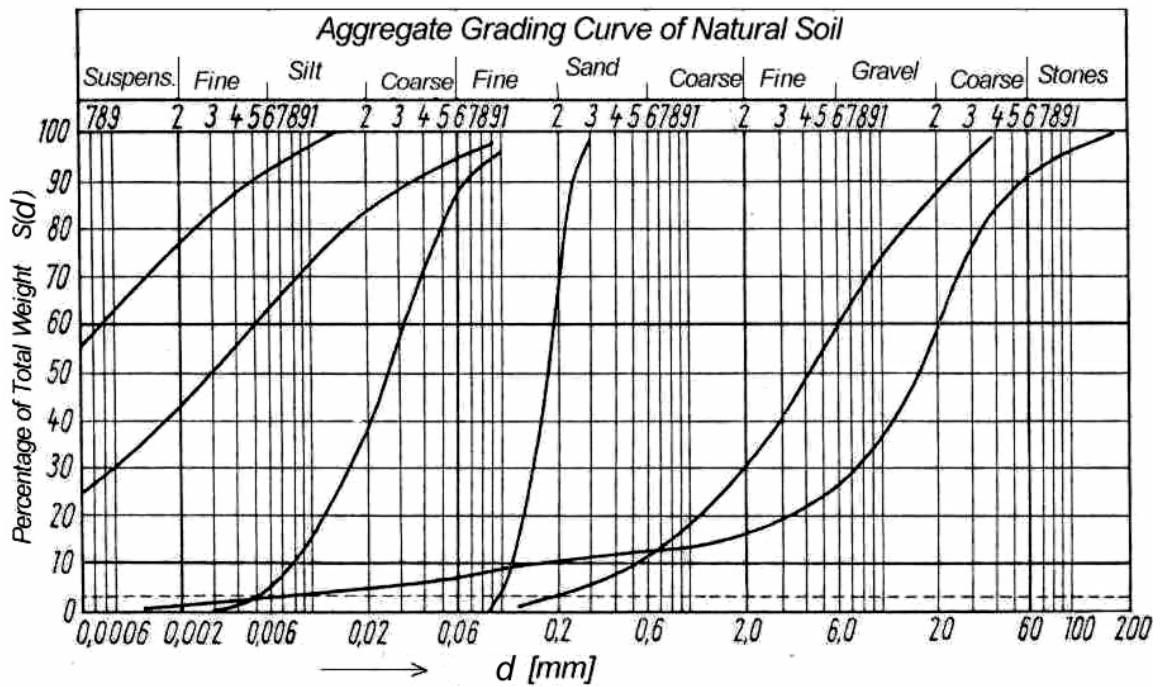
FIG. 7. Aggregate Grading Curve of Natural Soil (according to [57])

The parameter of uniformity U which is determined as the ratio of diameters at 60% of total weight and of 10% of total weight reflects the mean gradient of the aggregate grading curves at the significant transition.

Furthermore, the shape and roughness of natural soil play a significant role and are classified as follows:
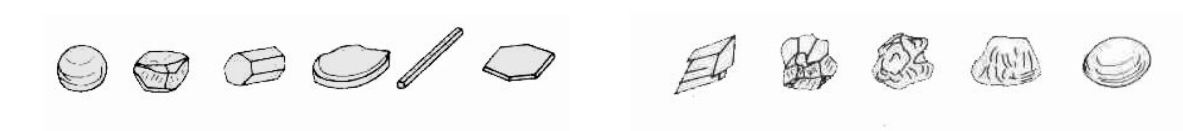
FIG. 8. Different Shapes and Roughness of Granules in Natural Soil (according to [58])

The possible shape of granules ranges from 'round' to 'flaky', while the roughness is described through attributes from 'sharp' to 'smooth'.

Finally, the following table according to [30] reflects some typical classes of granular soil, listed with possible values for the critical Angles of Friction $\varphi_c[^o]$, the average diameter $d_{50}[mm]$ and the Uniformity $U = d_{60}/d_{10}$ characterising the granularity.

Material	Av. Diameter d_{50}	Uniformity U	φ_c
Toyoura-Sand (angular/rounded)	0,16 mm	1,46	30°
Hochstetten-Sand (rounded)	0,20 mm	1,60	33°
Schlabendorf-Sand (rounded)	0,25 mm	3,09	33°
Hostun-Sand (angular/rounded)	0,35 mm	1,68	31°
Karlsruhe-Sand (rounded)	0,40 mm	1,85	30°
Zbraslav-Sand (angular/rounded)	0,50 mm	2,62	31°
Ottawa-Sand (round/rounded)	0,53 mm	1,70	30°
Ticino-Sand (angular/rounded)	0,55 mm	1,40	31°
Silver-Leighton-Buzzard-Sand (rounded)	0,62 mm	1,11	30°
Hochstetten-Gravel (rounded)	2,00 mm	7,20	36°
Polymer Granulate (elliptic cylinders $l = 4mm$, $d_1 = 3mm$, $d_2 = 4.5mm$)	3,00 mm	1,00	32°
Dry wheat (elliptic cylinders $l \simeq 6.6mm$, $d \simeq 3.7mm$)	3,70 mm	1,00	39°

Von Soos presents some more values in [58] for uniformly graded gravel where cohesion is measured $c \simeq 0$ and angles of friction in the range of $\varphi \simeq 34^o..42^o$ are obtained.

2. 5 Motivation for a Granular Model and Restrictions

The different aspects of grain to grain friction and the structural impact which presents itself also as a virtual frictional term motivated us to carry out some direct measurements of the force redirection ratio in a well defined two dimensional structural model of a granular arrangement.

The very simple model represents a small two dimensional section of a granular material. The shape of the granules is defined cylindrical, the frictional characteristics of the granules as well as the quality of the surface needs to be investigated. The granular arrangement ought to be characterised by a fixed distribution of granule diameters and by carefully described reproducible mixing and rearranging procedures. To be certain to include the observability of self organisation effects, the extent of predeformation needs to be varied. Then the arrangement of granules is to be loaded with forces, exposed to a precisely defined deformation history and finally surveyed concerning the redirection of forces in the direction transversal to the initial load. In order to separate the impact of grain to grain friction from the structural influence this experiment is to be made with granules of the same shape and distribution, but different surface materials causing different grain to grain friction.

Yet, the measurements introduced in this paper need to be positioned in the context of soil mechanics:

• Naturally, the structural mechanisms of redirecting forces and stress are of three-dimensional character. Yet, a 3D-model does not allow to visualize displacement processes nor areal force distributions, which are crucial to be surveyed. Using a 2D-setup, made from small cylindrical 'granules', the relevant mechanisms can be investigated fundamentally. Then, the evaluated mechanisms can be transferred to natural soil, but certainly not the quantitative values.

• Of particular importance in describing properties of natural soils is the most relevant fraction of water. Such impact needs to be excluded from the model since it introduces too many unknown parameters leading to mere fits instead of quantitative plausibility considerations.

- The model serves to understand principal interrelations, thus, the history of deformation needs to be defined and repeated in a reproducible way. In the present experiments, we need to survey the yield states and thus, have to be certain to exactly produce them.

- Considering the distribution of cylinder diameters, designed to be handled manually, the model represents the special case of uniformly graded coarse gravel.

- Measurements of the angle of friction of natural dry gravel lead to values of about 35° and higher which needs to correspond approximately to the cylinder surface friction. Other types of cylinders with the same geometry but different surface friction represent analogous granular material with less frictional influence but identical structural impact. Thus, surveying such models is expected to reveal some information about the structural contribution to the redirection of forces, not necessarily for material with less inherent friction. This means, that low friction cylinders leading to macroscopic angles of friction of some 15° do not represent e.g. some clay materials, since clay is known to comprise particles with a completely different distribution, emphasizing fine particles, a non-negligible fraction of water and is strongly influenced by other effects like electro-static adhesion, surface tension etc.

    Thus, projecting the results to natural soil is acceptable if variability of the scale does not have any influence. This might be true for absolutely hard and dry granules, where no parameters are depending on absolute sizes, pressures or weight but is certainly not applicable in general.

- A proper model specified for investigating force and stress distributions needs to be small. In this case, it is designed to represent a small section of the granular material (ca.20x20 granules). Hence, it is not a 'soil situation' but an 'infinitesimal' volume element. Again, this has no influence if the system can be assumed invariant to scaling, but not in general.

- In order to obtain significant differences in the structural arrangement of the granules, deformation values in the range of $\varepsilon \simeq 5$ % to $\varepsilon \simeq 20$ % are projected, which need to be judged in this respect. Referring to many different sources like [66], displacement values of $\varepsilon \gtrsim 2$ % are sufficient to produce completely sheared. Thus, one would not expect much of a difference between these limits. Yet, we need to consider the rough granularity of the model. Limited to a volume of about 200mm length filled with cylinders of about 10mm diameter, a compression of $\varepsilon \simeq 5$ % corresponds to a displacement within the

shearing joint of about *one* granule diameter while $\varepsilon \simeq 20$ % equals a shift length of *four* granule diameters.

- It is understood that besides the density the angularity and shape of grains influence most the macroscopic angle of friction, presumably more than the coefficient of grain to grain friction. Thus, the experiments described here refer to very simple structures, reducing the structural influence to circular cylinders but can easily be extended to more complex shapes as the computations solely rest on geometrical arguments.

- Investigation of the implicit elastic and plastic properties of the grains regarding strength and deformation of the granular assembly is not the subject of this paper. Therefore, grains in the present model are assumed to be not compressible and unbreakable.

- Since it is known, that uniformly graded gravel ($U < 6$) can hardly be compacted, the values of the packing fraction in our experiments will not develop that importance as they do on natural soil.

3 Experimental Setup

FIG. 9. Experimental apparatus
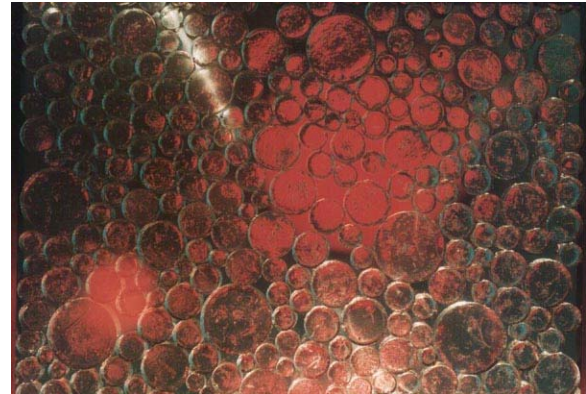
FIG.10. Close up of the granular model

3. 1 The Frame

The mechanical frame is based on a modular system of aluminium profiles and connectors supplied by FMS/Bosch. This allows for the flexibility that an experimental setup requires. A double frame surrounds the volume, which is formed by two parallel plates of glass, set at a distance of 12 mm. This permits good observation from the lateral side, while forces can be applied from any direction by moving steel boundaries ('walls') in and out. Forces up to 300 N can be imposed on the equipment without significant deformation. The inner surface of the 'walls' is covered with PTFE in order to minimize frictional boundary effects.

Looking very much like an aquarium, the frame acquired this nickname.
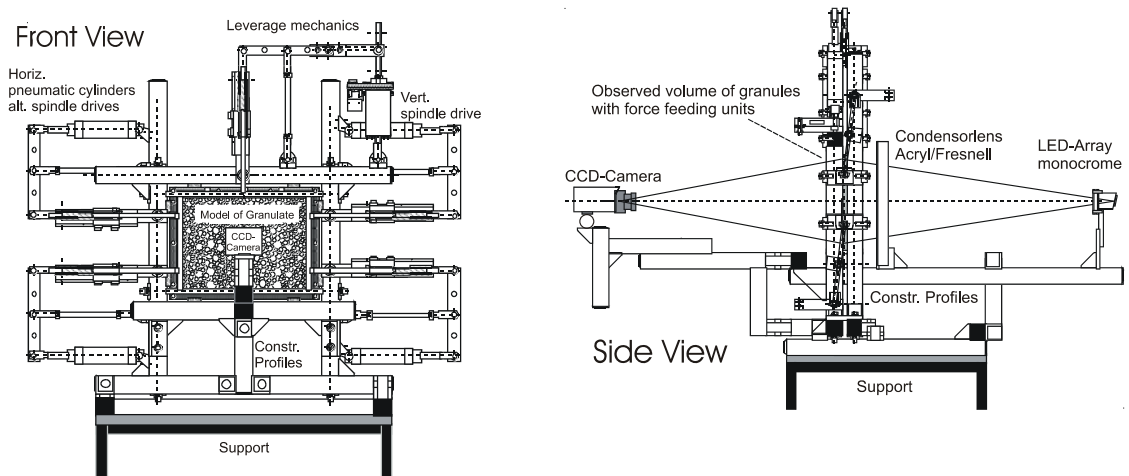
FIG. 11. Schematic view of the experimental setup

3. 2 The Granular System

The experimental volume of interest (240 mm x 210 mm x 12 mm) is filled with small cylinders, made from photo elastic plastics.

The distribution of cylinder diameters was chosen around a nominal value of 10 mm, allowing enough variance to inhibit effects derived from the symmetry. A minimum diameter of 8 mm was selected to avoid clamping, while only very few cylinders reach a maximum of 30 mm to ensure a sufficient number of contacts within the volume. A total number of about 400 cylinders in the volume provides an average of 20 contacts to each side wall, contributing to the particular force measurement.
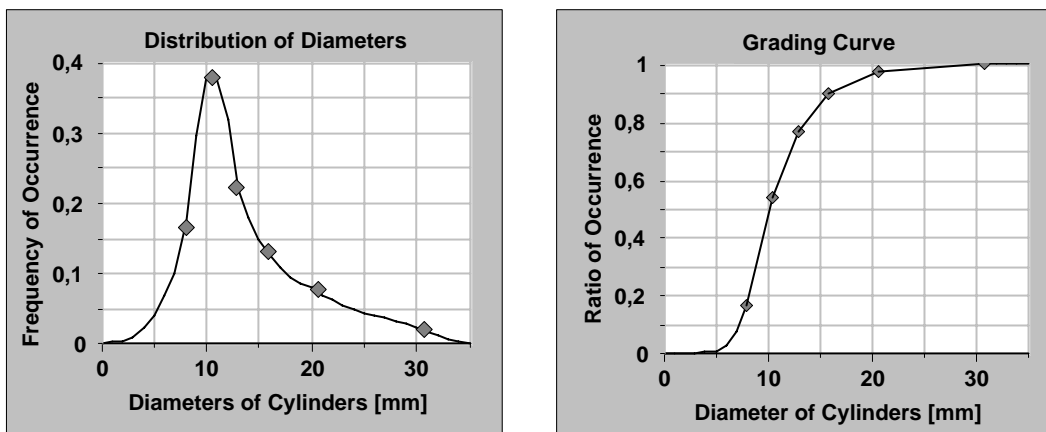
FIG. 12. 2D-model of granular material: Distribution of diameters. (File: FrequencyOfSize.123)

While the cylinder core material is mainly Polyester resin, the required variation in angles of friction is achieved by the use of different coatings applied to the circumference.

One set of cylinders was uncoated Polyester (PET), a second set was coated with Teflon tape (PTFE), and a third set was enveloped in Polyolefin (POC) sheathing. To enlarge the number of available coefficients of friction, a fourth type of cylinder was used, which is completely made of Polyvinylchloride (PVC). Though these elements cannot be used for photo elastic experiments, they contribute interesting additional observations.

FIG. 13. Samples of cylinders

PVC (red), Tinted PTFE *(blue),* PET *(transparent),* Covered POC (*black*:)

3. 3 The Polariscope

The photo elastic effect can be used to observe the building of force chains [26, 46, 47]. A monochrome, circular polarized LED source illuminates the window from behind, where an industrial CCD-camera takes the pictures from the front through a circular polarized analyser. A full-size condenser lens placed just behind the window allows for small and concentrated light sources. The pictures are captured by an electronic picture processing system which slightly enhances the contrast and color. With this, movies of any motion driven force development can easily be recorded and analysed.
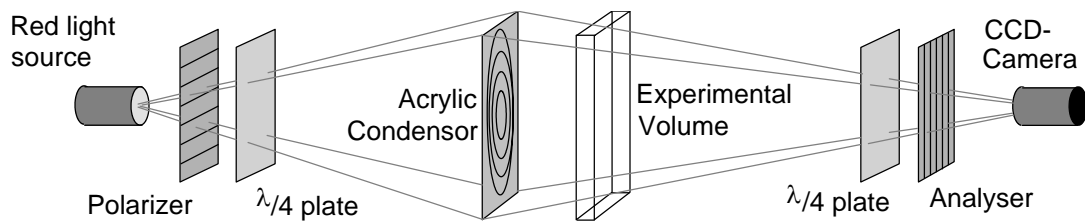
FIG. 14. Schematic view of the polariscope setup

The usage of circular polarised light in this arrangement allows for the visualisation of the difference of the principal stress ($\sigma_I - \sigma_{III}$) independent of the absolute angle of the direction of the principal stress with respect to the setup. Due to the singular character of the load at the contacts, synchronous increase of both stress components is rarely to be expected. Thus any grain exposed to stress or at least the surrounding area of a stressed contact simply lights up and indicates its participation in bearing forces.
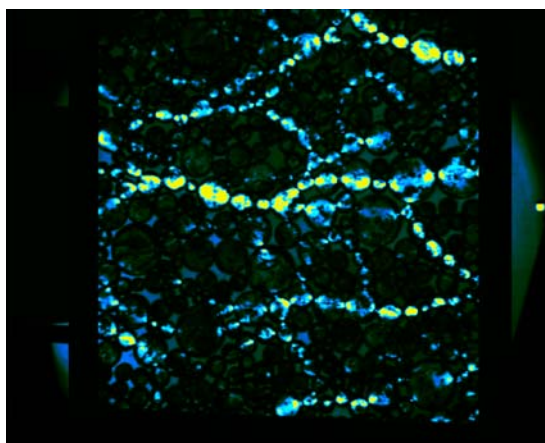
FIG. 15. Exemplary processed image, where the colour transition to yellow indicates bearing forces

3. 4 The Force Transmission

The setup allows the application of feeding forces up to 300 N from any side. Within this range electric spindle drives supply active positioning independent of forces, while low friction pneumatic cylinders allow for position-independent constant forces.

All forces are observed by industrial load cells, positioned within the mounting tappets of the moveable 'walls'. In this way, accumulated forces of the total granular volume are measured. The signals were recorded using a locking amplifier, fixed on a 1000 Hz sine wave excitation. Measurements are possible up to 100 Hz for up to 10 channels with an accuracy of ≈ 0.3 %

Positions are read out roughly through potentiometric sensors over a range of 100 mm (Accuracy ± 0.1 %), where small variations are observed using dial gauges (Accuracy 0.01 mm).

Data acquisition is run through a PC-based data logger, to be recorded, interpreted and stored.

3. 5 Universality

The described setup makes it easy to set up for diverse further measurements: Besides feeding stress and strain to a model of granular material and observing the resulting force chains with their accompanying lateral stresses and motion, any kind of additional detail can be investigated as well: coefficients of friction, angles of repose, elastic parameters and friction to walls are examples of the particulars to be tracked.

4 Measurements of Averaged Forces

Remark: The measurements described in this chapter, together with the obtained basic results are also discussed in [67].

4. 1 Friction Measurements

Besides the structural impact on the behaviour of granular material, the coefficient of grain to grain friction μ_0 can be taken to be the most important parameter.

While the common approach [3,4,5,8,9] defines the coefficient of friction inversely from the response of the system as a macroscopic effective parameter, the influences of structure and grain to grain friction need to be separated. Therefore, the microscopic coefficient of friction was measured carefully in advance in order to correlate it to the observed behaviour.

Efforts have been spent on understanding microscopic frictional mechanisms by a number of researchers [59,60]. Currently a continuous transition from static to dynamic friction is established based on a strong dependency on the velocity of a contact movement. In particular, *velocity weakening* causes the coefficient of friction μ_0 to increase significantly with decreasing contact velocity in the range of 10^{-1} *mm/s* to 10^{-4} *mm/s*. Thus, μ_0 can rather not be treated as a constant but needs to be corrected by a logarithmic function of the displacement speed. Measuring μ_0 at the state of incident failure would provide a correct static value, yet it still depends on the age of the contacts. This introduces some difficulty in choosing a proper method to obtain representative friction coefficient values μ_0.

Since this work aims at the structural impact on effective friction, the measure of the coefficients was taken under circumstances as close as possible to the conditions found in the granular system. As the granular material is sheared slowly by a spindle drive (see next section), lost contacts are constantly replaced by new contacts. Hence, we used the same model at the same velocity to obtain representative friction coefficients: A slowly moving contact is repeatedly opened and closed while the varying friction force is observed. In particular, the rise of the retaining force when closing the contact supposably represents the situation best and yields proper coefficients of friction for comparison purposes with the behaviour of complex granular material.

To implement such an experiment, a single contact of the particles involved was loaded with different forces and then moved slowly for a distance of some 10 mm in order to eliminate

local irregularities. The measurement is then repeated moving in the opposite direction, thus averaging mechanical effects.
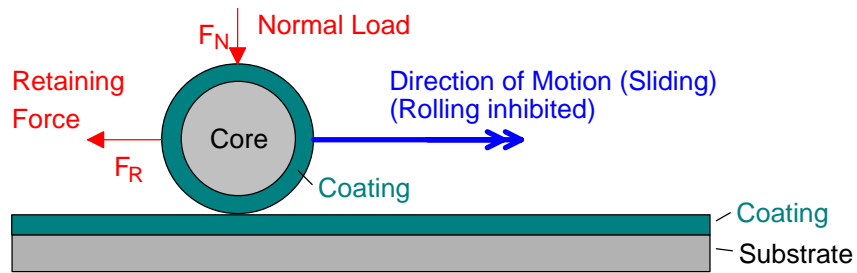
FIG. 16. Schematic view of the experimental setup used to measure friction parameters

Conventional load cells are used in conjunction with a sensitive Locking Amplifier to record the retaining friction force. The different loads are gauged using the same system prior to the actual measurement.

The speed of moving was set to about 0.25 mm/s to avoid the influence of dynamic effects. Constant speed could be ensured by using an electric motor spindle drive.

While moving, the load was repeatedly removed and reapplied. These reapplied load steps can be observed well, even on widely varying underground. After averaging the noise the amplitude of the steps were recorded for an ample number of transitions per load value. Then the number of measured retaining friction force values F_R corresponding to the particular normal force F_N which is given by the applied load allows for regressional analysis to determine the grain to grain friction as the ratio $\overline{\mu_0} = \dfrac{F_R}{F_N}$.
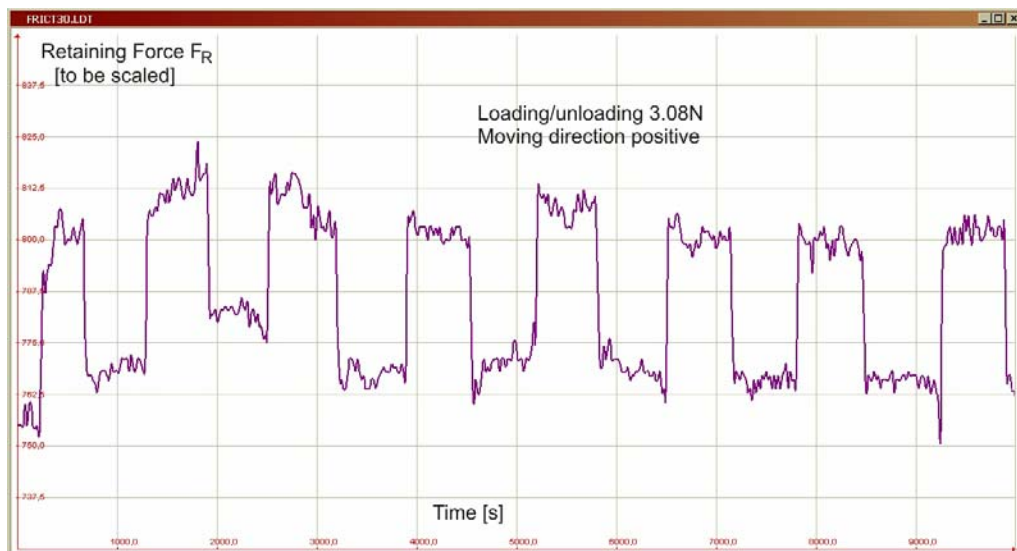
FIG. 17. Typical plot of friction force vs. measurement time during load steps (File:FrictionDemo.JPG)

The tested surface coatings were: Teflon (PTFE), Polyvinylchloride (PVC), Polyolefin (POC) and Polyester (PET).

In order to verify the reproducibility, some of the measurements were repeated with positively validating results.

Mean retaining force values $\overline{F_R}$ corresponding to a load F_N were plotted on graphs. Then regression lines were computed to represent the gradient $\overline{\mu_0}$. Since the interpolation lines meet the origin of the graph within their error margins, cohesion $c \simeq 0$ is obtained as expected for dry friction.

Fairly high coefficients of regression R^2 allow for a first order approximation of the result, neglecting nonlinear influences of the hertzian nature of the contacts. In order to obtain a reasonable error estimation, finally all results concerning a combination of materials were taken into account for further regression analysis.
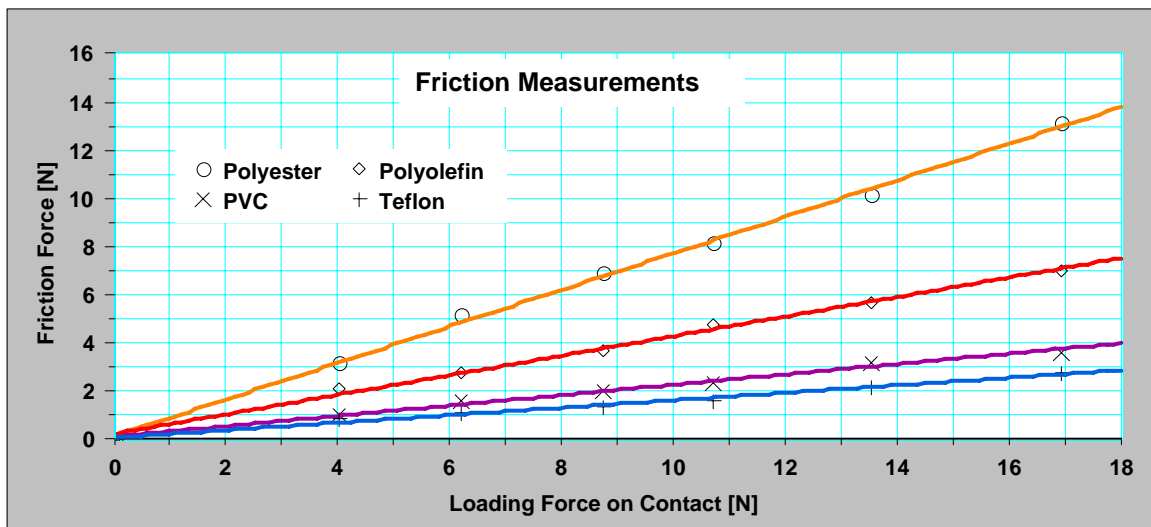
FIG. 18. Friction forces vs. normal load, experimentally obtained from different surface coatings (File: FrictionComplete.123)

As was expected, the single values show a wide variation due to the statistical nature of the contacts. Nevertheless, regression analysis of the measurement, taking into account about 150-200 'steps' per combination of materials yields amazingly good and reproducible results.

The following table shows the finally obtained values:

Material	Teflon	PVC	Polyolefin	Polyester
Coefficient of Regression(All)	0,761	0,678	0,824	0,917
Coefficient of Regression(Means)	0,975	0,990	0,997	0,996
Gradient $\overline{\mu_0}$	0,136	0,200	0,358	0,736
Accuracy (95%)	+/- 0,016	+/- 0,028	+/-0,028	+/- 0,052
Corresp. Angle of Friction $\arctan\overline{\mu_0}$	**7,75°**	**11,33°**	**19,71°**	**36,34°**
Interval of Confidence (95%)	+/- 0,86°	+/- 1,56°	+/- 1,60°	+/- 2,99°

Remark: The grain to grain angle of friction $\vartheta_0 = \arctan\overline{\mu_0}$ is not equivalent to the Angle of Friction φ, describing the shear resistance of the grain assembly, which is additionally dependant on the form, grain size, distribution and density of the assembly. Here it is specified only for clearness. In the following, $\overline{\mu_0}$ resp. $\vartheta_0 = \arctan\overline{\mu_0}$ is always used for the grain to grain friction, while φ represents the angle of friction of an assembly of grains.

4. 2 Estimation of Unevenness

Due to the fabrication process, the cast cylinders display significant unevenness. Assuming constant distribution of contacts over the whole range of angles, this property might be ignored, since such irregularities provide symmetrically rising and falling slopes, where additional positive and negative terms to the angle of friction cancel each other. Yet on the basis of self organising processes this symmetry cannot always be preconditioned.

In order to understand the circumstances of our measurements, the unevenness was recorded. While turning a cylinder between two sensing heads, the absolute height of irregularities for every type of surface material were surveyed and mapped:

	Polyester	Polyolefin	Polyvinylclorid	Teflon
Mean Roughness [mm]	0,24	0,23	<< 0,01	0,23
Error (95%) [mm]	0,07	0,09		0,11

The statistical errors are high due to the random selection of tested cylinders. Nevertheless, the amount of noise read from the smooth PVC cylinders produced on the lathe serves as a

well defined indication for the quality of the measurements. Thus the error can be assumed to be about 21%.

4. 3 Coefficient of Lateral Stress

Most of our work aims at the measurement of the lateral stress σ_3, responding to longitudinal stress σ_1, applied to a model of granular material with a well defined coefficient of friction in comparison to ancient approved theories like that of Rankine [5,6]. In contrast to his approach, we are observing not a complete 'soil'-situation but a volume, small enough to be independent of boundary conditions, but still large enough that discreteness of the grains has no more influence.

In order to allow precise observation of the granular material, all experiments had been carried out in two dimensions, while most approaches imply 3D-measurements. The impact of this restriction will be considered when comparisons are drawn.

4. 3. 1 Coordinate System

All measurements were carried out using the following coordinate system:
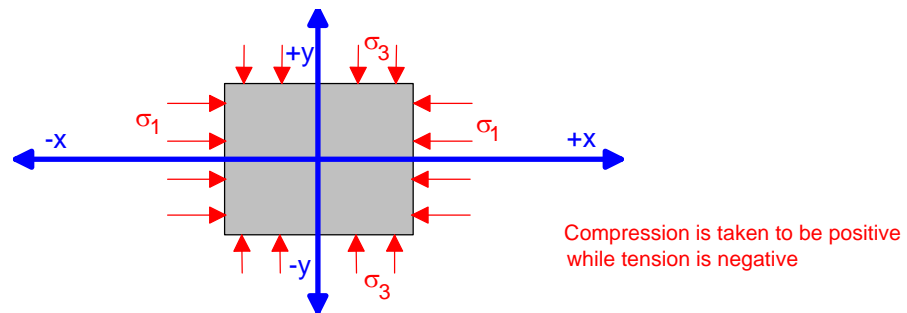

FIG. 19. Orientation and coordinate system used in this paper

4. 3. 2 Constructing an Unambiguous State

Due to the known nonlinear character of friction a grain contact can bear a wide range of tangential forces without making this visible to an external observer. Thus only the extreme border states, where friction helps most to withstand a deformation can be observed and are

of greater interest. These two available border states, in both positive and negative directions of movement are closely related to the 'Active' and the 'Passive' state defined by Rankine, and therefore denoted accordingly in this paper. Since the states are symmetrical in terms of stress (not in terms of deformation), it is sufficient to survey one of them. We define it by compressing a granular system in the horizontal direction, where friction between the grains impedes deformation. With increasing stress, sliding becomes possible because friction forces are now not strong enough to prevent movement. Vertical expansion is then observed, the stress no longer increases and the border state is reached.

However, well determined measurements presuming this state all over the volume can only be achieved by carefully creating a suited motion-history of the model. Due to the stochastic character of the building of structures like force chains, many motion cycles where one provides a single pair of values (σ_3, σ_1) as described below had to be executed and analysed in order to obtain reproducible results. An ample number of such pairs acquired with a certain set of granules where the grain to grain friction is known, finally allows for regression analysis to form a reliable average ratio $\overline{K} = \overline{\left(\dfrac{\sigma_3}{\sigma_1}\right)}$

All measurement cycles have been taken in the same manner (See following figure): Into a fixed two-dimensional volume, containing the granular material, the left wall is pushed inwards, forcing the granules to rise to the fixed top (Fig. Part a). Besides the small friction force introduced by the experimental apparatus, an additional basic force is needed to shear the system against its own weight. Then, with a little more pressure, the desired horizontal force is applied (Fig. Part b).

Holding this for a while, a bit of creep is observed, when single contacts are shifting to reach more stable positions. This behaviour tends to move the system away from the border state. Therefore, the upper wall of the volume is slowly lifted by about $300\mu m$ to allow the system to reach the 'active' state definitely (Fig. Part c). In this way, the vertical as well as the horizontal forces decrease slightly. At the end of this process to ensure the limiting state, the granular system immediately begins to lose this state again, proven by a small rise of the vertical force while horizontal forces are still decreasing.

Finally, the left wall is driven back to its initial state, where all the forces are expected to vanish and the set up is ready for another cycle (Fig. Part d).

a. Initial horizontal compression

b. Vertical contact, horiz. forces rise to desired value, vert. forces develop accordingly

c. Releasing vertical hold - reach active state

d. Releasing horiz. hold, all forces decay
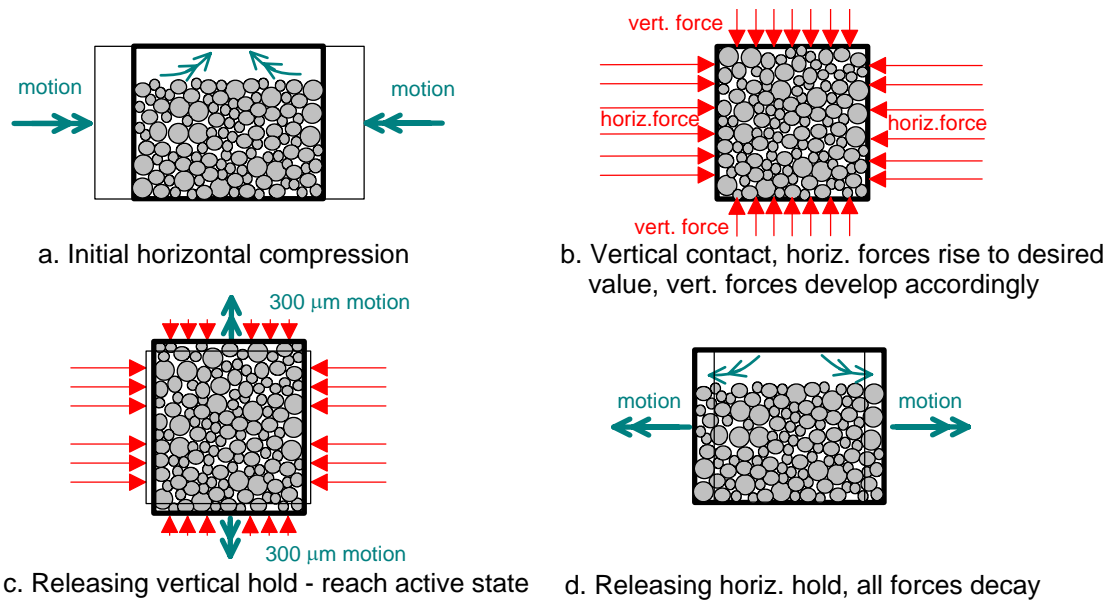
FIG. 20. Schematic view of measurement cycle to achieve an active state. Bold double arrows indicate motion while light arrows are forces

The characteristic stress development of such a cycle is exemplarily shown in the following figure:
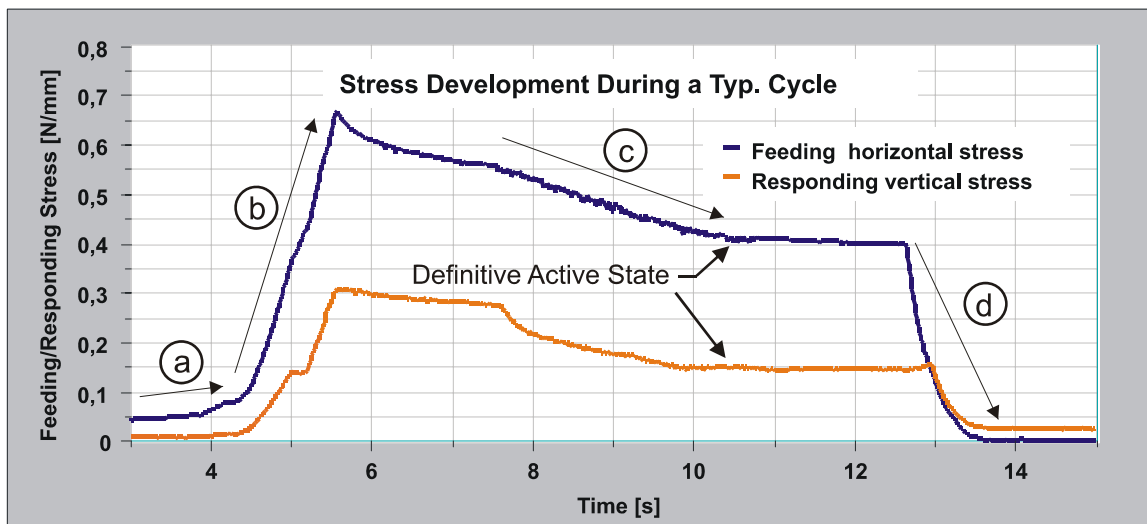
FIG. 21. Typical stress development during deformation cycle (File: MeasurementCycle UCT25.123)

Several aspects had to be considered carefully, to achieve a satisfactory acquisition of the factor $\overline{K} = \overline{\left(\dfrac{\sigma_3}{\sigma_1}\right)}$ accurately in the desired border active state:

- Calibration of the load cells has to be made before and after every set of measurements.

- The more or less constant friction forces of the setup must be eliminated.

- Care must be taken to certainly localize the final active state of the granular material for each measurement cycle. Further tests have been performed successfully in order to gain certainty of this state (See Chapter 4.5 *Excursion: Confirmation of Active State*)

- Because of the stochastic character of the problem, $\overline{K}$ can only be obtained as the result of regression analysis. In this case the regression coefficient R^2 does not tell much about the quality of the measurement, but indicates the broadness of responses to the possible states. Thus, many samples will indicate only the distribution of possible arrangements.

In order to interpret the cycles, the stress transmission σ_1 was displayed against the stress response σ_3 to obtain significant hysteresis diagrams.
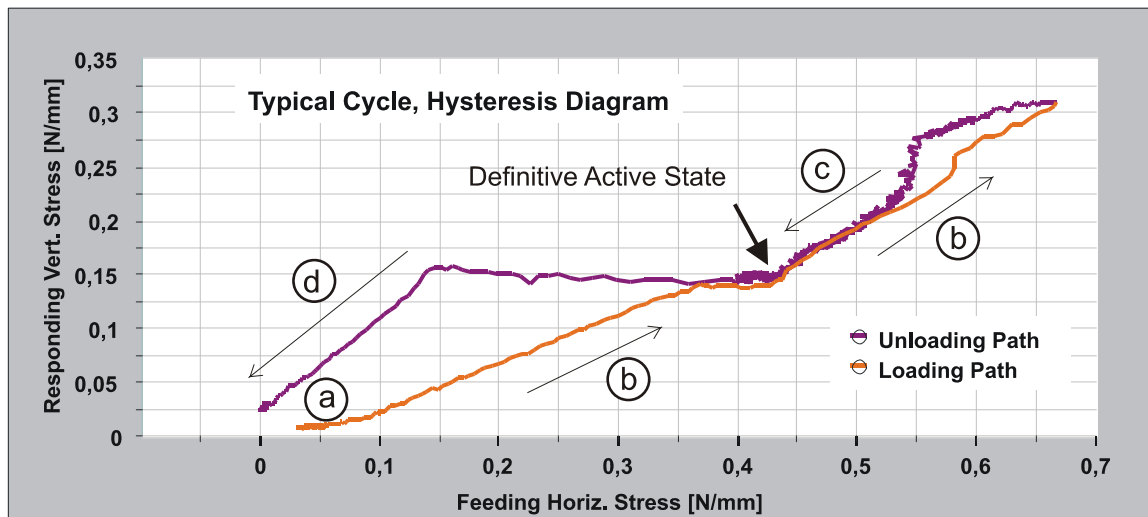
FIG. 22. Hysteresis diagram of typical deformation cycle (File: MeasurementCycle UCT25.123)

In preparation of the physical analysis, the hysteresis diagrams of all cycles were analysed with the following results:

In general, the properties, mentioned above, can easily be observed. Especially the point where the granular material is completely activated is well defined. Besides the fact that this point can be just "seen", it is bound to be the minimum gradient, observed within the cycle. Any other, higher gradient will not denote the active state.

It seems appropriate to select the last part of the activating line, which is linearly well correlated, to obtain the gradient, which is identical to $\overline{K}$. Linear regression analysis supplies the tools for it. Unfortunately, these lines are much too short to ensure small error bars.

The rising slope at the beginning of each cycle obviously displays the same gradient as at the end of the activation part of it. So regression analysis over this segment offers another way to interpret the readings. There we noticed at a certain - mostly constant height - a step in the hysteresis diagram. This step could be identified as the clearance of the mechanical set-up, but does not influence the results.

Due to the fact, that all the linear parts of the diagrams were too short and to widely spread to yield better results than such with up to 25 % uncertainty, a different way was needed to find a more satisfactory analysis.

For this reason, several cycles have been carried out with different maximum horizontal forces. Thus, each of the well-defined 'active points' of every cycle lies on a different force level. With a proper reference, eliminating systematic errors like the friction of the bearings of the experimental setup, the entirety of cycles yields a coverage of the force range that can be analysed with good results.

This raises the question of a good reference for each cycle.

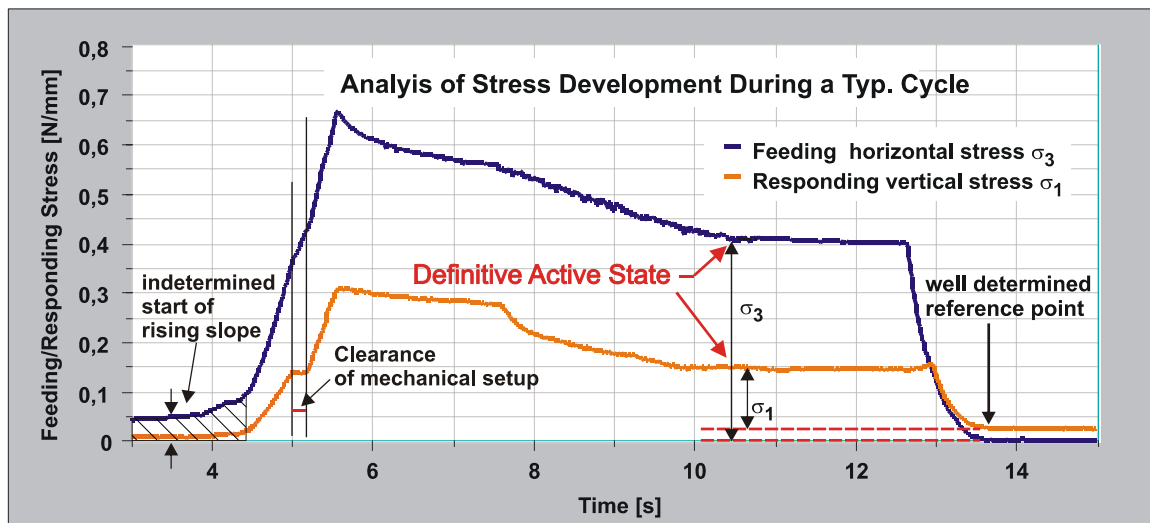FIG. 23. Typ. Stress development and possible reference point (File: Reference for MeasurementCycle UCT25.123)

From the hysteresis diagrams we note, that stress values σ_3 before and after each cycle do not vary significantly. Yet, we observe a greater horizontal base value at the beginning of the cycle, where the granules are sheared to fill the volume. Therefore a position on this base

value is not a very well determined reference, on the one hand because of its noisy character, on the other hand due to the insecure selection of a point on the soft knee at the beginning of the ascent.

The frictional contribution of the experimental setup is very obvious and can be taken into account. Using regression analysis these constant offset will have no effect on the calculation of the gradient.

Aside from this, sometimes a certain small offset on the vertical stress value σ_1 is noticed during some cycles. Nevertheless, we assume, that on the rising segment of the cycle where the main forces are applied, the vertical mechanics is set under pressure, which causes slightly enlarged parameters of friction within the setup. Certainly, this remains constant during the release period as all changes taking place during the measurement cycle are accomplished after the feeding force has been released. Thus the final state is the best reference for the most recent cycle.

Remark: Since the active state is defined as a situation, where grain to grain friction bears most of the applied force, it is characterised by the minimum of the ratio $\frac{\sigma_3}{\sigma_1}$. The following graph shows the typical progression of this value based on the reference discussed above for the considered unloading part of the experiment. The active state can clearly be obtained and verified at the time $\simeq 9.8$ s.
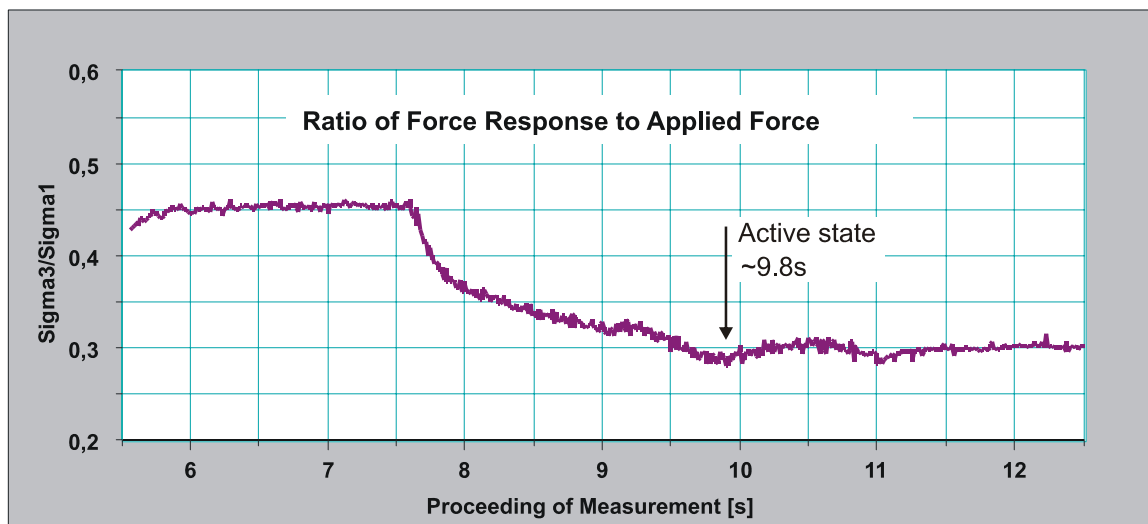

FIG. 24. Confirmation of active state as the minimum of the force ratio (File: MeasurementCycle Min UCT25.123)

4. 3. 3 Measuring the Lateral Stress Factors

It is known from shearing experiments that in dependence of the materials density the devia-tor σ_1/σ_3 $(= 1/K)$ develops through a peak to an asymptotical critical value when sheared. This behaviour is a consequence of the generation of shearing joints which is closely related to the variation of the void ratio e.
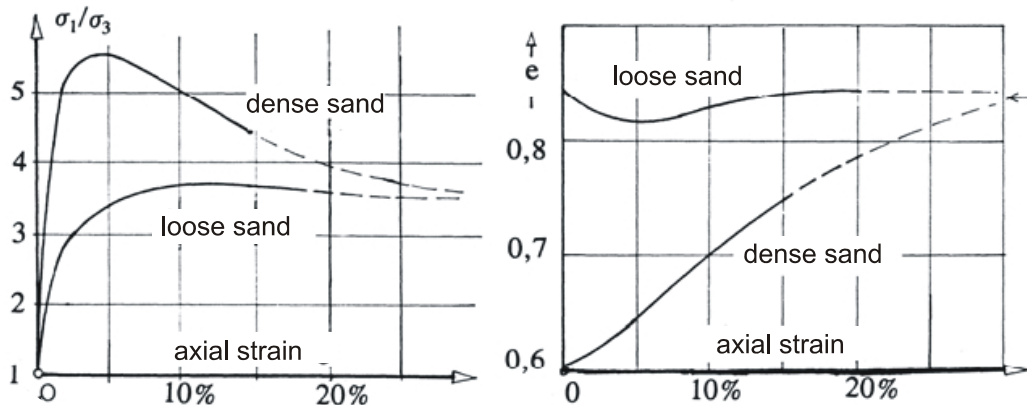

FIG. 25. Qualitative development of stress deviation and void ratio when sheared acc. To Herle [30] (File: AxStrain.wmf)

Hence in the simplified model surveyed in this project effects of different value and character are expected to be to observed, when the granular material is compressed horizontally to a variable extent, while it expands freely in the vertical direction. Such a procedure is likely to allow self organising mechanisms to develop, which cause significant differences in $\overline{K}$. On the other hand the same may lead to relaxation processes, provoking compensation by statis-tical averaging. Since the process of developing such behaviour corresponds to raising the level of organisation by forced deformation, in this paper, measurements are classified as being of High or Low Level of Organisation ('HLO' or 'LLO').

To understand these effects and possibly eliminate them, two types of cycles were performed:

For measurements with ***Low Level of Organisation*** ('**LLO**'), the volume is filled with carefully mixed cylinders. The size of the window had previously been preset, so that it can be completely filled. After that, the loading branch is characterized by a very small percent-age of horizontal compressing before the top is reached and forces begin to rise. The typical horizontal deformation in this process is approximately 5 % of the window size ($\simeq 1$ av. Diameter). In this configuration largely no structures generated by self organising

mechanisms corresponding to shear zones were observed and thus no significant impact of such is assumed.

Hence, expecting strong influences of the initial configuration, for each material thirty sequences were recorded, containing each at least five to six cycles. Ever after two sequences the granular material was remixed again to avoid the building of structures within the system. To be certain of the drift behaviour, horizontal as well as vertical gauging was analysed before and after every ten sequences. Thus, about 170 cycles were provided for further investigation for each of the four surface materials.

Measurements with **High Level of Organisation** ('**HLO**') are characterized by free horizontal deformation of about 20 % of the length ($\simeq$ 4 av. diameters), before the granules touch the upper bound and the forces begin to rise. These series allow for the development of observable shearing joints and are therefore assumed representative for a stationary state. Three sets consisting of sixteen sequences were executed. Anticipating balancing effects through the long range of predeformation, mixing and reloading the granules was done every two sequences. A sequence contains only two cycles, so overall this yields about 90 pairs of values for each surface material. Gauging again was done before and after each set to keep control over possible drifting effects.

Remark: Besides measurements of K for both the configurations, the variation of the density rsp. the packing fraction in both cases needs to be investigated, which is done in Chapter 5.

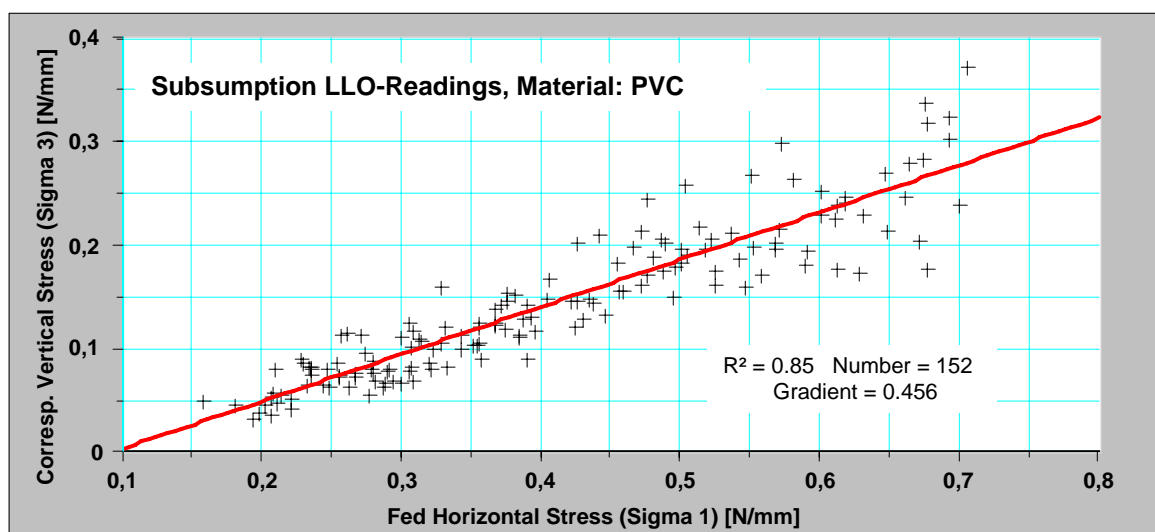Typical summaries of such a set of values look like this:

FIG. 26. Exemplary set of measured values: Horiz. stress vs. responding vert. stress (File: Subsumption UCV.123)

Depending on influences like creep, time dependent effects or low values, some of the measurements are wider spread than others. Regression analysis was used, to eliminate this as well as to give a good estimation for errors. Again, larger deviation from the mean, results from the stochastic character of the generating of structures.

4. 3. 4 Side Effects

The gradient of the regression line yields the total stress ratio $\overline{K^{total}}$, possibly consisting of several fractions contaminating the pure frictional and structural value.

In order to achieve a measure for the behaviour introduced by sliding contacts, the elastic contribution as well as the influence of other potential side effects needs to be investigated.

4. 3. 4. 1 Elastic Transversal Force

As for all materials, the resin cylinders exhibit elastic behaviour, which might contribute an additional value of lateral force response to the longitudinal force besides the frictional portion. Hence we find a possible additive correction

$$\overline{K^{total}} = \overline{K^{frict}} + \overline{K^{elast}}$$

activated by the impeded lateral strain which needs to be measured separately and judged for its influence on the readings.

In order to obtain at least the magnitude of the elastic contribution to the frictional and structural value K, two additional sequences of measurement had been performed: First a single cylinder, made of the selected resin, was loaded with varying forces while observing the lateral force, induced by the Coefficient of Poisson and the Modulus of Young. A second test was performed, reading the same values, but pressing on a miniature-structure, formed by four cylinders, glued together, in order to gain the shearing influence on the lateral force factor. A set of about 140 values per orientation, spread over a range of seven different loads was the basis for regression analysis and yielded the following results with small errors:
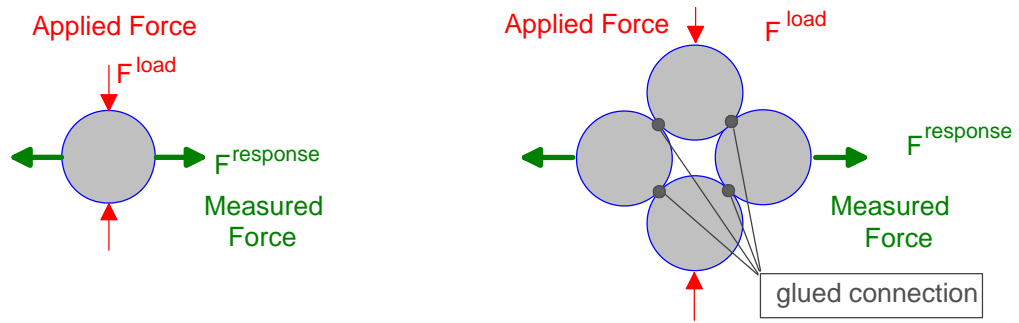
FIG. 27. Schematic view of measurement setup in order to obtain the elastic contribution

Taken in the two extreme orientations as shown, we obtain a small additional transverse force factor of

$$\overline{K^{elast}}_{vert} = \frac{F^{response}}{F^{load}} \simeq 0.030 \pm 0.00064 \text{ for the vertical and}$$

$$\overline{K^{elast}}_{diag} = \frac{F^{response}}{F^{load}} \simeq 0.042 \pm 0.0024 \text{ for the diagonal orientation.}$$

Additional tests were performed, to verify that the PVC-cylinders did not present significantly different corrections

The discrepancy between the measured values and the expected coefficient of Poisson $v \simeq 0.3 \simeq K^{elast}$ is a direct consequence of the difference between square elements and circular disks. On a rectangular element, the boundary condition of blocked strain effects is valid all over the boundary and therefore reactive stress is returned for every locus of the sample. In contrast to this, on circular disks the boundary condition only limits the strain at the small contact areas. Thus, most of the circumference is free to develop strain and hence returns much less reactive stress.
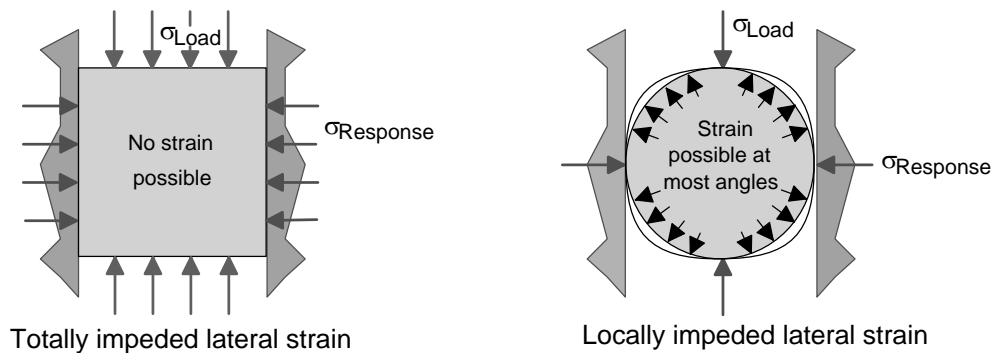

FIG. 28. Different consequences of impeded horizontal strain on rectangular and circular elements

Remark: Since the acquisition of the elastic contribution value (impeded longitudinal strain) does not completely reflect the situation of the granular material in the yielding state, the correction quantity is rated to be taken with care. Nevertheless the correction is assumed to be essential for the admissibility of proceeding further.

4. 3. 4. 2 Friction at the Glass Walls

Due to the cylindrical form of the granular elements, no significant force is fed into the contact to the glass walls. Short estimations gave evidence, that even in the worst case of configuration, the retaining force of friction is below some 0.1% of the initiating load. Thus its influence can be neglected in this context.

4. 3. 4. 3 Friction at the Limiting Side Walls

The side walls, which transfer all the forces to the granular model are subject to friction-forces too high to be disregarded. Taking the model as one compact block, even when having PTFE coatings on the side walls, they may reach $\mu_w = 0.05..0.2$ which would modify the read Lateral Force Factor significantly.

Fortunately the granular system does not act as a compact block. Rather being comparable to a loose conglomerate of cylinders, there is no need to really shift the elements contacting the side walls while compressing or expanding. Pictures from the polariscope may serve as additional proof for this, as they show no exceeding stress at the corners of the volume of interest, where the greatest deformation would be expected. Thus friction to the side walls can be completely left out of consideration.
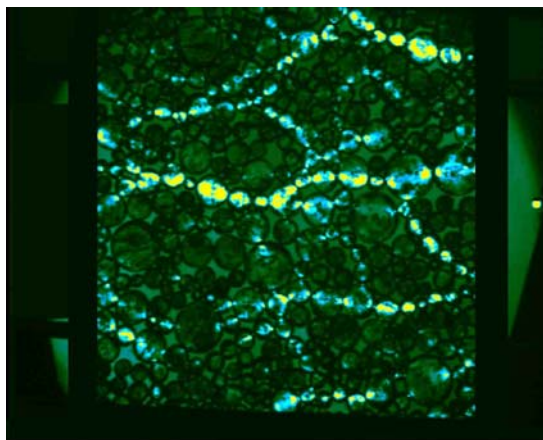

FIG. 29. Typical polariscope picture, indicating no exceeding stress at the corners

4. 3. 5 Final Readings

Finally, the results $\overline{K}$ of all the sequences are summarized in the following table. Now that they are definitely taken in an active state of the granular material, they can be called $\overline{K_a}$, in accordance with soil mechanics practice.

	Teflon	**PVC**	**Polyolefin**	**Polyester**
$\vartheta_0 = \arctan\mu_0$	**7,75°**	**11,33°**	**19,71°**	**36,34°**
Error +/-	+/-0,86°	+/-1,56°	+/-1,60°	+/-2,99°
$\overline{K_a^{total}}$ **(LLO)**	**0,344**	**0,456**	**0,272**	**0,200**
Error 95%	+/-0,025	+/-0,031	+/-0,031	+/-0,024
$\overline{K_a^{total}}$ **(HLO)**	**0,491**	**0,452**	**0,351**	**0,198**
Error 95%	+/-0,043	+/-0,039	+/-0,040	+/-0,031
elast. contrib.	-0,037	-0,037	-0,037	-0,037
$\overline{K_a^{frict}}$ **(LLO)**	**0,307**	**0,419**	**0,235**	**0,163**
$\overline{K_a^{frict}}$ **(HLO)**	**0,454**	**0,415**	**0,314**	**0,161**

In this table $\vartheta_0 = \arctan\mu_0$ is the angle calculated from the grain to grain coefficient of friction μ_0, where the angle of friction φ for an assembly of grains is assumed to be a function of μ_0. The row denoted **LLO** lists the Lateral Stress Factors for *States of Low Level of Organisation* (i.e. $\varepsilon \simeq 5$ %) while row **HLO** is the same for granular material with *High Level of Organisation* (i.e. $\varepsilon \simeq 20$ %). Error bars are calculated for the 95%-percentile. Elastic impact is eliminated from the final result.

The following graphs display the resulting $\overline{K_a^{frict}}$ *vs.* the grain to grain angle of friction $\vartheta_0 = \arctan\mu_0$. In order to illuminate the deviation, a theoretical line $K_a^R = \tan^2(\frac{\pi}{4} - \frac{\varphi}{2})$ in the style of a Rankine approach is added, where equivalence of the grain to grain Angle of Friction ϑ_0 and the Assembly Angle of Friction φ is assumed.
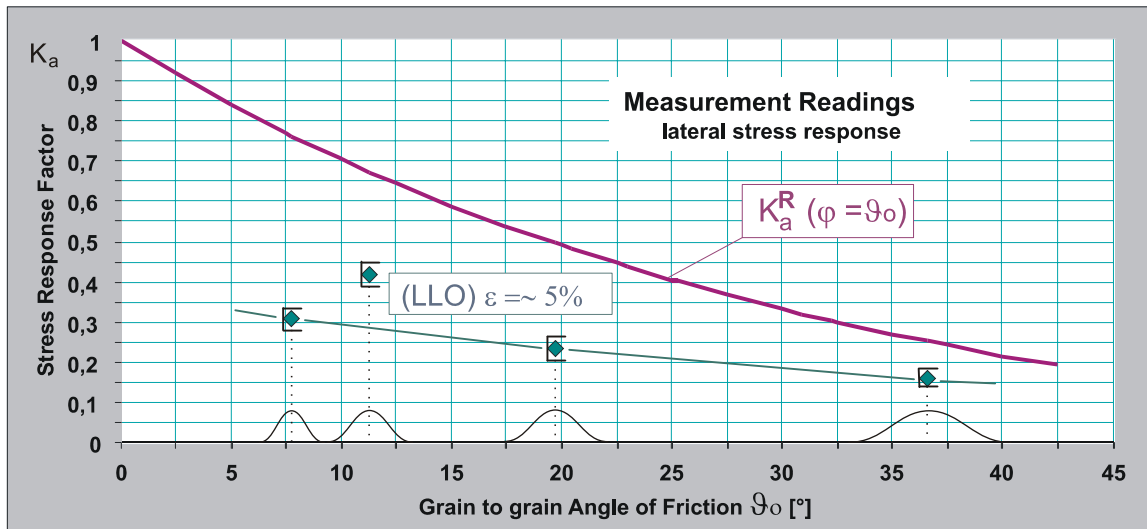
FIG. 30. Final measurement results for LLO-systems (File: Readings UC.123)
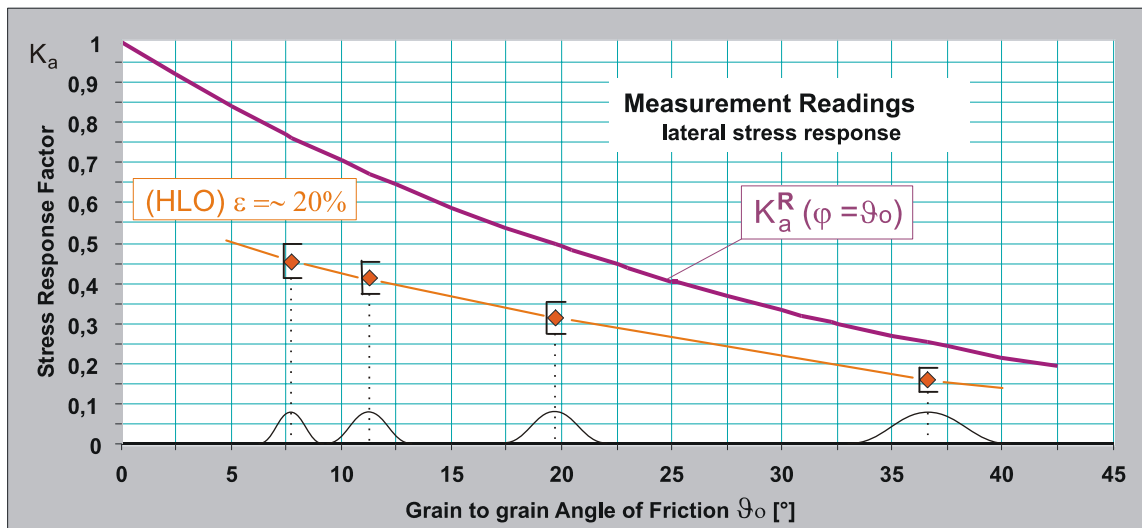
FIG. 31. Final measurement results for HLO-systems (File: Readings TC.123)

4. 4 First Discussion of Results, General Remarks

As the plotted errorbars indicate the results can be rated accurate enough to proceed to further analysis. Furthermore several series of measurements have been repeated to ensure reproducibility with no significant difference.

The first impression of the observed values is that completely different mechanisms are working on higher deformation (~20 %) than on low deformation (~5 %).

Starting from a more or less statistical state and allowing no restructuring, some force chains take over most of the longitudinal stress and therefore do not produce much lateral stress. Building up these force chains underlies mainly local selforganising effects, no restructuring processes are available to compensate. Nevertheless, the measurements exhibit a tendency to a smooth line, a good deal beyond the Rankine relation, where $\vartheta_0 = \varphi$ is assumed, with an exception of the PVC-Material value. This material obviously indicates an additional different effect.

Allowing for further restructuring, under deformation of some 20 %, this discrepancy has completely vanished. Images of the polariscope show well distributed patterns, with no observable difference between the miscellaneous surface materials. Thus we assume, that such a forced deformation enables restructuring processes to accomplish and, hence, can serve as a proper model for granular materials with a known history of unidirectional motion.

Remark: It must be kept in mind, that in this experiment a compression rate of $\varepsilon \simeq 5\%$ equals a displacement of about one average diameter of the granules, while $\varepsilon \simeq 20\%$ describes a displacement of four average diameters.

It can be clearly seen in both cases, that the grain to grain friction alone is not sufficient to explain the low ratio K_a^{frict}. Hence an additional structural impact is obvious and will be quantified and calculated in chapter 9 and 10 after all measurement procedures have been described and the results presented. In particular the variation of the density is expected to play an important role and will be discussed in chapter 7 and 8.

4. 5 Excursion: Confirmation of Active State

Since granular material always remains in a state between the active state and the passive state, it turns out to be difficult to be certainly observing the one or the other limit, especially when these border states possibly vary in dependence of a varying density.

In order to ensure, that the measurement cycles described above provide the active state, several additional measurements have been made.

Therefore the cycle, originally designed to ensure an *active state* (See figure, part a-c),was extended by a second compression section, where the top horizontal wall is pushed downwards until a certain force limit is reached (Fig. part d). Then, the vertical wall is drawn

back in steps, releasing the force again and thus providing a *passive state* (Fig. part e). The final removing of all forces leads back to the initial state of the experiment (Fig. part f). This procedure allows for comparison of the border states and gives a qualitative evidence for the validity of the previously obtained results.

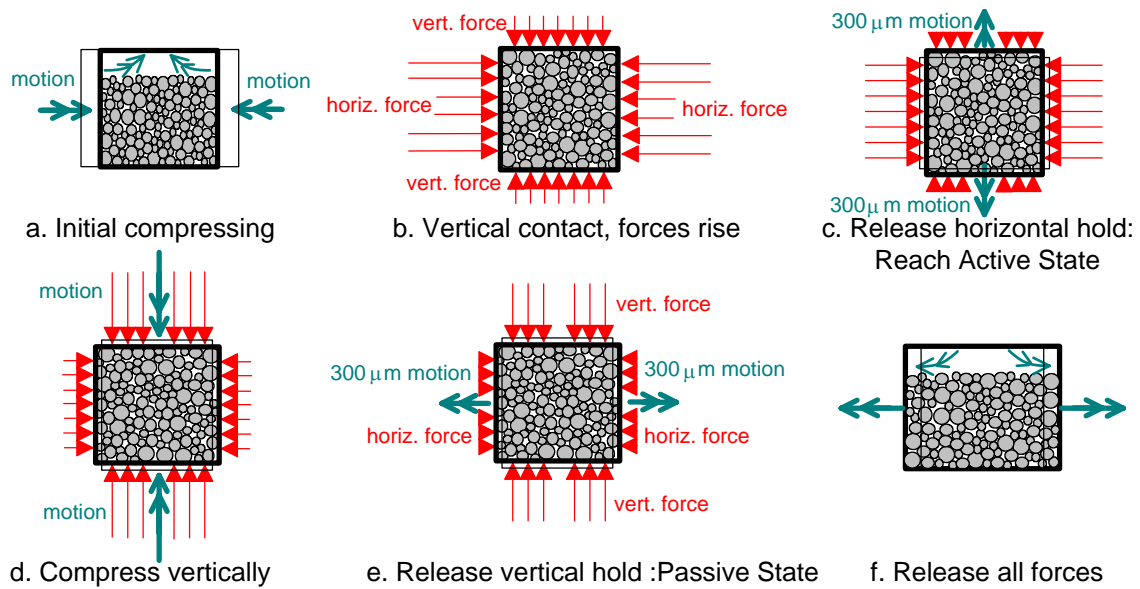The complete cycle can be described as follows:

FIG. 32. Schematic view of extended measurement cycle. Bold double arrows indicate motion while light arrows are forces

Several of these cycles have been recorded. Since this experiment is only needed as a qualitative argument, no statistical analysis over the lot of possible configurations is required. Therefore, only one surface material (PVC) was used for the tests and extra mixing procedures could be omitted.

The resulting diagrams show the variation of the vertical and the horizontal forces. The first releasing of forces provides the *active branch*, where the ratio of vertical and horizontal forces gives the lateral force factor $\overline{K_a}$ for the present configuration of contacts. It can be obtained easily as the gradient of the branch through regressional analysis of the regarded measurement points. Care must be taken, not to include some visible small horizontal steps, where single cylinders slide out of their position to make way for another contact.

The second releasing of forces constitutes the *passive state*. Thus regressional analysis of this branch yields the lateral force factor $\overline{K_p}$.

Some cycles needed to be excluded from the interpretation since a major rearrangement of the position occurred during the measurement; so active and passive branches were no more comparable.

A typical cycle hysteresis is shown in the following diagrams:
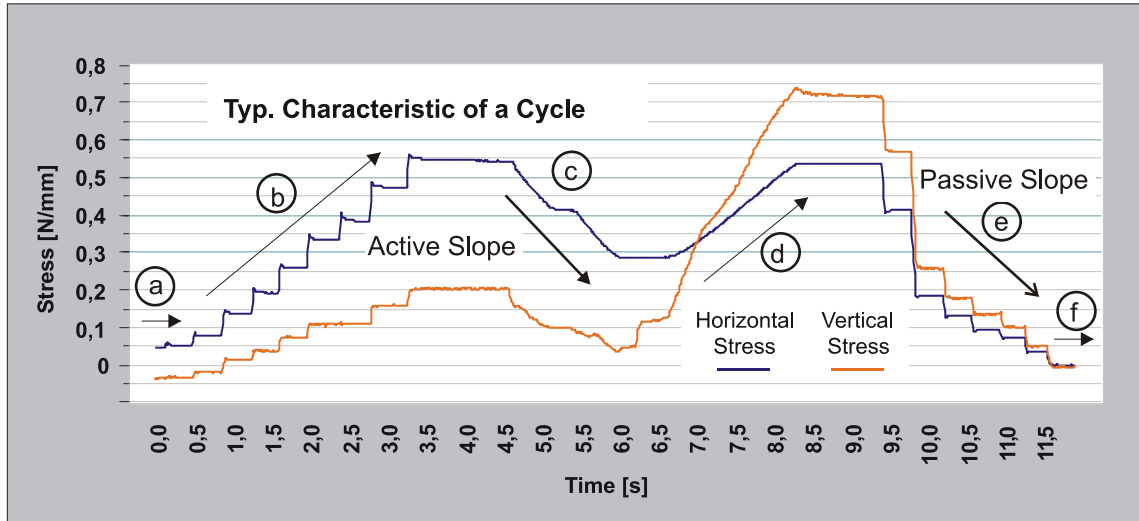

FIG. 33. Exemplary measurement I results confirming the achievement of an active state (File: PassV13 Diagram Disp.123)
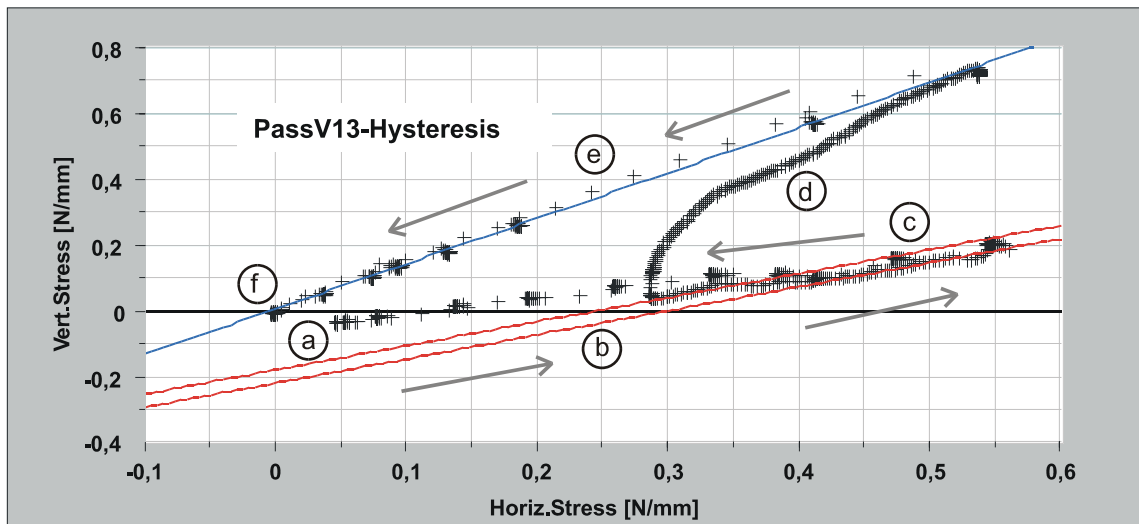

FIG. 34. Exemplary measurement II results confirming the achievement of an active state (File: PassV13 Diagram Disp.123)

Typically, the passive branch (Fig. part e) is well defined and shows no irregularities. Furthermore the changeover (part c-d) from the active to the passive state allows to observe

the reaching of the fully passive state. With this, the slope $\overline{K_p}$ can be obtained by regressional methods (line along e-f). Since it is much more difficult to extract the undisturbed slope of the active branch (c), two lines representing the theoretical active state on the basis of the inverted value $\overline{K_a} = \overline{K_p}^{-1}$ are drawn along section c. In this picture as well as in others, coincidences of the measured values descending with the theoretical lines, beyond single slipping contacts, give evidence, that the active state is reached with good reliability at this point of the cycle.

The influence of the small reconfiguration processes does not modify the slope itself, but needs to be taken into account when quantitative results are expected. Then, these are only some of the many restructuring processes, which are part of the history of the material to be considered.

In order to prove the reliability of generating active and passive states by the described deformation cycles, the correlation of the active branches to the corresponding passive branches was investigated. Since the validity of $\overline{K_a} = \dfrac{1}{\overline{K_p}}$ serves as a useful criterion both these values $\overline{K_a}$ and $\overline{K_p}$ have been read in pairs manually from the printouts of the measurements as the gradients of the corresponding branches. In this procedure all visible steps produced by restructuring processes have been eliminated. After all the values of each pair were multiplied and then plotted as a frequency distribution based on classes, each 0.1 units wide.
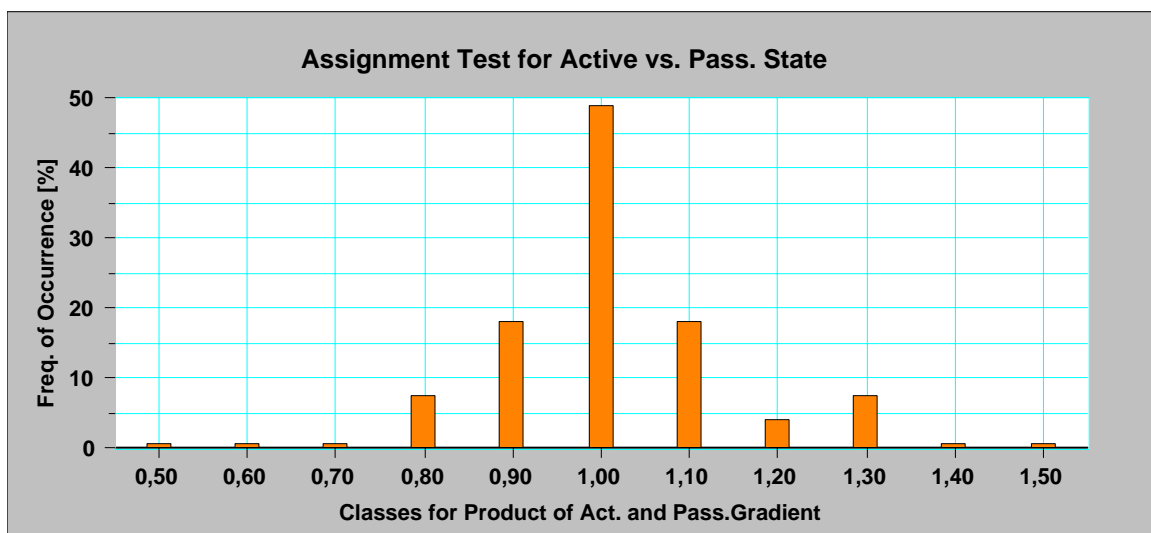

FIG. 35. Frequency distribution for $\overline{K_a}\overline{K_p}$ (File: ActPass-Analysis.123)

The clearly visible sharp maximum at $\overline{K_a}\overline{K_p} \simeq 1$ reflects satisfactory consistency of $\overline{K_a} = \overline{K_p}^{-1}$ as expected.

5 Measurement of Porosity rsp. Packing Fraction

In classic soil mechanics, the porosity $n = \dfrac{V - V_m}{V}$, i.e. the ratio of the pore volume to the total volume, plays a dominant role besides the coefficient of friction. It can be measured easily and reflects some information about the mechanical state of the granular material resulting from its deformation history. In order to gain an appropriate picture of the considered situation, we surveyed the 2D porosity of the granular model after being exposed to different displacement histories.

Remark: In many papers the packing fraction parameter κ (alternatively used symbol γ) is used instead, which is defined as the ratio of the massive volume to the total volume

$$\kappa = \frac{V_m}{V} = 1 - n$$

5. 1 Minimum Porosity/Maximum Packing Fraction

Since theoretical computations of porosity values are built on the basis of equally sized cylinders, the maximum density for the distribution of cylinder diameters used here needed to be measured directly. It was determined by experimental cyclic shearing of a defined set of cylinders; a procedure which, according to Herle [30] is likely to produce the minimum porosity.

Thus, a scaled set of cylinders on a horizontal table was manually deformed alternately in both directions until no more compacting was observed.
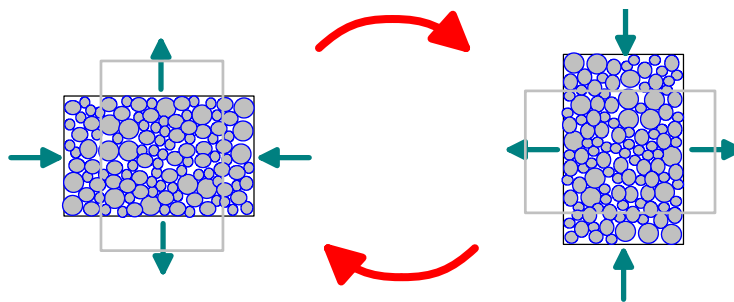

FIG. 36. Procedure to experimentally produce a minimum porosity for the granular model used here

Repeating such cycles several times a minimum porosity of

$$n_{\min}^{PTFE} \simeq 0.171 \pm 0.029 \quad n_{\min}^{PVC} \simeq 0.183 \pm 0.027 \quad n_{\min}^{POC} \simeq 0.197 \pm 0.024 \quad n_{\min}^{PE} \simeq 0.181 \pm 0.030$$

was obtained from the final extent of the bounds and the known volume of the cylinders. The repeated deformation is mainly useful to eliminate the impact of friction between the grains and finally reach a state which is only ruled by the structural properties of the granular material. Therefore a porosity value independent of the type of cylinder surface is expected which corresponds well to the obtained results.

Remark: The system resulting from this procedure can still easily be sheared and is therefore not completely compacted. Thus it corresponds best to the „critical state" rsp. transition state according to Behringer [26,27].

5. 2 Packing Fraction after Unidirectional Deformation

Since the surface friction is expected to have great influence on the development of the packing, the final porosity for the three different materials PET, POC and PTFE needed to be measured after exposing the granular system to a well defined linear unidirectional deformation.

The LLO-measurements were taken after having passed about $\varepsilon \simeq 5\ \%$ unidirectional deformation, while the HLO set-up had been exposed to about $\varepsilon \simeq 20\ \%$ unidirectional deformation as was done before in determination of the lateral stress response.

The final two dimensional volume was read from a video frame, selected at the point of maximum stress and corrected for geometrical aberrations of the image.

The volume of the sum of the cylinders was calculated from the mixture filled in and expanded by the thickness of the used coating. A minor correction was made to consider the thickness of the elastic Polyolefin coating in a compressed state.

Since a recording of the measurements concerning PVC cylinders was not available but the value was of great interest, the porosity *n* was measured manually after a very rough unidirectional deformation of about $\varepsilon \simeq 5\ \%$ and $\varepsilon \simeq 20\ \%$.

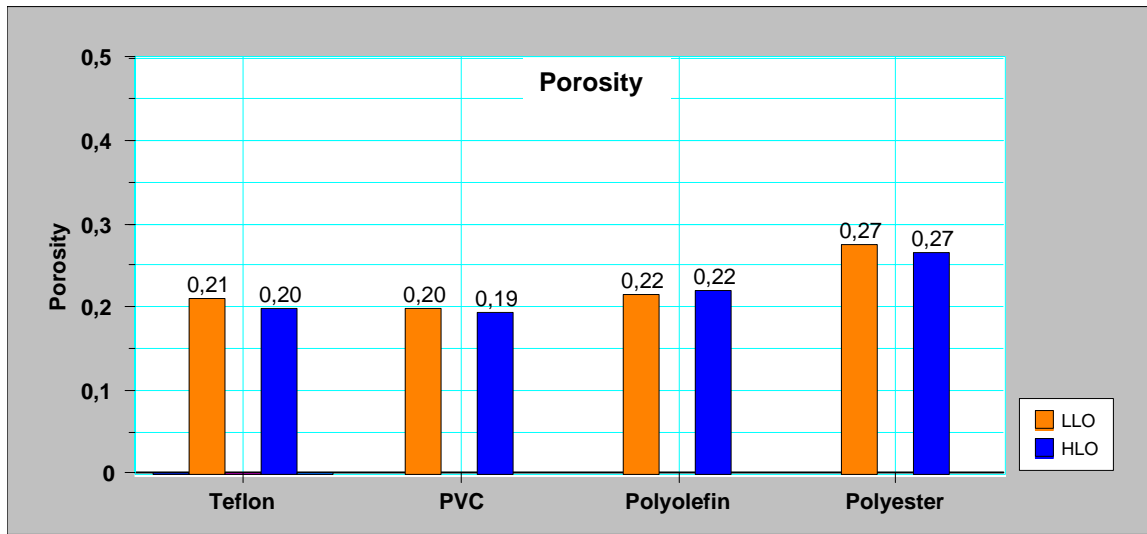The following graph shows the result:

FIG. 37. Measured porosity values (File: PackingDensity.123)

	HLO-Readings				LLO-Readings			
	Polyester	**Polyolefin**	**PVC**	**Teflon**	**Polyester**	**Polyolefin**	**PVC**	**Teflon**
Grain to grain friction ϑ_0	**36,34°**	**19,71°**	**11,33°**	**7,75°**	**36,34°**	**19,71°**	**11,33°**	**7,75°**
Av. Porosity	0,266	0,219	0,195	0,199	0,274	0,216	0,198	0,210
Error (95%Conf.Int)	0,035	0,050	0,024	0,048	0,034	0,049	0,030	0,043

Here we find some interesting characteristics:

- Obviously there is no significant difference in LLO and HLO measurements concerning the same type of cylinder surface. Further shearing only modifies positions and angles of contact to 'smoother' shearing joints but does not increase the porosity. This result strongly leads to assume that compressing in one direction under the influence of constant stress leads to a constant porosity. This again confirms that the higher level of organisation concentrates movements on some small shearing bands, which do not influence the average porosity.

- The absolute values do not vary much. Due to the fairly high error margins the gradient is only qualitatively significant. Yet we can assume that the less friction is involved the closer the final porosity approaches a final minimum with an exception of the PVC values. The measured value for PVC cylinders does not fit the series. Similar to the measurement results concerning the lateral force factor in LLO-systems, the behaviour of

PVC coated material seems to be governed by even less friction than PTFE cylinders in contrast to the measured microscopic frictional parameters.

- Referring to natural rounded gravel according to chapter *Granular Parameters in Soil Mechanics,* the completely compacted porosity readings $n_{min} \simeq 0.18$ match very well to the void ratios after being recomputed as porosity for two dimensions in the range between $n = 0.14$ and $n = 0.22$. A slightly higher porosity is obtained from the measurements based on the not completely compacting deformation history.

Hence, the model used here turns out to correspond fairly well to this type of granular soil.

6 Survey of the Macroscopic Structure

As the macroscopic structure formed by a force chain network is expected to have significant impact on the behaviour of granular material, the average meshsize and the distribution of the meshsizes as dominant parameters needed to be surveyed. Therefore, some polariscope images of different configurations have been recorded and analysed.
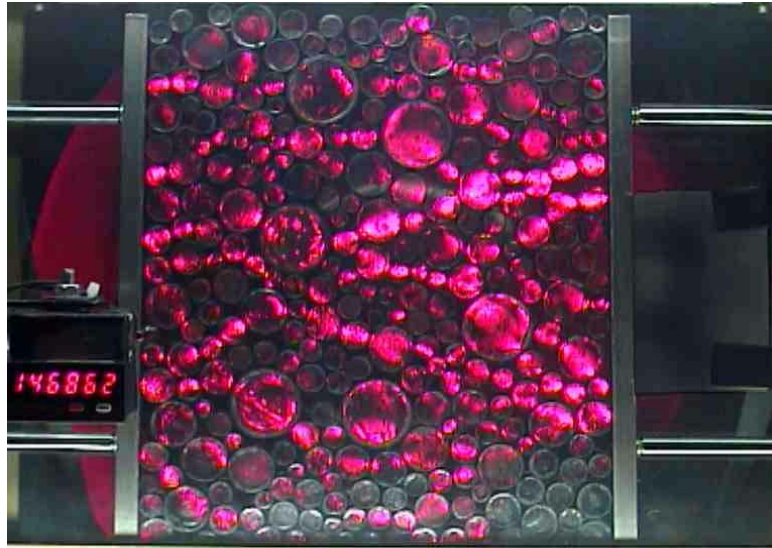

FIG. 38.   Unprocessed polariscope image, fairly overloaded to improve clearness

It can clearly be seen, that meshes do occur, but not in such regular patterns that their size could be measured. It turns out, that the average mesh size cannot be determined easily. Yet more sophisticated analysis tools reveal at least the character of the meshsize distribution and some numerical values, which are to be evaluated in plausibility considerations.

6. 1 Image Processing

Trying to obtain the distribution of forces using the stress induced illumination of photoelastic cylinders in a polariscope, requires to investigate the inhomogeneity of the resin displaying spots, the showing up of higher orders and last but not least the influence of forces fed into very small points, exposing a complete cylinder to stress, and finally the impact of the non-linear CCD-Camera recording the image.

In order to eliminate influences from the recording and data acquisition system, all the image processing was accomplished on both reference readings as well as final readings.

The polarisation apparatus was first adjusted optically to be certain of the mechanical alignment of the LED source of light, the condenser lens and camera system by focusing a small spot on the aperture of the camera.

Subsequently the camera was positioned to achieve an evenly illuminated image area on the directly attached 20" colour monitor. All automatic settings of the camera were switched off, Gamma was set to unity and the aperture was manually set to a value, where no image clipping occurred at the brightest spots.

Finally the polarizer foils were turned until least illuminance indicated orthogonal alignment of the analyser with respect to the polarisation filter. As a final check, manual compression of a reference resin cylinder guaranteed the working condition of the set-up.

Weak diffusive environment illumination was applied additionally in order to make mechanical rearrangements, deformation and sliding visible. The LED source for the polarizer was chosen as monochrome red, since it supplies high intensity at small extent of monochromatic light able to produce a well focusable reproduction of the stress distribution.

Recording the results in the process of applying variable forces to a set of cylinders was achieved by conventional video technique using separated Y/C cabling and a digital video recorder (Compression 1:5). From this digital source, bitmaps of the required sector, size and time slot were extracted and processed further.

It turned out, that the most instructive visual representation was obtained by shifting colours by -139° on the standard colour circle, then squaring the intensities of all colours separately and finally inverting the picture. After normalising the result to conventional RGB signals, it can by viewed on any screen.

Shifting the colours effects in particular the transformation of the red colour to the blue component adding a little bit of cyan to the image, where due to the different weighting of colours the bright spots indicating force concentrations show up more intensely, while the diffusive background is suppressed. This step of the process is used for measurements too, carefully handled equally for references as well as for the acquisition of data. Here we make use of the unknown weighting of colours, but eliminate the missing link by taking it in to the references. Since the source colour is sited well inside the red range, where no variation of the red component occurs and the shifted value still remains in the blue range, where also no modification to the blue component is made, the final intensity of the evaluated component underlies no falsification either.
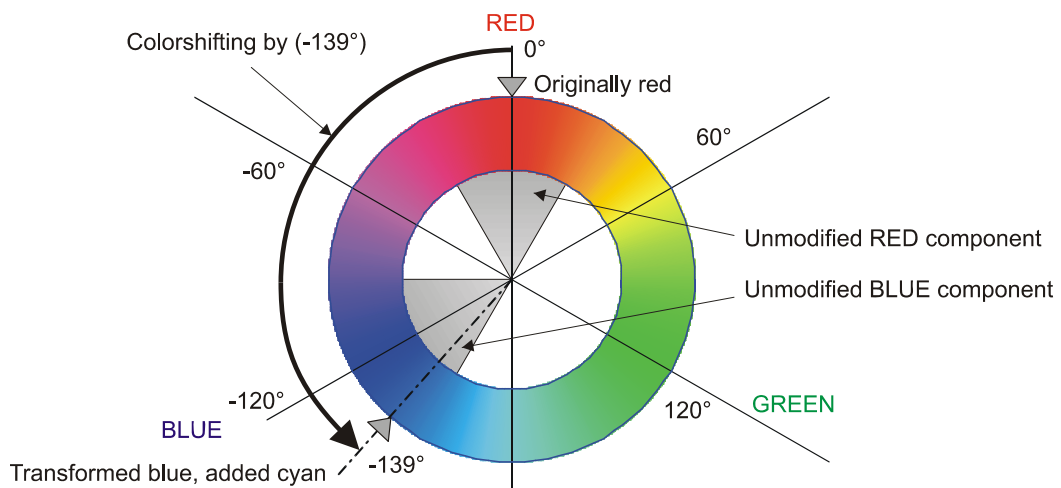
FIG. 39. Consequences of the colorshifting process applied to polariscope images (File: ColorcircleFinal.cdr)
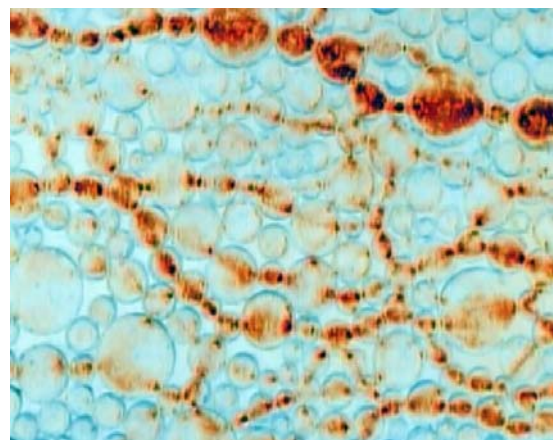
The inversion procedure and the squaring of intensities serves only for enhancement of the visual contrast and is not applicable for the acquisition of data since it brings in further nonlinearities.
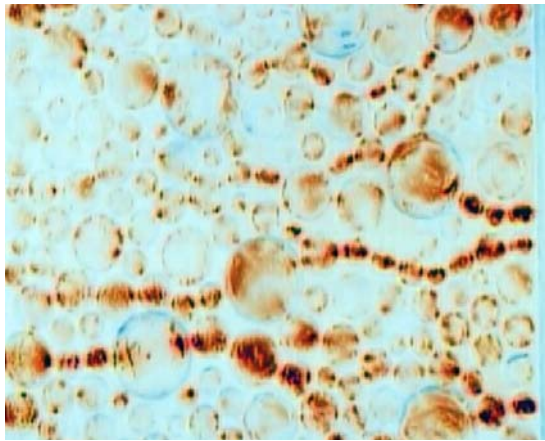

6. 2 Visualisation Results

Typical results prepared as described above are presented in the following pictures, one for every type of surface coating. Additionally investigating the influence of the Level of Order we surveyed HLO states ($\varepsilon \simeq 20$ %) as well as LLO states ($\varepsilon \simeq 5$ %) separately:
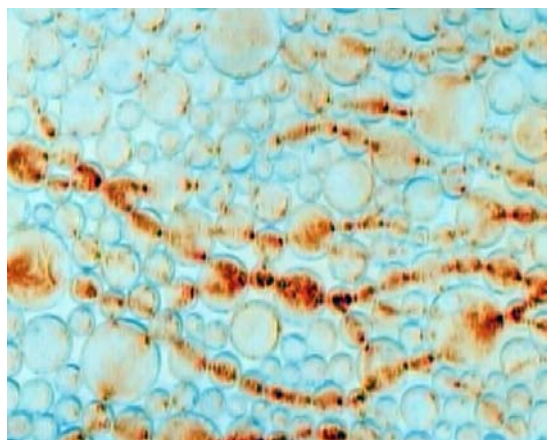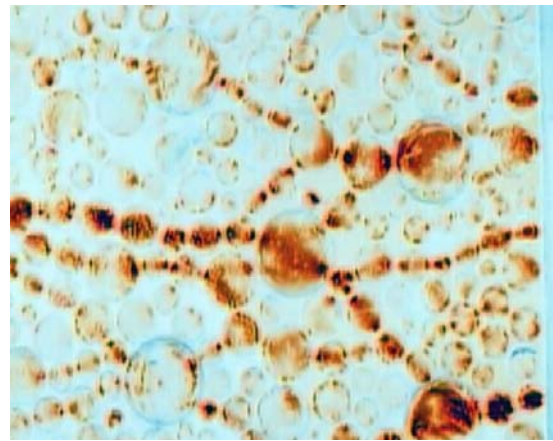

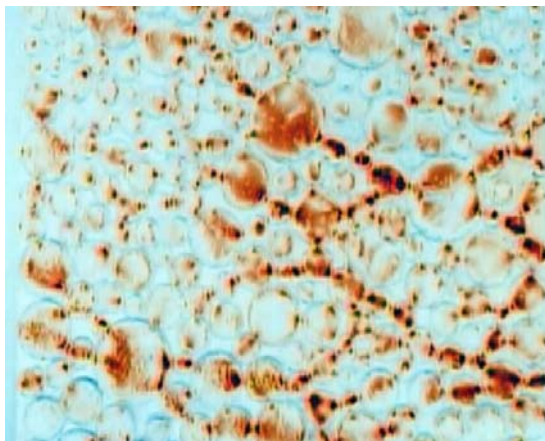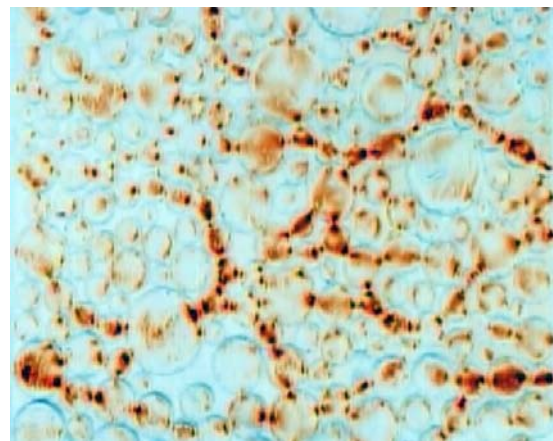Polyestercoating LLO (UCN01.jpg)　　　　Polyestercoating HLO (TCN01.jpg)

Polyolefincoating LLO (UCP01.jpg)　　　Polyolefincoating HLO (TCP01.jpg)

Tefloncoating LLO (UCT01.jpg)　　　Tefloncoating HLO (TCT02.jpg)

FIG. 40. Processed images from the polariscope

6. 3 Approval of Linearity

The assignment of forces to the illumination of a certain colour needs to be verified prior to any serious - even qualitative - statement. It is described in more detail e.g. in Ref [64] Chapter 5, or by [47].

In fact, this dependency is very complex since contact forces are concentrated on the infinitesimal small points of contact, where they produce planar distributions of stress. The illumination of a pixel observed through a polarizer apparatus is then: $I \sim \sin^2(\alpha)$, where $\alpha \sim \sigma_2 - \sigma_1$. Due to the varying size of both the grains and the area of contact, the pattern

cannot be generally evaluated. Some attempts have been made with good results by reading out the average gradient of the light intensity in order to exploit the number of orders shown in the image [26]. In our context, we are only interested in a very small range of forces, where we can approximate the overall dependency of the resulting light intensity vs. the applied forces as linear.

Confirming this approach, a sequence of very simple measurements yielded a good linear dependency as long as the stress is kept low enough not to produce higher order images and well below the rise of nonlinearities of the recording system:

Such a measurement could easily be achieved by compressing the standard volume horizontally in steps up to the limit of 160N, where the data acquisition system is still in good working condition and no visible clipping occurs. The responding image of the polariscope was simultaneously recorded on videotape, synchronised with the data recording by acoustic marks. After applying the image processing operations described above, the overall illumination of the blue component, averaged over all the picture was extracted and plotted on graphs vs. the applied force. The influence of the developing macroscopic structures can be neglected since, once they are set up, they remain stable with the increasing forces (due to the only very small variation of the volume extent) and hence keep the distribution of forces unaltered. Furthermore, some additional tests confirmed the ample linearity of the illumination of single cylinders with rising forces which prevents hidden nonlinearities to be covered by the averaging procedure.

In building the mean value, the influence of macroscopic structures is completely eliminated, yet different structures on each compression cycle make them not directly comparable. Nevertheless the degree of linearity can be derived easily as the coefficient of regression.

Thus we obtain exemplary for a series of six measurements, where the linearity of the relation of the applied forces to the resulting light intensity is evaluated as the coefficient of regression:

Check for Linearity: Intensity of light vs. Applied forces						
Measurement ID	M1a	M1b	M2a	M2b	M3a	M3b
Coeff. of Regression	0,96	0,93	0,97	0,92	0,91	0,92

Since the surface parameters were of no importance in this investigation, the measurement was made with only one type of resin cylinder, coated with Teflon. Finally, all measurements were individually corrected in gradient and offset for matching structures and combined in

the following plot. Thus only the deviation from linearity i.e. the coefficient of regression is of importance yielding a fairly good substantiation.
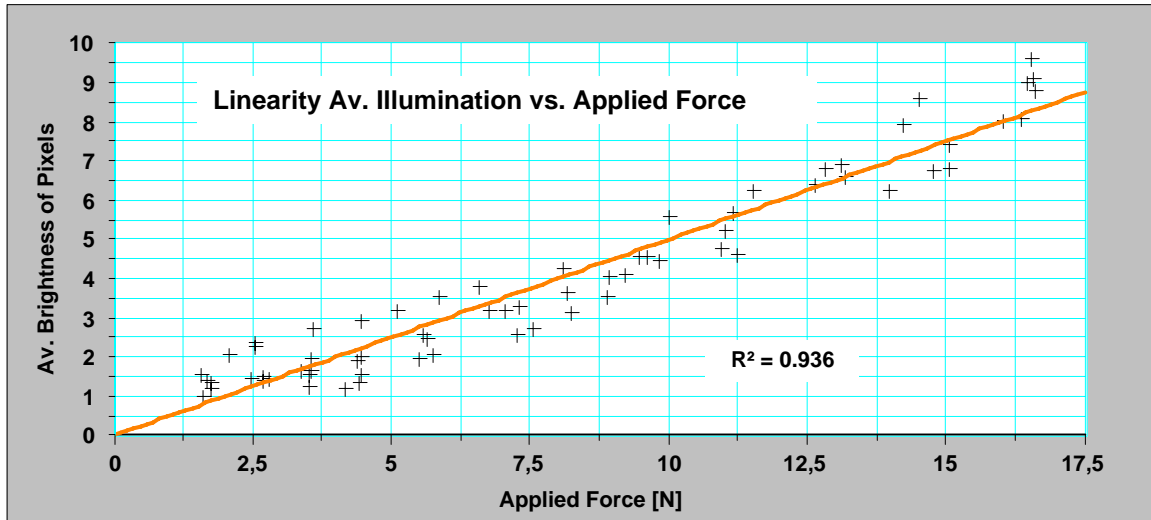

FIG. 41. Confirmation of a linear dependency of illumination values vs. the applied forces (File: Force-Illum-Dep.123*)*

6. 4 Distribution of Intensities and Forces

In order to obtain the characteristics of the force distribution and from this an estimation for average mesh sizes in the pictures shown above, we first extracted the distribution of illumination $W_{Load}(\omega)$, where ω is the light intensity of a certain class. Since we were interested in the modification brought in by applied forces, we also recorded the illumination distribution $W_0(\omega)$ of the unloaded system as a reference.

Remark: The pictures shown were made during the rise of applied forces well before the maximum had been reached to ensure the measurement remaining within the linear range. The maximum intensity was only useful for intuitive exploiting of the images, but far away from the evaluable range. The reaching of this limit was determined by the occurrence of a peak at the high illumination end of the spectrum.
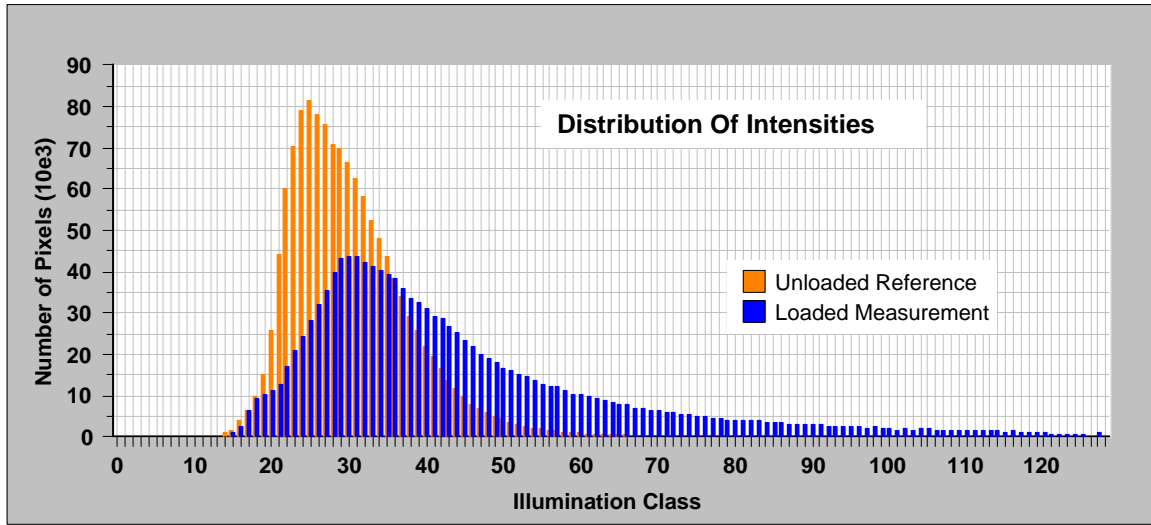
FIG. 42. Exemplarily shown distribution of light intensities $W_{Load}(\omega)$ and $W_o(\omega)$ (File: Demo-TCN-Distrib.123)

The background illumination can be clearly seen as the large peak on the left side in both diagrams. The right end of the loaded diagram $W_{Load}(\omega)$ uncovers the limited illumination range of the camera as we would expect no definitive end but an asymptotic behaviour of the distribution. The small peak at the end contains the pixels with too high illumination to be displayed, which are collected at the upper end of the available range.

The distribution effectuated by the load can easily be derived from this by calculating

$$W(\omega) = W_{Load}\left(\int_{0}^{\omega\,max} W_0(\omega')(\omega - \omega')d\omega' \right)$$

This process is based on the assumption, that a frequency of occurrence W_{Load}, measured at the intensity ω had been shifted by the applied stress from an intensity ω' weighted by the probability of the stressless occurrence of this intensity, which is given by $W_0(\omega')$. Thus the integral over all available source intensities determines the average intensity from which the measured value is derived.

This operation modifies the distribution and finally reveals its significant shape. The resulting distribution is valid for the measured intensities and therefore equally valid for the contact forces within the granular media. An example of an individual image is shown in the next figure.
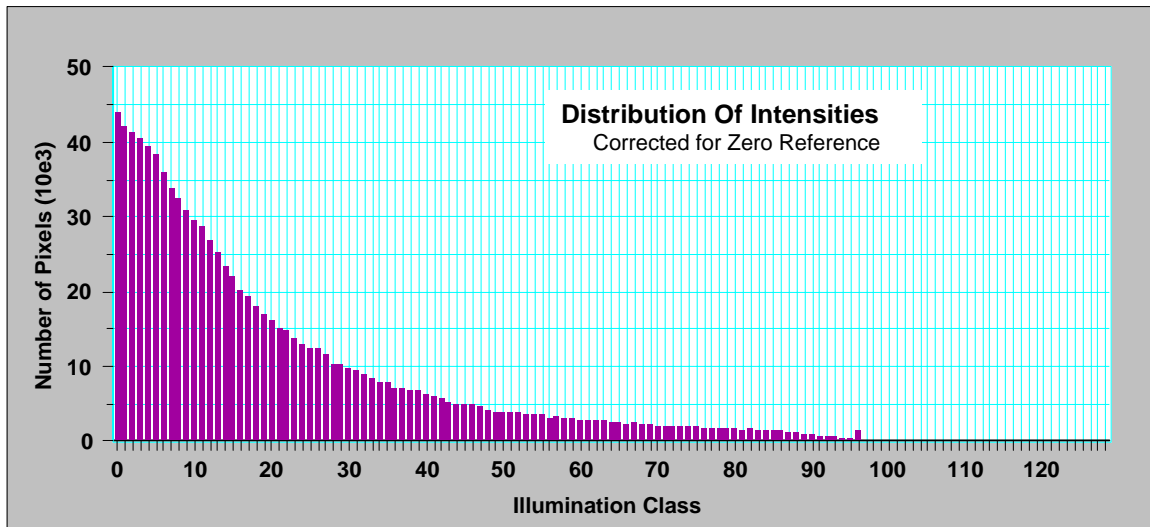
FIG. 43. Exemplary distribution of light intensities, corrected for the zero load reference (File: Demo-TCN-Distrib.123)

Surveying several images of the same configuration in this manner, in fact reproduces the picture above with not much difference, but determines the error obtained. For example all the HLO-readings using cylinders with Polyester coating (TCN) lead to the following graph, displaying the average distribution together with its error margins (assuming a confidence interval of 95%). Errors are apparently concentrated at low intensity values as they are not easy to separate from the background.
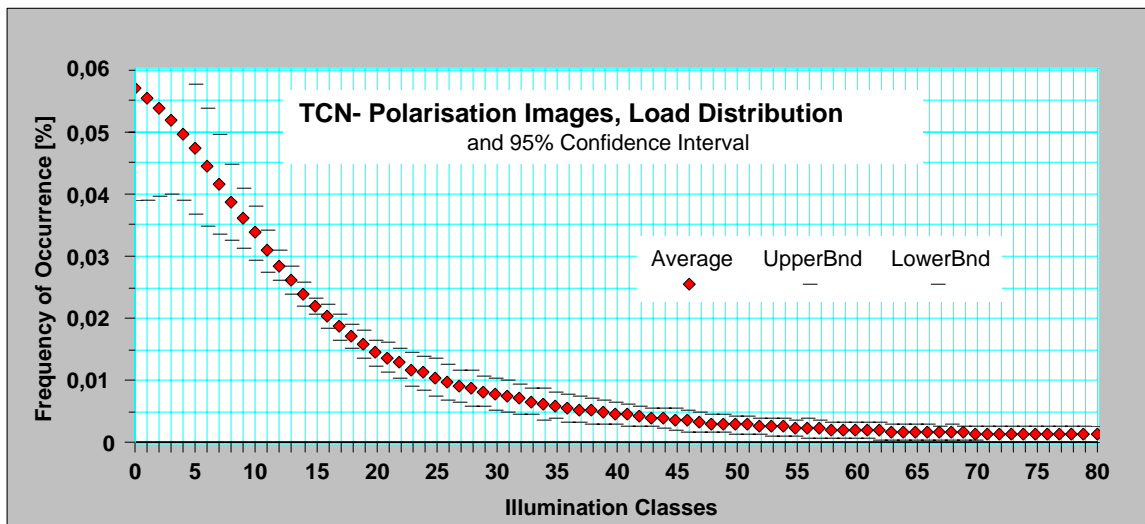

FIG. 44. Typical analysis of light intensities of several images, obtained from Polyester cylinders (File: TCN-Distrib.123)

6. 5 Mesh Size Acquisition

Since average mesh sizes cannot be taken from the pictures directly, an indirect way was chosen: First the mean intensity $\overline{\omega}$ of the each distribution was calculated, i.e. the centre of gravity. This value compared to the maximum intensity supplies the ratio $\lambda = \overline{\omega}/\omega_{\max}$ of fully illuminated pixels with respect to all pixels within the image. This allows to derive an estimation for an average mesh size under assumption of a regular isotropic mesh all over the granular system by dividing the plane in units, which are either fully illuminated or not at all. Since the scale does not play a role, this works for pixels as well as for bigger units; the resulting mesh size is always determined in units of the width of a visible force chain.

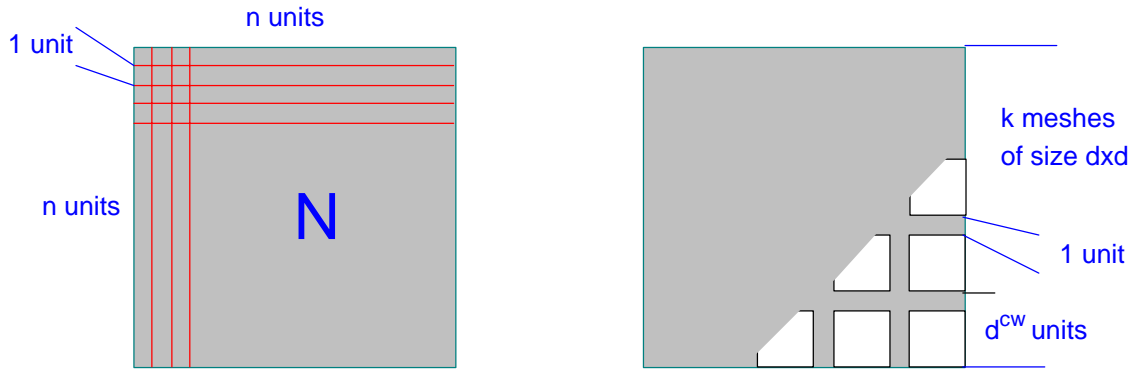Exercising this for a two dimensional plane of size $N = n \times n$ units, we derive:

FIG. 45. Geometrical aspects of a network with meshlines of finite width

With a meshsize d^{cw} in units of an average chain width we obtain $k = \dfrac{n}{d^{cw}}$ regular meshes at one border. Thus the fraction of highly illuminated units along one dimension is $\dfrac{k}{n}$ since each mesh contributes one chain width to the lot.

In two dimensions the unilluminated fraction is determined as $\dfrac{(n-k)^2}{n^2} = 1 - \lambda$, where λ is the known two dimensional fraction of illuminated pixels.

$$1 - \lambda = \frac{(n-k)^2}{n^2} = \frac{\left(n - \dfrac{n}{d}\right)^2}{n^2} = \left(1 - \frac{1}{d}\right)^2.$$

Resolved to derive the mesh size in units of chain widths, we obtain:

$$d^{cw} = \frac{1}{1 - \sqrt{1 - \lambda}} \; .$$

Since we aim at a mesh size estimation in units of the average grain size and because the chain widths are not identical to the diameter of the granules, a further correction is required:

We measured the diameter of illuminated spots, which made up the visible force chains, scaled them to the average size of the granules and thus calculated a geometrical factor f^{geom} to convert illumination width to the granule diameter.

Furthermore we introduced a factor $f^{spots} = \dfrac{r^2\pi}{2r \cdot 2r} = \dfrac{\pi}{4}$, taking into account that force chains consist of a sequence of circular spots and therefore the mean visible width of a chain is a bit less than the spots diameter.
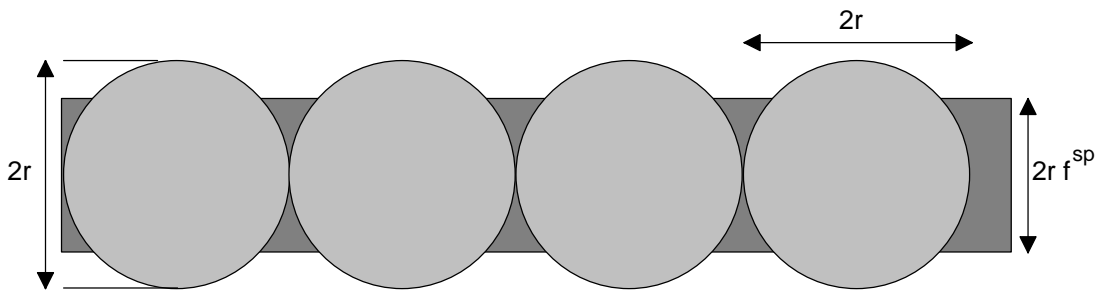

FIG. 46. Correction due to the circular shape of the grains

Finally we obtained measured mesh size values and their error margins from several acquisition cycles as follows:

	High Level of Organisation			Low Level of Organisation		
	Polyester	Polyolefin	Teflon	Polyester	Polyolefin	Teflon
Angle Of Friction ϑ_0 [°]	**36,34°**	**19,71°**	**7,75°**	**36,34°**	**19,71°**	**7,75°**
Diam. 30mm Gran.[mm]	30,8	30,8	30,8	30,8	30,8	30,8
Av. Diam. All Gran. [mm]	12,56	12,56	12,56	12,56	12,56	12,56
Av. Meas. Diam30Gran [px]	193,6	193,7	195,9	187,8	193,2	193,8
Std. Deviation [px]	7,7	6,12	5,84	6,68	9,13	6,48
Rel. Error	4,0%	3,2%	3,0%	3,6%	4,7%	3,3%
Av. Meas. Spotwidth [px]	24,86	25,18	23	20,94	23,08	20,64
Std. Deviation [px]	6,87	6,82	6,74	6,51	5,55	4,78
Rel. Error	27,6%	27,1%	29,3%	31,1%	24,0%	23,2%

Av. Meas. Linewidth [px]	19,52	19,78	18,06	16,44	18,13	16,21
Std. Deviation [px]	5,4	5,36	5,29	5,11	4,36	3,76
Rel. Error	27,6%	27,1%	29,3%	31,1%	24,0%	23,2%
Av. Grain.Diameter [px]	78,95	78,99	79,89	76,58	78,79	79,03
Factor Graindiam./Linewidth	4,04	3,99	4,42	4,66	4,35	4,87
Std. Deviation	1,12	0,85	1,02	1,14	0,82	0,89
Meas.Center of Gravity λ	16,30%	20,05%	20,26%	14,11%	19,20%	20,42%
Av. Meshsize /Av. Linewidth	11,75	9,45	9,34	13,66	9,89	9,27

This leads to averaged meshsizes, summarized in the following table:

	High Level of Organisation			Low Level of Organisation		
	Polyester	Polyolefin	Teflon	Polyester	Polyolefin	Teflon
Angle Of Friction ϑ_0 [°]	**36,34°**	**19,71°**	**7,75°**	**36,34°**	**19,71°**	**7,75°**
Av. Meshsize /Av. Diam.	**2,91**	**2,37**	**2,11**	**2,93**	**2,28**	**1,9**
Std. Deviation	**0,8**	**0,5**	**0,49**	**0,72**	**0,43**	**0,35**

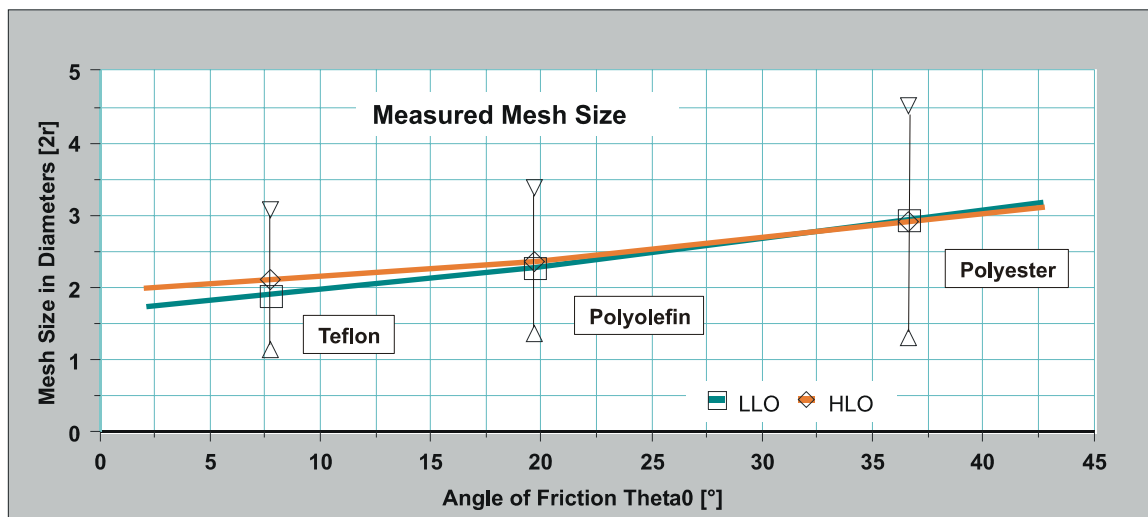The relevant excerpt of data from the table is plotted to the graph.

FIG. 47. Experimentally obtained av. meshsize (File: MeshSizeInterpr.123)

Obviously, this experiment yields, despite the large error bars, a well defined magnitude of averaged meshsizes: Any stress applied to a granular system which is comparable to our model is transferred by every second to every third granule.

The measurement indicates slightly increasing mesh size with rising angle of friction, which corresponds to our intuition, but can not be confirmed by the experiment due to the large error bars.

Apparently there is no significant difference between HLO- and LLO-readings, where one would expect self organising mechanisms to have greater impact.

7 Discussion of Results: Overview

In general the obtained results qualitatively meet the expected dependencies. For all surveyed types of cylinders, the measured ratio σ_1/σ_3 is plotted to the qualitative development. The dotted development of the ratio against the increasing shearing parameter is only intended to illustrate the expected characteristic. At this stage of the investigation the values are only assigned to the used surface material i.e. the grain to grain friction, and not to the angle of friction, since this will possibly be subject to some modification by structural impact.
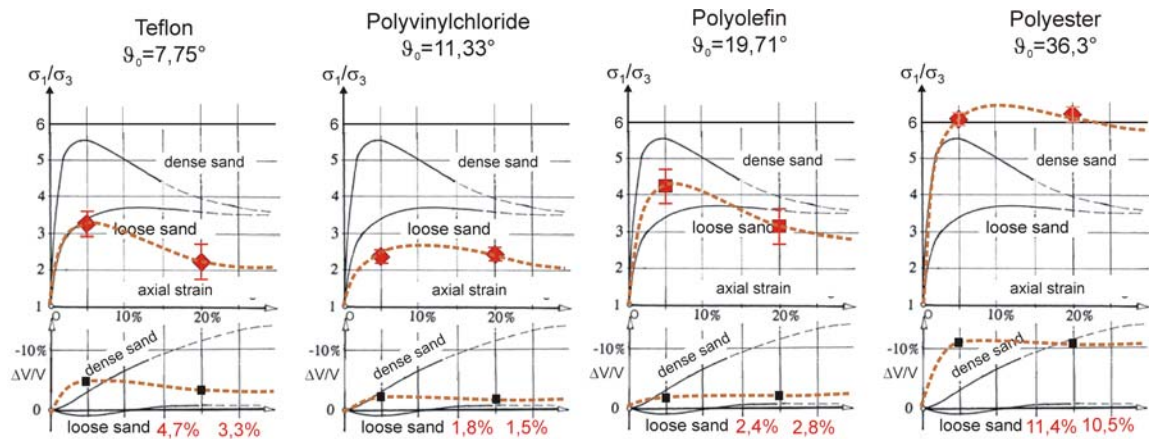

FIG. 48. Measured values entered in qualitative drawing(File: AxStrainQualitativ.cdr)

In the lower diagram the range of the measured density variation with respect to the state of maximum density is plotted. It can be clearly seen, that no significant dilatancy occurs during the shear process between 5 % and 20 %, in contrast to the very beginning of the shearing process depending on the material used. This behaviour is interpreted to indicate the fairly well ordered most dense state, which is not typical for a stochastic set but for an artificial 'block-system'. After some shearing deformation of about 5 %, the density has reached a mainly constant value where the positioning of the single cylinders is expected to still be ordered stochastically, but no more as part of a compacted system but as the positioning of independently moving particles. While shearing further up to a value of 20 %, the density varies no more, but a new order may have been established by self organising mechanisms, governed by shearing joints. This behaviour is expected for uniformly graded round granular material in accordance to round gravel which is known to be more or less incompactible.

The most compacted state can not be surveyed easily and is however of no further interest in this context, since it represents a well ordered state. The following investigation concentrates

on the two states $\varepsilon \simeq 5$ % (LLO-regime) and $\varepsilon \simeq 20$ % (HLO-regime) as assumed models for a stochastic situation and in contrast to this as a situation, where the building of shear joints is expected to be the dominant mechanism. Undoubtedly there is no hard transition from one regime to the other. Increasing shear deformation is expected to produce more and more local shear zones which join until the HLO regime governs the total volume. Yet the lateral stress σ_3 varies significantly during the shearing process in this total range and additionally is different for every type of surveyed cylinders which leads to investigate the mechanisms of the shearing process.

However the detailed development of the ratio σ_1/σ_3 and the density in dependence of the shearing procedure is not the subject of this paper. It can be clearly seen, that the measured values are in accordance with the expected behaviour, but vary strongly with the surface properties of the used cylinders. The investigation described in this paper is focussed on the influence of the grain to grain friction separated from the structural impact of the circular grains to the absolute ratio σ_3/σ_1.

Based on this overview it is assumed, that in some way different mechanisms are dominantly active in the LLO and the HLO regime.

Obviously the LLO sets are close enough to the completely unorganised state. Therefore a set of cylinders at statistically independent angles and positions is investigated in order to explain the different contributions of structure and grain to grain friction to the ratio σ_3/σ_1.

In contrast to this the higher ordered state of systems in the HLO regime seems to have developed shear joints, where all deformation is localised. Thus, for the HLO systems, a model using shear joints generated by self organising processes in accordance to the Rankine conception is evaluated.

8 Discussion of Porosity Measurements

In soil mechanics the porosity resp. the void ratio of a sample of natural soil reflects the history of compaction and shearing as well as the ability of the single grains to yield or deform. Thus, this value represents the actual state of a granular medium including the deformation path it was exposed to.

In the presently used model consisting of hard circular shaped cylinders the elastic and plastic properties of single grains are obviously of less importance. An elastic correction has been applied to the measurement values, while yielding of the cylinders turns out to be far out of the observed range. However, the behaviour of granular material is nevertheless largely assumed dependent of the packing fraction, respectively the distance of the actual porosity rsp. packing fraction to a transition value [26-30, 32, 50]. In order to consider this criterion, the porosity values observed for several states of the granular system, which are achieved through a different history of deformation and on varying surface materials need to be analysed at least qualitatively.

8. 1 Theoretical Limiting Densities

As can easily be accomplished, the theoretical density of a two dimensional granular system, consisting of equally sized cylinder grains in different border states is determined as

- $\kappa_{hc} = \dfrac{\dfrac{r^2\pi}{2}}{r \cdot 2r\cos\dfrac{\pi}{6} + \frac{1}{2}\left(r \cdot 2r\cos\dfrac{\pi}{6}\right)} = \dfrac{\pi}{6\cos\dfrac{\pi}{6}} = \dfrac{\pi}{3\sqrt{3}} = 0.605$, corresponding to a porosity value of $n = 0.395$ for honeycomb lattice,

- $\kappa_{sqr} = \dfrac{r^2\pi}{(2r)^2} = \dfrac{\pi}{4} \simeq 0.785$, corresponding to a porosity value of $n = 0.215$ for a square lattice and

- $\kappa_{opt} = \dfrac{r^2\pi}{(2r)^2\cos\dfrac{\pi}{6}} = \dfrac{\pi}{4}\cos^{-1}\dfrac{\pi}{6} \simeq 0.907$ corresponding to a porosity value of $n = 0.093$ for the optimal packing (triangular lattice).

The coordination numbers z are given as the number of contacts for a single grain.
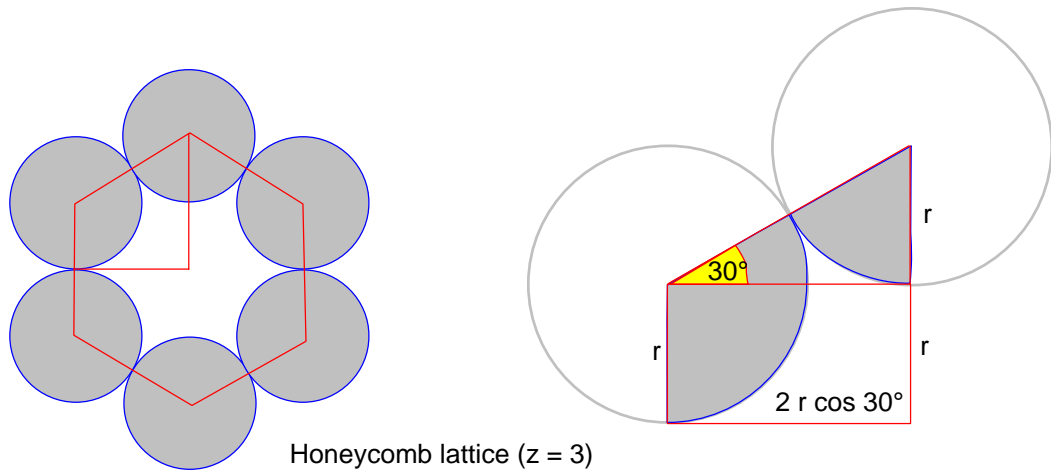
FIG. 49.　Theoretical porosity of a honey comb lattice
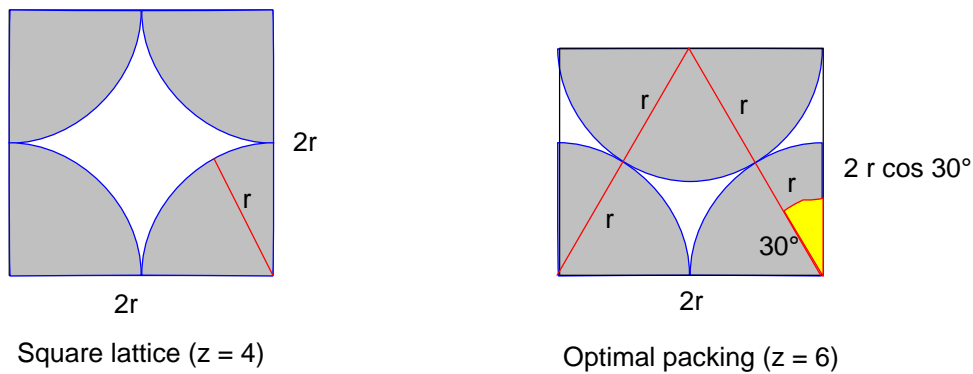
FIG. 50.　Theoretical porosity values of square and optimal lattices

The random close packing provides a maximum density of $\kappa_{rnd} \simeq 0.82$ [see 26], confirmed by a very basic estimation:

Considering a cell as shown below, but let the top cylinder be positioned randomly at every angle a. Then, the size of the cell containing four fourths of a cylinder is:

$$A = 2r \cdot 2r\frac{6}{\pi} \int_0^{\frac{\pi}{6}} \cos a \; da = 4r^2 \cdot \frac{6}{\pi} \sin \frac{\pi}{6} = 4r^2 \cdot \frac{3}{\pi}$$

Thus the random density is determined: $\kappa_{rnd} = \dfrac{r^2\pi}{A} = \dfrac{r^2\pi^2}{4r^2 3} = \dfrac{\pi^2}{12} = 0.822$, corresponding to a porosity value $n = 0.178$, while the coordination number is close to $z \simeq 4$.
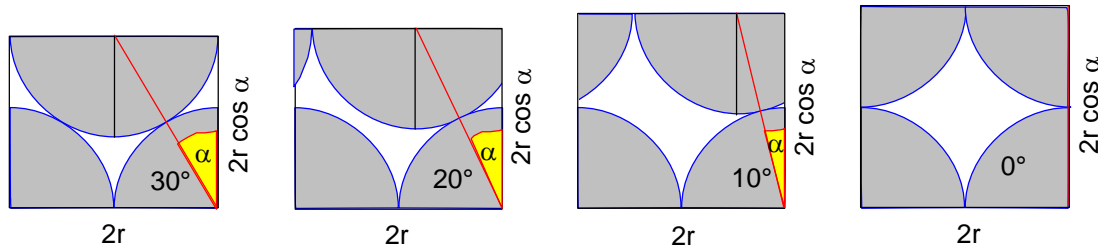

FIG. 51. Estimation of packing fraction of a random close packing

8. 2 Referring to Measurements

As described in the measurement section of this paper, we obtained a maximum density value of $\kappa_{\max} \simeq 0.817 \pm 0.009$ for the granular model used in our experiments. Furthermore, surveying protocol images of the compression experiments yielded some porosity values after exposing the granular material to unidirectional compression of $\varepsilon \simeq 5\,\%$ (LLO-measurements) and $\varepsilon \simeq 20\,\%$ (HLO-measurements), which are repeated here for convenience:
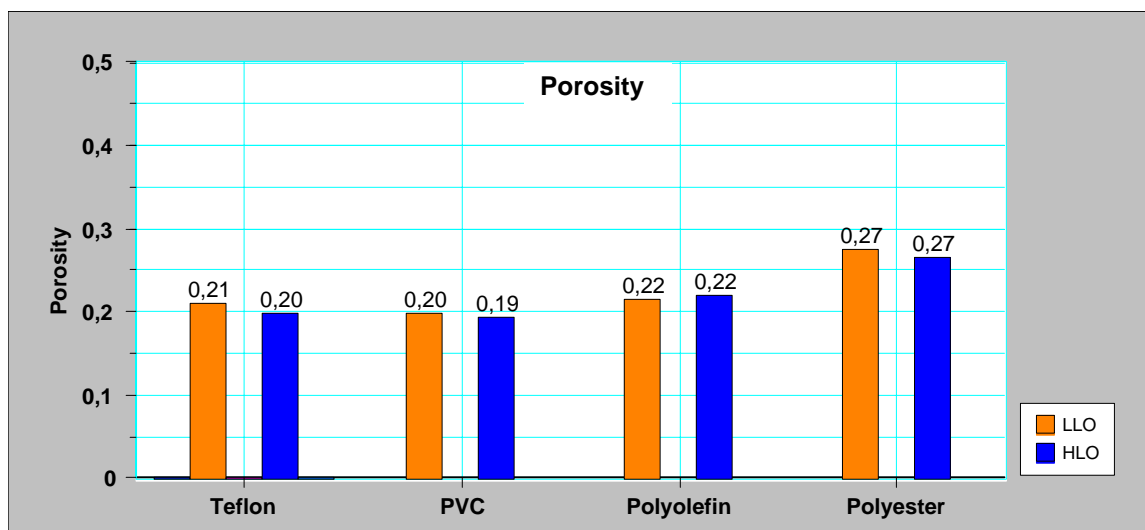

FIG. 52. Measured porosity values (File: PackingDensity.123)

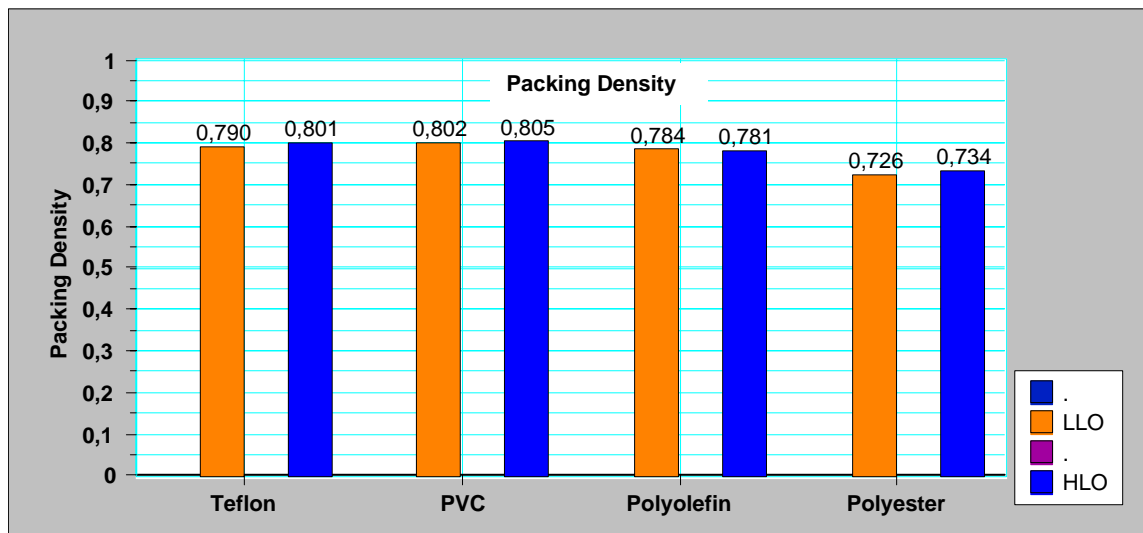|	HLO-Readings				LLO-Readings			
	Polyester	**Polyolefin**	**PVC**	**Teflon**	**Polyester**	**Polyolefin**	**PVC**	**Teflon**
Grain to grain friction ϑ_0	**36,34°**	**19,71°**	**11,33°**	**7,75°**	**36,34°**	**19,71°**	**11,33°**	**7,75°**
Av. Porosity	0,266	0,219	0,195	0,199	0,274	0,216	0,198	0,210
Error (95%Conf.Int)	0,035	0,050	0,024	0,048	0,034	0,049	0,030	0,043

FIG. 53. Measured packing fraction values (File: PackingDensity.123)

As already mentioned, the difference between HLO-readings and LLO-readings is not significant. From this we conclude confirmation that shearing in this range takes place in shear bands of very small width, so that the deformation process ordering and organising the grains has no large influence on the porosity value. Furthermore, regarding soil mechanics, this result matches the well known incompactibility of uniform gravel which is best represented by the model used here. This leaves the results to be interpreted on the basis of friction and structure.

Intuitively, we accept that friction and surface irregularities have a lot of influence on the packing process of unidirectional deformation, while their impact is mainly eliminated on repeated bi-directional deformation. Thus we expect friction and surface irregularities to prevent singular locations from further compaction, the earlier the higher the frictional parameters are. This motivated us to extrapolate the measured values to a packing fraction value, where granular material with no friction is expected to end up. It can be regarded as the state of the system, defined only by the structural impact: Considering the coefficient of friction μ_0 between the single grains leads to a decreasing dependency, obviously ending up at a definite point. $n^{\mu_0=0} \approx 0.180$ rsp. $\kappa^{\mu_0=0} \approx 0.820$ (coefficient of regression: $R^2 = 0.956$):
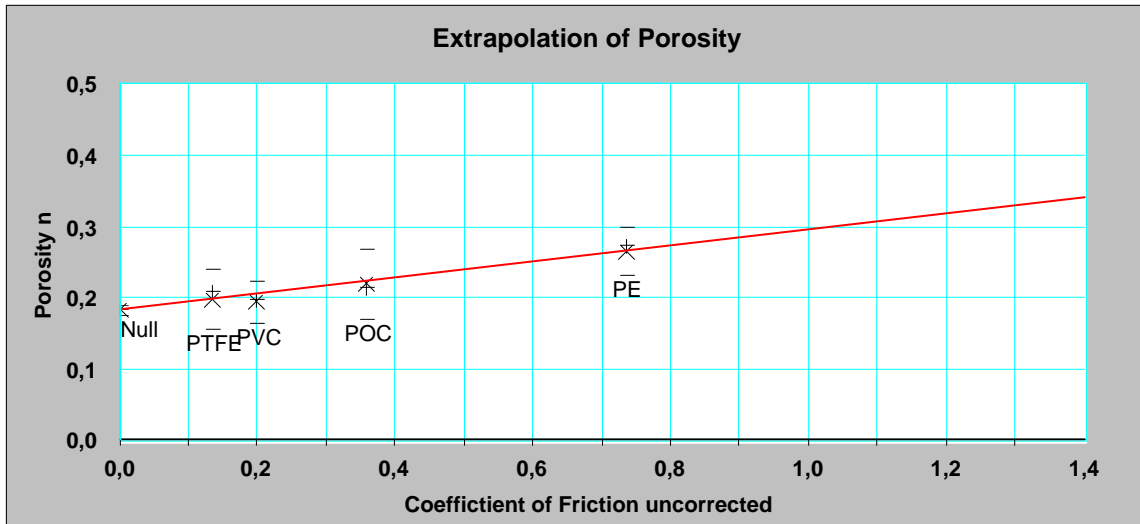
FIG. 54. Linear interpolation for measured porosity values (File: InterpolationOfPackingFraction.123)

In a later chapter (10.2) it will be pointed out, that small surface irregularities can be treated as an offset of some degrees to the angle of grain to grain friction in all cases where no statistical positioning of cylinders averages the effect. As already noted, the value for PVC seems to be an exception to the linear correlation, probably due to this effect. Since the influence of irregularities at the cylinder surfaces can be obviously assumed to effect the same consequences as friction does, regardless of the amount of applied deformation, another test was made anticipating an offset of roughly 12,5°. This results in a very well matching linear correlation, however leading to about the same interpolated value of $n^{\mu_0=0} \approx 0.179$ corresponding to $\kappa^{\mu_0=0} \approx 0.821$ for a frictionless medium ($R^2 = 0.978$):
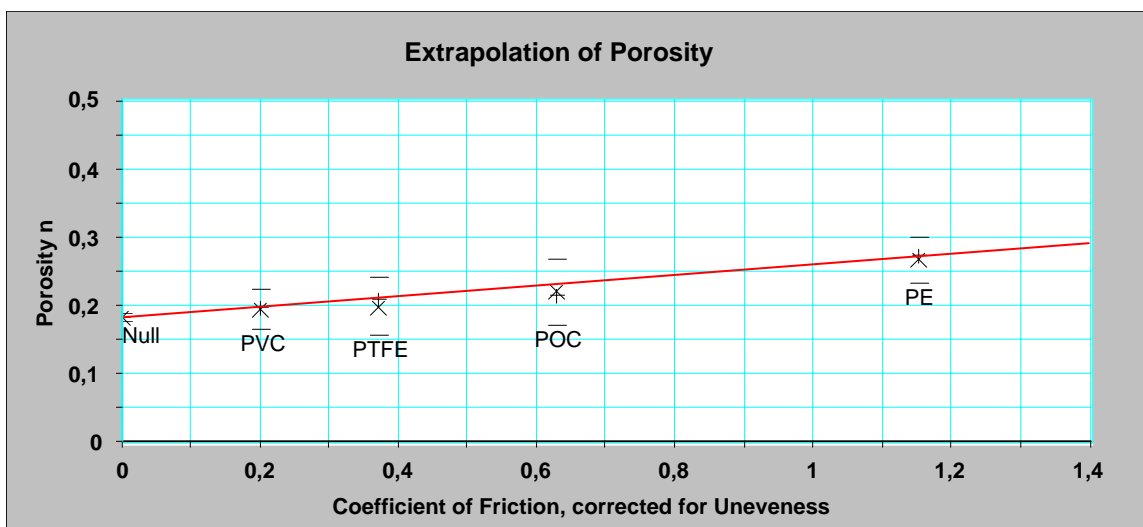

FIG. 55. Linear interpolation for measured porosity values, corrected for irregularities (File: InterpolationOfPackingFraction.123)

However, this result, describing a system which is compacted only by gravity without friction, independent of a possibly applied correction due to irregularities on the surface, matches fairly well the measured extreme value of $\kappa \simeq 0.817^{\pm 0.009}$ representing a comparable system, where friction is eliminated by the process and the own weight is without influence.

8. 3 The Granular State prior to Force Measurements

These findings viewed in the context of Howell, Behringer [26] et al. and Herle[30] et al allow to interpret the development of the granular model during the initial deformation prior to the force measurements.

They investigated the average stress in a slowly sheared two-dimensional granular system in dependence of an increasing packing fraction. At low packing fraction values the elements are mainly not interacting and therefore the mean stress is constantly low. At a transition state, identified by still vanishing stress, high compressibility and maximum shearability, the packing fraction is at minimum and shearing just begins. With increasing density, the average stress rises and thus the need for higher forces to have the system sheared. As the stress becomes infinite, the maximum packing fraction has been reached and the system cannot undergo further deformation. This transition takes place within a variation of κ of not more that 4 % above κ_t.
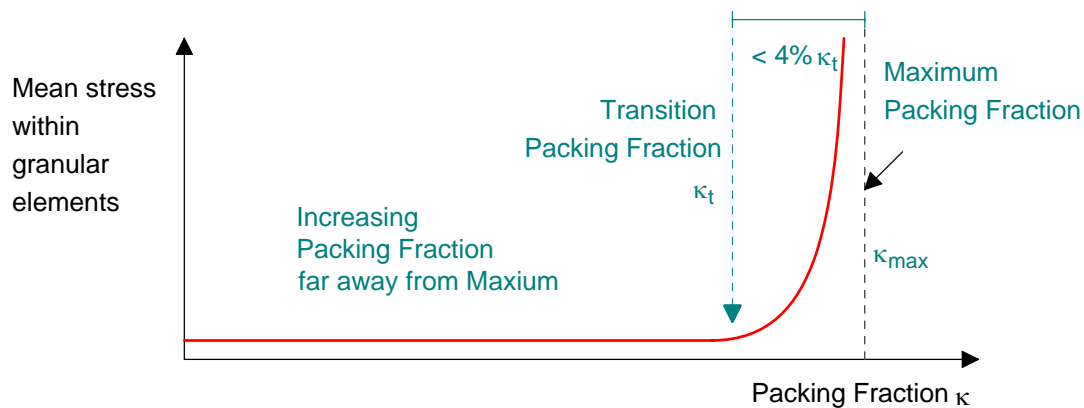

FIG. 56. Qualitatively rising mean stress with increasing packing fraction

The value of the transition packing fraction κ_t was described as mainly system dependent, but close to the square lattice density (regarding cylinders of elastic polymer in [27]). The rise of stress above κ_t seems to be determined by the structural impact only and is assumed to be much steeper on stiffer cylinders. In comparison to the soft type of cylinders used in [27] the cylinders deployed in our measurements are very solid.

The following drawing summarises the different values, from theory, from Behringer, Veje et al. [26,27] and taken from the measurements of this paper:
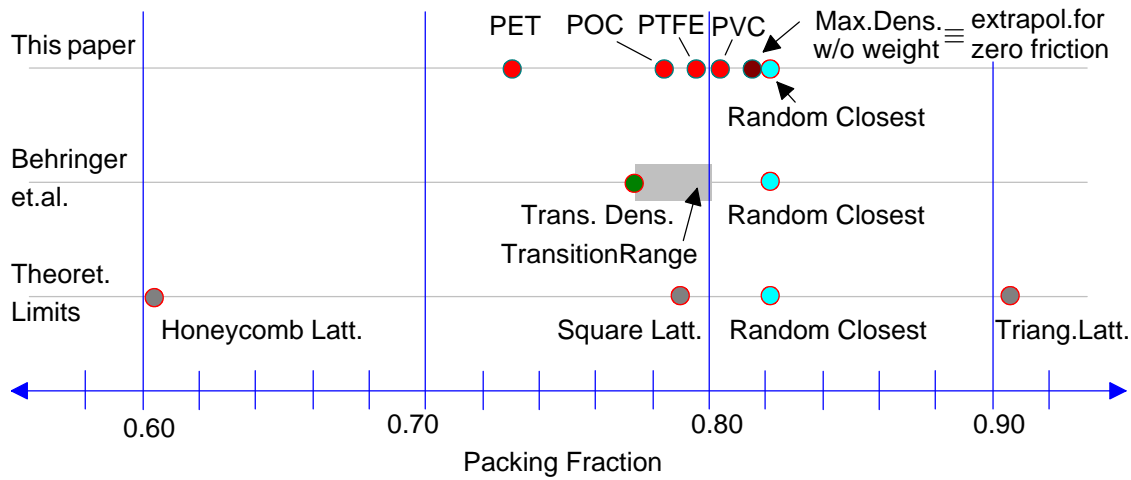

FIG. 57. Comparison of packing fraction values obtained by different sources

Since we are observing systems of identical structure under stress produced by frictional impact, we assume from this the immediate reaching of an equilibrium condition, when beginning to apply unidirectional deformation.
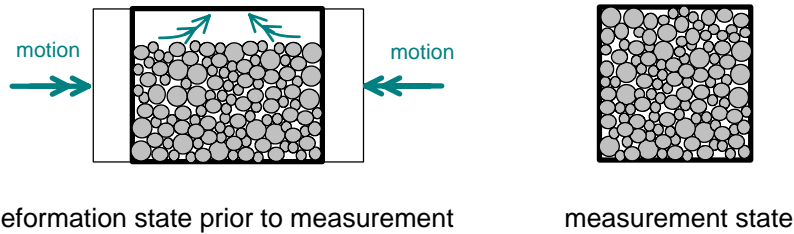

FIG. 58. Schematic development of measurement state

At the very beginning of the compression, the packing fraction rises until the shearing stress balances the own weight under the actual frictional parameters. Thus the packing fraction does not vary with the deformation process, as long as the own weight does not play a significant role compared to the frictional contribution. As soon as the test volume is completely filled, the transition state is reached, the mean stress begins to rise and the system is ready for the measurement to be taken. Due to the minor influence of the own weight we assume, that besides the structural effects the transition value κ_t depends at most on the frictional coefficients of the granular material.

The acquired measurements of packing fraction rsp. porosity in dependence of the frictional parameters μ_0 allow for a rough estimation of κ_t. Since the absolute rise of stress in

dependency of the packing fraction is not known, only a qualitative result can be given here. For very soft cylinders, Veje [27] specifies a rising length of about 4% from κ_t to the point, where the granular system is completely compacted.

On the basis of the hard cylinders used in our experiments, we assume a very high gradient leading to the possible negligence of the difference between the transition density $\kappa_t(\mu_0)$ at the root point of the rising stress and the maximum packing fraction.

Preconditioned by this argumentation, we obtain as a rough estimation for the transition packing fraction κ_t extrapolated for zero friction including an error range of 4% due to the unknown distance to the completely packed situation. However this findings lead to no strong dependency between the transition value and the frictional parameters.
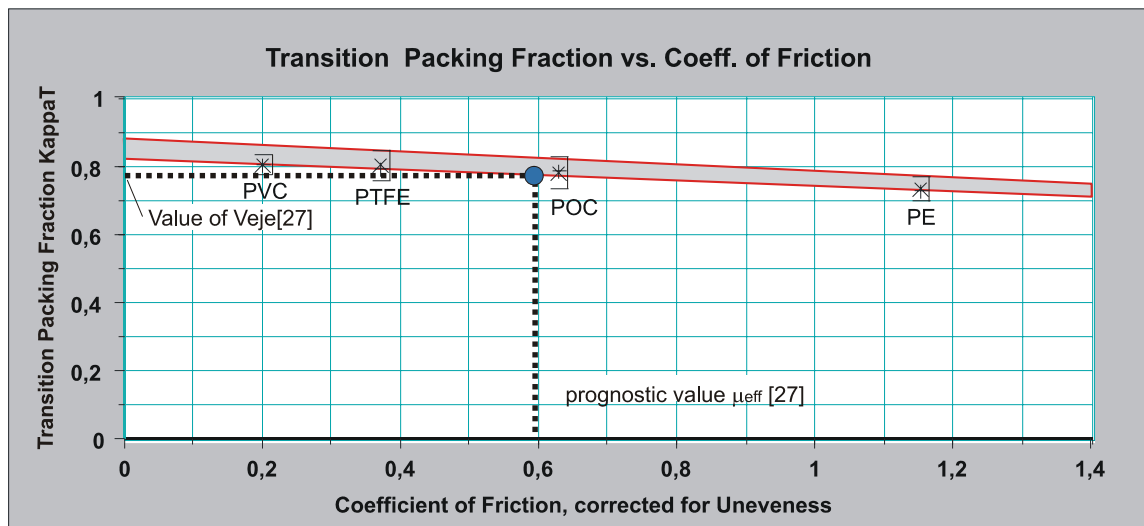

FIG. 59. Estimation of development of packing fraction (File:CriticalPackingFraction.123)

From these considerations, we assume the granular system to undergo deformation, as long as it does not touch the upper wall, representing a state very close to the transition.

Having eliminated the influence of frictional parameters to the shearing process, the system can easily be sheared and the average stress is very low in comparison to the forces applied and measured later. Particularly since the variation of density is low both on the proceeding of the shearing process and on the variation of the different surface materials, we conclude that not much alteration of the state occurs until the upper wall is touched.

At this moment no more deformation is possible, the mechanical and geometrical situation is 'frozen' and serves as a solid and reproducible initial state for the performed measurement of the Lateral Stress Factor.

9 Discussion of Results: Well Organised Granular Material

Taking the highly organised state (HLO) as the model for granular material which was subjected to ample deformation to balance inherent forces, a comparison to the concept of Mohr-Coulomb [3,4] and the resulting border states according to Rankine [5,6] can be made:

9. 1 The Mohr-Coulomb Concept

The basic idea of the Mohr-Coulomb concept was to evaluate a macroscopic coefficient of friction μ_0^{eff} from the ratio of the shearing stress τ and the normal stress σ in the sliding joint since experiments yielded the state of failure as: $\frac{\tau}{\sigma} = \mu_0^{eff} = \tan\varphi$ (as far as cohesion c can be assumed $c = 0$). This defines the yield surface as a triangle in the $\tau - \sigma$ –diagram, symmetrically to the stress axis. Any stress state, defined by the principal stresses (σ_I, σ_{III}) shows up as a circle in this space. The position on this circle is given by the definition of a coordinate system turned by an angle α against the designated system where $\tau = 0$ and (σ_1, σ_2) are identical to the principal stresses (σ_I, σ_{III}). If this circle touches the limiting triangle the state of failure is reached, indicated by the ratio $\frac{\tau}{\sigma} = \mu_0^{eff} = \tan\varphi$. Thus, the sliding plane is defined by the angle α in this case.
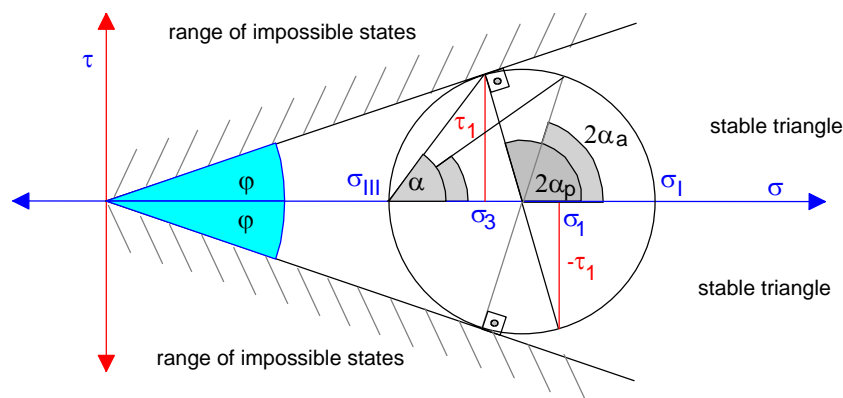

FIG. 60.   The Rankine border states, shown on the Circle of Mohr-Coulomb

According to the limiting characteristic of a frictional force, two limits depending on the direction of movement can be observed, here, according to Rankine, called the active state and the passive state. The lateral stress factor for the active state is derived as

$$K_a = \tan^2 \alpha_a = \tan^2\left(\frac{\pi}{4} - \frac{\varphi}{2}\right) = \frac{1 - \sin\varphi}{1 + \sin\varphi}, \text{ where } \varphi = \arctan\mu_0^{eff}$$

The active state is defined, where the lateral wall is yielding and friction is helping to hold the state. Thus, $K_a = \frac{\sigma_3}{\sigma_1}$ is less than unity, because σ_3 is reduced by friction. In the passive state the lateral wall tries to move inward and is held stable by σ_1. In this case friction increases σ_3 which leads to K_p greater than unity. According to the drawing above K_p is determined to be the reciprocal value of K_a.

Originally this approach was designed for three dimensions. Since it implies, that the medial principal stress has no influence on the characteristics, it can be used for two dimensions as well, as long as the missing dimension has no impact. In our experimental setup this is perfectly fulfilled; the cylindrical form of the granules ensures that no forces are acting in the third direction.

This concept is based on the perception of a continuous material, which begins to decompose as soon as shearing forces reach the possible retaining forces induced by normal stress. It does not contain any structural impact and therefore supplies a kind of effective coefficient of friction μ_0^{eff}, leading to the macroscopic Angle of Friction φ, which includes the true coefficient of friction μ_0 between the particles as well as the influence of granularity i.e. unevenness of the sliding joint. We expect the dimensionality of the model to have great impact on exactly this contribution since the statistics of this surface is completely different on cylinders in contrast to spheres.
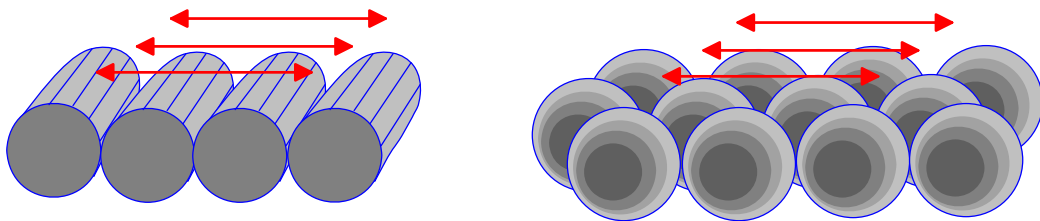

FIG. 61. Clarifying different ranges of contact positions in two and three dimensions

Yet, as the model consists of cylinders, the structural impact needs to be considered in two dimensions; different results are expected for spherical models.

9. 2 Comparison to the Rankine Border States: Structural Contribution

In order to evaluate the HLO-measurements in comparison to the border value K_a according to Mohr/Coulomb and Rankine, the results are repeated here for convenience:
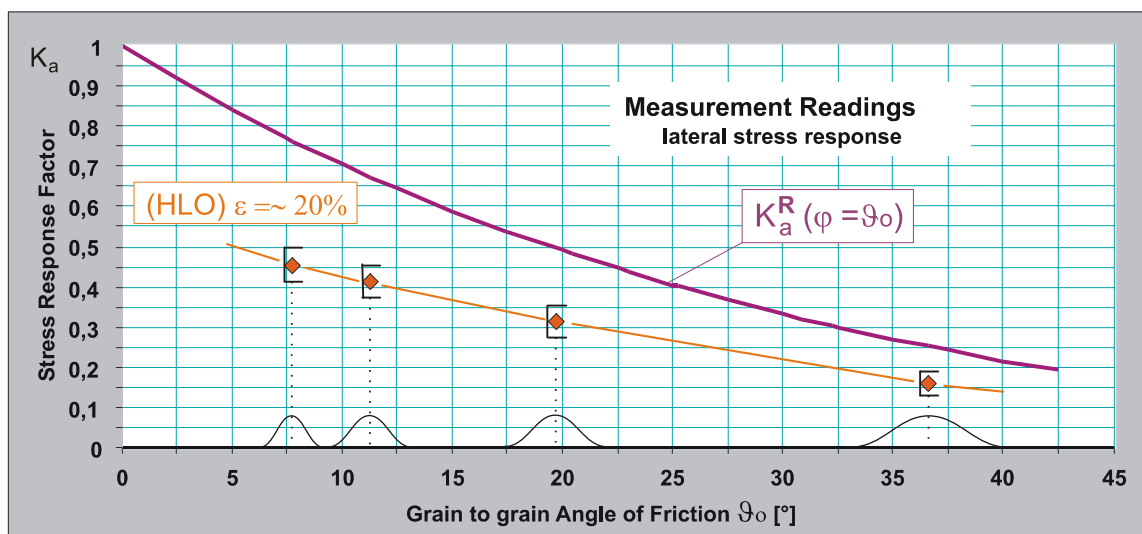

FIG. 62.   Repeated results of HLO Stress Response Factor (Readings.123)

The measurements shown above display a significant difference to the Rankine equilibrium state, which can be interpreted as the structural contribution in two dimensions.

Since we observe that the only type of cylinder (PVC) produced on the lathe with no significant macroscopic irregularities on the surface fits the continuous development of the measured values very well, we assume, that such are of no major influence. Hence, no correction of the grain to grain friction is made which needs to be discussed further.

The shearing process in the sliding joint of a granular material is based on many contacts at varying angles χ within a limit $[-\delta, \delta]$. This is given by the shape of the cylinders as well as the self organising process, which is assumed to smoothen the joint, forcing the bedding cylinders into a more or less perfect line.

Therefore, the grain to grain coefficient of friction $\mu_0 = \tan\vartheta_0$ is different from the effective operating coefficient of friction $\mu_0^{eff} = \tan\varphi$.
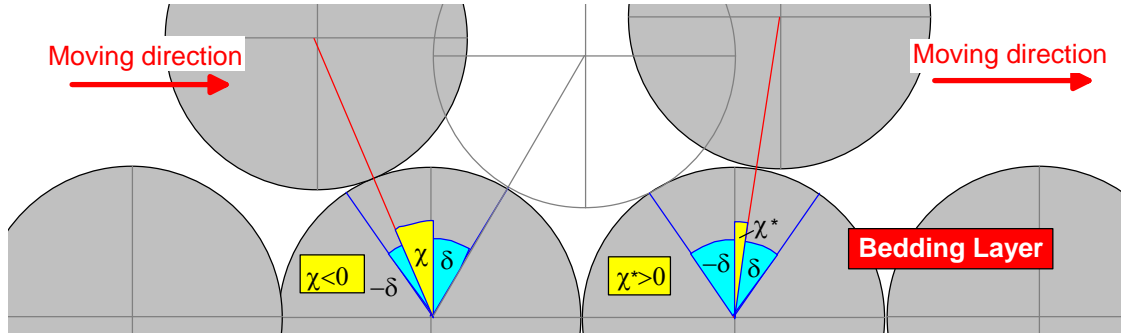

FIG. 63.　Geometrical situation in the sliding joint (Clockwise oriented angles are positive).

The local coefficient of friction $\mu_0 = \tan\vartheta_0$ in dependence of a contact angle χ can be calculated like this:
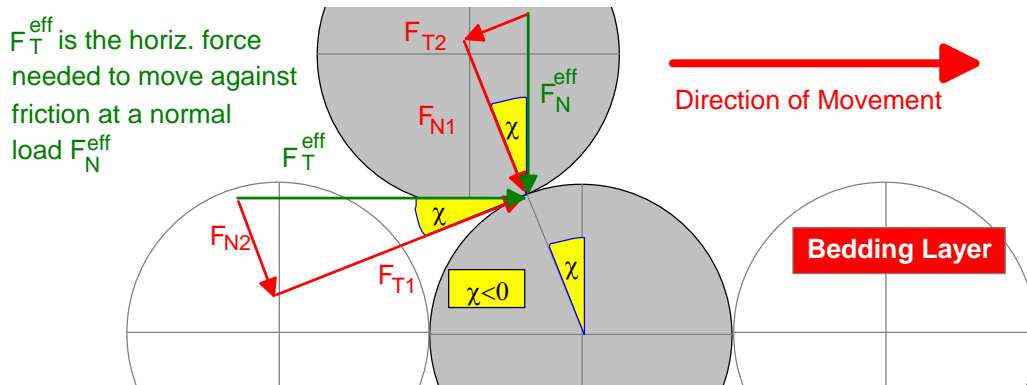

FIG. 64.　Composition of forces within a sliding joint

$$F_N = F_{N1} + F_{N2} = F_N^{eff}\cos\chi - F_T^{eff}\sin\chi$$

$$F_T = F_{T1} + F_{T2} = F_T^{eff}\cos\chi + F_N^{eff}\sin\chi$$

$$\mu_0 = \frac{F_T}{F_N} = \frac{F_T^{eff}\cos\chi + F_N^{eff}\sin\chi}{F_N^{eff}\cos\chi - F_T^{eff}\sin\chi}.$$

Describing the scene in the sliding joint by the macroscopic angle of friction

$$\varphi = \arctan\mu_0^{eff} = \arctan\frac{F_T^{eff}}{F_N^{eff}}, \text{ we write } \tan\vartheta_0 = \frac{\tan\varphi + \tan\chi}{1 - \tan\varphi\tan\chi}.$$

This is to be resolved for φ and leads to:

$$\tan \varphi = \frac{\tan \vartheta_0 - \tan \chi}{1 + \tan \vartheta_0 \tan \chi} = \tan(\vartheta_0 - \chi), \text{ which identifies: } \varphi = \vartheta_0 - \chi$$

(Hence, a negative angle of contact $\chi < 0$ virtually enlarges the shear resistance)

In order to obtain the mean value, the range for χ to vary needs to be defined. As the drawing above indicates, the geometrically possible location is limited by an angle $\pm\delta$, given by the straightness of the bedding layer. For perfectly straight lines formed by cylinders of equal diameter we have $\delta = 30^o$, under less ideal circumstances it might be a bit more.

The equation above additionally yields a natural limit, for φ must not be negative, thus we obtain $\chi \leq \vartheta_0$ and therefore $\chi \in [-\delta, \vartheta_0]$.

Sufficient forced deformation of the granular material as considered here, causes selforganising processes establishing shear zones, where the granules are **shifted collectively**. Since the collective remains compound, each of the single contacts is not governed by local criteria of friction and movement, but can be assumed evenly spread over all possible conditions. Therefore, the measured unevenness of the cylinders produces as many rising edges as falling edges, where none of these preferably influences the characteristics of a mean contact. Hence, the previously neglected influence of the macroscopic irregularities in fact plays no role since the symmetry of such irregularities balances its consequences as long as the motion history generates the contacts within the sliding joint at stochastically independent angles. This turns out to be a very important observation and corresponds well to the perception of shearing deformation being strongly localized in shear bands [11-16,43,44,63].

Assuming **constant probability** $P_\chi d\gamma = \dfrac{d\chi}{\delta + \vartheta_0}$ within this range, the effective coefficient of friction can be gained through

$$\overline{\tan \varphi} = \overline{\mu_0^{eff}} = \frac{1}{\delta + \vartheta_0} \int\limits_{-\delta}^{\vartheta_0} \frac{\tan \vartheta_0 - \tan \chi}{1 + \tan \vartheta_0 \tan \chi} d\chi,$$

Integrating is done via expansion into partial fractions and yields:

$$\overline{\tan \varphi} = -\frac{\ln(\cos(\delta + \vartheta_0))}{(\delta + \vartheta_0)}$$

Applied to the measurement, φ is calculated from ϑ_0 and under assumed evenness of sliding joints, the results fit the theoretical considerations very well. Best fit is gained under the assumption of $\delta = 37.0^o$ with a mean deviation of 1.38^o.

It should be kept in mind, that this value is a mere fit, but it appears to be very plausible, knowing that a perfectly smooth joint is characterized by $\delta = 30^o$. Completely rough joint

surfaces would be the normal on stochastic mixtures, far away from equilibrium, which occur on states with low level of organisation.

Improvement might be expected from specifying the **probability of contact proportional to** $\cos \chi$, keeping in mind the projection of the surface to the slide joint as the relevant face (explained more in detail in chapter *Statistical Approach: Less Organised Granular Material*, section *Coefficient of Geometry*). Such an approach yields:

$$\overline{\tan \varphi} = \overline{\mu_0^{eff}} = \frac{1}{\sin \delta + \sin \vartheta_0} \int_{-\delta}^{\vartheta_0} \frac{\tan \vartheta_0 - \tan \chi}{1 + \tan \vartheta_0 \tan \chi} \cos \chi \, d\chi$$

which can be solved fundamentally to

$$\overline{\mu_0^{eff}} = \frac{\cos \vartheta_0 - \cos \delta + \sin \vartheta_0 \ln \tan\left(\frac{\pi}{4} + \frac{\vartheta_0 + \delta}{2}\right)}{\sin \delta + \sin \vartheta_0}$$

This gives an effective angle of friction φ, which is slightly lower ($\approx 0.5^o$) than the one given by a constant distribution of probability. As before, the measurement results can be approximated on the basis of $\delta = 38.1^o$, resulting in a mean deviation of 1.12^o. The arising effective angle of friction is less than 1% away from the one obtained by the much simpler linear approach.

The following graph shows the structural adjustment to the measurements on highly organised granular material using the COS-distribution. Hence, taking into account angle of contact distributions leads to a friction dependent correction to the Rankine approach, which is compatible with the experimental results.
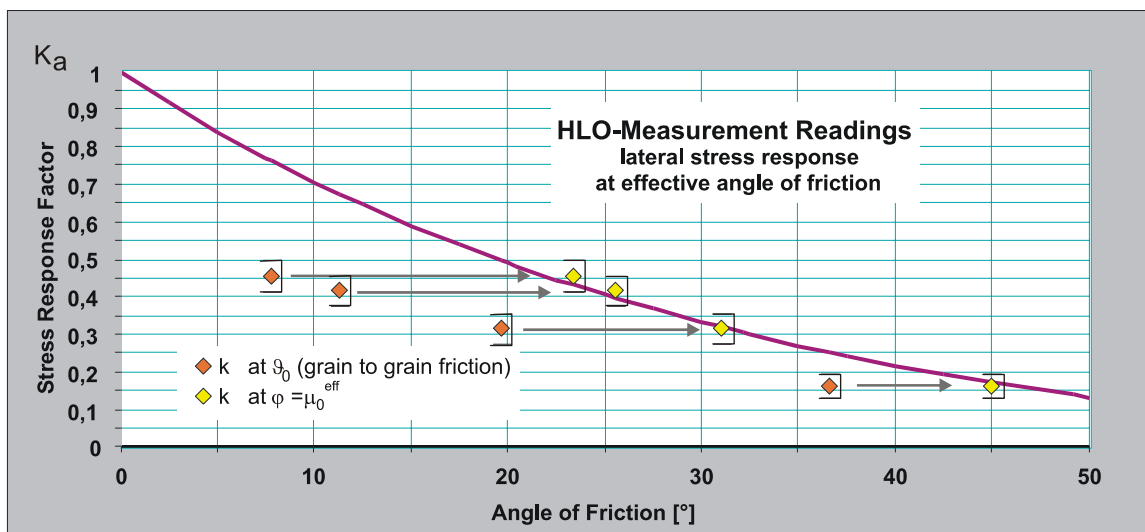

FIG. 65. Structural modification through the use of a COS distribution for the angles of contact (File: Readings.123)

Remark: Such a mechanism in the sliding joint as described above is closely related to the concept of dilatancy. A purely stochastic arrangement of cylinders leads to a maximum contact angle of $\delta \simeq 60^o$ which, averaged over all possible positions, corresponds to an initial angle of dilatancy of about $\psi_D \simeq 30^o$. From the state of balanced forces considered here we obtain a much better estimation of $\psi_D \simeq 19^o$ which is compatible e.g. with the value of Reynolds, presented by [68].

9. 3 Estimation of Self Organising Effects

Since rearrangement processes have obviously compensated for the local effects after a continuous deformation of $\varepsilon \simeq 20\%,$ the self organisation effect needs to be justified by a quantitative estimation:

The initial state of a stochastically arranged granular material is dominated by the maximum angle of contact $\delta_0 = 60^o$ within any sliding plane.

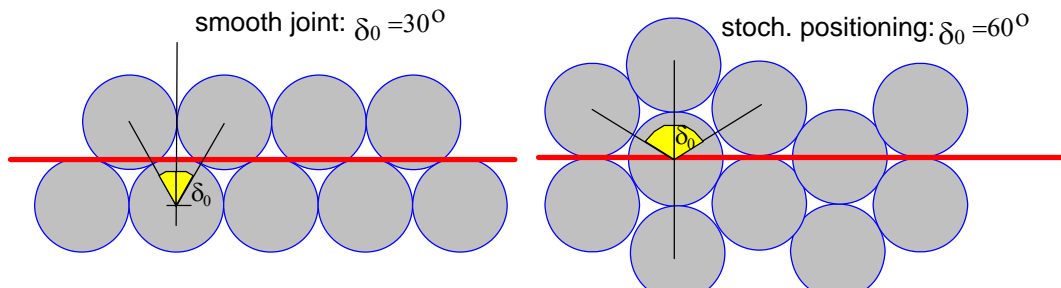smooth joint: $\delta_0 = 30^O$ stoch. positioning: $\delta_0 = 60^O$

FIG. 66. Dependence of δ_0 on the smoothness of the shear joint

Shearing forces tend to smoothen the joint. Therefore, self organisation expressed as deformation ε effectively lowers the maximum angle of contact $\delta_0 \to \delta(\varepsilon)$.

9. 3. 1 Consequence of continuous deformation

Compression of a granular system in the direction of a shearing joint pushes contacts at certain angles χ to smaller angles and hence reduces the maximum angle of contact $\delta_0 \to \delta(\varepsilon)$ in the same way.

Distributing continuous compression ε_{joint} of a granular system along a shearing joint equally to all contacts, the deformation shifts δ from $\delta_0 = 60^o$ to: $\delta = \arcsin[(1 - \varepsilon_{joint})\sin\delta_0]$
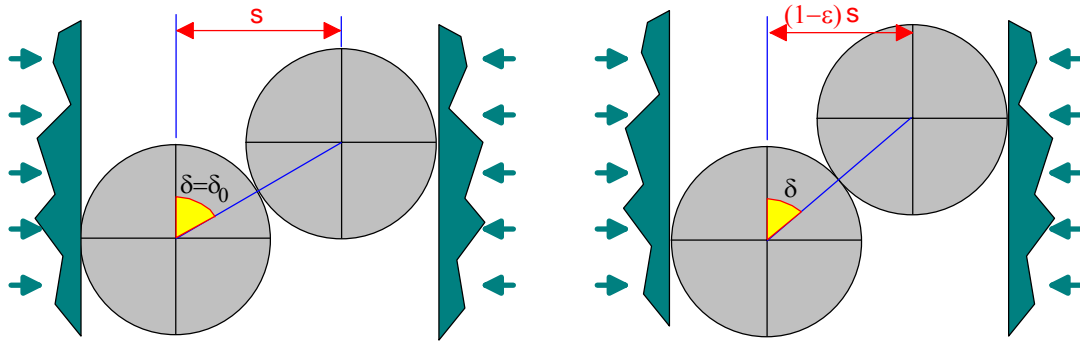

FIG. 67. Deriving δ as a function of the deformation ε

However, in order to evaluate the smoothing of a joint by a certain amount of deformation along the joint, first, the angle of the joint a is needed. With this, the overall compression ε in the horizontal direction is transformed into the angular compression:

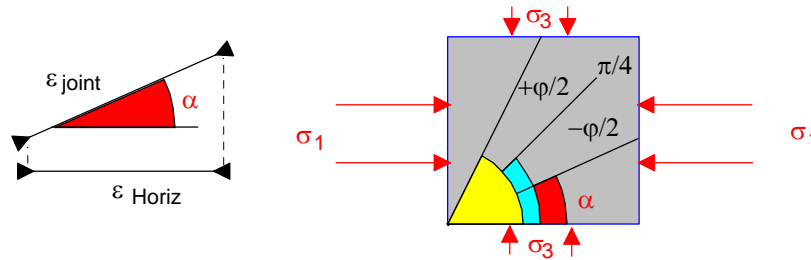$$\varepsilon_{joint} = \frac{\varepsilon}{\cos a}$$

FIG. 68. Transforming horizontal compression to angular compression

Based on the considerations made above, the angle of the shearing joint can be calculated according to Rankine as $a = \frac{\pi}{4} - \frac{\varphi}{2}$, using the overall angle of friction φ. Yet, this angle of friction φ consists of the known term ϑ_0 representing the coefficient of friction and the structural impact, which is not yet available but to be estimated here from the smoothing of the joint.

$$\varphi := f(\vartheta_0, \delta) :\overset{\delta = f(\delta_0, \varepsilon, a)}{=} f(\vartheta_0, \delta_0, a, \varepsilon) :\overset{a = f(\varphi)}{=} f(\vartheta_0, \delta_0, \varphi, \varepsilon)$$

Unfortunately this circular relation cannot be resolved, but it can be handled by iteration. Starting with a very rough estimation of $\varphi = \vartheta_0$ leads to the angle of the joint α which allows to calculate the smoothing effect $\delta_0 \rightarrow \delta(\varepsilon)$ from the horizontal compression ε. From this we obtain a better estimation for φ improving the repeated calculation. We found that the influence of this recursion is so weak, that values of φ converge very fast. Two iterations already reduce the error to approximately $1^o/_{oo}$.

9. 3. 2 Influence of varying diameters of elements

As the granular material consists of cylinders of different diameter, the limiting angle δ_0 is not absolutely fixed to $\delta_0 = 60^o$. Simulating all combinations through the real distribution of the model cylinder diameters, we obtain this frequency distribution for δ_0:
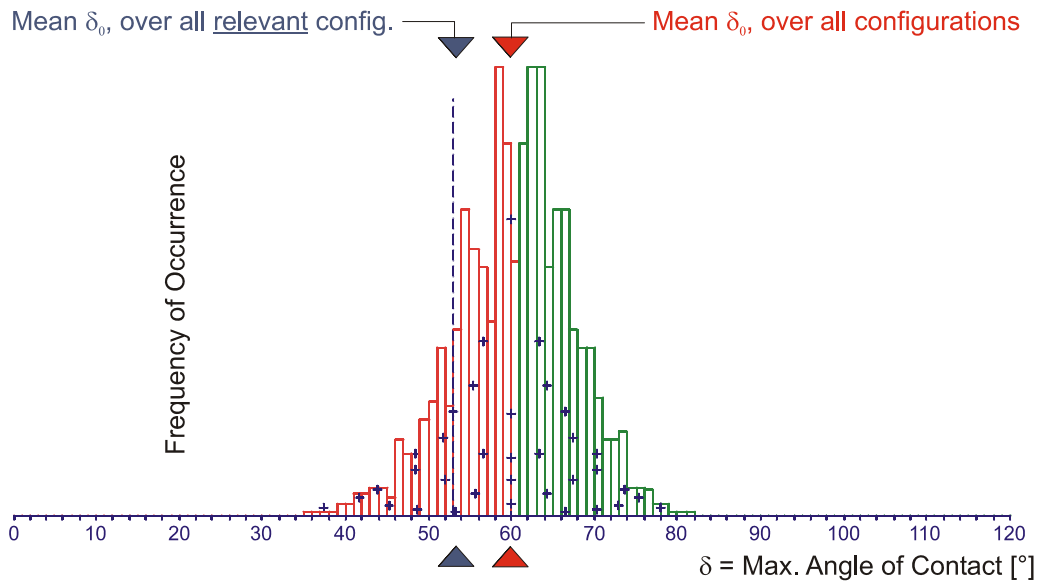

FIG. 69. Numerically obtained distribution of the max. Angle of Contact for the set of cylinders used here.

As expected, the mean value is $\delta_o \simeq 60^o$, but this neglects the fact, that the sliding joint is not forced to use a certain stochastically given contact, but is free to choose the best one, i.e. the one with the least necessity to be shifted out of the way. For each contact at a maximum $\delta_0 \gtrsim 60^o$, being the consequence of a special combination of radii, the concerned cylinder can

be taken as part of the bedding layer and not be shifted away. Therefore a corresponding contact $\delta_0 \lesssim 60^o$ can be found, which will preferably be used. The restructuring processes always make use of the least available resistance.
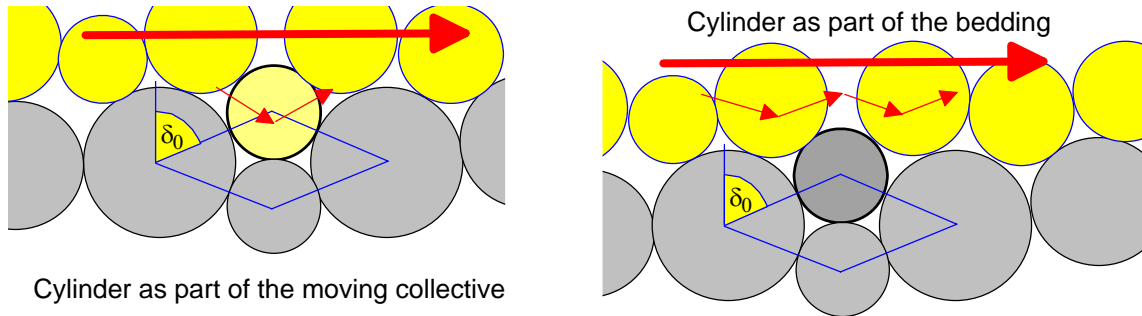
FIG. 70. Changeover of a single cylinder in the sliding joint from the moving block to the bedding

Thus within the distribution of δ_0 the lower limiting angles $\delta_0 \lesssim 60^o$ are not compensated by other contacts with $\delta_0 \gtrsim 60^o$, but simply limited at $\delta_0 = 60^o$

Accepting this mechanism, the upper half of the distribution needs to be cut off and the mean value of the remainder serves as a good estimation for the maximum limiting angle $\delta_0 \simeq 53^o$ as indicated by the dashed line.

9. 3. 3 Estimated structural impact

Taking all these factors together, the calculated effective angle of friction φ_0 is determined as:

	Fit [δ=37°]	Fit [δ=38.1°]	Estimation [ε =20%]	Estimation [ε =20%]
	const. Distrib.	COS-Distrib.	const. Distrib.	COS-Distrib.
ϑ_o	φ_o	φ_o	φ_o	φ_o
7,75°	23,66°	23,42°	23,93°	23,04°
11,33°	25,82°	25,56°	26,21°	25,27°
19,71°	31,22°	31,01°	31,91°	30,93°
36,61°	44,55°	44,99°	46,32°	45,57°

The estimated structural impact meets the fit very well. Differences, using the COS-distribution seem not to be significant. All estimations produce values, which are well positioned within the error bars of the measurement readings.

Typically, the following graph illustrates only the most sophisticated approach, which is the estimation using the COS-distribution:
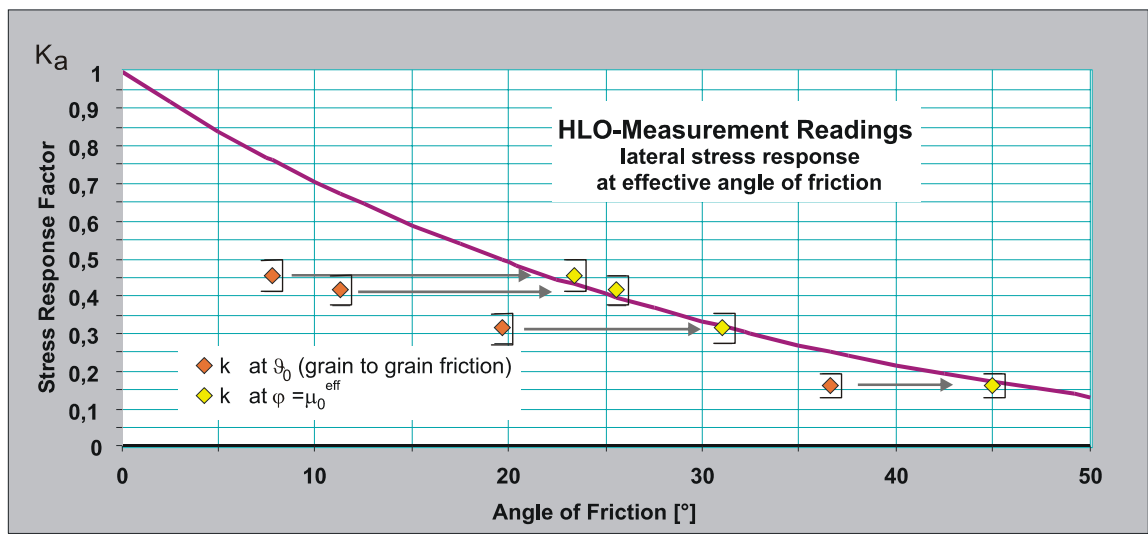

FIG. 71. Measured values, transformed using $\delta(\varepsilon)$ instead of δ_0 correspond to the Rankine approach (File: Readings.123)

This results in a structural offset up to 15 degrees to the Microscopic Angle of Friction ϑ_0, manifestly decreasing with rising friction.

Within the range of normal Coefficients of Friction, it turns out to be an approximately linear dependency, displayed in the following graph:
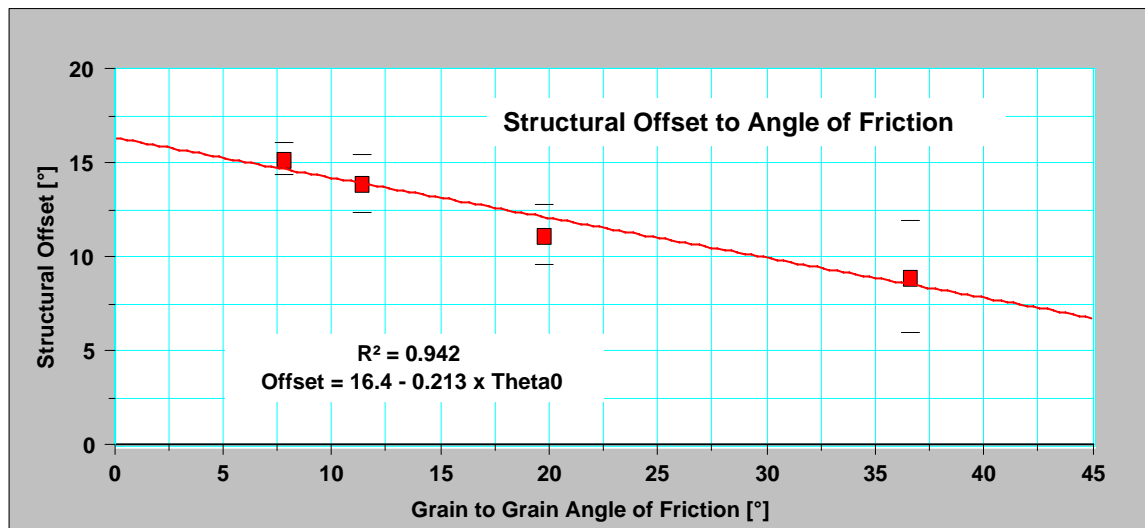
FIG. 72. Linear fitting approach for the structural offset to the Rankine model (File:StructuralOffsetTCFit.123)

Extrapolation of this linear approach to higher values of friction may give rise to the idea of a completely vanishing structural offset at some value. After all, we find that the obtained error-ranges allow no substantiation of such a characteristic.

10 Discussion of Results: Less Organised Granular Material

As the measurements regarding LLO granular material are to be discussed here, the results are repeated for convenience:
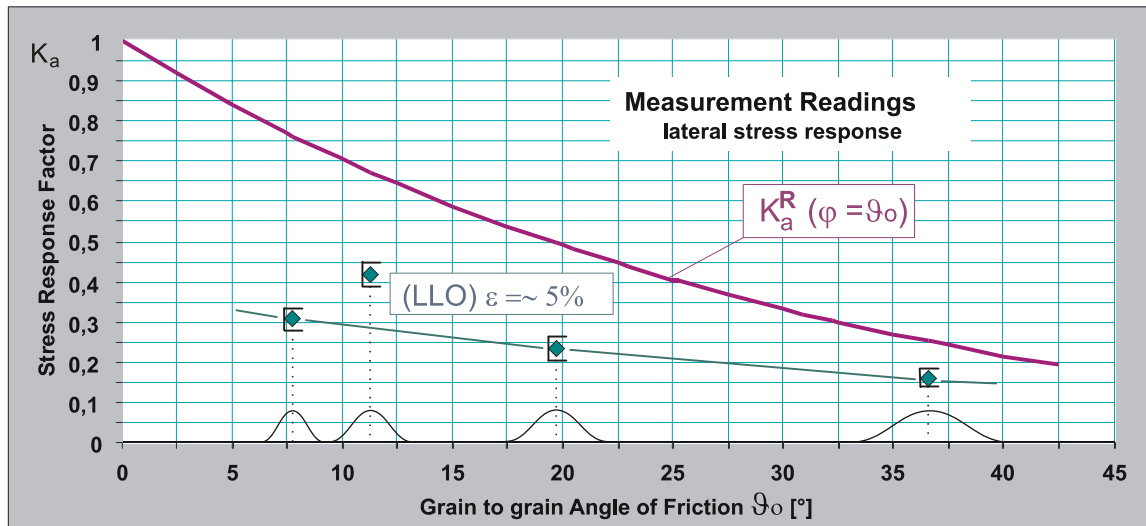

FIG. 73. Final measurement results for LLO-systems (File: Readings.123)

To gain certainty about the characteristics, the results on scarcely organised granular material were repeatedly confirmed by additional series of measurements. They are reproducible and display the shown properties.

The most remarkable attribute is the non monotonous progression of the lateral force with the rising coefficient of friction. Especially the value obtained from the PVC-material presents itself as a strong misfit.

Even under the assumption that this value is the result of a systematic error, which is not very likely, the remaining data cannot be fitted like the highly organised sequences. Furthermore allowing not much compensating processes, the approach of Rankine is presumably not applicable here.

On the basis of stochastic positioning of the cylinders, sliding joints cannot be established and therefore cannot serve as a reference for a designated direction. This state is much closer to a statistical model, telling something about the building of force chains which bear most of the load. In this view, contact angles δ are to be defined in a different way, referring to a

virtual direction of a force chain. Then in a system of stochastically positioned cylinders, contact angles δ up to 60° may occur, before contacts are replaced by others using smaller angles.

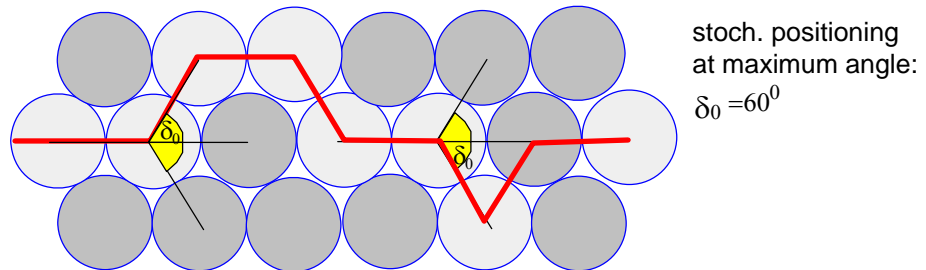stoch. positioning
at maximum angle:
$\delta_0 = 60^0$

FIG. 74. Maximum Angle of Contact δ_0 in a stochastically positioned set of cylinders

Since the readings are much lower than predicted by a quasi continuous model, and as the polariscope images indicate, such a stochastic perception is very likely to hold. Unfortunately there is no way to perform the experiments completely without any deformation and thus organisation, so mixtures of states as well as effects triggered by small self organisation rates contaminate the results.

At first and before any attempt can be made to interpret the obtained readings, the mechanism which produces the observed irregularity needs to be identified. Its authenticity is additionally confirmed by the measurements of the porosity n, where also PVC cylinders behave as if they were subject to much less friction than even PTFE coated cylinders in contrast to the measured microscopic friction parameter.

The only property, where the PVC-cylinders differ from the other is the observed unevenness of the circumference surface. Being produced on the lathe they are much smoother, while all other cylinders had been cast and show small, sharp irregularities.

So, contrary to the arguments discussed before on the highly organised systems, here the local unevenness of the cylinders seems to play a most important role:

The discontinuity displayed by the measurements concerning PVC and Teflon-Cylinders is obviously not supported by any physical argument. There is no reason, why the relation between the angle of friction and the produced transversal force, should not be monotonous but exhibit a kind of sharp maximum at any value.

Remark: Nonlinear equations ruling chaotic systems are nevertheless likely to produce similar characteristics. Such approaches were applied to comparable systems and promise a

good understanding. Yet, motivated by the good reproducibility of the results under varying circumstances, we deduce this not to be the source of the peak.

More probably, the self organising processes find positions of contacts, where the effective angle of contact is enlarged by a local unevenness.

10. 1 Assumed Self Organising Process based on Unevenness

In this case the self organising process is assumed to be very elementary:

Beginning from a pure stochastic distribution of contacts, every angle of contact in the range $[\simeq -60^o, \simeq 60^o]$ can be found with constant probability. Depending on the microscopic angle of friction, the contacts need to be separated into rolling contacts, where the friction is sticking and in gliding contacts, where friction is to low to hold.

Small deformation of the granular medium starts to shift the gliding contacts to higher angles. Within this process, cylinders with rolling contacts are supposed not to contribute much to the deformation due to the redundant definition by other contacts, holding the element in place. Yet, cylinders with gliding contacts tend to slip to higher angles as long as they are not stopped by a positive slope, introduced by a sharp bump on the surface. Consequently, the gliding contacts just above the limit of the gliders, pick up positions on positive slopes and convert to sticking contacts. The range of angles, where this effect occurs, is defined by the mean maximum slope, i.e. by the mean size of the unevenness. Thus, the granular material can be characterized by its intrinsic angle of friction ϑ_0, enlarged by the size χ_u of the range, where the conversion is possible.

This scenario should be valid until the relaxation processes discussed in the High Level of Organisation Section begin to dominate.

10. 2 Quantitative Estimation of the Self Organised Stability

Any unevenness can be characterized by its height, as long as its shape is assumed to be sharp. The effect is easily quantified using the following model:
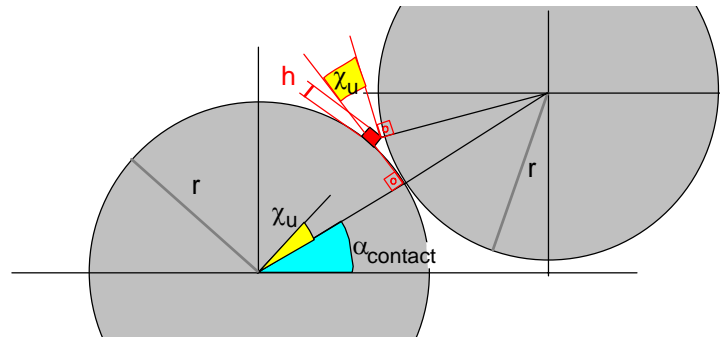
FIG. 75. Unevenness on the cylinder surface characterized by its height

A perturbation of height h increases the angle of contact, where gliding is just possible, by an angle χ_u, thus adds χ_u to the microscopic angle of friction ϑ_0.

χ_u is given by the difference between the surface angle at the contact and the surface angle at the ridge. Restricting to circular cylinders, the surface angle is defined by the tangent to the surface.
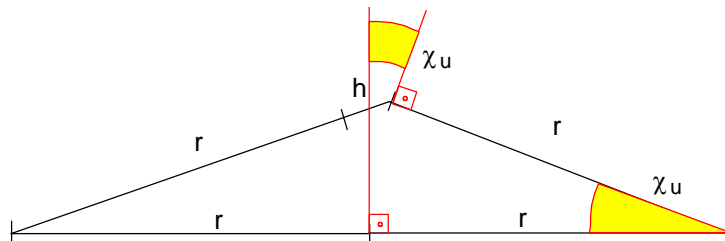
Thus χ_u is defined by the following structure:

FIG. 76. Schematical view of the geometrical situation

From the law of cosines we obtain, setting $u = \dfrac{h}{r}$ as relative perturbation:

$$\chi_u = \arccos\left(1 - \frac{u}{2} - \frac{u^2}{4} \right)$$

Referring to the aquired mean values for the unevenness, this yields:

	Polyester	Polyolefin	Polyvinylchlorid	Teflon
Mean Roughness[mm]	0,24	0,23	<< 0,01	0,23
Statist. Error (95%)	0,07	0,09		0,11
Rel. Perturbation $\bar{u}$	4,76%	4,66%		4,68%
Add. Angle χ_u [deg]	**12,7°**	**12,5°**		**12,6°**
Abs. Error (Ref)[deg]	1,35°	1,37°		1,37°
Abs.Error (Stat) 95%[deg]	1,98°	2,67°		3,01°

The cylinders, produced from PVC on the lathe are significantly better and serve as an absolute reference for measurement noise. The resulting absolute error margins, one taken from the reference, the other taken from the statistical errors, is scaled by the derivation:

$$\frac{\partial \chi_u}{\partial u} = \frac{2 + 2u}{\sqrt{16u + 4u^2 - 4u^3 - u^4}}$$

As the function rises very fast, but soon reaches a more or less stagnating state, the high statistical errors do not result in a great uncertainty in the final values for χ_u .

Under the assumption of this consideration, the readings need to be modified as follows and are much more plausible:
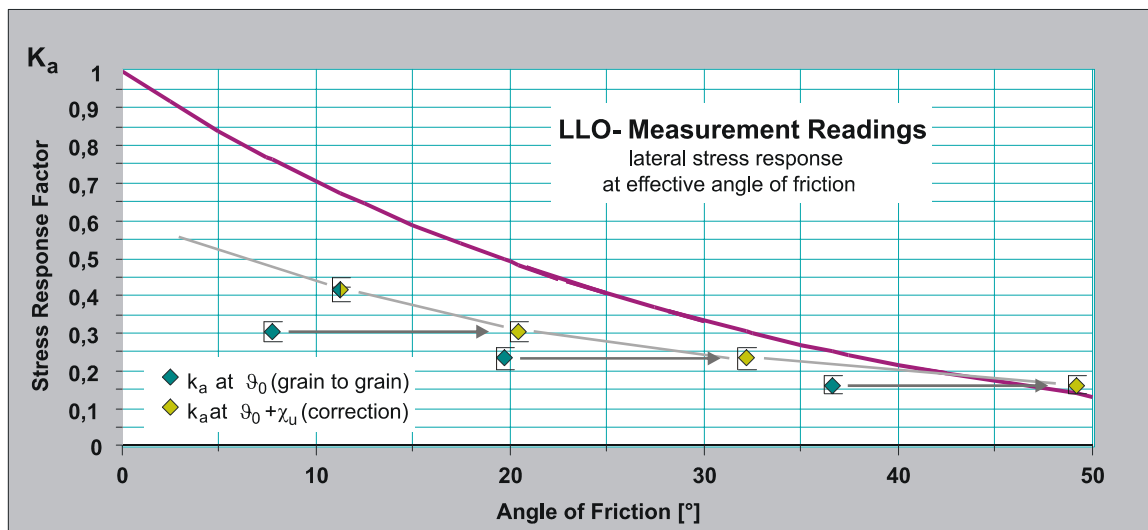

FIG. 77. Correction to measured values due to surface unevenness (File: Readings.123)

Any trial to interpret this reading, using models like that of Rankine, corrected by the structural impact, are doomed to fail, since the granular system is dominated by stochastically generated contacts which are not balanced by ample restructuring processes to be described by approaches based on deformations on a comparably large scale.

The very small deformation ε in this case would predict a fairly large structural impact and thus leads to expect mainly vanishing lateral forces at the upper end of the scale.

So beyond a well based explanation by statistical means which is addressed in the next chapter, the readings of K_a need to be at least parameterized.

10. 3 Descriptive Parameterizing Approach

Aiming at an appropriate **approximation** of the measurement data, we presume the deformation ε to have no quantitative impact, but just to activate the surface traps to enlarge the angle of friction.

Furthermore, we observe, that even under vanishing friction, the stress response factor K_a rises to a value significantly less than 1 due to the structural impact itself.

Presupposing this, we can formulate a convenient exponential approximation with a high coefficient of regression and remaining well within the error margins:

$$K_a(\vartheta_0 + \chi_u) = a \cdot \exp[-\beta\,(\vartheta_0 + \chi_u)]$$

Such an exponential description implies the existence of a well defined value at the point of no friction and finally vanishing lateral stress in the limit of high angles of friction.

Drawn on a single logarithmic scale, the parameters are obtained easily from linear regression analysis as: $a = 0.528^{+0.07}_{-0,04}$ $\beta = 0.0244^{+0.005}_{-0,0045}$
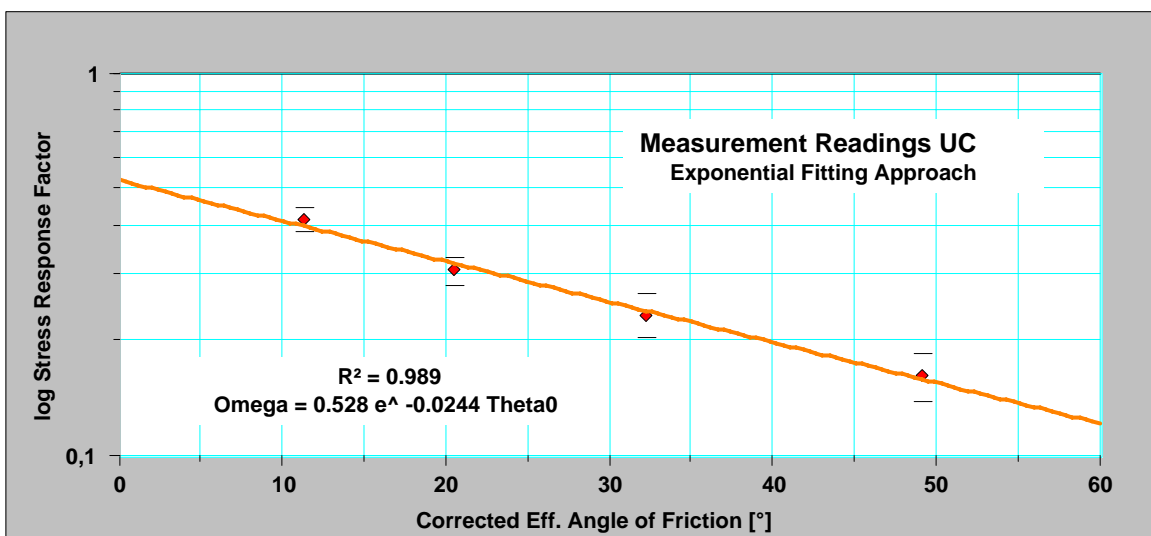

FIG. 78. Exponential approximation for the corrected measurement values (File: Readings.123)

The exponential approach predicts $K_a(\mu_0 = 0, \chi_u = 0) \simeq 0.528^{+0.07}_{-0.04}$, but due to its character as an extrapolation this value is very sensitive to variations of the parameters. It needs to be taken with care, but at least serves as a good argument for the broken equilibrium in the selforganising state.

Furthermore, the measured value corresponds fairly well to the '*coefficient of redirection towards the wall*' for frictionless monodispersed granular media, $K \simeq 0.58$, cited by Duran [52].

11 Statistical Approach: Less Organised Granular Material

Granular systems consist of a multiplicity of elements, contacting their adjacent neighbours at random angles. As soon as motion is introduced, the angles of contact are no more evenly distributed, but are dominantly ruled by the selforganising processes. Under the influence of sufficient forced deformation, completely different mechanisms are working.

Yet on scarcely sheared systems, statistical approaches should be applicable. The following considerations are made in order to find a basic state of the granular material, where the deformation development is assumed to start from.

The readings concerning granular material with low level of organisation ($\varepsilon \simeq 5\ \%$) (LLO) are supposed to be close to this state and may verify this model.

11. 1 Preliminary Test Using a Highly Simplified Model

In order to obtain a first impression of a lateral stress factor which a stochastically positioned granular media may provide, a very simple model was chosen:

We assume longitudinal stress to be split into several longitudinal force chains, which lead to a number of lateral force chains where the local mechanical situation allows. For reasons of simplicity, this is assumed to be a symmetrical construction described only by the angle of contact ψ as shown in the drawing:
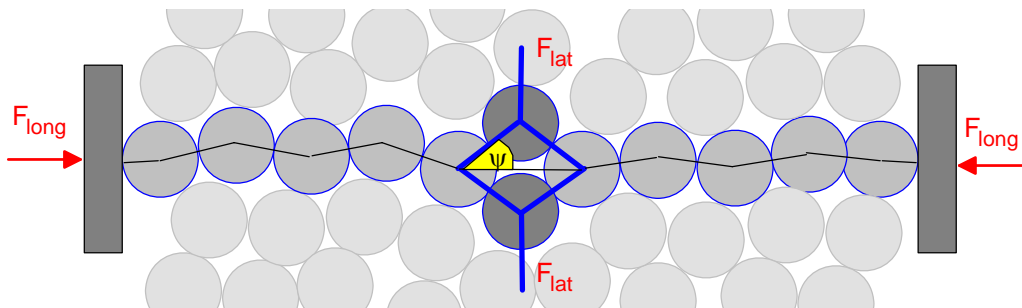

FIG. 79. Highly simplified model as a preliminary test

Building of lateral chains, i.e. redirection of forces is considered possible, if the angle of contact ψ is greater than the angle of friction ϑ_0 as depicted in the next figure.

Using $F_T = \sin \psi \, (-F_{long})$ and $F_N = \cos \psi \, (-F_{long})$, we obtain the condition of stability where no gliding of adjacent cylinders is possible:

$$\mu_0 = \tan \vartheta_0 \geq \frac{F_T}{F_N} = \tan \psi \quad \text{and thus} \quad \psi \leq \vartheta_0.$$
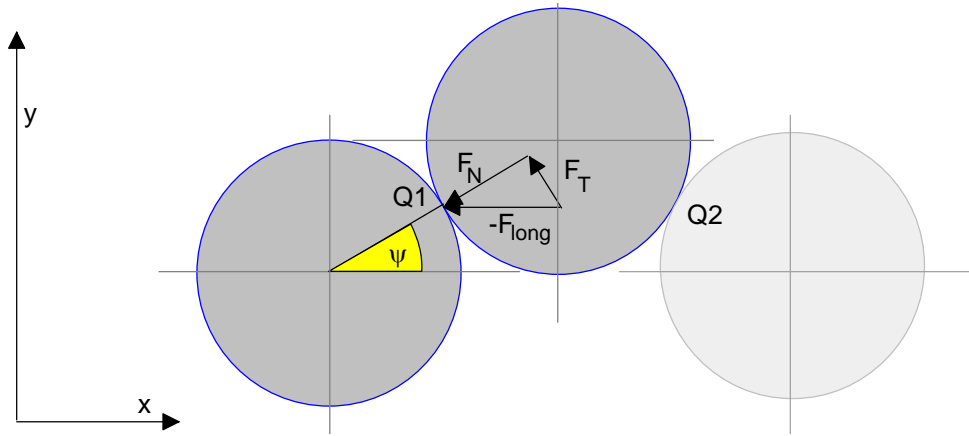

FIG. 80. Criterion of Gliding in preliminary model

For the case, where the situation provides a gliding structure at contact Q1 (and symmetrically at Q2, yet here considered only Q1) the operant forces can be easily derived by using the principle of virtual displacements. A small virtual modification $-dx$ of the longitudinal distance of two adjacent cylinders interacting with force $-F_{long}$ causes a geometrically defined variation of the angle of contact ψ and therefore a modification dy to the lateral distance where the force $-F_{lat}$ is acting. No other movement is considered possible, the impact of elasticity, weight and other side effects is assumed to be of negligible order in comparison to the mechanical contribution.
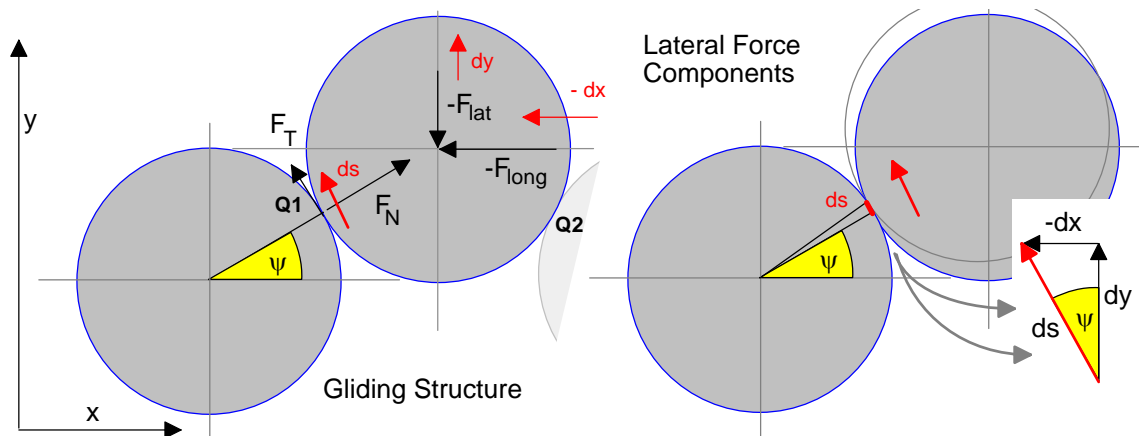

FIG. 81. Redirection of forces in preliminary model

Page 94

Considering the virtual work of such a limited mechanical frictionless system allows to derive the ratio of the lateral force $-F_{lat}$ to the longitudinal force $-F_{long}$ in dependence of the angel of contact ψ (The gliding amount ds at Q1 contributes no virtual work since $ds \perp F_N$ as long as no friction is assumed $F_T = 0$):

Using $dx = \sin\psi$ and $dy = \cos\psi$ yields:

$$(-F_{long})(-dx) + (-F_{lat})\,dy = 0 \text{ and thus } F_{lat} = \tan\psi\, F_{long} = \hat{K}\, F_{long}.$$

Additionally considering the retaining friction force at the contact Q1, the virtual work needs to be extended by a frictional term which is given by the virtual displacement ds at the contact, the normal force F_N at this point and the effective coefficient of friction $\mu_0 = \tan\vartheta_0$ between the grains where corrections contributed by irregularities of the surface, described by χ in the former chapter need to be included in μ_0 as well. Beyond the condition of stability, the „active" state is assumed, where the frictional component effects the maximum resistance to the deformation:
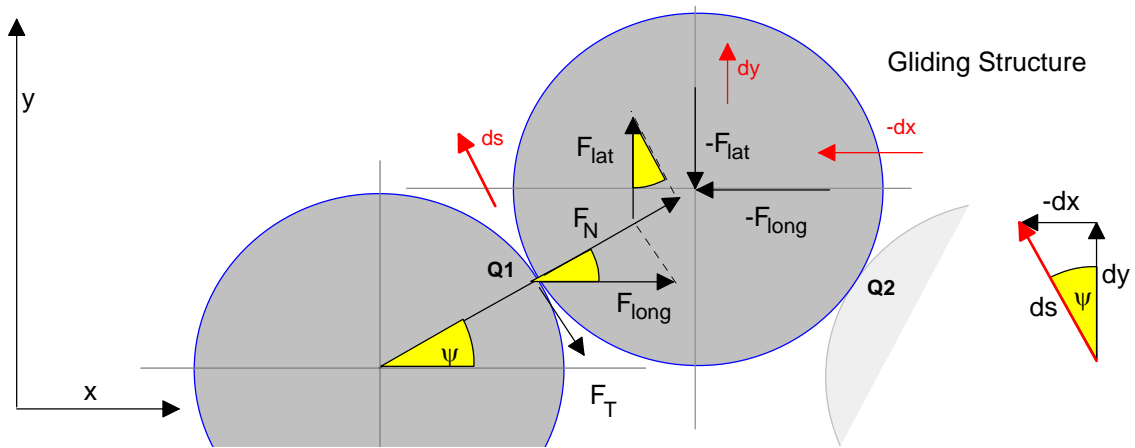

FIG. 82. Retaining friction forces in preliminary model

$$(-F_{long})(-dx) + (-F_{lat})\,dy + \mu_0 F_N(-ds) = 0$$

$$F_{long}\,dx = F_{lat}\,dy + \mu_0 F_N\,ds = F_{lat}\,dy + \tan\vartheta_0(\sin\psi F_{lat} + \cos\psi F_{long})\,\frac{dy}{\cos\psi}$$

$$F_{long}\,\frac{dx}{dy} = F_{lat} + \tan\vartheta_0 \tan\psi F_{lat} + \tan\vartheta_0 F_{long}$$

$$F_{lat}\,(1 + \tan\vartheta_0 \tan\psi) = F_{long}\,(\tan\psi - \tan\vartheta_0)$$

$$F_{lat} = F_{long}\left(\frac{\tan\psi - \tan\vartheta_0}{1 + \tan\vartheta_0 \tan\psi}\right) = F_{long}\,\tan(\psi - \vartheta_0)$$

Remark: In this simplified model the torsional moment introduced by friction at contact Q1 is expected to be compensated by the identically working mechanism at the opposite contact Q2 in the symmetric case.

Under such perception, the average lateral stress factor $\overline{K}$, which is taken from the force per grain, is determined by the tangents of the reduced angle of contact, weighted by the number of contacts exceeding the Angle of Friction and therefore contributing to the lateral stress. All other contacts are taken to be completely stiff since they are overdetermined by immobile adjacent cylinders. The average is to be taken for all angles of contact ψ up to the limit $\xi = \frac{\pi}{3}$ which is the geometrically maximum possible angle of contact for monodispersed cylindrical media.

This most basic approach results in: (with substitution $u = \psi - \vartheta_0$ and therefore $du = d\psi$):

$$\overline{K} = \frac{3}{\pi} \int_{\vartheta_0}^{\frac{\pi}{3}} \tan(\psi - \vartheta_0) \, d\psi = \frac{3}{\pi} \int_{\vartheta_0 - \vartheta_0 = 0}^{\frac{\pi}{3} - \vartheta_0} \tan(u) \, du = -\frac{3}{\pi} \ln \cos\left(\frac{\pi}{3} - \vartheta_0\right)$$

The resulting stress factors are plotted to the graph together with the LLO measurements readings for comparison:
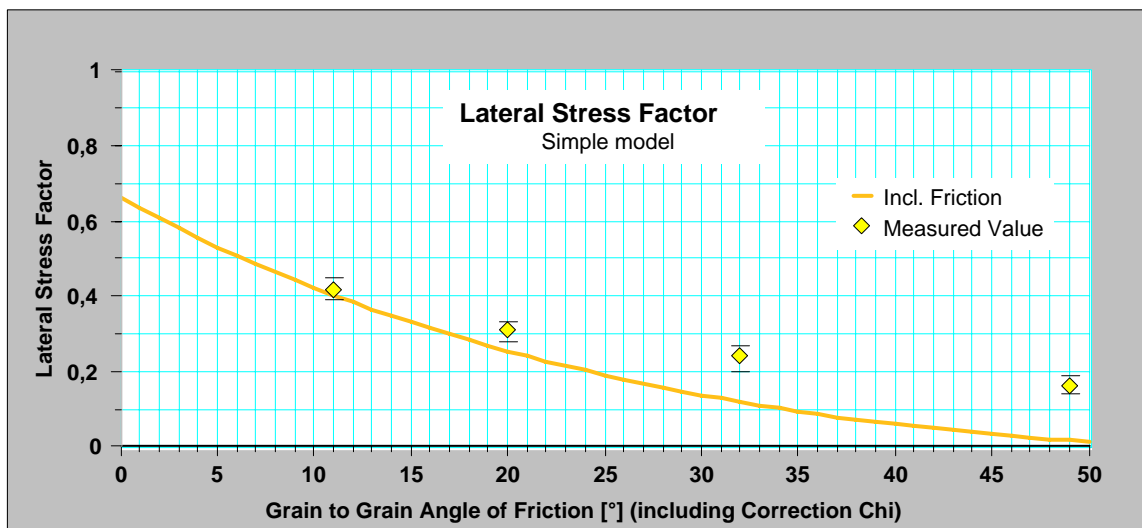

FIG. 83. LLO-Measurement of Lateral Stress Factor and result of highly simplified model (File: SimplifiedModelLLO.123)

Obviously, this model is too fragmentary for the measurement readings to describe. Nevertheless, it leads to some interesting conclusions:

- Even for frictionless granular media, this concept does not result in a Lateral Stress Factor of 1 but about $\overline{K}(\vartheta_0 = 0) \simeq 0.67$ which points out some structural influence besides the pure frictional portion.

- In general, even the improved model highly underestimates the Lateral Stress Factor, measured in our experiment, especially for high angles of friction. Thus, the approach made here serves as a rather incomplete model and requires considering many more details.

11. 2 Monte Carlo Modelling

Improving the model, we need to carefully consider possible configurations and situations of a single grain in a granular environment which may occur. Doubtless, only a small selection of mechanisms can be treated, but the model discussed in the section above was apparently much too restricted. After all, the selforganising processes are assumed to have not much influence on the LLO-situation. Yet, we need to include the most significant mechanisms in order to gain a more compatible model.

11. 2. 1 Modelling Force Chains

The more general system consists of a set of parallel chains of cylinders, bearing the longitudinal force F_x and generating lateral forces per grain F_y which are taken over and responded by the adjacent chains in order to keep the equilibrium.
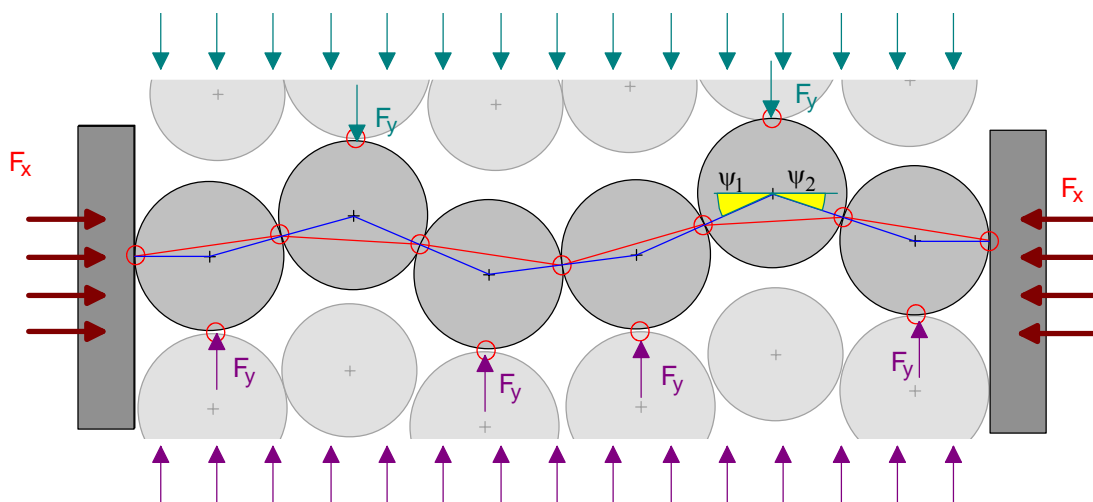

FIG. 84. Model of parallel chains of cylinders bearing the longitudinal force

Since all chains are moved synchronously, the interaction of the parallel chains is assumed to be low. Within each chain the contacts between the cylinders are equally distributed within a geometrically possible range of contacting angles. For every cylinder in the chain, mechanisms can be established which yield the lateral forces while the equilibrium of forces and torsional moments are strictly observed. In conjunction with the probability of the occurrence of such contacts, an averaged lateral force of such a contact may be calculated.

Geometrical considerations contribute the mean size of a chain like this and allow to transform the forces to mean stress values, which may serve for comparison to the values read from the experiment.

11. 2. 2 Simulational Approach

In a multi-particle system like a granular medium, every change in the value of a variable at a certain location consequently alters the complete system. Equilibrium can only be fulfilled all over the total model. Thus, any attempt to isolate a part of it actually implies the assumption of a limited range for any interaction by damping or self organisational mechanisms. This aspect is discussed in detail in a later chapter (13.3. *Modelling Structures in Granular Material*).

The basic model cannot be restricted to a single contact nor can it comprise the whole two-dimensional matrix of cylinders. In the present approach only force bearing chains are separated from the granular system. Interaction between each chain and the surrounding granular system is assumed to be restrictable to normal contacts transmitting normal and possibly transversal forces.

Since the intention of the present considerations aims at mere plausibility computations, we accept the restriction to force chains and averaged lateral forces. Yet, equilibrium of forces and torsional moments needs to be fulfilled for every single cylinder in the chain, which necessitates to consider the impact of a local modification to the complete chain. For instance, the introduction of a longitudinal force propagates through all the chain and thus affects every single member in the same way as does the application of a torsional moment at any point of the chain.

In order to treat this long range interaction in a proper way, we decided to compute a stochastic set of complete force chains by classical Monte Carlo Methods.

11. 2. 3 Software Aspects

All the simulation software was written in Object Pascal and developed in Borland Delphi 7.0 environment. This 'Integrated Development Environment' allows for easy encoding on a direct graphic surface in order to simplify the user interface on the one hand, on the other hand permits very basic operations directly written in assembler code.

As no general Simulation Software was used, the computation was formulated directly in the code written for a unique application. Several additional software components, originally written for other projects, were available to display the results and provide simple graphic cross-checks.

The code can be found on the attached Compact Disc, which also includes a Runtime-Version of the software.

All data were collected and computed in one large data array allowing fast processor access and displayed in detail on a data grid in order to check results easily. Furthermore the geometrical situation and the calculated forces and torsional moments were shown on a graphical panel giving a direct overview of the current iterations.
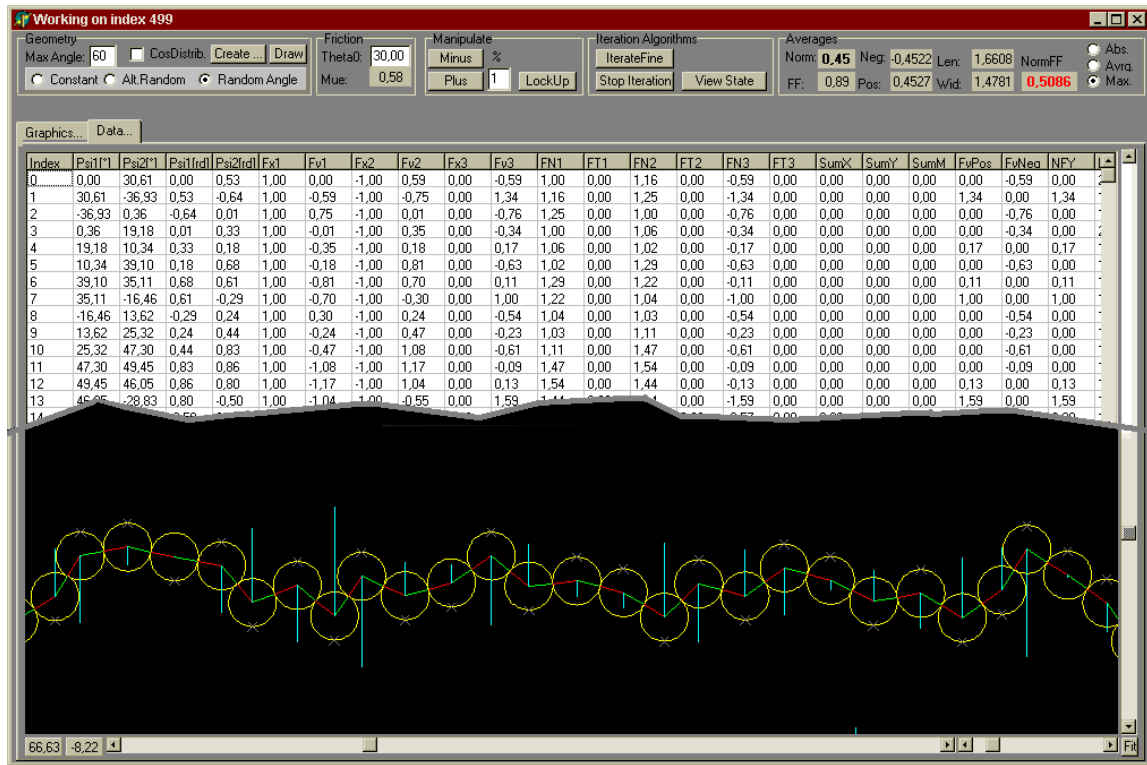
FIG. 85. Screen Display of Simulation Software

11. 2. 4 Proceeding

A virtual force chain is built up following some rules of construction: In accordance with previous considerations, a contact is placed on any point at the circumference at an angle of contact $\psi \leq \xi$, taking into account the geometrical restriction of cylinders with equal radii. A rather large number of cylinders are assembled (5000) in order to obtain results of good statistical significance. The distribution of the contact angles was chosen constant or alternatively proportional to $\cos \psi$.

After building the chain, a longitudinal force $F_x = 1$ is applied to the leftmost cylinder. Then, step by step the force resulting at the next contact is calculated based on equilibrium of forces and torsional moments depending on the angles of contact. Lateral contacts on top or at the bottom of the cylinders are used to support the chain introducing only normal forces but no transversal forces.

Under such load, the mean transversal supporting forces were calculated with respect to the applied longitudinal chain force. Transmitting no torsional moments, this state is equal to the only situation, which a granular force chain can form when frictional parameters are zero.

As soon as friction is introduced, all contacts are capable to transmit torsional moments as well. The active state requires all contacts to bear most of the lateral forces just by friction and leave only the minimum of supporting lateral forces to the environment. In order to simulate this situation, every triple of cylinders is recalculated, unloading the supporting central contact by a small percentage while keeping the border situation to both the left and the right adjacent cylinders unmodified.

After such a step all concerned contacts are checked to be certain of transmitting only torsional moments which are covered by the possible friction at the contact. In case the moments exceed the ability of the contact, the trial is revoked otherwise the new state is kept and another step is applied.

When no more unloading is possible all over the considered chain without exceeding the limit of frictional transmission of tangential forces, the state is assumed to be 'active' and thus represents the minimum lateral supporting force.

11. 3 The Stochastic Model in Detail

11. 3. 1 The Basic Cell

A single cylinder is taken to be the basic cell, of which a granular chain consists. It's possible contacts to the neighbours, together with their probability, define the mean forces of the cell.

A single cylinder is held in it's place by the bearing contacts. In two dimensions there is a maximum number of six contacts available, but in reality only very few contacts in fact transfer forces, because otherwise the equations of equilibrium are highly over-determined. Considering the two vectorial equations yielded by the equilibrium of forces and torsional moments, we can reduce the number of effective contacts within a chain to two. Additional lateral contacts are assumed to only respond to the created lateral forces, where further retro-activity is not taken into account.
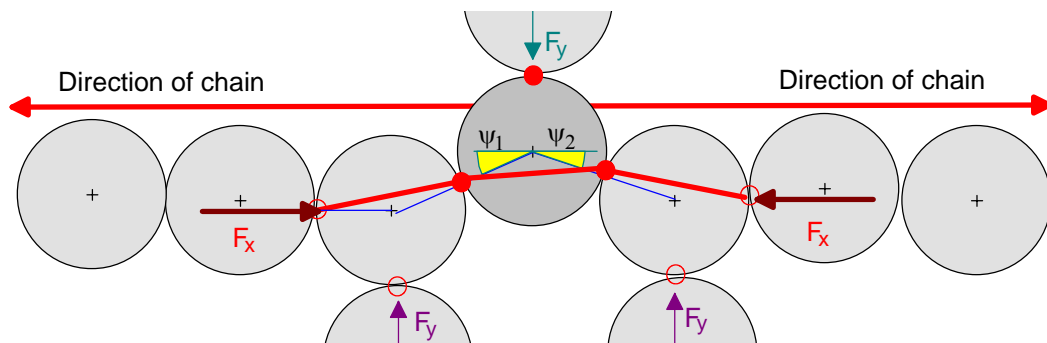
FIG. 86. Single cylinder within a chain, three dominating contacts

Remark: Certainly the process of filling the volume with cylinders under the influence of gravity already introduces braking of symmetry and constitutes more contacts than two. Nevertheless the first steps of deformation concentrate the forces to the relevant contacts, all others are assumed to be released and have no more influence.

11. 3. 2 Limit of Possible Angles

At the first glance we introduce a limit $\xi = 60^o$ for the possible angle of contact ψ, because equally sized granules underlie this structural boundary in two dimensions:
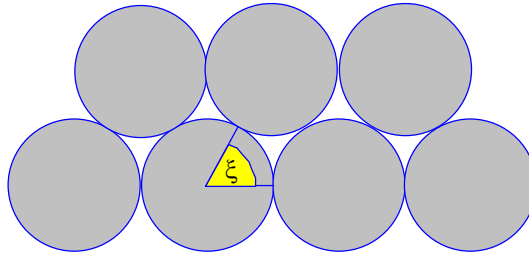
FIG. 87. Constant maximum angle of contact in monodisperse media

Under the influence of differently sized granules according to a grading curve, this limit needs affirmation. Therefore, a simple test has been performed by simulation:

The maximum angle of contact ξ is given by the contact of two elements, when a third element is touching both of them:
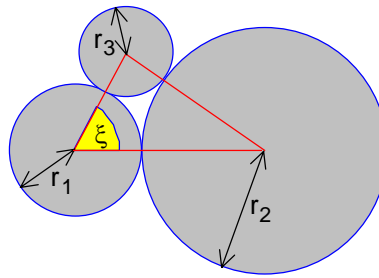

FIG. 88. Possible maximum angles of contact in polydisperse media

Thus we calculate ξ from the three radii according to the law of cosines:

$$\cos \xi = \frac{(r_1 + r_3)^2 + (r_1 + r_2)^2 - (r_2 + r_3)^2}{2(r_1 + r_3)(r_1 + r_2)}$$

This value is calculated for each configuration of $[r_1, r_2, r_3]$ and weighted by the combined probability $P^{conf[r1,r2,r3]} = P(r_1) \cdot P(r_2) \cdot P(r_3)$, given by their frequency of occurrence in the set. Impossible configurations are ignored.

The results are plotted vs. ξ and read like this:
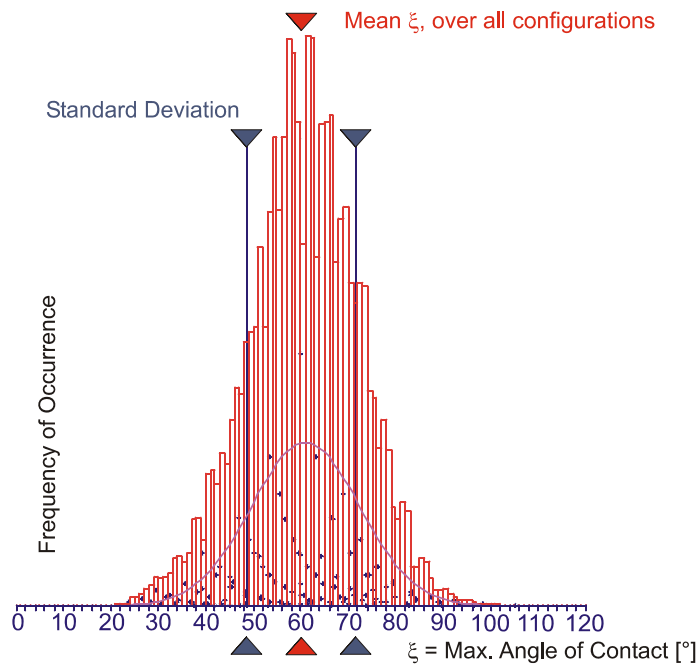
FIG. 89. Numerically obtained distribution of maximum angle of contact, based on the set of cylinders used here.

The weighted mean value results in exactly $\overline{\xi} = 60^o$, meeting our expectation due to reasons of symmetry. On the basis of the real distribution of radii, we obtain the shown standard deviation of 11.42^o. A higher number of really big granules (30mm) would increase the broadness of the distribution, but keep the mean value constant.

Remark: This result is only valid as long as the volume of interest is large enough to average the influence of inhomogeneities caused by small locally ordered structures as discussed in a later chapter (13.5.). Anticipating this discussion, the extent of such structures is found to be limited to 2 or 3 times the average diameter of a cylinder while the volume of the present measurement is of the order 20-30 cylinders per dimension. Thus, the estimation made above appears applicable in this case. Yet, investigating local effects in later chapters the local occurrence of order needs to be taken into account.

11. 4 Modelling a Frictionless Chain

11. 4. 1 Equilibrium of Forces on a Single Cylinder

A single cylinder within a force chain is held by three contacts $Q_{1..3}$, where Q_1 and Q_2 are the contacts at angles ψ_1, ψ_2 within the force chain. Q_3 is the supporting contact keeping the

chain stable. The later can be positioned at the top ($t = 1$) or at the bottom ($t = -1$) of the cylinder depending on the angles ψ_1 and ψ_2. In the approach employed here, where stochastic positioning of the cylinders is assumed and where macroscopic structures have not yet been generated by the shear deformation, no variation of the position Q_3 is taken into account since the central position is expected in average.
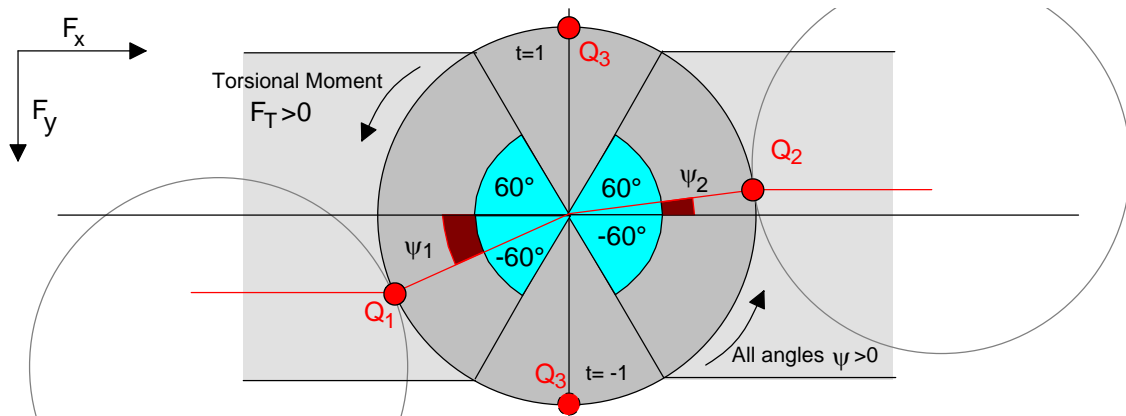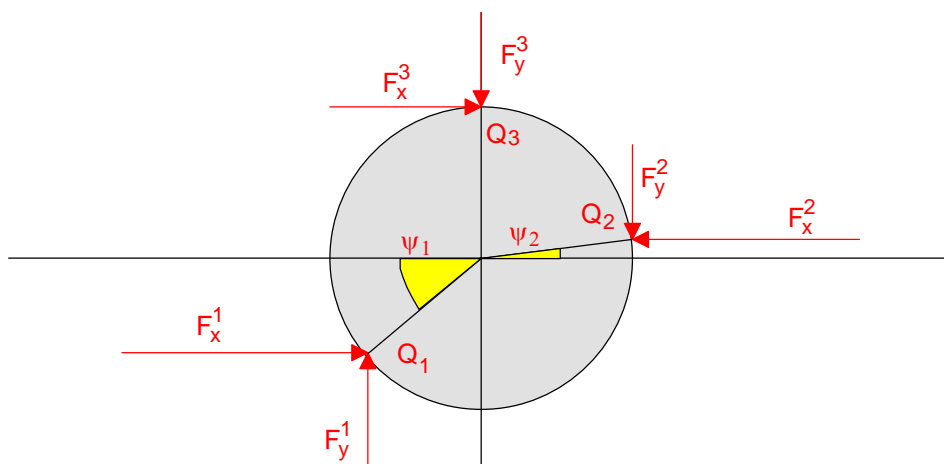

FIG. 90. Definition of possible contacts for an isolated cylinder

At each contact Q_i forces are determined:

Contact Q_1: F_x^1 and F_y^1

Contact Q_2: F_x^2 and F_y^2

Contact Q_3: F_x^3 and F_y^3

In order to compute torsional moments, the rectangular forces can be expressed as tangential and normal forces:

Contact Q_1:

$$F_N^1 = F_x^1 \cos \psi_1 - F_y^1 \sin \psi_1$$

$$F_T^1 = F_x^1 \sin \psi_1 + F_y^1 \cos \psi_1$$

Contact Q_2:

$$F_N^2 = -F_x^2 \cos \psi_2 + F_y^2 \sin \psi_2$$

$$F_T^2 = -F_x^2 \sin \psi_2 - F_y^2 \cos \psi_2$$

Contact Q_3:

$$F_N^3 = -t \cdot F_y^3$$

$$F_T^3 = -t \cdot F_x^3$$

Equilibrium requires to fulfill three equations simultaneously:

$$\sum F_x = F_x^1 + F_x^2 + F_x^3 = 0$$

$$\sum F_y = F_y^1 + F_y^2 + F_y^3 = 0$$

$$\sum M = F_T^1 + F_T^2 + F_T^3 = 0$$

Based on this and depending on the considered situation, the lateral force F_y^3, with respect to the applied longitudinal force $F_x = 1$ can be calculated and averaged through all possible combinations of contact angles ψ_i

11. 4. 2 Basic Solution: Propagation of a Longitudinal Force

The very basic case of a vector force (F_x^1, F_y^1) applied at the left side of a force chain propagating through the chain to the right side can be calculated easily:

Forces F_x^1 and F_y^1 are given, only normal forces F_y^3 are assumed to support the chain setting $F_x^3 = 0$ This implies that no torsional moment is introduced or lost through the supporting contacts, i.e. contact Q3 is assumed frictionless.

In this case three unknown variables correspond to three equations of equilibrium. Thus, a linear system of equations is determined:

$$\sum F_x = 0: \qquad F_x^1 + F_x^2 + F_x^3 = 0$$

$$\sum F_y = 0: \qquad F_y^1 + F_y^2 + F_y^3 = 0$$

$$\sum F_T = 0: \qquad -F_x^2 \sin \psi_2 - F_y^2 \cos \psi_2 + F_x^1 \sin \psi_1 + F_y^1 \cos \psi_1 - t \cdot F_x^3 = 0$$

which yields:

$$F_x^2 = -F_x^1 - F_x^3$$

$$F_y^2 = \frac{-F_x^1 \sin \psi_2 - F_x^3 \sin \psi_2 - F_x^1 \sin \psi_1 - F_y^1 \cos \psi_1 + t \cdot F_x^3}{\cos \psi_2}$$

$$F_y^3 = \frac{-F_x^1 \sin \psi_2 - F_x^3 \sin \psi_2 - F_x^1 \sin \psi_1 - F_y^1 \cos \psi_1 + t \cdot F_x^3 - F_y^1 \cos \psi_2}{\cos \psi_2}$$

Setting $F_x^3 = 0$, we obtain:

$$F_x^2 = -F_x^1$$

$$F_y^2 = \frac{-F_x^1 \sin \psi_2 - F_x^1 \sin \psi_1 - F_y^1 \cos \psi_1}{\cos \psi_2}$$

$$F_y^3 = \frac{-F_x^1 \sin \psi_2 - F_x^1 \sin \psi_1 - F_y^1 \cos \psi_1 - F_y^1 \cos \psi_2}{\cos \psi_2}$$

Substituting the results to the equations of equilibrium confirms the computation (see Appendix MAPLE Files on the attached Compact Disk).

This result evaluates to a Lateral Force Factor of

$$\widehat{K^{stoch}} = -\frac{\sin \psi_1 + \sin \psi_2 + \eta(\cos \psi_1 + \cos \psi_2)}{\cos \psi_2}, \qquad \eta = \frac{F_y^1}{F_x^1}$$

which could be averaged with no effort for all sensible angles of contact $\psi_{1..2}$. However, the unknown ratio η is given by the situation of the adjacent cylinders and therefore allows for none but an iterative i.e. simulational determination.

Remark: Since the geometrical extent of the cell is not yet introduced, $\widehat{K^{stoch}}$ describes the ratio of forces per cell. Later on it will be related to a length unit and be written as K^{stoch}.

11. 5 Introduction of Torsional Moments

The force chain system described before does not introduce torsional moments, neither from the application point nor at the supporting contacts. Therefore no torsional moments are transmitted by any contact. This is the case, where no friction is needed or available.

As soon as non zero friction allows for the transmittance of torsional moments, the supporting lateral force can be diminished while the longitudinal contacts Q_1 and Q_2 take over the necessary moments to keep equilibrium. These moments are transmitted through all the chain until they are compensated by the moments of another unloaded lateral contact.

Since the overall equilibrium of torsional moments needs to be fulfilled, the average moment in comparably small volumes is zero. Thus, the balancing takes place as close as possible.

11. 5. 1 Unloading Lateral Contacts

In order to model this section of a force chain the equilibrium of three adjacent cylinders was computed. Their basic state is taken from the already computed force chain in equilibrium. Then, the lateral force $^{1..3}F_y^3$ is reduced by a certain small percentage and the equilibrium is recalculated while keeping the contact forces $^1F_x^1$, $^1F_y^1$ and $^3F_x^2$, $^3F_y^2$ at the border of the section unmodified. In this way, the chain remains mainly as it is, but the local supporting forces decrease. The tangential forces at the chain contacts $^1Q_2$ and $^2Q_2$ which unload the contact $^1Q_3$ increase as long as they can be taken over by the given friction.

Since the friction limit may be exceeded by every step, it must be observed continuously during the unloading process. Furthermore the unloading steps need to be very small in order to approach the active state as close as possible.

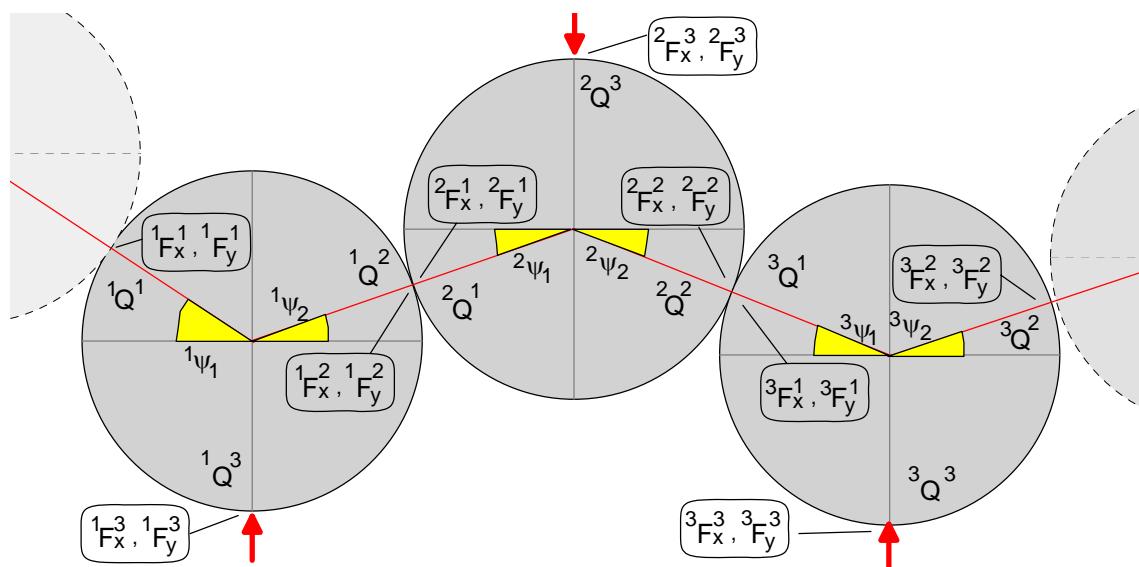The following drawing defines the variables used in calculating the equilibrium:

FIG. 91. Identification of variables at three adjacent cylinders

Due to the symmetry of the system some identities are given:

$$^1\psi_2 = {}^2\psi_1, \quad {}^2\psi_2 = {}^3\psi_1,$$

$$^1F_x^2 = -{}^2F_x^1, \quad {}^1F_y^2 = -{}^2F_y^1,$$

$$^2F_x^2 = -{}^3F_x^1, \quad {}^2F_y^2 = -{}^3F_y^1.$$

A total of nine equations of equilibrium corresponds to nine independent variables. Thus, the border forces and the vertical supporting force of the central cylinder are to be preset, all the rest is determined by the linear system of equations.

$$^1F_x^3 + {}^1F_x^2 = -{}^1F_x^1$$

$$^1F_y^3 + {}^1F_y^2 = -{}^1F_y^1$$

$$-t_1 \cdot {}^1F_x^3 - {}^1F_x^2 \sin{}^1\psi_2 - {}^1F_y^2 \cos{}^1\psi_2 = -{}^1F_x^1 \sin{}^1\psi_1 - {}^1F_y^1 \cos{}^1\psi_1$$

$$-{}^1F_x^2 + {}^2F_x^3 + {}^2F_x^2 = 0$$

$$-{}^1F_y^2 + {}^2F_y^2 = -{}^2F_y^3$$

$$-{}^1F_x^2 \sin{}^2\psi_1 - {}^1F_y^2 \cos{}^2\psi_1 - t_2 \cdot {}^2F_x^3 - {}^2F_x^2 \sin{}^2\psi_2 - {}^2F_y^2 \cos{}^2\psi_2 = 0$$

$$-{}^2F_x^2 + {}^3F_x^3 = -{}^3F_x^2$$

$$-{}^2F_y^2 + {}^3F_y^3 = -{}^3F_y^2$$

$$-{}^2F_x^2 \sin{}^3\psi_1 - {}^2F_y^2 \cos{}^3\psi_1 - t_3 \cdot {}^3F_x^3 = {}^3F_x^2 \sin{}^3\psi_2 + {}^3F_y^2 \cos{}^3\psi_2$$

This system can be solved and leads to lengthy expressions for all the internal forces

$$^1F_x^2 = -{}^2F_x^1, \quad {}^1F_y^2 = -{}^2F_y^1, \quad {}^2F_x^2 = -{}^3F_x^1, \quad {}^2F_y^2 = -{}^3F_y^1.$$

and for the lateral supporting forces $^{1..3}F_y^3$, $^{1..3}F_x^3$, which can be found in full length on the attached Compact Disk as Maple-Files.

11. 5. 2 Unloading Lateral Forces in Symmetric Cases

The equations derived above unfortunately diverge for mathematical reasons for the particular cases $(t_1 = -1,\ t_2 = +1,\ t_3 = -1)$ and $(t_1 = +1,\ t_2 = -1,\ t_3 = +1)$ while they are uncritical for all other cases.

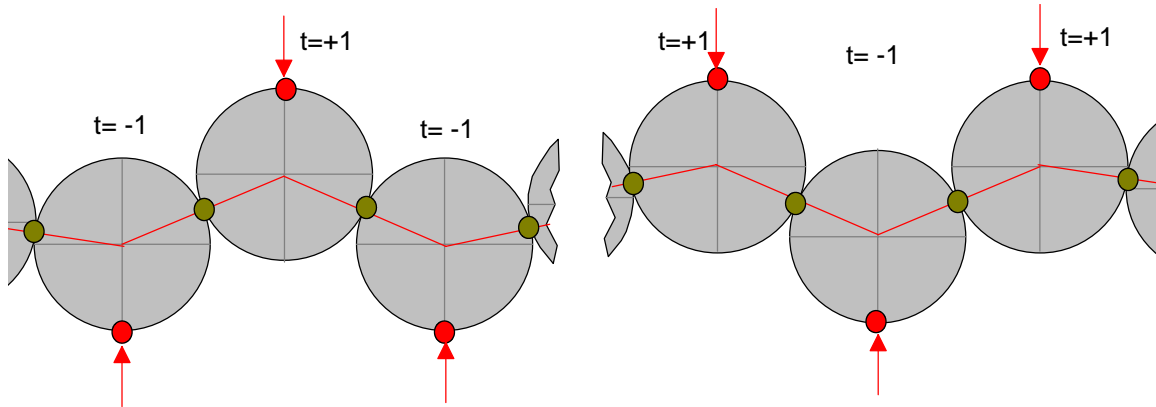Thus, these two particular situations need to be considered separately:

FIG. 92. Symmetrical cases needing extra consideration

Since forces are superimposable, it is sufficient to calculate only the variation of the central supporting force at $^2Q_3$, where longitudinal chain forces are not affected. Therefore, the contacts at the left and the right of the section $^1Q_1$ and $^3Q_3$ within the chain can be neglected at all and the following simplified systems remains for the **first case** ($t_1 = -1, \ t_2 = +1, \ t_3 = -1$):
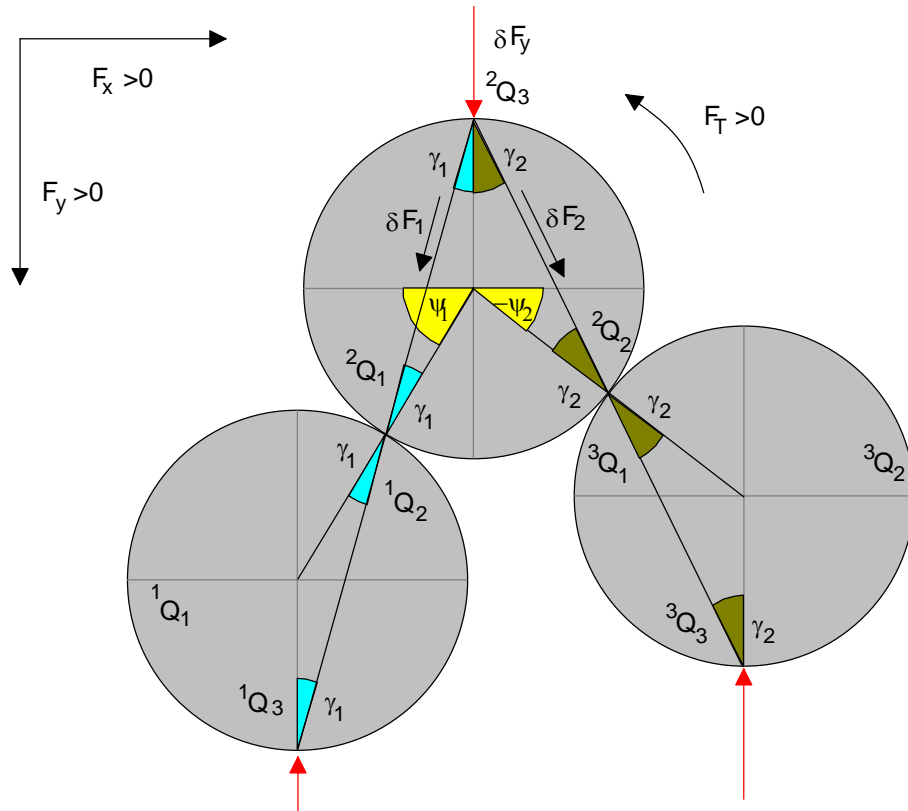
FIG. 93. First case, identification of variables

The newly introduced angles $\gamma_{1..2}^{(-,+,-)}$ are determined (both counted positive):

$$\gamma_1^{(-,+,-)} = \frac{\pi}{4} - \frac{\psi_1}{2} \quad \text{and} \quad \gamma_2^{(-,+,-)} = \frac{\pi}{4} + \frac{\psi_2}{2}$$

The variation of the central supporting force δF_y splits up into the forces $\delta F_{1..2}$ along the straight lines through the contact points:

$$\delta F_1 \cos \gamma_1 + \delta F_2 \cos \gamma_2 = \delta F_y$$

$$\delta F_1 \sin \gamma_1 - \delta F_2 \sin \gamma_2 = 0$$

Solving this set of equations results in:

$$\delta F_1 = \delta F_y \frac{\sin \gamma_2}{\sin(\gamma_1 + \gamma_2)}$$

$$\delta F_2 = \delta F_y \frac{\sin \gamma_1}{\sin(\gamma_1 + \gamma_2)}$$

This leads to force components at the relevant external contact points ${}^1Q_3$ and ${}^3Q_3$:

Contact ${}^1Q_3$:

$$\delta^1 F_N^3 = \delta F_1 \cos \gamma_1$$

$$\delta^1 F_T^3 = -\delta F_1 \sin \gamma_1$$

$$\delta^1 F_x^3 = -\delta F_1 \sin \gamma_1$$

$$\delta^1 F_y^3 = \delta F_1 \cos \gamma_1$$

Contact ${}^3Q_3$

$$\delta^3 F_N^3 = \delta F_2 \cos \gamma_2$$

$$\delta^3 F_T^3 = \delta F_2 \sin \gamma_2$$

$$\delta^3 F_x^3 = \delta F_2 \sin \gamma_2$$

$$\delta^3 F_y^3 = \delta F_2 \cos \gamma_2$$

Internal force components at contact points $^1Q_2$ rsp. $^2Q_1$ and $^2Q_2$ rsp. $^3Q_1$ are calculated accordingly:

Contact $^1Q_2$ rsp. $^2Q_1$

$$\delta^1 F_x^2 = -\delta^2 F_x^1 = -\delta F_1 \sin \gamma_1$$

$$\delta^1 F_y^2 = -\delta^2 F_y^1 = \delta F_1 \cos \gamma_1$$

Contact $^2Q_2$ rsp. $^3Q_1$

$$\delta^2 F_x^2 = -\delta^3 F_x^1 = -\delta F_2 \sin \gamma_2$$

$$\delta^2 F_y^2 = -\delta^3 F_y^1 = -\delta F_2 \cos \gamma_2$$

Absolute normal and tangential forces at the contacts $^1Q_{2..3}$, $^2Q_{1..3}$, $^3Q_{1..2}$, are calculated by adding the particular offset δF to the basic forces of the previous state. The contacts $^1Q_1$ and $^3Q_2$ remain unaltered.

The **second case** ($t_1 = +1$, $t_2 = -1$, $t_3 = +1$) is calculated in the same way:
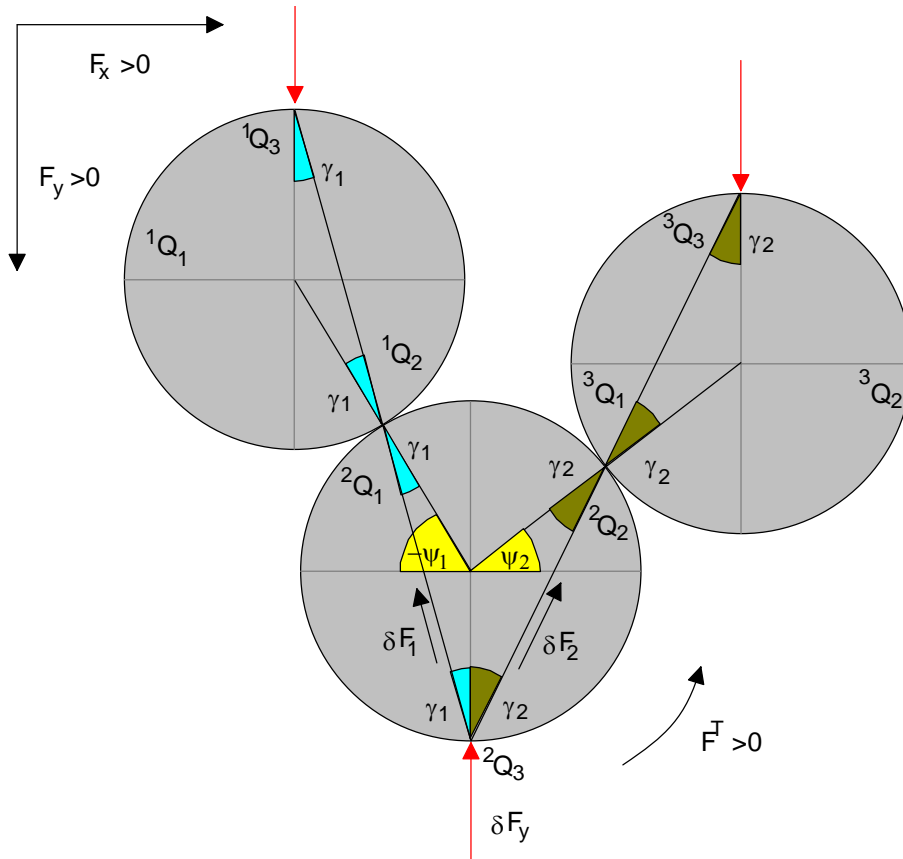
FIG. 94. Second symmetric case, identification of variables

Since angles $\gamma_{1..2}^{(+,-,+)}$ are also counted positive, they are determined:

$$\gamma_1^{(+,-,+)} = \frac{\pi}{4} + \frac{\psi_1}{2} \quad \text{and} \quad \gamma_2^{(+,-,+)} = \frac{\pi}{4} - \frac{\psi_2}{2}$$

Splitting δF_y into $\delta F_{1..2}$ yields as before:

$$\delta F_1 = \delta F_y \frac{\sin \gamma_2}{\sin(\gamma_1 + \gamma_{2)}}$$

$$\delta F_2 = \delta F_y \frac{\sin \gamma_1}{\sin(\gamma_1 + \gamma_{2)}}$$

This again leads to force components at the external contact points $^1Q_3$ and $^3Q_3$:

Contact $^1Q_3$:

$$\delta^1 F_N^3 = \delta F_1 \cos \gamma_1$$

$$\delta^1 F_T^3 = \delta F_1 \sin \gamma_1$$

$$\delta^1 F_x^3 = \delta F_1 \sin \gamma_1$$

$$\delta^1 F_y^3 = \delta F_1 \cos \gamma_1$$

Contact $^3Q_3$

$$\delta^3 F_N^3 = \delta F_2 \cos \gamma_2$$

$$\delta^3 F_T^3 = -\delta F_2 \sin \gamma_2$$

$$\delta^3 F_x^3 = -\delta F_2 \sin \gamma_2$$

$$\delta^3 F_y^3 = \delta F_2 \cos \gamma_2$$

Contact $^1Q_2$ rsp. $^2Q_1$

$$\delta^1 F_x^2 = -\delta^2 F_x^1 = \delta F_1 \sin \gamma_1$$

$$\delta^1 F_y^2 = -\delta^2 F_y^1 = \delta F_1 \cos \gamma_1$$

Contact $^2Q_2$ rsp. $^3Q_1$

$$\delta^2 F_x^2 = -\delta^3 F_x^1 = \delta F_2 \sin \gamma_2$$

$$\delta^2 F_y^2 = -\delta^3 F_y^1 = -\delta F_2 \cos \gamma_2$$

Remark: These equations can be identified with the first symmetric case, defining:

$$\gamma_1^{(-,+,-)} = \frac{\pi}{4} - \frac{\psi_1}{2} \quad \text{and} \quad \gamma_2^{(-,+,-)} = \frac{\pi}{4} + \frac{\psi_2}{2}$$

$$\gamma_1^{(+,-,+)} = -\left(\frac{\pi}{4} + \frac{\psi_1}{2}\right) \quad \text{and} \quad \gamma_2^{(+,-,+)} = -\left(\frac{\pi}{4} - \frac{\psi_2}{2}\right)$$

Using these equations allows to directly evaluate the modification of force components at every contact which results from a small unloading the central contact while equilibrium is kept all over the force chain.

11. 6 Coefficient of Geometry

The statistical considerations above only supply average forces per contact, respectively per basic cell. In order to make them comparable to measurements of stress the average extent of the basic cell needs to be known. This can be computed easily, observing the available angles of contact, weighted with the probability of occurrence.

11. 6. 1 Parameters

Two parameters turn out to be of significant influence: The type of distribution $P(\psi)d\psi$ of angles of contact ψ and the limiting angle ξ, up to which contacts are possible because of geometrical constraints.

Concerning distributions only two alternatives are to be discussed:

On the basis of a pure stochastic approach, the angles can be assumed evenly distributed.

$$P(\psi)d\psi = const.$$

Yet, if even a small amount of deformation needs to be taken into account, this assumption will not hold true. A minor mechanism of self organisation will shift contacts while deforming, until lateral forces are answered by appropriate lateral contacts and the local movement is stopped. Thus, compression in the longitudinal direction, which does not force any lateral motion will not be stopped while compression causing large lateral motion will be stopped immediately.
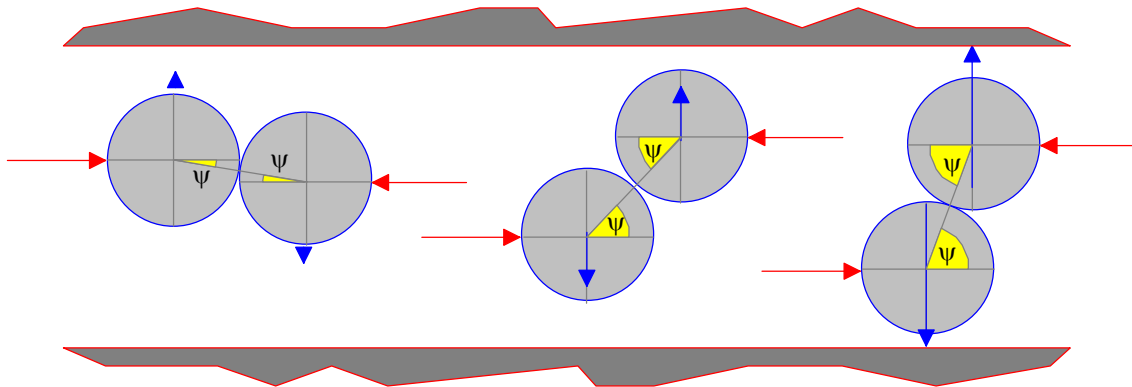
FIG. 95. Stopping probability depending on angle of contact ψ

Therefore, in a granular medium exposed to unidirectional motion we find angles of contacts only after the granules have contacted the sidewalls of a cell. Hence, contact angles will not occur with equal probability, but following a distribution like:
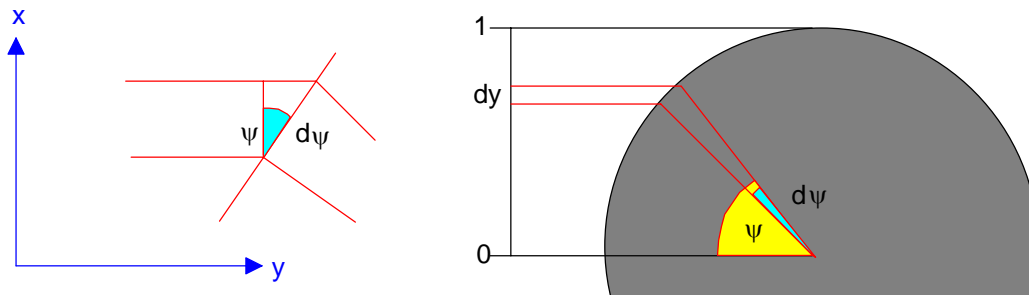
$$P(\psi)d\psi \sim \cos\psi \; .$$

FIG. 96. Linear deformation, leading to a COS distribution of contact angles

A constant probability Pdy , using $dy = \cos\psi \, d\psi$ yields

$$Pd\psi = C\cos\psi \, d\psi$$

In addition to this, the maximum available angle of contact ξ plays a significant role since averaging needs to be done over all possible configurations.

11. 6. 2 Definition of a Cell

A cell which represents a section of a force chain supported by one lateral contact at each side can be defined in the following manner:
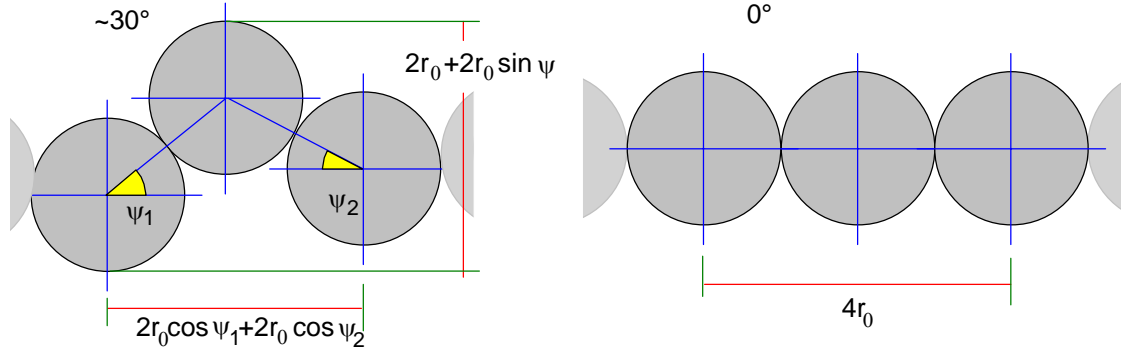
FIG. 97. Geometric extent of 'basic cell' depending on angles of contact ψ

Here, the horizontal extent of the basic cell, i.e. in the direction of the force chain, is given as:

$$\bar{s}_x = 2r_0 \cos \psi_1 + 2r_0 \cos \psi_2 \equiv 4r_0 \cos \psi \text{ (for averaging purposes),}$$

while the vertical height, i.e. the lateral with of a chain is

$$\bar{s}_y = 2r_0 + 2r_0 \sin \psi = 2r_0(1 + \sin \psi)$$

The form factor g is determined to correct the ratio of vertical to horizontal forces $\widehat{\widehat{K}} = \dfrac{F_y}{F_x}$ when transformed to measurable stresses $\overline{K} = \dfrac{\sigma_y}{\sigma_x} = g \cdot \widehat{\widehat{K}} = g \cdot \dfrac{F_y}{F_x}$ into a basic cell.

Using $F_x = \sigma_x \cdot \overline{s_y}$ and $F_y = \sigma_y \cdot \overline{s_x}$ we find the formfactor:

$$\frac{\sigma_y}{\sigma_x} = g \cdot \frac{F_y}{F_x}$$

$$g = \frac{\sigma_y \cdot F_x}{\sigma_x \cdot F_y} = \frac{\sigma_y \cdot \sigma_x \cdot \overline{s_y}}{\sigma_x \cdot \sigma_y \cdot \overline{s_x}} = \frac{\overline{s_y}}{\overline{s_x}}$$

11. 6. 3 General Formulation of the Form Factor:

Presuming *constant distribution* of angles of contact ψ up to the limiting angle ξ the norm is calculated:

$$1 = C \int_0^\xi d\psi = C(\xi - 0) \text{ resp. } C = \frac{1}{\xi}$$

Thus, we have

$$\overline{s_x^e} = \int_0^\xi \frac{2}{\xi} \cos \psi \; d\psi = \frac{2}{\xi} \sin \xi - 0 = \frac{2 \sin \xi}{\xi}$$

and

$$\overline{s_y^e} = 1 + \int_0^\xi \frac{1}{\xi} \sin \psi \; d\psi = 1 - \frac{1}{\xi} \cos \xi + \frac{1}{\xi} \cos 0 = 1 + \frac{1}{\xi} - \frac{\cos \xi}{\xi}.$$

This yields a general formfactor

$$g^e = \frac{\overline{s_y^e}}{\overline{s_x^e}} = \frac{1 + \dfrac{1}{\xi} - \dfrac{\cos \xi}{\xi}}{\dfrac{2 \sin \xi}{\xi}} = \frac{\xi + 1 - \cos \xi}{2 \sin \xi}$$

Using a *cos-shaped distribution* for the probability of an angle of contact ψ up to the limiting angle ξ changes the formulation as follows:

$$1 = C \int_0^\xi \cos \psi \; d\psi = C(\sin \xi - \sin 0) \;\; \text{resp.} \;\; C = \frac{1}{\sin \xi}$$

Thus, we have

$$\overline{s_x^c} = \int_0^\xi \frac{2}{\sin \xi} \cos^2 \psi \; d\psi = \frac{2\xi}{2 \sin \xi} + \frac{2}{4 \sin \xi} \sin 2\xi - 0 = \frac{1}{\sin \xi}\left(\xi + \frac{1}{2} \sin 2\xi\right)$$

$$\overline{s_x^c} = \frac{1}{\sin \xi}(\xi + \sin \xi \cos \xi)$$

and

$$\overline{s_y^c} = 1 + \int_0^\xi \frac{1}{\sin \xi} \sin \psi \; \cos \psi \; d\psi = 1 + \frac{1}{2 \sin \xi} \sin^2 \xi - 0 = 1 + \frac{1}{2} \sin \xi$$

which yields:

$$g^c = \frac{\overline{s_y^c}}{\overline{s_x^c}} = \frac{1 + \dfrac{1}{2} \sin \xi}{\dfrac{1}{\sin \xi}(\xi + \sin \xi \cos \xi)} = \frac{\left(1 + \dfrac{1}{2} \sin \xi\right) \sin \xi}{\xi + \sin \xi \cos \xi} = \frac{\sin \xi + \dfrac{1}{2} \sin^2 \xi}{\xi + \sin \xi \cos \xi}$$

The result of these two calculations is displayed in the following drawing:
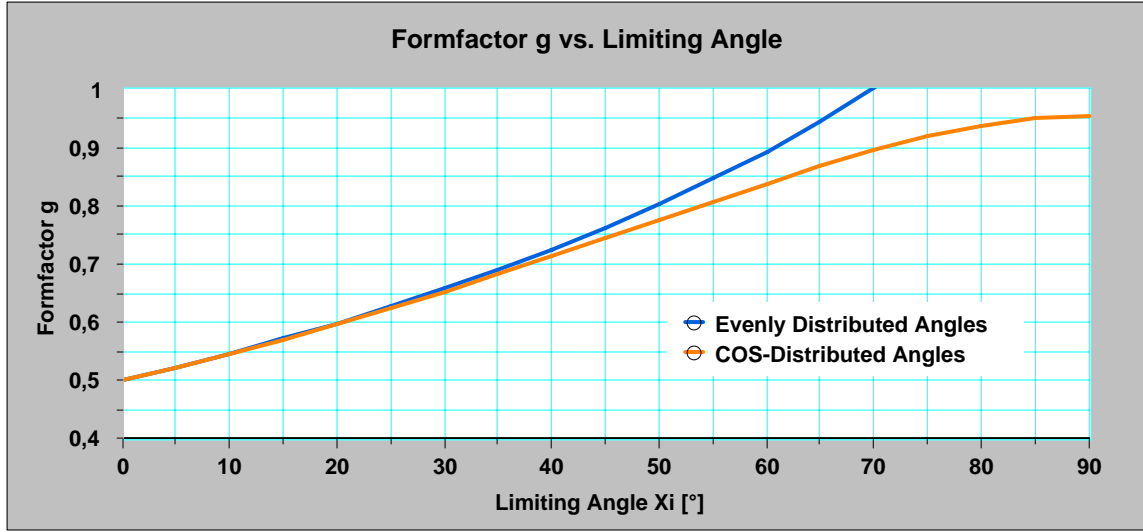
FIG. 98. Form factor *g* derived from the extent of a 'basic cell'   (File: Formfactor, General.123)

The form factor for the commonly used limiting angle $\xi = 60^o$ is determined to be

- $g^e(\xi = 60^o) = 0.893$ for evenly distributed angles of contact

- $g^c(\xi = 60^o) = 0.838$ for angles of contact following a COS-distribution.

11. 6. 4 Packing Ratios

From the calculated mean density of a force chain $2 \cdot \overline{s_x}$ and the associated width $\overline{s_y}$ of such a chain, the resulting mean packing ratio κ^{stoch}rsp. pore volume : $n^{stoch} = 1 - \kappa^{stoch}$, preconditioning monodisperse cylinders can be computed:

A two-dimensional volume of size a^2 is filled with n_y parallel chains comprising n_x cylinders with radius R.

$$n_y = \frac{a}{\overline{s_y}} \qquad n_x = \frac{a}{2 \cdot \overline{s_x}}$$

Hence the theoretical packing ratio is determined:

$$\overline{\kappa^{stoch,e}} = \frac{a^2}{2 \cdot \overline{s_x^e} \cdot \overline{s_y^e}} \frac{\pi R^2}{a^2 R^2} = \frac{\pi \xi^2}{4 \sin \xi (1 + \xi - \cos \xi)} \text{ (for constant distribution)}$$

$$\overline{\kappa^{stoch,c}} = \frac{a^2}{2 \cdot \overline{s_x^c} \cdot \overline{s_y^c}} \frac{\pi R^2}{a^2 R^2} = \frac{\pi \sin \xi}{2(\xi + \sin \xi \cos \xi)\left(1 + \frac{1}{2}\sin \xi\right)} \quad \text{(for COS distribution)}$$

The following graph shows the characteristics:
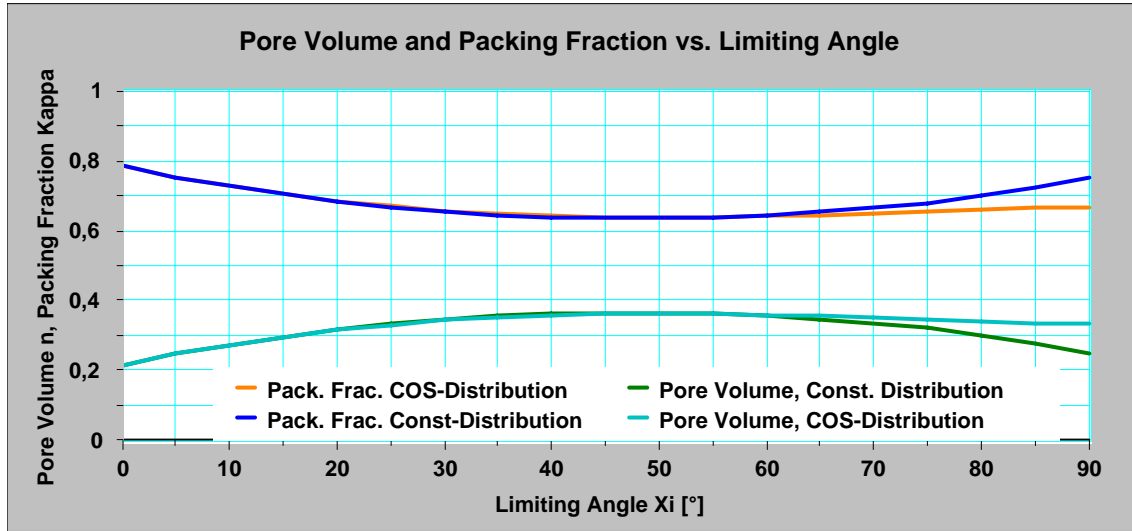
FIG. 99. Pore Volume *n* and packing fraction γ derived from the extent of a 'basic cell'   (File: Formfactor, General.123)

In particular, the theoretical packing fraction for the limiting angle $\xi = \frac{\pi}{3}$ is determined:

- $\kappa^{stoch,e}(\xi = 60^o) \simeq 0.643$ rsp. $n^{stoch,e}(\xi = 60^o) \simeq 0.357$ for evenly distributed angles of contact

- $\kappa^{stoch,c}(\xi = 60^o) \simeq 0.641$ rsp. $n^{stoch,e}(\xi = 60^o) \simeq 0.359$ for angles of contact following a COS-distribution

11. 7 Building Mean Values

The formulae developed in the previous chapter have been implemented to the compute simulation environment. Proceeding further, the results and the respective boundary conditions are discussed here.

11. 7. 1 Generating Force Chains

A virtual force chain is built by appending one cylinder after the other, beginning from the left boundary. Angles of contact were chosen stochastically by the internal random number generator of the DELPHI environment (Borland Inc.).

The distribution of contact angles was selectable as CONSTANT or proportional to the COS of the angle, always limited by a presetable angle ξ, which is set to $\xi = 60^o$. Two additional alternatives are available for test purposes: Alternating random and constant angles of contacts allow for preliminary checks.

In order to gain significant results, a fairly high number of 5000 cylinders was chosen.
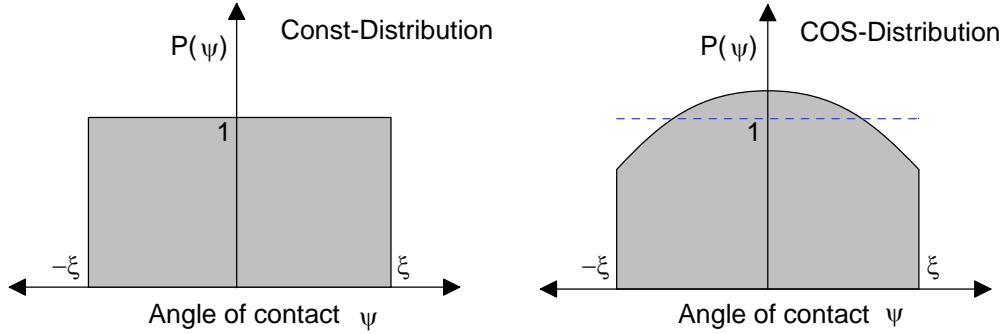
FIG. 100. Constant Distribution of contact angles vs. COS Distribution

11. 7. 2 Frictionless State

Modelling the equilibrium state for all concerned cylinders, a single horizontal force $F_x = 1$ was applied to the leftmost cylinder at $\psi = 0$.

After this, equilibrium for every cylinder was computed by the force propagation formulae. Supporting contacts were assumed at the top or at the bottom of the cylinder, basically depending on the difference of the contact angles. After finishing the computation the Top/Bottom indicator t is adapted to the resulting sign of the supporting lateral force F_y in order to model the support respectively.

Three equations of equilibrium require three preset variables to determine further three variables. Thus, besides the force components at the left contact F_x^1 and F_y^1 the tangential frictional force at the supporting contact F_x^3 needs to be preset. Its value was chosen $F_x^3 = 0$. This corresponds to the frictionless case where no contact is producing a moment due to the centre of each cylinder.

The supporting forces F_y^3 of every cylinder were weighted with the applied longitudinal force $F_x = 1$ and averaged over all cylinders:

$$\widehat{K_{9=0}^{stoch}} = \overline{F_y^3} = 0.463^{\pm 0.006}(95\% \text{ percentile})$$

This value needs to be converted into the conventional stress ratio by applying the geometrical form factor g^e resulting in:

$$K_{\vartheta=0}^{stoch} = 0.519^{\pm 0.007}(95\% \text{ percentile})$$

11. 7. 3 Unloading Support Contacts by Friction

Friction at a certain contact allows for transmittance of not only normal but also tangential forces. Yet, the amount of tangential force is not defined but only limited by the frictional ratio $\tan\vartheta_0 = \mu_0 = \dfrac{F_T}{F_N}$. In this paper, the „active state" which is subject to the present measurements is defined by the state where friction is used to unload the supporting lateral contacts as much as possible.

Since this state cannot be computed directly, it is approached iteratively by repeated attempts to reduce the supporting force at every member of the chain.

As already discussed, we know, that unloading a lateral (top/bottom) contact leads to tangential forces at the chain contacts which compensate for the lacking force. Such a variation is only applicable if the grain to grain friction allows to transmit the tangential force and if this is balanced in close proximity in order to observe the mean local equilibrium.

Modelling this mechanism, a loop tries to modify every contiguous triple of cylinders unloading the central supporting contact by $0.1\ ^o/_{oo}$ using the equations of equilibrium which are derived in the chapter before. After every step, the compatibility of the transmitted tangential forces with the frictional parameters is checked and hence the step possibly revoked.

For each triple of cylinders a maximum of 10 steps is tried, then the next triple becomes the subject of the unloading process. After all cylinders of the chain have been processed in this way, the chain is treated again in backwards direction to avoid systematical errors due to a preferred processing order.

Such operation is repeated up to 2000 times until the computed average lateral force factors improvement is less than $1\ ^o/_{oo}$, indicating that no more unloading can be done without exceeding the frictional limit of the granular force chain.

Several simulation cycles were conducted for different types of angular distributions (const and COS-shaped) and for a set of representative Angles of Friction $\vartheta_0 = 0...50^o$ with varying limiting angles $\xi = 55..65^o$.

The results already including the influence of the geometrical form factor are shown in the following graph:
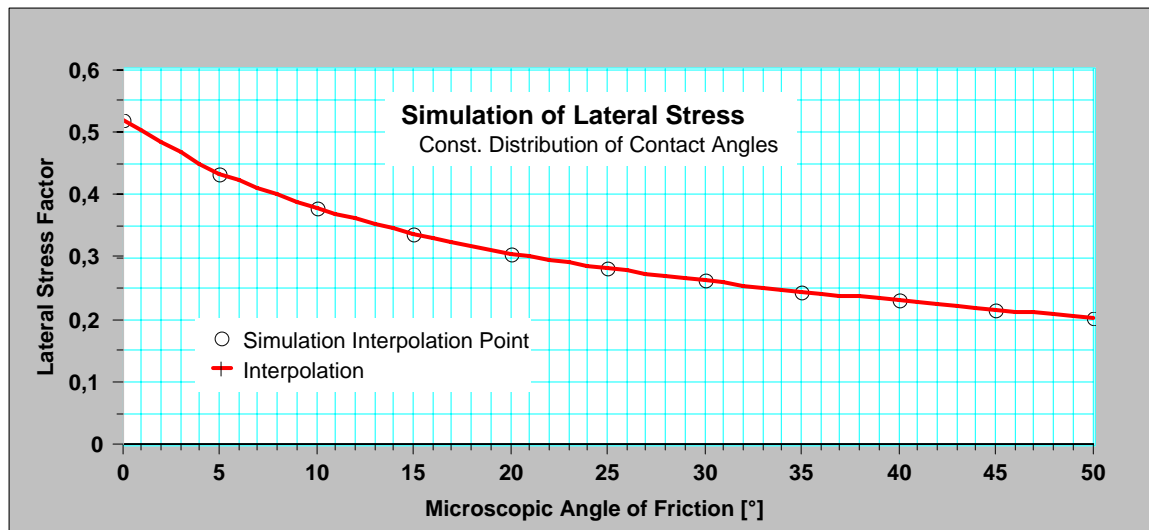

FIG. 101. Averaged lateral stress factor, using a constant distribution (File: NumSimulation.123)

Calculating the same on the basis of a distribution $P(\psi)d\psi \sim \cos\psi$ yields slightly different values, reflecting mainly the lower form factor g^c.
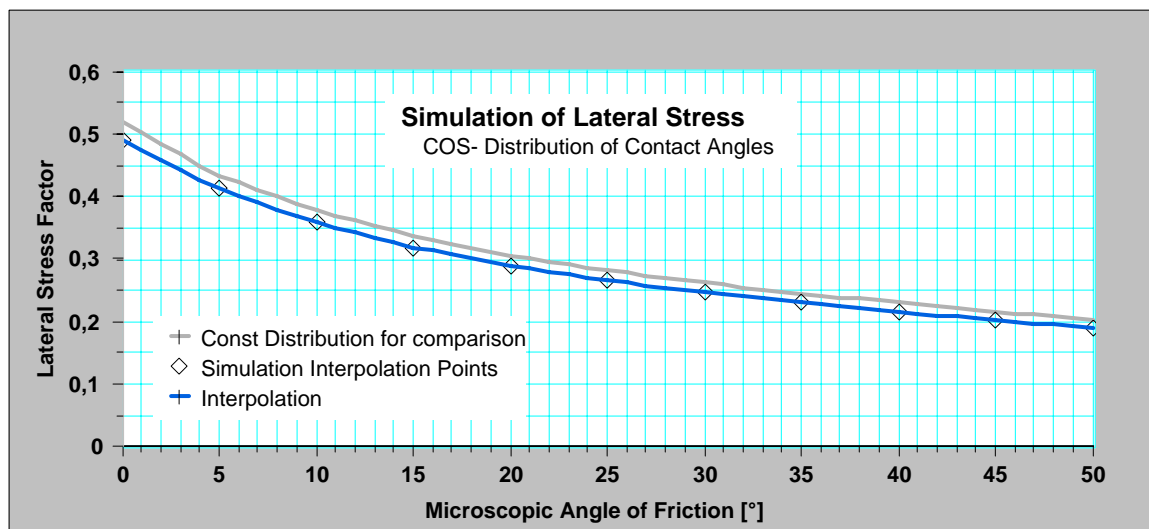

FIG. 102. Averaged lateral stress factor, using a COS distribution (File: NumSimulations.123)

The sensitivity of results against the selection of a different maximum angle of contact $\xi = 54^o$ is shown in the following graph:
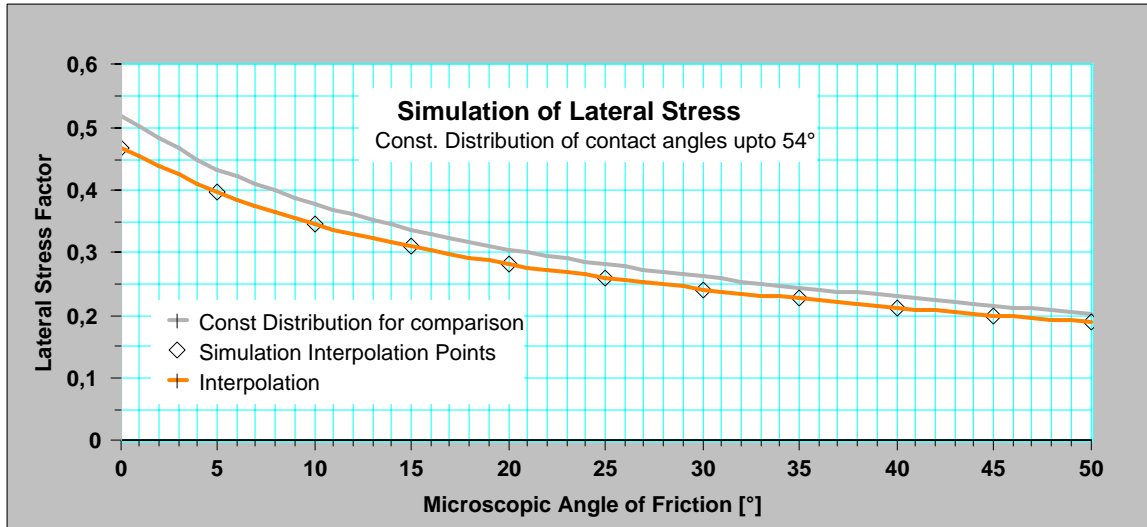
FIG. 103. Lateral Stress Factor using a Const. Distribution limited to 54° (File: NumSimulation.123)

This reduction of the Lateral Stress Factor caused by a reduced range of contact angles will imply some consequences on the extent of macroscopic structures and is discussed in later chapters.

11. 8 Discussion of Results

Comparison to the measured values leads to the need of some adaptive measures. The simulation results are stable and reproducible.

Yet, the simulated packing fraction value of $\kappa^{stoch} \simeq 0.64$ rsp. the porosity $n = 0.36$ does not match the values obtained in experiment for LLO-systems:

	LLO-Readings			
	Polyester	**Polyolefin**	**PVC**	**Teflon**
Grain to grain friction ϑ_0	**36,34°**	**19,71°**	**11,33°**	**7,75°**
Av. Packing Fraction κ^{meas}	0,726	0,784	0,802	0,790
Av. Porosity $n = 1 - \kappa^{meas}$	0,274	0,216	0,198	0,210

This is certainly the consequence of the difference between the idealised simulated situation and the real conditions during the experiment as the simulation was conducted for uncompressed granular material, which is not the case for the experimental results.

LLO-Measurements were accomplished after exposing the system to 'low' level of organisation which implies an unnegligible compression of $\varepsilon \simeq 5$ %. This is assumed not to alter the extent of the basic cell significantly but to initiate some reorganisation within the granular material which will have some impact discussed later.

As a consequence, some modification to the distribution of contact angles certainly occurs but can be neglected due to the low sensitivity of the simulation results against such influence. However it will be taken into account by using a maximum angle of contact of $\xi \simeq 56.6^o$ instead of $\xi \simeq 60^o$. This modification corresponds to the perception of all contacts beyond $\simeq 56.6^o$ to be shifted out of the 60° range and replaced by contacts at lower angles when a pair of cylinders is compressed to about 5 % of an average diameter.
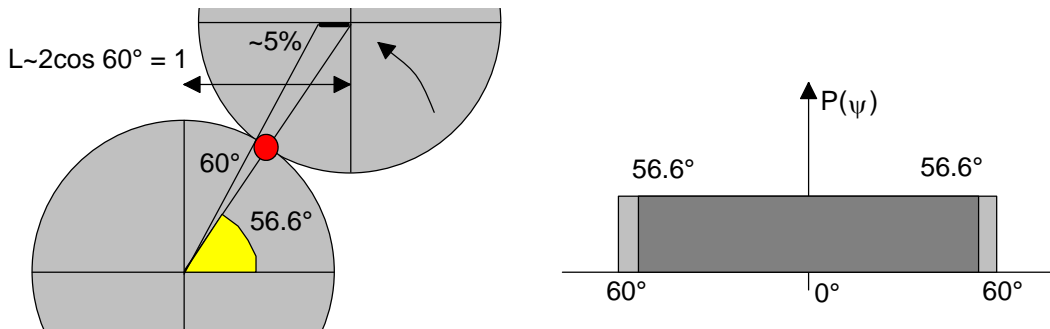
FIG. 104. Limiting the range of contact angles to 56.6° by a deformation of ~5 %

The most significant difference is assumed to be the possible overlap of parallel lateral force chains which reduces the average width of the chains. Idealised, the width of a force chain was calculated on the basis of exclusively normal supporting forces at the outermost positions of the cylinders. The applied minor deformation in LLO cases is expected to sufficiently cause a major overlap and hence increase of the lateral stress factor:
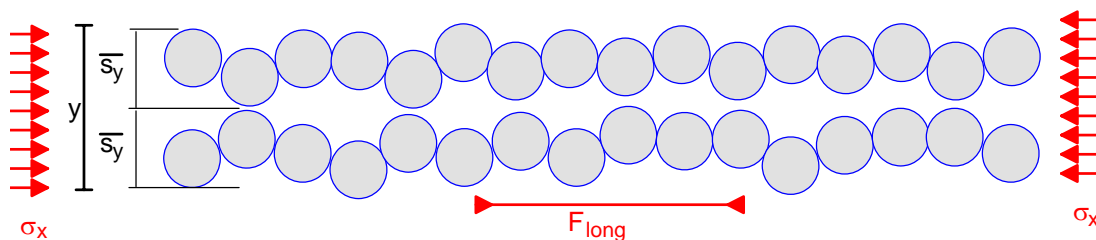
FIG. 105. Correction by overlapping adjacent chains

The average width of a chain had been calculated on the perception of independent cylinder chains as the mean value of the local size of basic cell which leads to an assumption of the longitudinal force $F_{long} = \dfrac{\sigma_x \cdot y}{s_y}$ for each chain. Since in reality the wide gaps between the chains are filled a certain overlap of the chains is unavoidable. Such synchronisation is assumed to have no significant impact on the stochastic nature of the arrangement. Yet, the stress σ_x is distributed on more chains causing the longitudinal force F_{long} to be somewhat less why in consequence the measured ratio $K = \dfrac{F_y}{F_x}$ increases.

Thus, a correction to the measured values needs to be made in order to transpose them to the ideal situation which is the basis of the simulation model. The packing fraction of a particular measurement compares to the resulting theoretical packing fraction from the simulation and hence defines the percentage of overlap of adjacent force chains:

$$\frac{K^{stoch}}{K^{meas}} = \eta_{overlap}$$

In this way, the measured Lateral Stress Factor is adapted to the simulational situation by:

$$\overline{K_{LLO}^{frict}}^{SIM} = \eta_{overlap} \cdot \overline{K_{LLO}^{frict}}$$

	Teflon	PVC	Polyolefin	Polyester
$\vartheta_0 = \arctan \mu_0$	**7,75°**	**11,33°**	**19,71°**	**36,34°**
corr. for irregularities	20,35°+/-3,01°	11,33°	32,21°+/-2,67°	49,04°+/-1,98°
$\overline{K_a^{frict}}$ (LLO)	0,307	0,419	0,235	0,163
Error 95%	+/-0,025	+/-0,031	+/-0,031	+/-0,024
Packing Fraction	0,790	0,802	0,784	0,726
Error 95%	+/-0,043	+/-0,030	+/-0,049	+/-0,034
Overlap Correction	81,01%	79,80%	81,63%	88,57%
Transposed Result	**0,249**	**0,334**	**0,192**	**0,144**
Error 95%	+/-0,035	+/-0,038	+/-0,039	+/-0,029
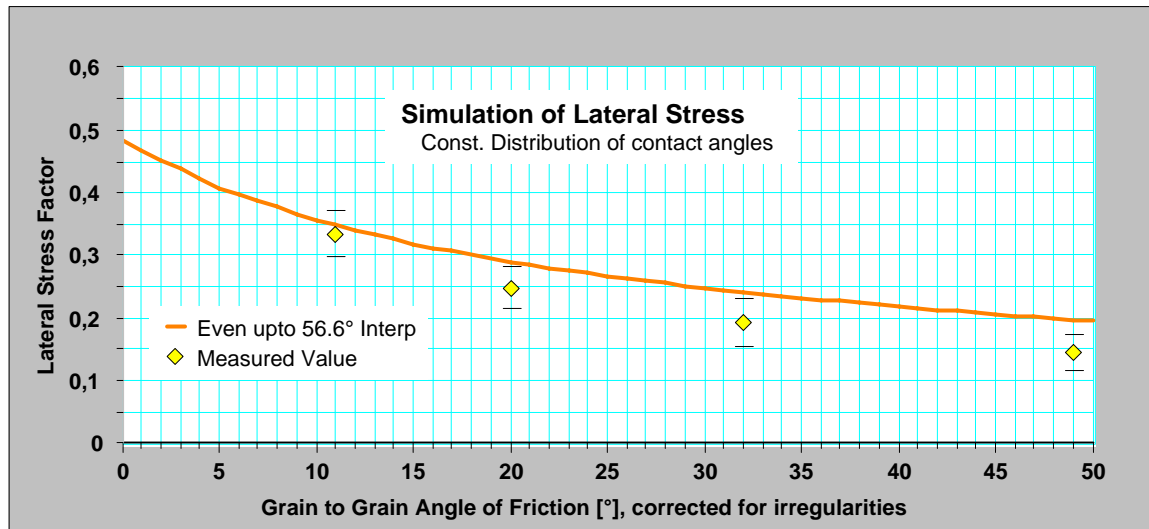
FIG. 106. Averaged lateral stress factor in comparison to measured values (File: NumSimulation.123)

11. 8. 1 Major Characteristics

The constant distribution of contact angle matches the measurement data acceptably well within or at least close to the given error margins. Hence, the consideration of parallel force chains satisfying local equilibrium of normal and tangential forces seems sufficient to describe the stochastical behaviour in LLO systems. Some inaccuracy of the model is indicated by the tendency of the measured values at high angles of friction to lower stress factors, meeting the simulated graph somewhat below the error bar.

This behaviour is certainly the consequence of a neglected mechanism of significant influence. In fact a stochastic approach can only cover completely unorganised systems, while the observed granular medium has been subject to some compressing deformation which allows for at least small modification to the structure. Therefore some deviation of the measurement values with respect to the simulation results must be expected.

Obviously the impact is a further small reduction of the Lateral Stress Factor which is mainly proportional to the angle of friction. A very plausible explanation for such behaviour can be given qualitatively and is easily confirmed by visual observation of the compacted granular system:

While constructing all configurations of cylinders, some can be found which are stable by friction without any lateral support. These are dependant on the radii of the participating cylinders, the orientation of the subsystem and finally the angle of friction between the surfaces.
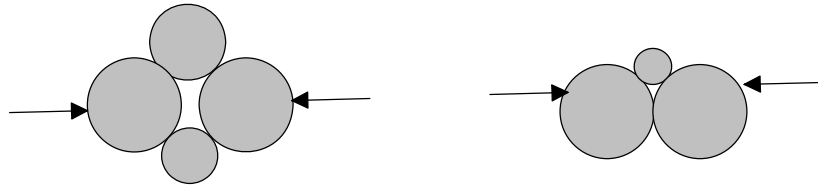
FIG. 107. Some configurations of higher order causing 'Locking Areas' inducing no Lateral Stress

Needless to say, that none of these configurations remains stable on vanishing friction while the ratio of stable systems and orientations increases with rising friction. It is common to all the considered combinations, that they comprise more simultaneous contacts than are employed in stochastically built granular media. Therefore the probability of occurrence is neglectably low. Yet, considering granular media exposed to some even low compressing deformation, single cylinders are pressed out of their position and move to 'better' contacts, i.e. searching for a more stable situation. In detail we assume that the cylinders at the most exposed positions contributing most to the average lateral stress are subject to the highest forces and therefore most easily move out until a locally stable position is found where no lateral stress is generated. In such a configuration called 'Locking Areas' no contribution to the Lateral Stress Factor is made and thus its mean value decreases.
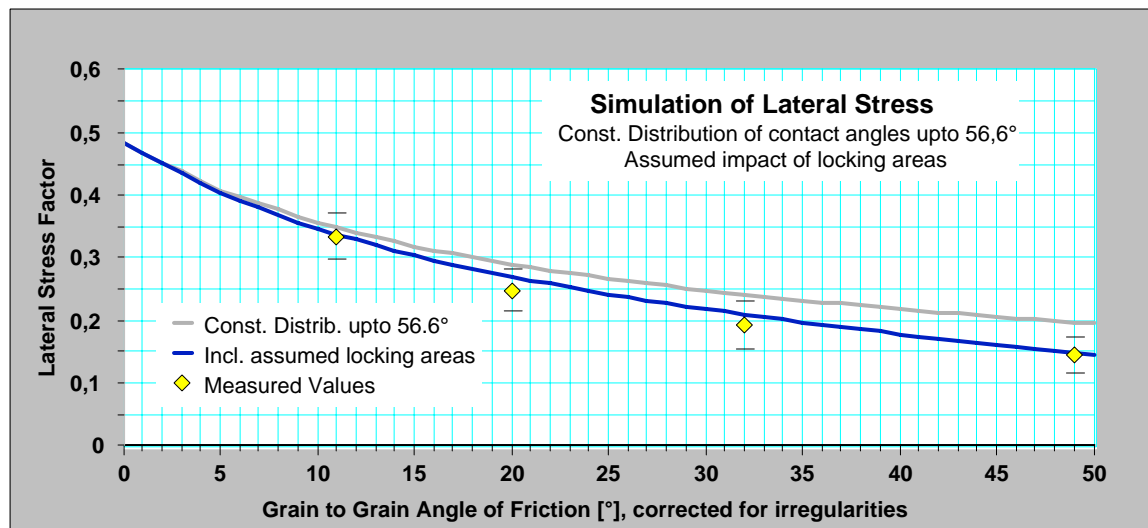
FIG. 108. Simulation results with assumed locking areas in comparison to measured values (File: NumSimulation.123)

However, since the model is not intended to serve as theory but as a plausibility calculation, such improvements are not persecuted in this context. Only the order of correction was

estimated by the assumption of an neglected impact linear with the angle of friction ϑ_0. Then, a very small further offset of $1^o/_{oo}$ per degree makes the measurement values match well.

This leads to the assumption that 4,5 % of the contacts are subject to such locking mechanisms at an effective angle of friction $\vartheta + \chi \simeq 45^o$

11. 8. 2 Summarized Observations

- Since the difference between constant distribution of contact angle and COS-distribution in the simulation is less than the expected error of the measurements, no conclusion can be made whether a displacement of $\varepsilon \simeq 5$ % is sufficient to activate a COS-distribution.

- Simulation computing provides a fixed packing fraction which is not matched by the measurements. Thus, we conclude significant impact by the deformation process, even if displacement is as low as $\varepsilon \simeq 5$ %. However, only the overlap of force chains needs to be adapted to match the reality.

- The permission of only a limited range for the possible angles of contact is of great importance. Its omission would lead to unrealistically high estimations for the lateral stress factors. The restriction can be determined by the constant limit $\xi = \frac{\pi}{3}$, even on the basis of a non uniform distribution of grain radii. Presumably, this is valid only if the distribution is centred around a sharp value and not too wide.

- Again, the value for vanishing friction in a completely unorganised system is confirmed to be about $k_s(\vartheta_0 = 0) \simeq 0.52$ in fairly good accordance to Duran [52]. Comparison of the simulated results including the assumed impact of locking configurations to the prediction of Rankine shows that a structural component of friction for such a model which develops to zero for $\vartheta_0 \to \simeq \frac{\pi}{4}$ is evident.
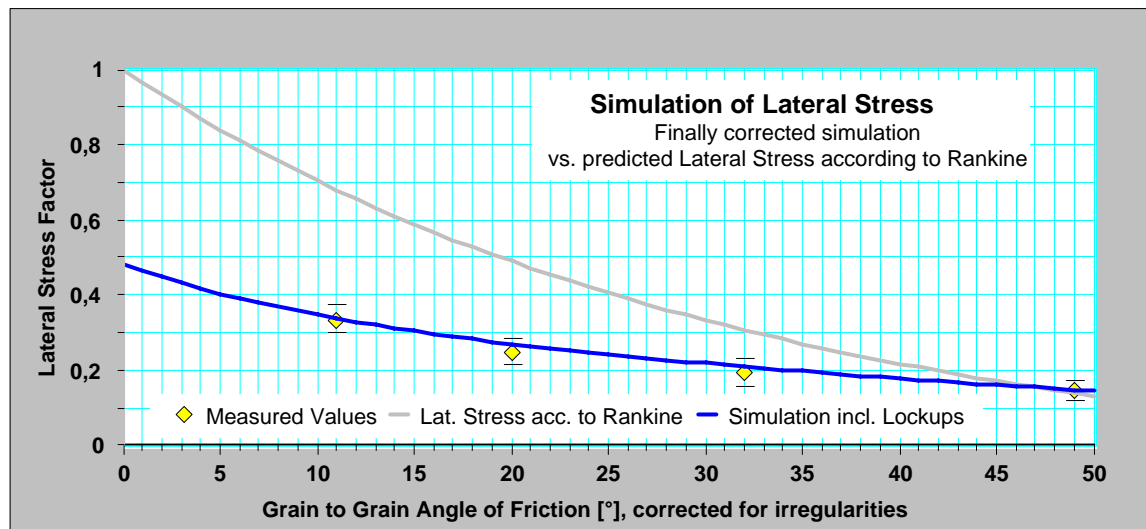
FIG. 109. Simulation results with assumed locking areas in comparison the Rankine prediction (File: NumSimulation.123)

The well matching description of LLO measurements by a pure stochastic approach leads to understand the importance of selforganising mechanisms in granular media. Based on a displacement of up to one average grain diameter, only very local processes are activated e.g. the effects of the unevenness of surfaces and the building of locking configurations. Furthermore, friction seems to impede the packing process a lot, so actual values of packing fraction need to be taken into account. Beyond this, no more mechanisms need to be considered, the overall behaviour is fairly well determined by stochastic positioning.

Yet, this state is of relevance for dry granular media, but largely not for soil, since soil is always exposed to a tectonic or grown deformation history which dominates the behaviour and, thus, shifts the characteristic to the range of the HLO-measurements with much higher deformation than by some four grain diameters.

12 Review on HLO and LLO Measurements

Obviously the measured lateral stress factor in dependence of the grain to grain friction parameter behaves differently for highly and lowly organised systems and therefore different mechanisms are found to be dominating the two extreme situations investigated here. There is no sharp transition expected to separate them, however the observed situations seem to be far enough away from this transition to display the particular characteristic of each type. Computations based on the expected effects allow to reproduce the obtained measurement results with ample closeness in both cases.

Nevertheless at least an attempt must be made to compare the two cases by trying to apply the found mechanisms for the respectively other situation. This may serve to improve the understanding of the transition.

For **HLO granular systems** dominated by the development of shear joints the following expression had been found, which yields the effective angle of friction $\arctan \overline{\mu_0^{eff}}$ from the grain to grain angle of friction ϑ_0 and the maximum available angle of contact in a shear joint δ. This dependency turns out to be well compatible with the measurement results.

$$\overline{\mu_0^{eff}} = \frac{\cos \vartheta_0 - \cos \delta + \sin \vartheta_0 \ln \tan\left(\frac{\pi}{4} + \frac{\vartheta_0 + \delta}{2}\right)}{\sin \delta + \sin \vartheta_0}$$

For straight shear joints in a set of equally sized circular cylinders δ was equal to 30° where small deviations from this state were indicated by slightly larger values of $\delta \approx 30^o..40^o$. In this range the resulting transformation is an offset of about $10^o - 20^o$.

However testing this approach for the extreme state of stochastically positioned cylinders (LLO) requests to use a value of $\delta \simeq 60^o$. It can be clearly seen that in this case the offset to the grain to grain friction values ϑ_0 rises to 30° but becomes infinite for all friction values larger than 30°. This leads to virtually infinite friction which implies a vanishing contribution of the shear joints to the lateral stress factor. The main part in this case is expected to be a direct consequence of the force chains themselves.

Therefore an approach based on more or less smooth shear joints can affirmatively not be applied for granular sets dominated by stochastically positioned cylinders.
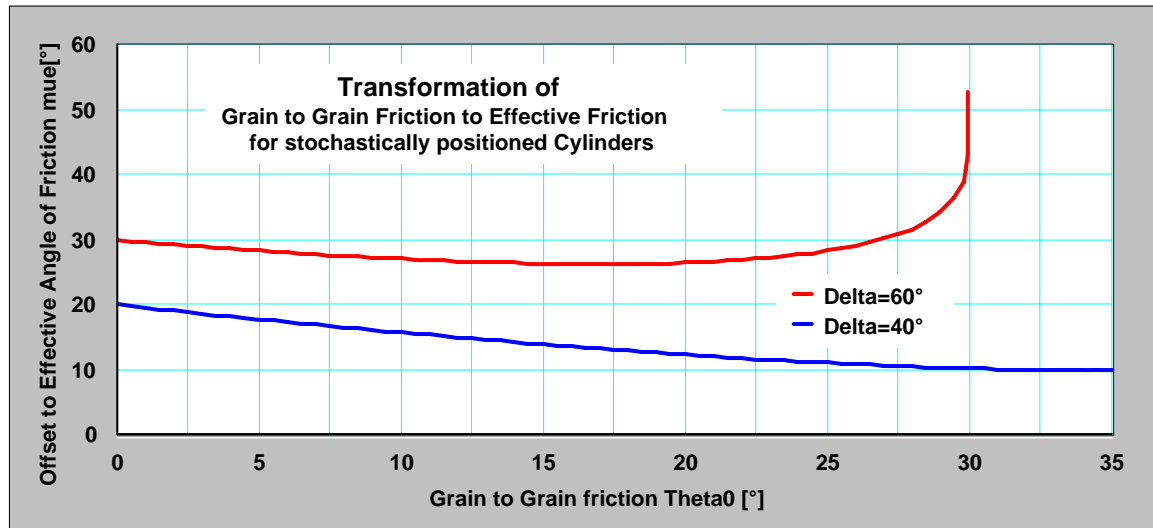

FIG. 110. Transformation of Grain to Grain Friction ϑ_0 to effective friction μ_0^{eff} for stochastically positioned cylinders

(File: HLO-Mechanism for LLO.123)

The central idea of describing the lateral stress factor by the situation in the shear joint is obviously unsustainable if no shear joints are generated.

On the other hand the simulational approach well describing the behaviour of a set of stochastically positioned cylinders in a **LLO system may be tested for the HLO material** as well. In this case the angle of contact in a force chain needs to be restricted to very small values of about 10°, representing the unevenness of the chain. The basic value of 30° is already considered in a perfectly straight force chain.

In order to investigate the contribution of the force chains themselves, even if shear joints are existing, the simulation software described before was set to create and calculate appropriate force chains with contact angles evenly distributed between $-\xi$ and ξ where $\xi = 10^o$. The resulting lateral stress factor was additionally plotted to the final result of the realistic simulation, which mirrors the stochastic (LLO) situation in accordance with the measured stress values:
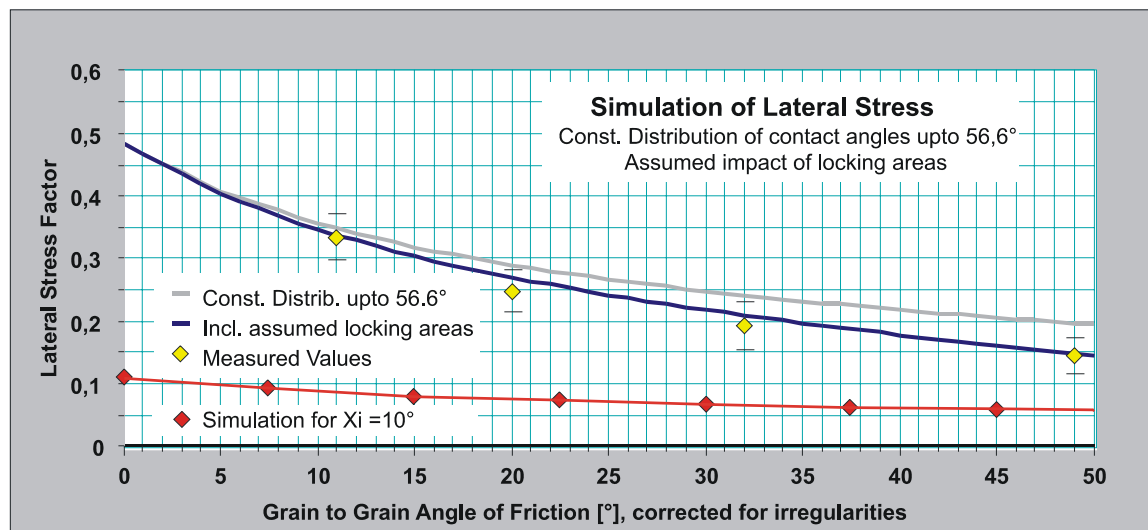
FIG. 111. Simulation of very straight force chains, lateral stress (File: NumSimulation.123)

It must be kept in mind, that such an approach is based on the assumption that the lateral stress is mainly produced by the force chains themselves, not by the interaction of the chains. Therefore the contribution of the chain is far too low to explain the measurement results. Thus the assumption of a dominating situation in the shear joint for HLO systems is evident.

13 Structures in Granular Material

Obviously, granular material cannot be treated as if it was continuous. Yet the approaches used by soil mechanics are well founded and do not comprise any structural implications. The following chapter concentrates on the influence of the inherent structure of the single cylinders as well as the macroscopic structures built by self organising mechanisms.
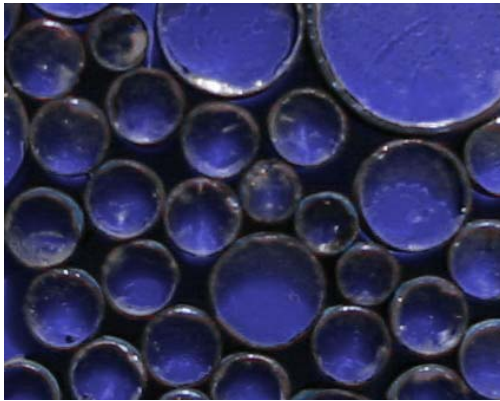
FIG. 112. Inherent Structure
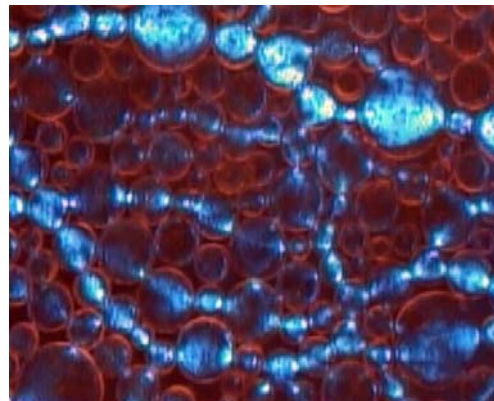
FIG. 113. Macroscopic Structure

13. 1 Inherent Structure

13. 1. 1 Influence in Highly Organised Granular Material

As has already been shown in previous chapters, the consistency of granular material as a conglomerate of cylinders has significant consequences. Concerning highly organised systems, where we expected continuous theories like Rankine to be applied best, a discrepancy between the Angle of Friction φ as a result of the averaged behaviour of the material *versus* the Angle of Friction ϑ_0 derived from the Coefficient of Friction between the interacting particles was substantiated.

We found $\varphi = \vartheta_0 + f(\overline{\delta}, \varepsilon)$, where the structural offset $f(\overline{\delta}, \varepsilon)$ was reaching values between 12° and 15° in the present experiments. The offset $f(\overline{\delta}, \varepsilon)$ had been the expression of the uneven surface within the sliding joint. This dependency is certainly closely aligned to the distribution of the particle sizes as well as their shape and angularity.

Since classic considerations expect a material with no inherent friction $\vartheta_0 = 0$ to present itself like a frictionless liquid; the Coefficient of Lateral Stress $K_a(\vartheta_0)$ is expected to be 1. Yet this is not valid for a material with an inherent structure:

Such behaviour can be observed in the case of vanishing effective Angle of Friction φ, meaning nothing else than the combination $\varphi = \vartheta_0 + f(\bar{\delta}, \varepsilon)$ to become zero. Thus the Microscopic Angle of Friction is expected to compensate the influence of the inherent structure $\bar{\delta}$. Since friction cannot be negative, i.e. $\vartheta_0 \geq 0$, this situation will actually never occur.

As a matter of fact, the macroscopic definition of φ is made from a view that summarises all frictional and structural response of the material to meet exactly this anticipation $K_a(\varphi = 0) = 1$. Such an approach comprises the perception, that friction is the only contribution of granularity to the characteristics, which can be held true as long as structural effects can be described as an additional frictional term. Yet as the experiments indicate, this term seems to be not constant but a more or less linearly decreasing function of the frictional parameter. Nevertheless, since in general applications the Angle of Friction is commonly determined through experiments and scarcely extrapolated to other materials, this is only of academical interest.

13. 1. 2   Influence in Statistical Approaches on Lowly Organised Granular Matter

13. 1. 2. 1 Structural Impact on Granular Material under Vanishing Friction

In the same way, concerning granular material of low organisation, the impact of the inherent structure is also evident.

The computations, done before, yield a lateral stress factor of about $\bar{K}(\vartheta_0 = 0) \simeq 0.45..0.55$, depending on the applied distribution, but certainly not close to 1. Since the operating mechanism is different in comparison to the highly organised structures, a well founded relation between ϑ_0 and φ can not be formulated. Nevertheless the values different from unity at $\vartheta_0 = 0$ can easily be justified:

The model consists of cylinders with more or less equal diameters. Such a model, introduced for a typical granular material, cannot be valid for a continuous system like a fluid.

In a situation with $\vartheta_0 = 0^o$ we imagine frictionless sliding cylinders. Nevertheless the structure remains real; even frictionless movements are accomplished by contacts, defined through geometrical conditions and statistically distributed positions and angles. At each contact longitudinal forces are transformed into lateral forces. Thus, it stands to reason that statistically distributed frictionless contact orientations are in no way forced to produce an average lateral force factor of 1.

Remark: This consideration is valid for the statistical case of a system with no or only low level of organisation. As soon as forced deformation begins to play a role, self organising mechanisms start trying to reach a state which is characterised by $\overline{K}(\varphi = 0) = 1$:

All motion in one direction is redirected in all other directions and thus no special direction is preferred since no friction provides an asymmetrical contribution to movement and forces. Thus, the situation finally can only end at a symmetrical state, where the - non existing - friction and the structural share lead to $K = 1$ in common.

13. 1. 2. 2 Lateral Force Factor in Extreme Configurations

In order to gain a comparative value for an obtainable Lateral Stress Factor, two theoretical borderline cases are considered:

Let all cylinders be of equal diameter $d = 1$. In case A below, all particles are ordered in exact lines. Then, assuming infinitely hard granules and thus, neglecting elastic effects derived from the poisson factor, the Lateral Force Factor is obviously determined $\widehat{K_a^A} = 0$ as well as the Lateral Stress Factor $K_a^A = 0$. Case B below considers parallel lines, horizontally displaced by half a diameter, so that the cylinders are positioned in the most dense packing. In the most extreme situation, the cylinders in a line are just not touching their left or right partner resulting in the transmission of forces running zigzag between the lines.
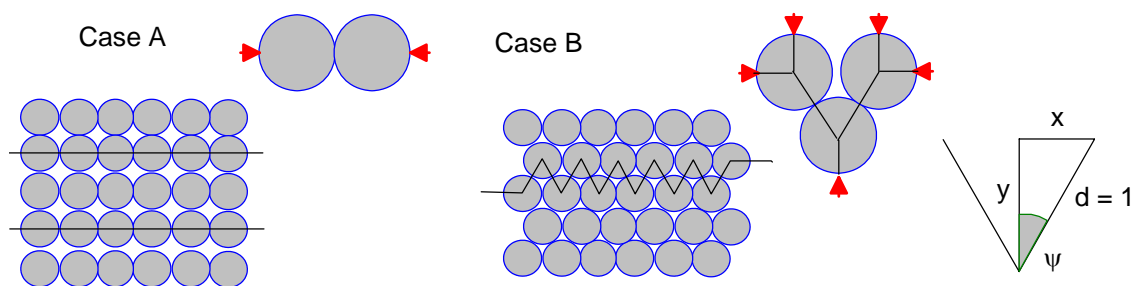
FIG. 114. Two distinct extreme arrangements of cylinders

Then, the Lateral Force Factor is calculated using $x = \sin \psi$, $y = \cos \psi$ and $\frac{x}{y} = \tan \psi$, rsp.

$$x = y \tan \psi$$

The differential is determined:

$$dx = \tan \psi \, dy,$$

which yields for the value of interest $\psi = 30°$:

$$dx = \frac{1}{\sqrt{3}} dy$$

As has been already derived in chapter 11.1 „Highly simplified Model" the forces can also be obtained by using the principle of virtual displacements. A small virtual modification dx of the longitudinal distance of two adjacent cylinders interacting with a force F_{long} causes a modification dy to the lateral distance where the force F_{lat} is acting. The impact of elasticity, weight and other side effects is again assumed to be of negligible order in comparison to the mechanical contribution. Considering the virtual work of such a limited mechanical friction-less system yields

$$F_x |dx| = F_y |dy|$$

which again leads to

$$\widehat{K^B} = \frac{F_x}{F_y} = \left| \frac{dy}{dx} \right| = \sqrt{3} \approx 1.73$$

Considering stress instead of forces, the coefficient K needs to be corrected by the extent of the basic cell, depending on the actual angle of contact:

$$\sigma_x = \frac{F_x}{y}, \ \sigma_y = \frac{F_y}{x}$$

$$K^B = \frac{\sigma_x}{\sigma_y} = \frac{xF_x}{yF_y} = \frac{x}{y} \left| \frac{dy}{dx} \right| = \tan \psi \left| \frac{dy}{dx} \right| = \frac{\tan \psi}{\tan \psi} = 1$$

More generally, we consider a symmetrically packed granular system formed by cells of four cylinders, where angles of contact ψ are possible in the range $\psi \in [30^o, 60^o]$, denoted as range I.
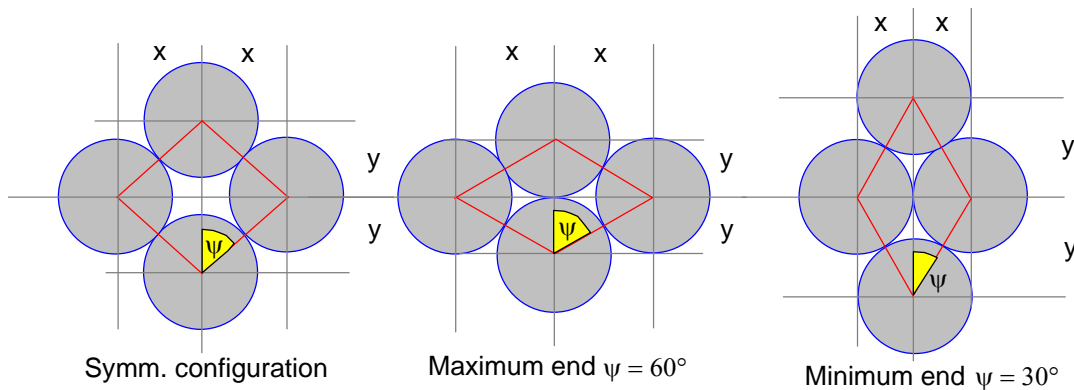
FIG. 115. Symmetrical arrangement of equally sized cylinders

With $x = d \sin \psi$, $y = d \cos \psi$, and thus $x = y \tan \psi$, $dx = dy \tan \psi$, the Lateral Force Factor for ϑ_0 can be written:

$$F_x \, dx = F_y \, dy \quad \Rightarrow \quad \widehat{K_a^I} = \frac{F_y}{F_x} = \frac{dx}{dy} = \tan \psi$$

Using $\sigma_x = \frac{F_x}{y}$ and $\sigma_y = \frac{F_y}{x}$, we obtain as the Lateral Stress Factor:

$$K_a^I = \frac{\sigma_y}{\sigma_x} = \frac{y \, F_y}{x \, F_x} = \cot \psi \, \tan \psi = 1$$

independent of the angle of contact $\psi \in [30^o, 60^o]$.

Yet, the angle of contact ψ cannot always be restricted to the denoted range I. If it becomes less than 30° (range II), the symmetry of the structure gets lost and a completely different mechanism begins to work:
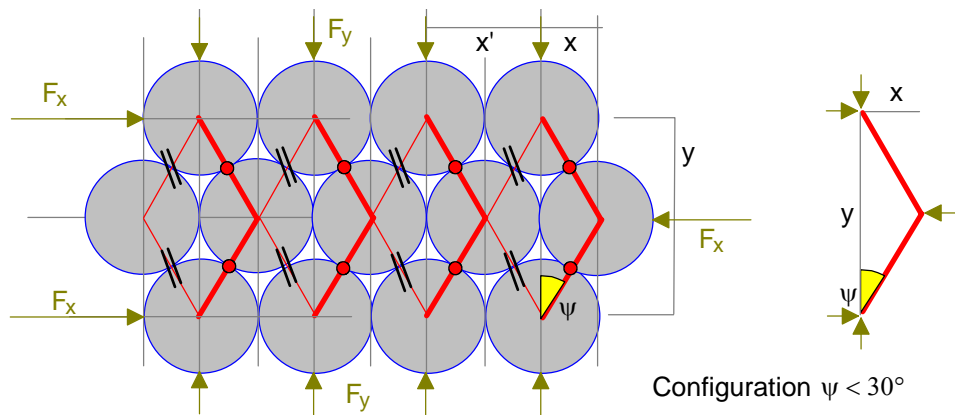
FIG. 116. Arrangements of cylinders, where symmetry is broken

The contacts marked by the black double bars are breaking up, the points (●) are taking over all the force and the bold lines remain as force bearing chains:

In this case we obtain: $x = d \sin \psi$, $y = 2d \cos \psi$ and thus: $x = \frac{y}{2} \tan \psi$, $dx = \frac{dy}{2} \tan \psi$.

Finally, the consideration of virtual displacements as shown above leads to:

$$F_x \, dx = F_y \, dy \quad \Rightarrow \quad \widehat{K_a^{II}} = \frac{F_y}{F_x} = \frac{dx}{dy} = \frac{1}{2} \tan \psi.$$

Converting this to a Lateral Stress Factor we need to use the full width of a cell: $x' = d$ and thus:

$$K_a^{II} = \frac{\sigma_y}{\sigma_x} = \frac{y\,F_y}{x'\,F_x} = \frac{2d\,\cos\psi}{d}\frac{1}{2}\tan\psi \; = \sin\psi \qquad \text{for } \psi \in [0..30^o\,]$$

The combination of these two situations is displayed in the following graph:
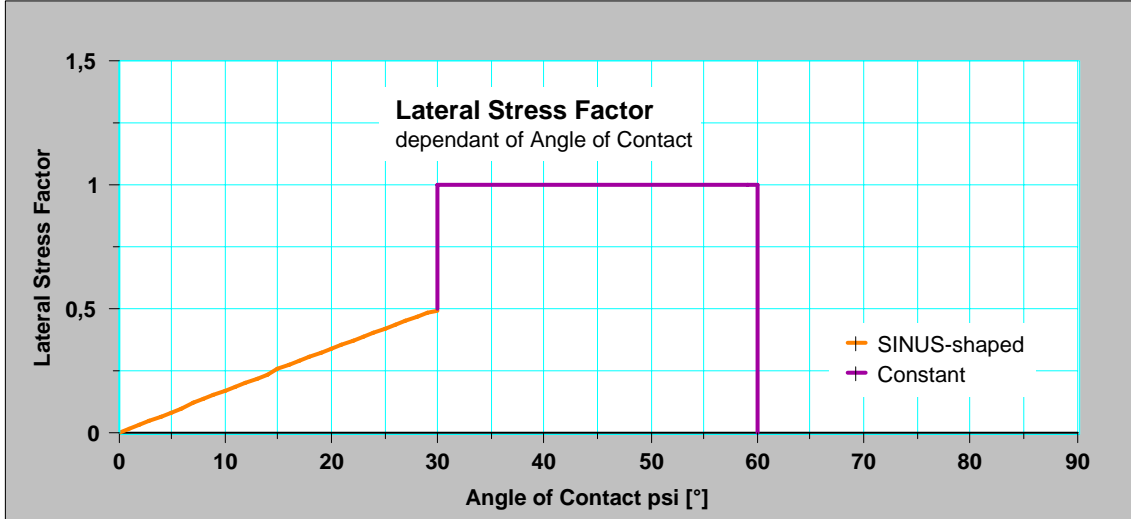
FIG. 117. Lateral Stress Factor for special arrangements of cylinders, where $\vartheta_0 = 0$ (File: ExtremeCasesSymm60°.123)

Since every granular system comprises of all these types of mechanisms, we expect an overall Lateral Stress Factor definitely smaller than unity, even on vanishing friction. Assuming equally distributed angles $\psi \in \left[0, \frac{\pi}{3}\right]$, we obtain an average Lateral Stress Factor of:

$$\overline{K_a} = \overline{\left(\frac{\sigma_y}{\sigma_x}\right)} = \frac{3}{\pi}\int_0^{\frac{\pi}{3}} \frac{\sigma_y(\psi)}{\sigma_x(\psi)}\,d\psi = \frac{3}{\pi}\int_0^{\frac{\pi}{6}} \sin\psi\,d\psi + \frac{3}{\pi}\cdot\frac{\pi}{6} = \frac{3}{\pi}\left(1 - \cos\frac{\pi}{6}\right) + \frac{1}{2} = 0.627$$

Remark: This corresponds very well to the results obtained from both the HLO as well as the LLO measurements extrapolated to frictionless granular systems. Furthermore it rather matches the value cited by Duran [52], *who denotes a 'coefficient of redirection towards the wall' for frictionless monodispersed two dimensional granular media of* $K \simeq 0.58$.

Friction has not yet been taken into account and reduces the possible Lateral Force Factor. As derived before (see chapter 11.1 *Statistical Approach: Less Organised Granular Material, Simplified Model*), we obtain for a sliding contact at angle ψ including the influence of friction ϑ_0:

$$\widehat{K_a^g} \sim \tan(\psi - \vartheta_0)$$

For illustration, the result for grain to grain Angles Of Friction $\vartheta_0 = 0..45^o$ is drawn for the two cases I at $\psi = 30^o..60^o$ and II at $\psi = 0^o..30^o$ in the following graph:

$$K_a^I = \frac{\tan(\psi - \vartheta_0)}{\tan \psi} \qquad \text{for} \qquad \psi = 30^o..60^o$$

$$K_a^{II} = \cos \psi \tan(\psi - \vartheta_0) \qquad \text{for} \qquad \psi = 0^o..30^o$$
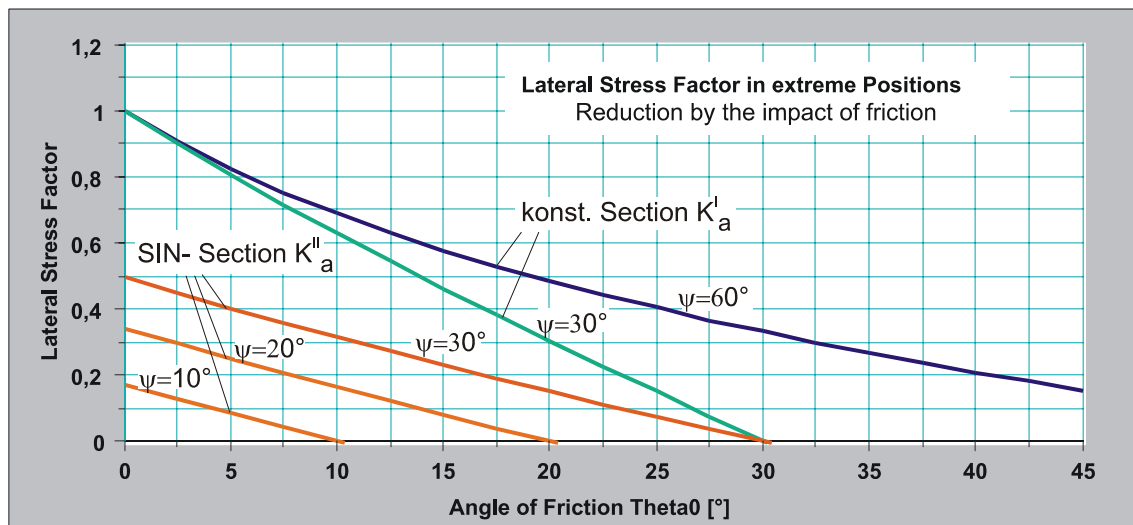
FIG. 118. Lateral stress factor for extreme cases (File: ExtremeCasesSymm60°.123)

13. 2 Building Of Mesh Structures

As all the polarisation images show and as easily can be imagined, forces are not borne equally by all granules in a granular material [17]. Instead, force chains are built, which transfer most of the force, being stabilised and supported by the environmental grains. Friction and helpful geometrical configurations provide good stabilisation of high longitudinal forces by very low supporting forces. Self organising mechanisms are controlling the size, orientation and symmetries of this mesh structure as soon as motion gives rise to alteration of structures at all. Up to this point, stochastic positioning and contacting dominates the local formation of structures.

The following paragraphs are intended to consider qualitatively the mechanisms of building macroscopic structures as well as to point out some quantitative estimations of their possible extent.
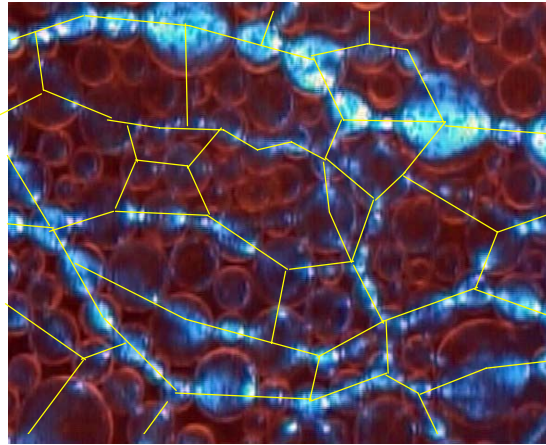
FIG. 119. Picture from the polariscope, displaying the building of a force network

13. 2. 1 Originating Macroscopic Structures - Qualitative Description

When exposing a granular system to a longitudinal compressing force, positions and angles of contact can not be predicted. Thus the force is passed on by stochastic chains, wherever stable configurations can be found [21,22]. However, a granular system which is not exposed to any stabilising force has no stable contacts at all, let alone stable chains. These are always the product of more or less deformation of the system and therefore created by self organising mechanisms. The resulting lateral forces reflect the distribution of contact angles and friction stabilised structures, averaged by the lot.

Generating a contact is always the result of at least a small compression in a certain direction. This may happen even on a very low level of force, e.g. applied by the own weight of the cylinders or by the friction between the cylinders or between the walls and the cylinders. Then, a macroscopic deformation of a granular system in direction x is distributed equally to all cylinders lined up in the direction of the deformation. The probability $P(\psi)$ of generating a contact in a direction ψ is determined proportional to $\cos \psi$ and thus preferring contacts in direction x.
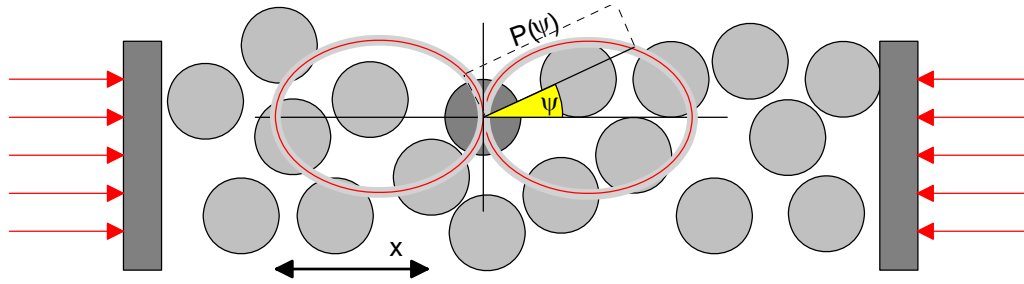
FIG. 120. Schematic view of the probability of generating further contacts (neglecting own weight)

The closer an angle of contact is to $\psi \approx 0$, the more stable it is in the view of the compression in direction x, generating low lateral forces

Since a stable contact allows no further compression of this pair of cylinders, the deformation in direction x is distributed to the rest of the cylinders in the line, resulting in a somewhat higher compression as the chain grows. Assuming the probability of generating contacts to rise with the amount of compression, any existing contact serves as a kind of initiating point, where further stable contacts tend to attach and build longer lines. With this, the intrinsic inhomogenity of the granular material comes to be the basis for the larger mesh structure.
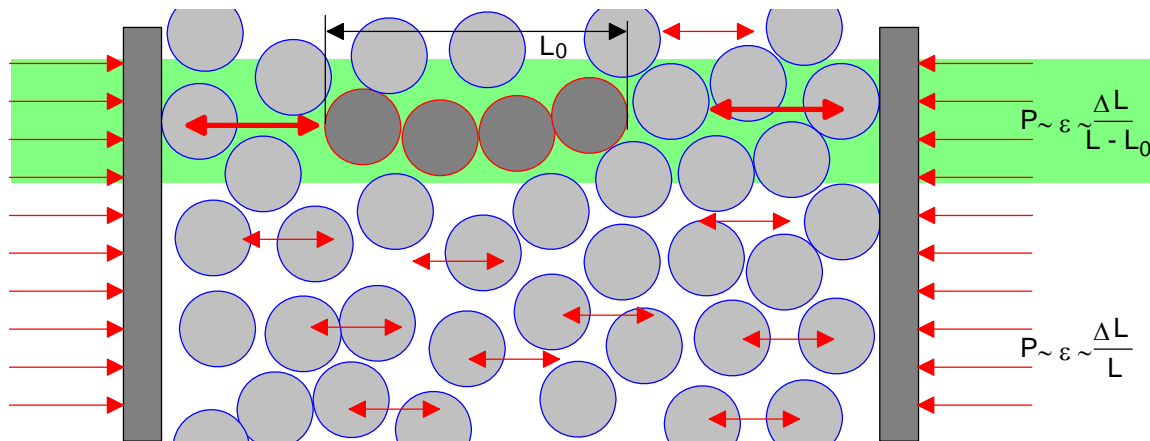
FIG. 121. Inhomogenities become the seeds for building longer force chains

Since friction and lateral forces are coupling parallel movement, another parallel line is not very likely to be created in the direct neighbourhood of an existing line. Thus a starting chain wants to elongate itself while keeping other competing lines away. The range of this interaction, elongating as well as protecting, depends on the interplay of a chain with its environment and will be quantitatively estimated in further chapters.

Not all contacts, created in this way are stable. Therefore a chain is terminated by a single contact not hitting centrally at $\psi \simeq 0$ and thus redirecting the force to somewhere else. With ongoing compression, the number of unstable contacts is increasing and starting to redirect the compression to any other direction. This initiates the same process in the transversal direction too and begins to create transversal force chains. Having reached a stable state the motion in direction x equals the motion in the lateral direction y. Thus, allowing a sufficient amount of deformation enhances symmetry and produces as many longitudinal as transversal force chains, thus meshes occur with mainly equal height and width (This consideration concerns only the extent of meshes, not their shape, where intuitively honeycomb structures are expected).

During the phase of compression nothing of the structures can be made visible, because the forces are too low to be displayed by the polariscope. Only when all motion has come to an end where the granular material touches the walls of the experimental container, forces are rising while no more deformation is accomplished. This quasi 'frozen' state can be made visible and is available for further investigations.

13. 2. 2 Impact of the Mesh Structure on Lateral Forces vs. Measurement

Computing lateral forces leads to a factor $\widehat{K_a} = \dfrac{F_{lat}}{F_{long}}$, where the average lateral force F_{lat} per length of a grain is calculated with respect to the longitudinal force F_{long} in a one diameter wide chain. Distributing the horizontal stress σ_{long} not to all available chains, but on some highlighted chains, i.e. every m^{th}, chain, accidentally bearing more of the stress, the longitudinal force is expected to be higher by the factor m. Thus the resulting lateral force is determined to be locally increased by the factor m too.
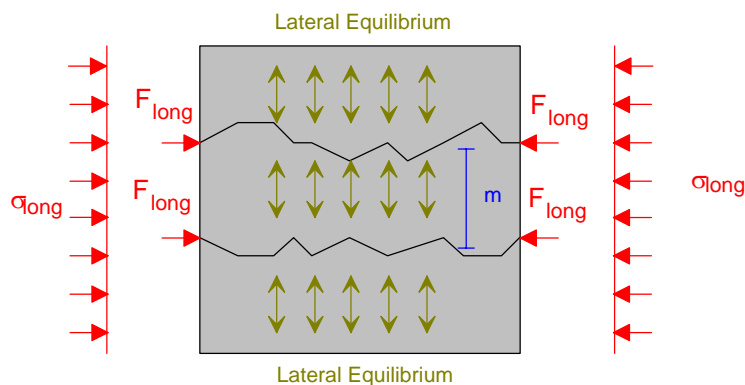
FIG. 122. Overall equilibrium of stress in networks

Yet, observations of the polarisation images clarify, that the distance *m* of the bearing force chains is of the size 2 to 3 diameters (See picture at the beginning of this chapter), while quantitative measurements, not considering the macroscopic mesh structure, confirm the lateral force factors fairly well (See chapter '*Discussion of Results: Less Organised Granular Material'*).

Consequently, we are forced to assume a selforganised mechanism, which is capable to adapt the lateral force in a chain appropriate enough to keep equilibrium with adjacent chains all over the granular system. Under this perception, the visible structure just mirrors the inhomogeneous bearing of the forces as the applied stress is distributed on all the chains, each bearing so much of the charge as it can, producing the same averaged lateral force.

13. 3 Modelling Structures in Granular Material

In order to investigate the influence of mesh structures to the well founded continuous models, which are after all known to describe granular material fairly well, we need to estimate the mechanisms as well as the dimensions of the selforganised activities. This leads to the necessity to find discrete models, still qualitative ones, but accurate enough to provide values and ranges:

13. 3. 1 Estimating the Scope of an Irregularity

A very basic consideration, derived from previously achieved characteristics of granular material, allows to estimate the reach out of a disturbance in homogeneity as a force bearing chain certainly is.

The mesh structure itself cannot provide any information about its extent, since the probability of a lateral supporting chain does not depend on the length of the longitudinal chain, rsp. the lateral force is not fading on a growing chain length. In particular, the fact of an existing lateral chain does not reduce the probability of another lateral chain further up the line.
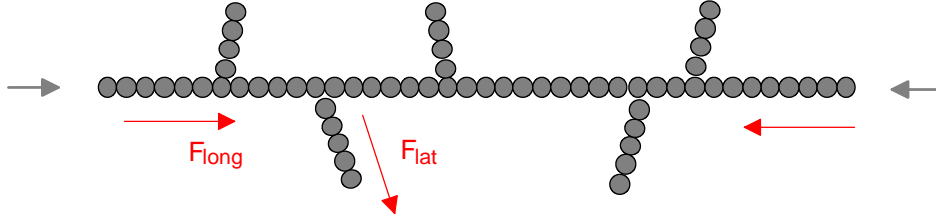
FIG. 123. Single force chain in a mesh structure, no interaction with the environment

The only obtainable information comes from the interaction of a chain with its environment, which is ruled by the Lateral Stress Factor $\overline{K}$ generated by the chain itself. The lateral force per grain, $\dfrac{\overline{K} F_{long}}{g^e}$, weighted with an effective Coefficient of Friction μ^{av}, adds up a backward force along the extent of the chain until the primary longitudinal force F_{long} is fully compensated. Since the force F_{long} as well as the Lateral Stress Factor $\overline{K}$ and last but not least the effective Coefficient of friction μ^{av} are dominated by stochastic processes, the result can only be an average value too.
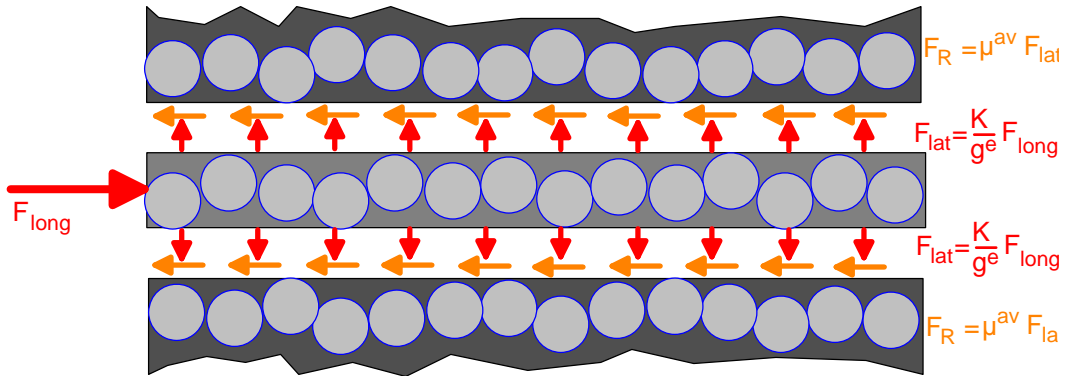
FIG. 124. A single force chain limited in length of effectiveness by friction μ^{av} versus environment

Consequently, the reduction of force dF over a length dx is:

$$dF_{long} = -\mu^{av} F_{lat} = -\frac{\mu^{av}\overline{K}}{g^e} F_{long}\ dx$$

As this simple differential equation is solved by the exponential function:

$$F_{long} \sim \exp(-\frac{\mu^{av}\overline{K}}{g^e}x)$$

we obtain an average scope $\overline{W} = \dfrac{g^e}{\mu^{av}\overline{K}}$.

In order to achieve at least rough estimates for this value, both the approach made for granular systems with a *high level of organisation* as well as the one for *low level of organisation* yield comparable results:

The numerical evaluation for **granular media in the LLO-state** leads (See chapter '*Discussion of results: Granular Material with Low Level of Organisation*') to an average Lateral Stress Factor $\overline{K}$ of:
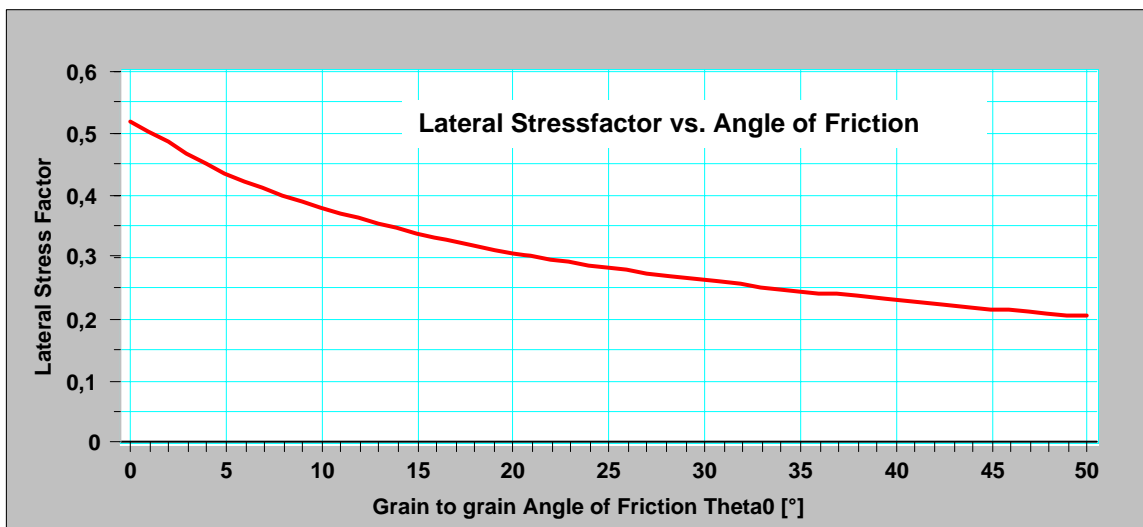
FIG. 125. Numerically obtained lateral stress factor for LLO systems (File: NumSimulation ReachOut.123)

Since smooth sliding planes cannot be presupposed, the coefficient of friction needs to be corrected.
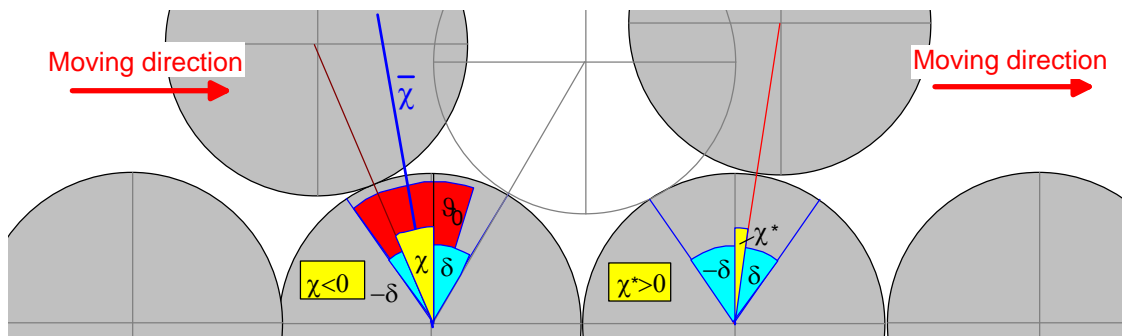
FIG. 126. Effective friction in a sliding joint, represented by average angle $\overline{\chi}$

Remembering the adjustment made for uneven sliding joints (chapter 9.2), the available geometrical range for lateral contacts $\chi \in [-\pi/3, \vartheta_0]$ (i.e. completely unordered: $\delta = \pi/3$) may

be represented here by the average angle $\bar{\chi}$ as a constant offset to the grain to grain angle of friction ϑ_0:

$$\bar{\chi} = \frac{-\pi/3 + \vartheta_0}{2}$$

and thus

$$\mu^{av} \simeq \tan(\vartheta_0 - \bar{\chi}) = \tan\left(\vartheta_0 + \frac{\pi/3 - \vartheta_0}{2}\right) = \tan\left(\frac{\vartheta_0 + \pi/3}{2}\right)$$

With this we obtain the following estimation, where an offset of 1 is added, in order to signal the scope of interaction to the next neighbour and further.
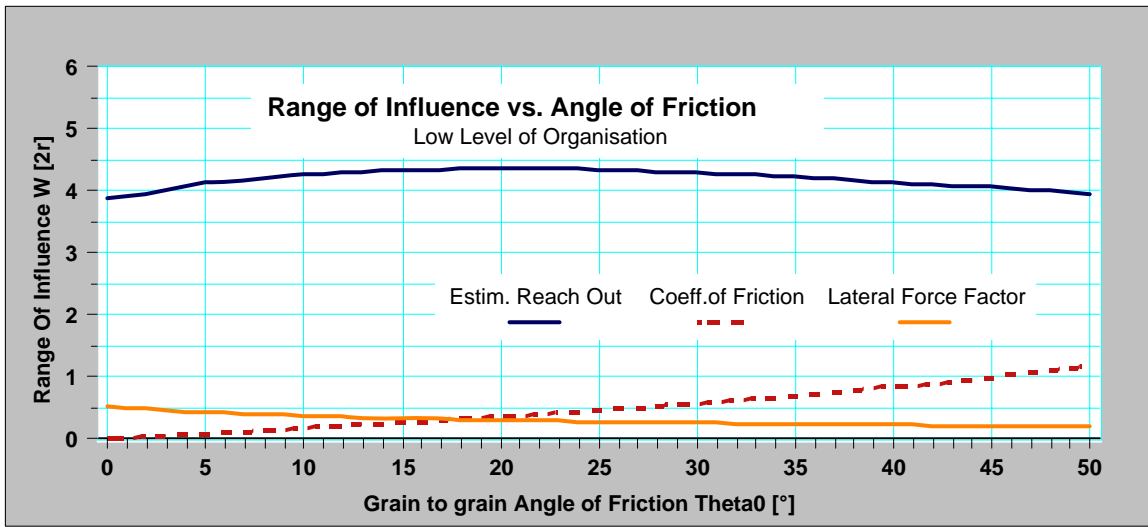
FIG. 127. Range of influence, limited by inherent friction in lowly organised systems (File: NumSimulationReachOut.123)

As the parameter of friction rises, it also reduces the lateral forces and thus the scope of influence is more or less kept constant at values ranging from 4 to 4.5 average diameters as long as reasonable Angles of Friction are considered. Unaltered structural influence prevents the system from reaching more extended values.

Using the obtained values for **granular material with higher level of organisation (HLO-state)** produces approximately the same result:

We found, that the concept of Rankine is met very well, if the Macroscopic Angle of Friction φ is replaced by the corrected Microscopic Angle of Friction $\varphi \simeq \vartheta_0 + f(\varepsilon, \delta)$. This leads to results for the lateral stress factor $\overline{K_a}$ close to $K_a = \tan^2(\frac{\pi}{4} - \frac{\varphi}{2})$. Furthermore, friction within the sliding joint can be written as $\mu^{av} = \tan\varphi$. Yet this parameter is only valid along the

smoothened sliding joint, which is not vectored in direction of F_0 but deflected by the angle $a = \frac{\pi}{4} - \frac{\varphi}{2}$. Thus, the arrangement being ordered best in this direction, grows worse in every other direction leading to a non isotropic range. Referring to the chapter *Discussion of Results: Well Organised Granular Material*, we can describe the 'worst case' exemplarily by:

$$\mu^{av} = -\frac{\ln(\cos(\delta + \vartheta_0))}{\delta + \vartheta_0}$$

where the range of possible contacts δ can be up to $60°$. Since this value is not realistic, we put $\delta \simeq 50^o$ for a rough check. Using these values we obtain the scope with respect to the macroscopic Angle of Friction φ, which is known to be some 10° to 15° greater than ϑ_0.
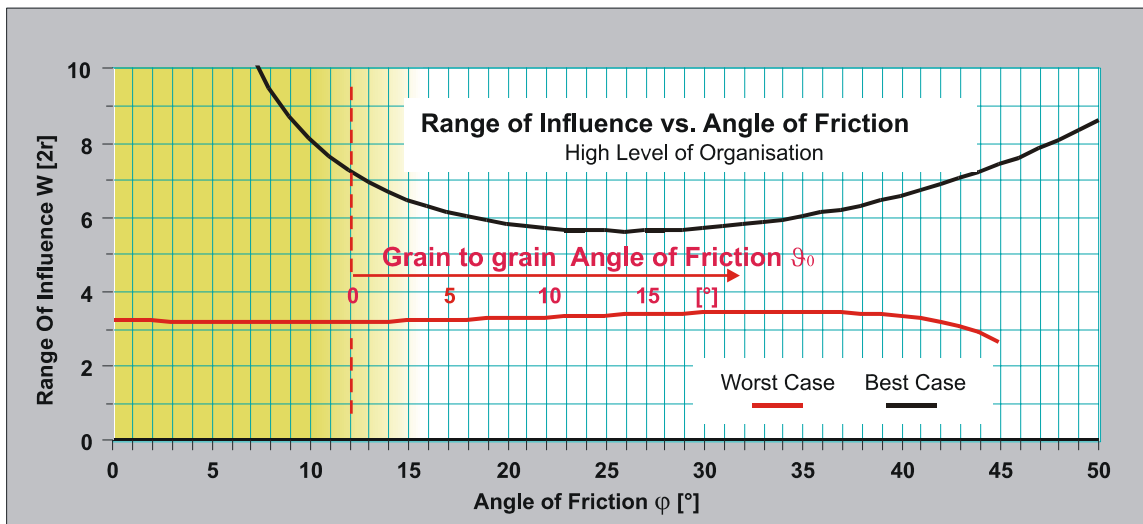
FIG. 128. Range of influence, limited by friction in highly organised systems (File: NumComputation ReachOutTwoCases.123)

This approach leads to a slightly enlarged reachout of about 6 to 8 grain-diameters in the optimal direction and a bit more than 3 diameters in every other direction. Furthermore, we note, that optimised structural arrangement of the granular systems invokes infinite scope of inhomogeneity for vanishing friction, as could be expected. Yet this implies vanishing of the structural impact itself as well and is therefore no realistic range.

Overall we conclude a range limited by several grain-diameters, where influences from force chains are expected to have disappeared. Thus, self organisational structures normally remain smaller than the magnitude of 10 diameters and averaging approaches covering more than this size are assumably not affected by structural impact.

13. 3. 2 Basic Model for Chain Lengths

13. 3. 2. 1 Probability of Stable Chains

In order to acquire a rough estimation for the resulting mesh size, a very simple model can be of great help:

Not considering a network, but just a mesh, we state a stable force bearing chain, if all members of the chain are fulfilling a condition of stability. This criterion may be derived from different considerations; here we need only the probability $P_0(\vartheta_0)$, possibly depending on the Angle of Friction ϑ_0, for a single cylinder to meet the condition.

Then the probability of such a line of length n is determined to be $P(\vartheta_0,n) = P_0(\vartheta_0)^{n-1}$ as every elongating contact multiplies its probability to be stable on the lot.

Since normalisation was done on the probability of a single contact, the result is already normalised.

Using

$$\sum_{m=0}^{\infty} mP^m = \sum_{m=0}^{\infty} PmP^{m-1} = \sum_{m=0}^{\infty} P\frac{\partial}{\partial P}P^m = P\frac{\partial}{\partial P}\sum_{m=0}^{\infty} P^m = P\frac{\partial}{\partial P}\frac{1}{1-P} = \frac{P}{(1-P)^2}$$

allows to calculate the average length $\overline{N}$ of a line:

$$\overline{N} = \sum_{n=1}^{\infty} nP_0^{n-1} = \sum_{m=0}^{\infty}(m+1)P_0^m = \sum_{m=0}^{\infty} mP_0^m + \sum_{m=0}^{\infty} P_0^m$$

$$\overline{N} = \frac{P_0}{(1-P_0)^2} + \frac{1}{(1-P_0)} = \frac{P_0+1-P_0}{(1-P_0)^2} = \frac{1}{(1-P_0)^2}$$

13. 3. 2. 2 Simple Model Using the Angle of Friction

A first approach can be the assumption, that a contact between two consecutive cylinders in a chain keeps stability if the contact angle is small enough not to let the cylinders glide but only to roll i.e. it is not a 'gliding' but a 'rolling' contact. In chapter 11.1. *'Highly Simplified Model for Less Organised Granular Material'* the condition of stability by friction was derived as $\mu_0 = \tan\vartheta_0 \geq \frac{F_T}{F_N} = \tan\psi$ and thus $\psi \leq \vartheta_0,$ using $F_T = \sin\psi\, F_{long}$ and $F_N = \cos\psi\, F_{long}$.
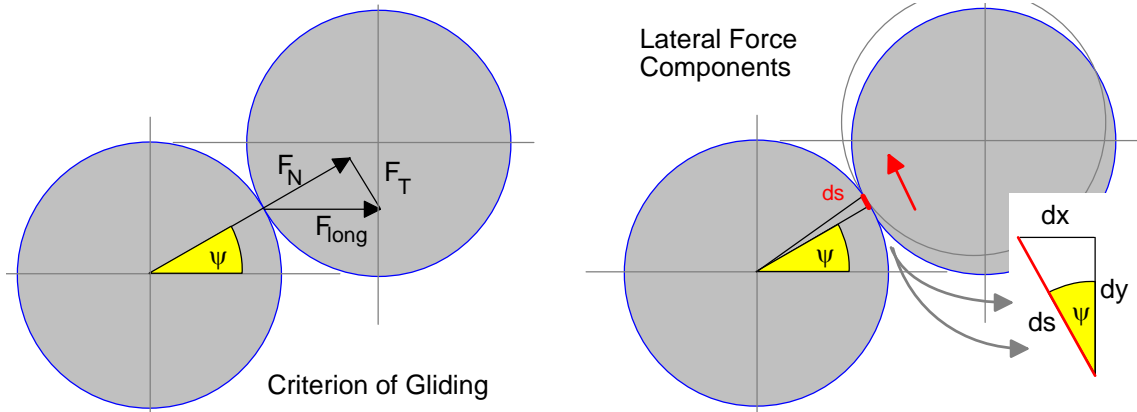
FIG. 129. Redirection of forces in preliminary model

In this respect the first gliding contact $\psi > \vartheta_0$ terminates the stable chain. Furthermore we need to hypothesise that the last cylinder of the chain, where the next is to be attached is held tight in its position by neighbouring elements.
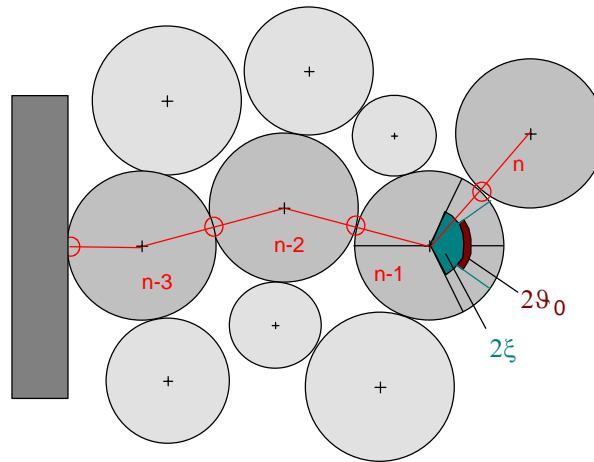
FIG. 130. Model of force chain, defined by fixed cylinders, where the first non rolling contact terminates the chain.

In this case we can state the probability to be $P_0 = \dfrac{\vartheta_0}{\xi} = \dfrac{3\vartheta_0}{\pi}$ leading to an average length of stable chains of:
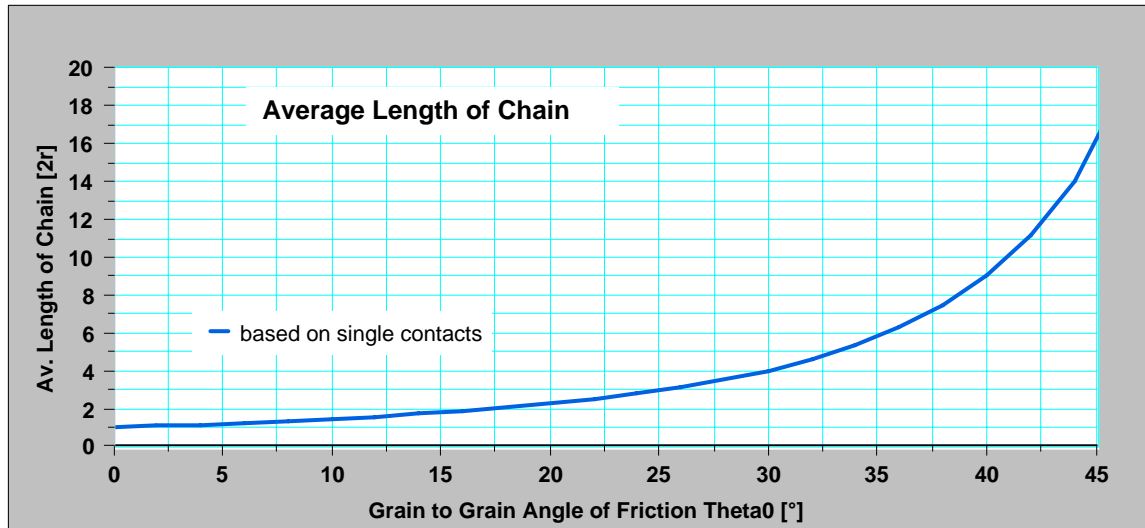
FIG. 131. Av. length of chains, derived from 'rolling vs. gliding' criterion (File: LineLengths.123)

This simple model ignores the contribution of rolling contacts to the lateral force, which reaches significant values on higher angles of contact. Therefore, the model predicts infinite chain lengths at $\vartheta_0 = 60^o$, since exceeding this limit leads to all geometrically possible contacts being rollers and therefore adding a stable contact to the chain. Taking the influence of rollers into account will effectuate a much lower gradient, but has no effect on low angles of friction.

13. 3. 2. 3 Characteristic of Distribution

Taken quasi continuously, the distribution of line lengths can easily be written as exponential function:

$$P(\vartheta_0, n) = cP_0^{n-1} = c\, e^{(n-1)\ln P_0}$$

Regardless of how the final probability is calculated, this exponential characteristic corresponds very well to measurements conducted by [20] and other more simulational approaches like the q-model [18,19,21,22]. Here the run is taken from the probability of a contact beyond the limit of $\psi = \vartheta_0$, again under the restriction of having not considered the influence of the rolling contacts.
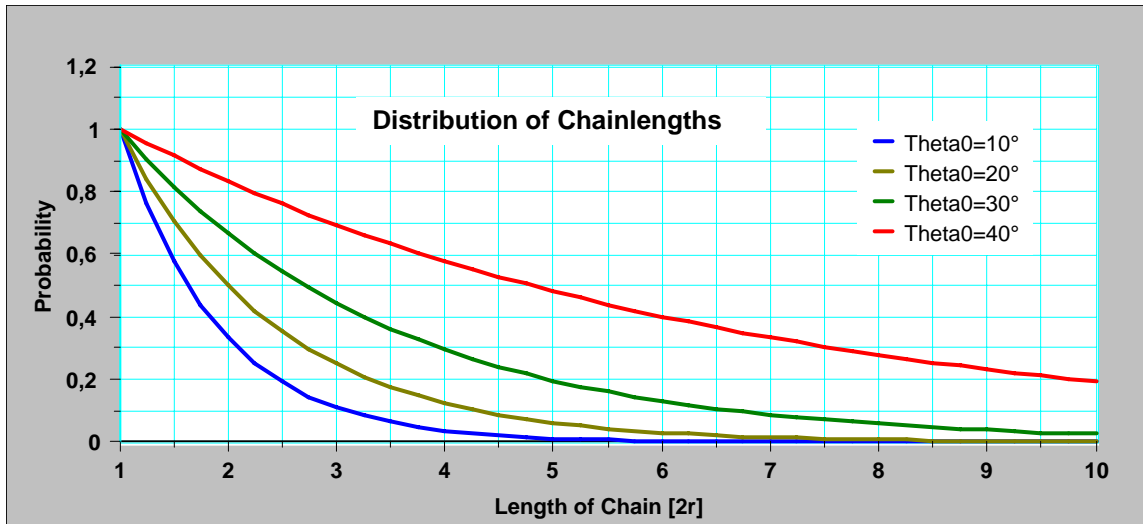
FIG. 132. Fundamental exponential character of chain lengths (File: LineLengths.123)

This rough estimation of mesh sizes is obviously very sensitive to the choice of the criterion defining P_0 and therefore only of use for investigating the exponential characteristic. Determining the absolute value of chain lengths needs a much more precise approach.

Remark: Lengths of chains are not determined unwound but as the number of grain-members. In order to find an absolute value of mesh sizes, a scaling form factor as computed before needs to be taken into account.

13. 3. 3 Improved Model for Mesh Sizes (Argument of Equilibrium)

The visible mesh structure is obviously created by inhomogeneities in transformation of longitudinal to transversal forces as discussed before. Nevertheless the system is still in equilibrium, locally as well as averaged over a greater extent. Thus the most bearing force chains need to keep equilibrium with the less bearing environment. Investigating stability and probability of such chains under the precondition of averaged isotropy supplies a better estimation for mesh sizes.

13. 3. 3. 1 Contacts in a Reduced Range of Angles

More stable force-chains are stimulated by the accidental or self-organised reduction of the range available for angles of contact between adjacent cylinders. Let ξ be the average maximum angle of contact, given by the structural restriction of equally sized cylinders. Any limitation to this is described by the reduced maximum angle $\xi_r \leq \xi$
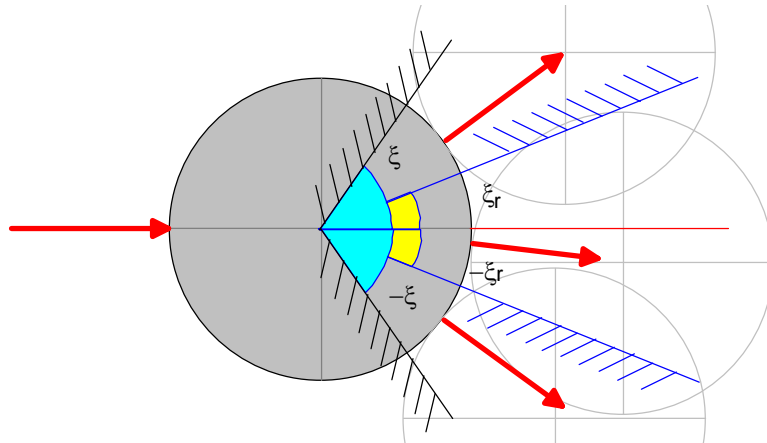
FIG. 133. Definition of a reduced range for contact angles

From simulations shown in chapter [11.3.2] the average value $\xi = \pi/3$ is known. Yet this wide range is valid only for contacts independent from each other, which is the case for very loosely packed granular material. Considering more densely packed material only very few degrees of freedom are observed, hence forcing contacts to a much smaller range of angles.

In particular for equally sized cylinders this can easily be shown: Approaching the maximum packing fraction of a hexagonally ordered system the mean deviation $\Delta\psi$ from an expected angle of contact ψ_m vanishes completely since all contacts are forced to the symmetrical angles $\psi_m^0 = [0^o, 60^0, 120^0, 180^o, 240^o, 300^o]$, defined in a freely rotating coordinate system around any arbitrary cylinder.
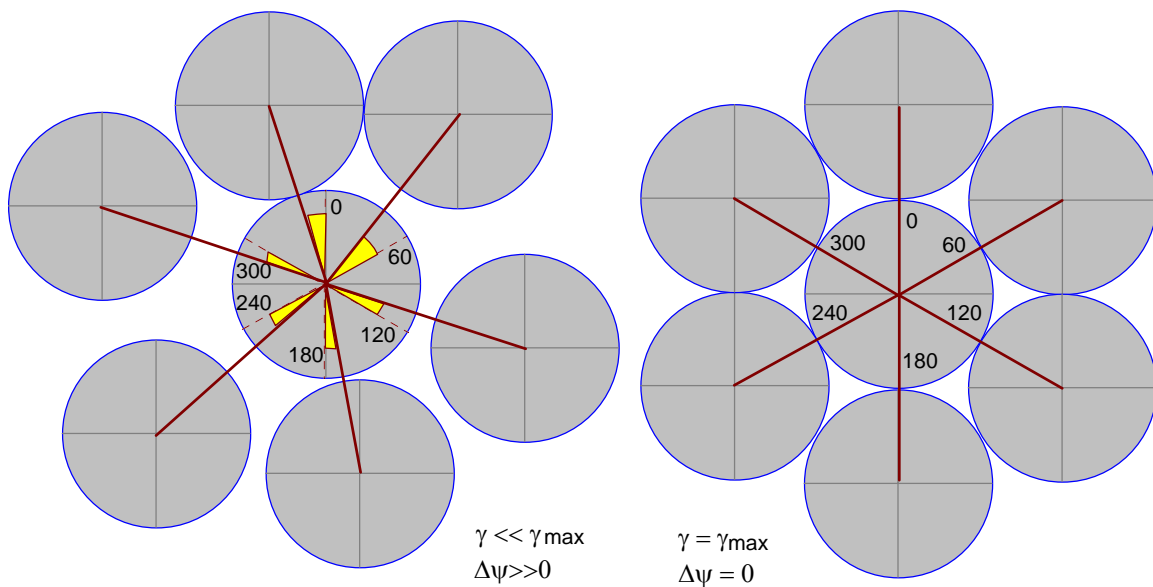
FIG. 134. Reduced degree of freedom in dependency of packing fraction (monosized cylinders)

The dependency of the extent of the distribution of contact angles from the packing fraction for equally-sized cylinders has been investigated in detail by Gervois et al.[50] using methods of Voronoi-tesselation. The following graph shows the experimental results together with a bilinear approximation curve:
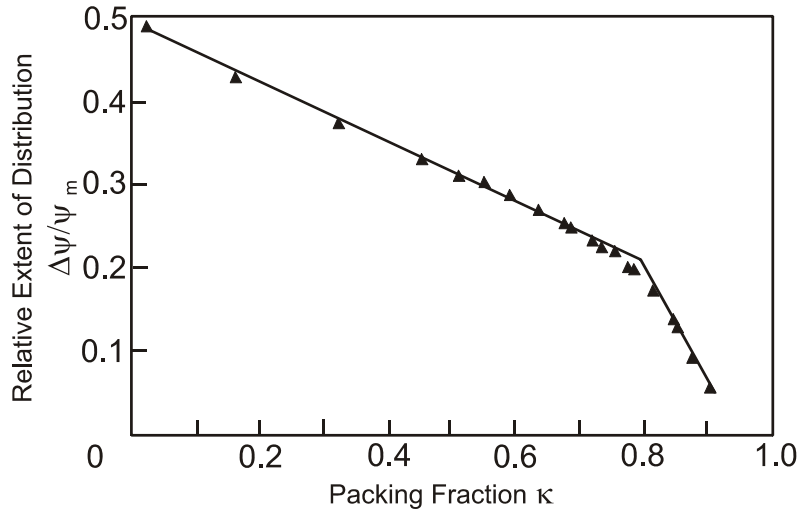
FIG. 135. Extent of contact angle distribution in dependency of packing fraction (monosized cylinders)

The expected angle between two adjacent cylinders with respect to any arbitrary central cylinder is $\psi_m = \pi/3$ for equally-sized particles. Thus for a value of packing fraction approaching zero, the angles are completely independent of each other covering the circumference with constant probability and hence the mean deviation from the ordered state becomes $\dfrac{\Delta\psi}{\psi_m} = 0.5$:
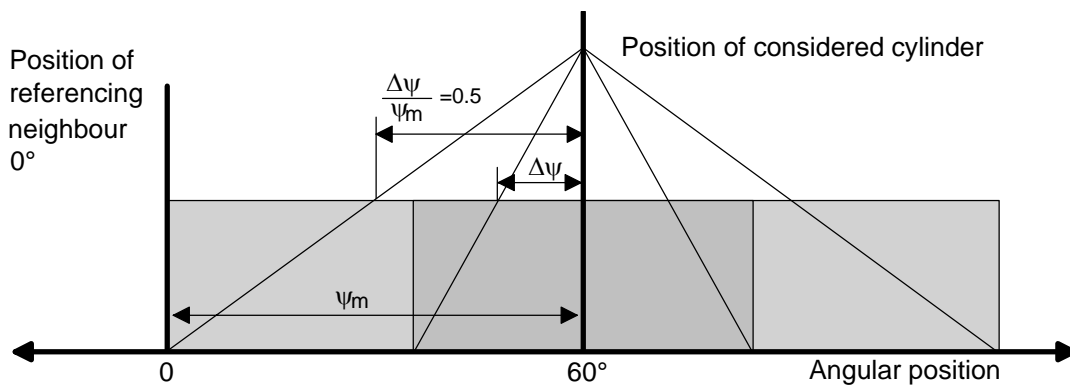
FIG. 136. Extent of contact angle distribution for infinite packing fraction (monosized cylinders)

Since the reference position varies independently too, the extent needs to be distributed to two absolute positions. Hence, the mean deviation from an assumed absolute position for each of the participating contacts is about $\Delta\psi/2\psi_m$ considering monosized systems.

However, the system employed in our experiment rarely fulfils this condition. The simulation described in chapter [11.3.3] provided the mean angular distance between adjacent cylinders in the most ordered state of $\xi = 60^o$ as for equally-sized elements but also a mean deviation from this value of $\Delta\xi \simeq 11.4^o$ for the set of cylinders used in our experiments. Therefore, the distribution given by [50] in dependence of the packing fraction needs to be expanded by the possible variation of the opposite contact position, which is expected to be about three times the measured extent for adjacent cylinders considering the position of three cylinders ordered along a line:
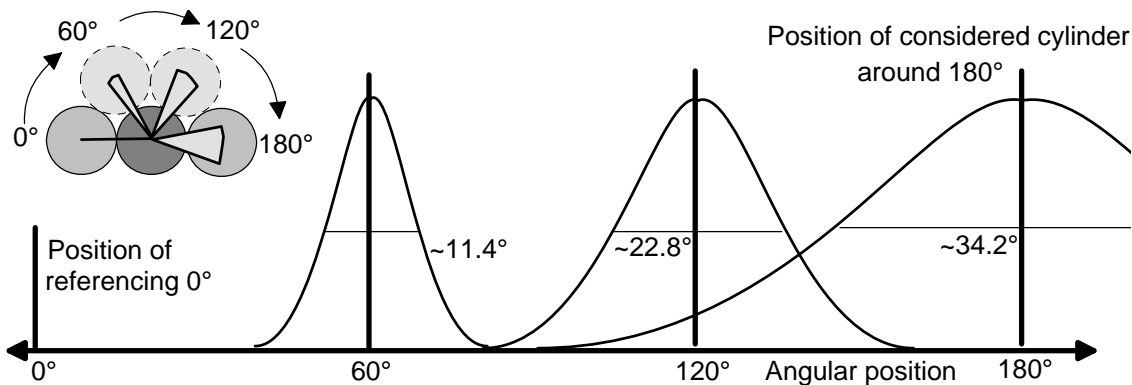
FIG. 137. Extent of contact angle distribution for the set of cylinders used in this paper

In order to confirm this very rough estimation, another simulation calculation was done using dedicated software written in Object Pascal:
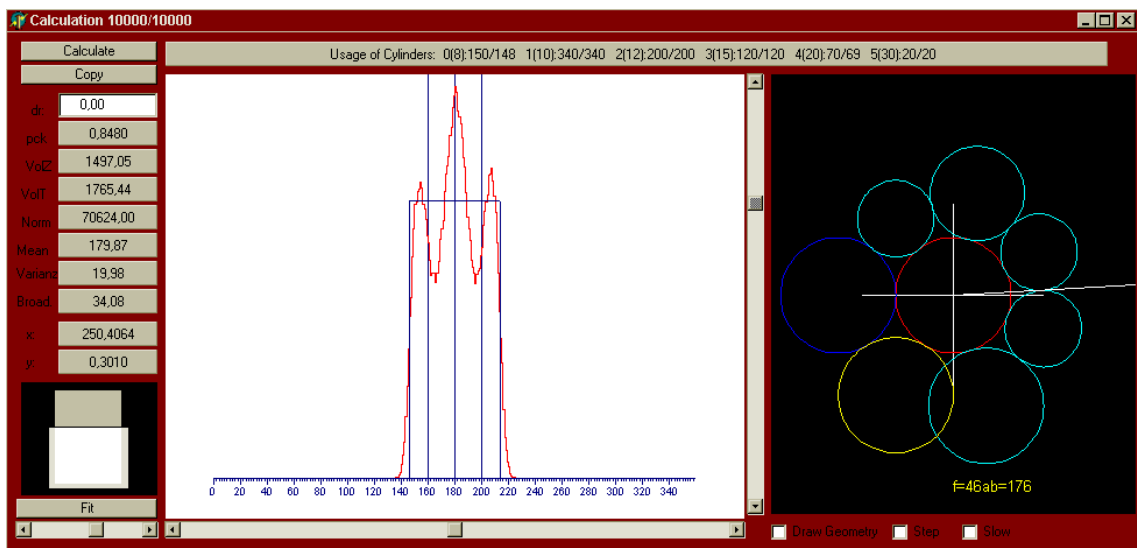
FIG. 138. Screen shot of the simulation software, investigating the distribution of contact angles

After selecting a central cylinder diameter from the pool of available values, it was closely encircled by a set of more cylinders until the circle was closed. The remaining gap extent was then distributed equally to all contacts around the central element. After this, the contact which matches the position 180° best referring to the initial contact was recorded together with its fraction of the gap as possible freedom of variation. Selecting cylinders was always done stochastically, carefully observing the probability of occurrence given by the distribution of diameters.

Furthermore, taking into account the dependency of the packing fraction, every cylinder was surrounded by a virtual 'layer' of predefined thickness, allowing for some well defined distance of the cylinders. The range of free movement for the considered configuration was increased by this thickness since it represents an additional clearance. Finally, the packing fraction value was estimated by comparison of the participating cylinders sections to the total area covered by the polygon which is defined by the centres of the surrounding cylinders.

A typical graph containing data of a series of 10000 simulations is shown in the following graph:
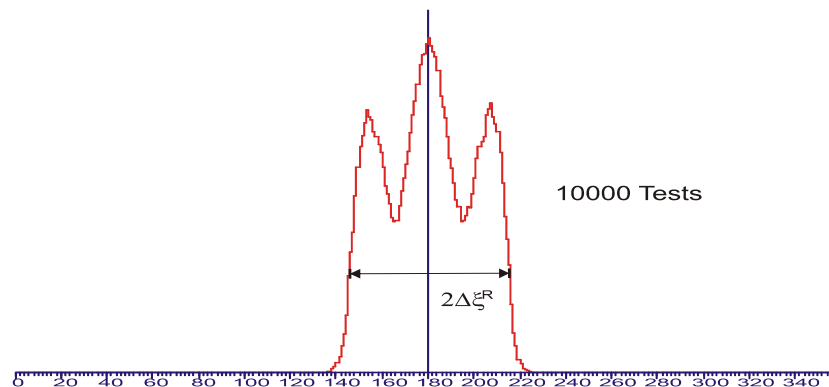
FIG. 139. Typical distribution of contact angles for the used set of cylinders

Obviously, we obtain a broad, compact distribution, sharply limited by well defined angles. Two symmetric peaks at $\simeq 180^o \pm 30^o$ result from the discrete structure of the diameter distribution which allows only for definite configurations. Varying the packing fraction has not much impact on the qualitative figure shown above. Thus, only the extent ξ' of the distribution is used in further considerations. As expected, this value represents a new maximum angle of contact introduced by the discrete character of the cylindrical elements in short ranges.

The results of six series of 10000 simulations each, applying twenty-three different 'cover'-clearance values representing different packing fractions is shown in the following graph:
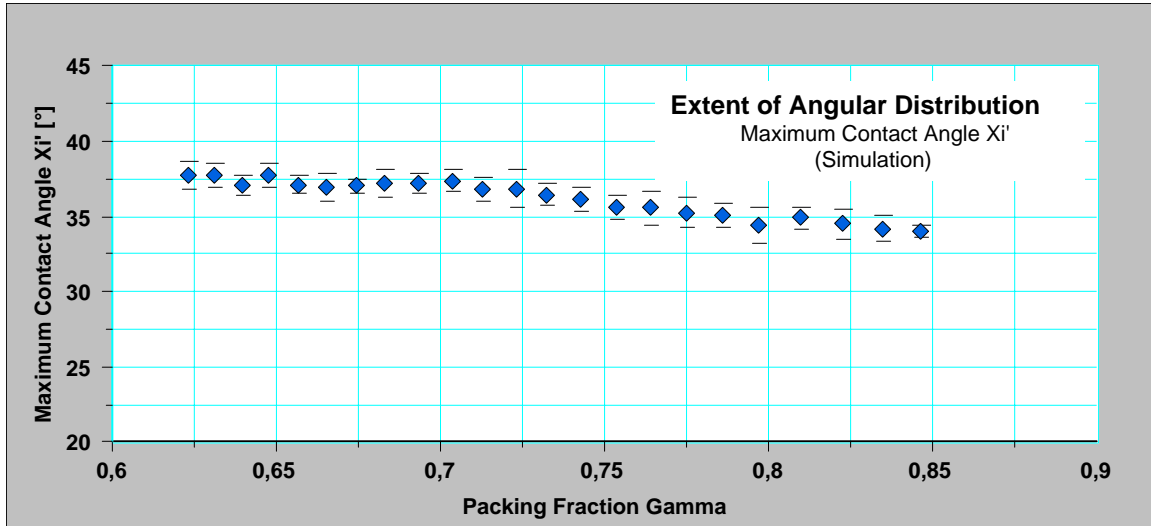

FIG. 140. Extent of the distribution of contact angles vs. Packing fraction (File: SimulationOfOrder.123)

Since the simulation procedure starts at the state which is ordered best, the observed packing fraction value is not the random closest packing ($\gamma_{RCP} \simeq 0.82$) but somewhat higher($\gamma \simeq 0.84$). However, in contrast to the results of Gervois [50] the extent of the distribution of contact angles in the opposite direction of the initial contact is ranging from $\xi' \simeq 35^o..37^o$. This is a clear consequence of the high grade of order, the monosized system approaches on high packing fraction, where the set of cylinder diameters used in our experiments leads to constantly high variations of angles in a force chain, yet limited to a value significantly smaller than the isotropic range of $\xi \simeq 60^o$
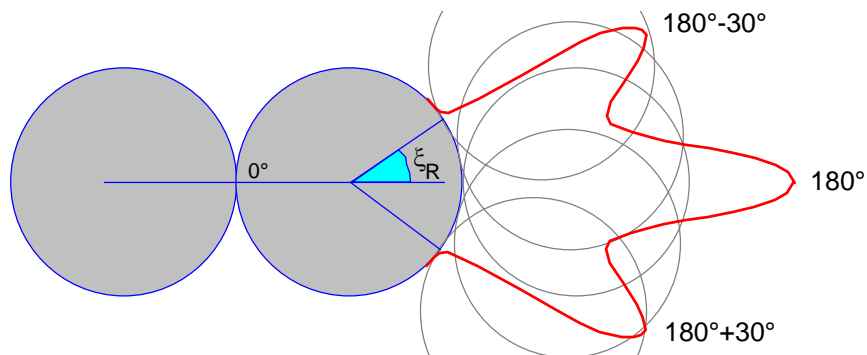
FIG. 141. Typical distribution of contact angles

Remark: The simulation results match the estimated value of $\xi' \simeq 3 \cdot 11.4^o = 34.2^o$ fairly well. The obtained dependency on the packing fraction can not be taken significant due to the coarse method of acquisition.

Altogether, we note the existence of some order in small scales responsible for the building of force chains, where the maximum angle of contact is no longer $\xi \simeq 60^o$ as is valid in average for larger volumes but $\xi' \simeq 36^o$ as a consequence of the cylindrical shape of the elements in interaction with the narrow distribution of cylinder diameters.

13. 3. 3. 2 Equilibrium

In a granular medium treated quasi continuously, each small volume is well balanced in all directions. This implies that any longitudinal chain of cylinders, reaching from the feeding point of force to the border of the granular system bears the same longitudinal fraction of force and produces the same average lateral force keeping local equilibrium with all neighbouring chains.
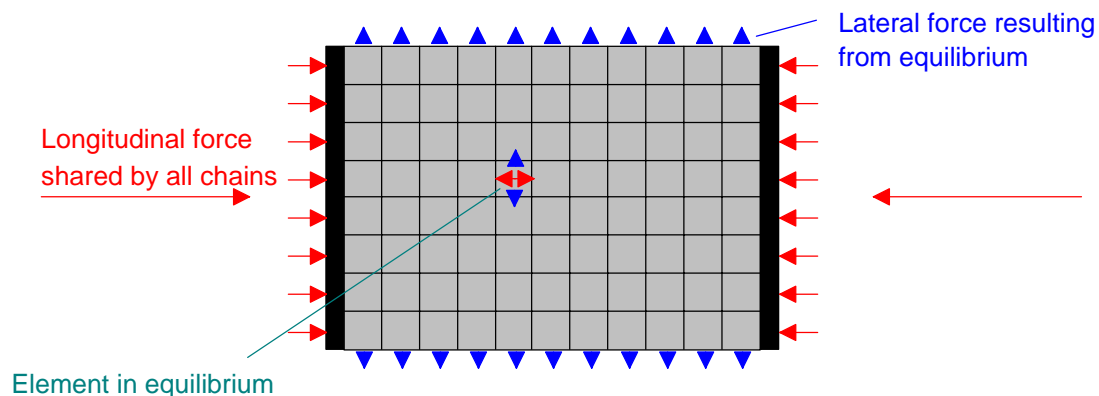
FIG. 142. Equilibrium in a quasi continuous system

Contrary to this, all photo elastic experiments show discrete lines, which obviously are bearing higher longitudinal forces. Nevertheless, they are in equilibrium with their neighbourhood. In particular, adjacent chains are loaded far less, but still supply the local lateral forces needed for equilibrium.
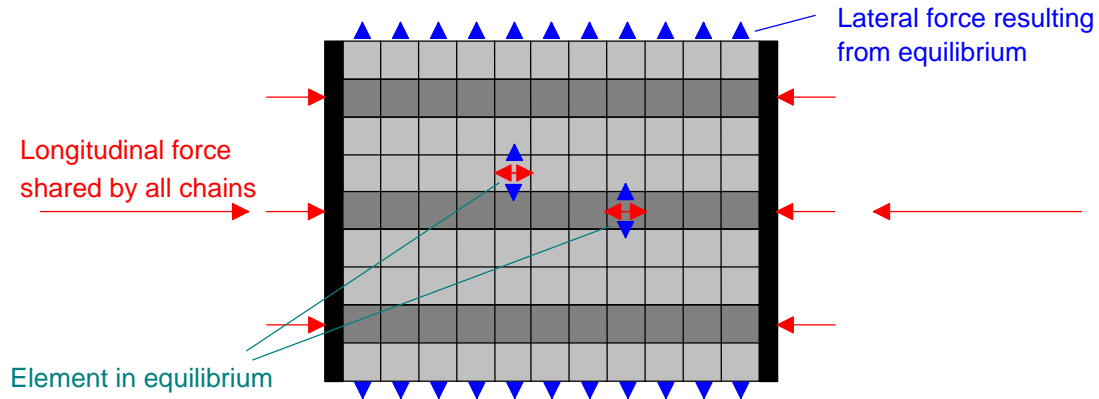
FIG. 143. Equilibrium in a granular system**,** where some chains bear most of the longitudinal stress

Additionally, the observation of much lower angles of contact within visible highlighted chains, mainly far less than the values suggested by the isotropic maximum angle of contact $\xi \simeq 60^o$, leads to the following interpretation:

In order to keep the local equilibrium, small local rearrangements are necessary. Nevertheless, the mean lateral force of any chain needs to be equal, regardless of its capability to bear longitudinal forces. This is possible as soon as the highlighted, and thus more bearing chains are built by angles of contact, which do not utilise the range up to the maximum Angle of Contact $\xi = \frac{\pi}{3}$, but are much less, e.g. only up to $\xi_r \le \xi$. In this case, the Lateral Stress Factor $\overline{K}(\xi_r, \vartheta_0)$ is much lower too.
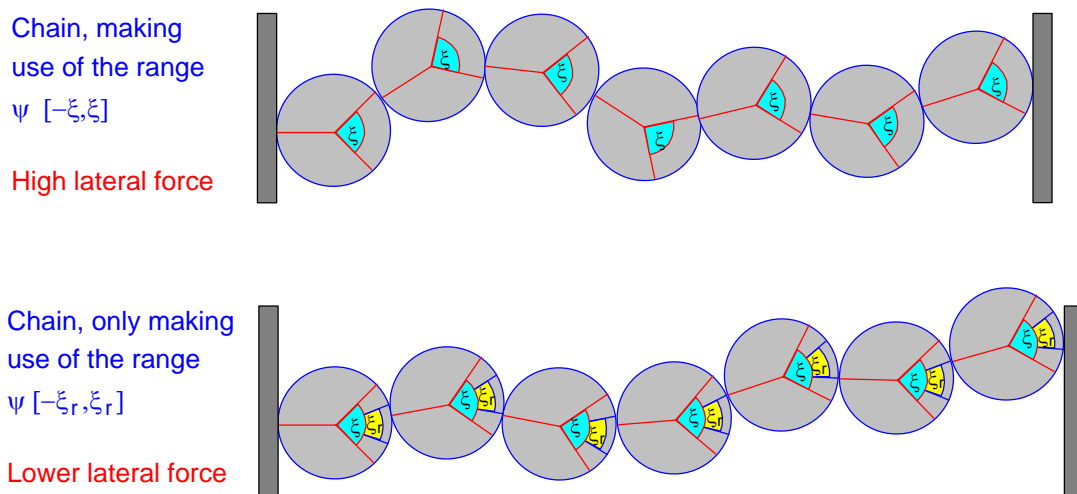
FIG. 144. Reduction of lateral stress by limiting the range of possible contact angles

Thinking macroscopically, a reduced limiting angle of contact ξ_r implies a reduced lateral force factor $\overline{K}(\xi_r, \vartheta_0)$. The condition of equilibrium requires this lateral force to equal the average lateral force within the granular system as a whole. In order to achieve this, such a chain can occur only infrequently. One out of m parallel chains can be of such configuration, if

$$ m = \frac{\overline{K}(\xi, \vartheta_0)}{\overline{K}(\xi_r, \vartheta_0)}. $$

Only in this case, the longitudinal force of each chain F_{chain} is enlarged exactly by this factor m and thus enlarges the reduced lateral force $\overline{K}(\xi_r, \vartheta_0) \cdot F_{chain}$ to meet the equilibrium.

Based on this, the factor m can be interpreted as the average distance of bearing chains in the horizontal direction.
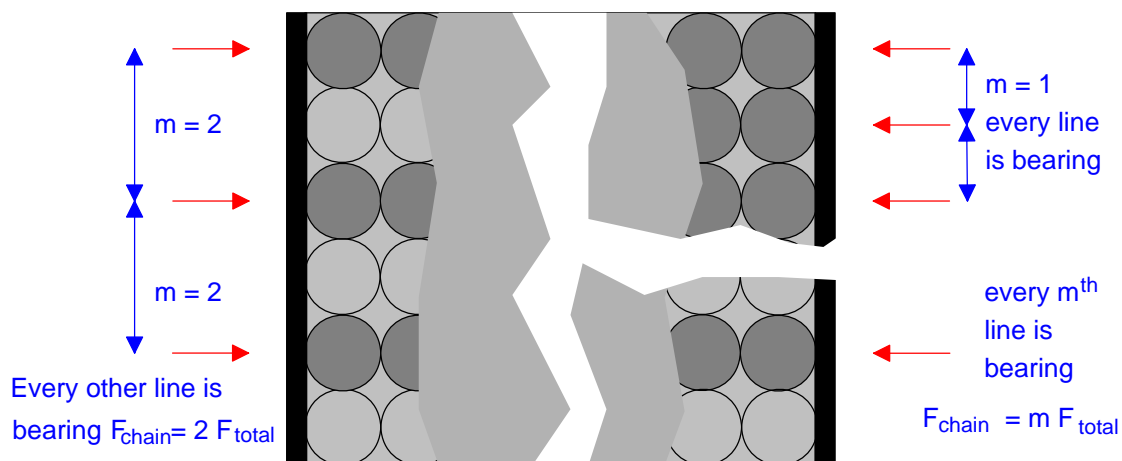
FIG. 145. Condition of equilibrium in inhomogeneous granular material

In order to determine this information, the lateral force factor $\overline{K}$ was calculated numerically for a range of Angles of Friction $\vartheta_0 \in [0, 45^o]$ and for different limiting Angles of Contact $\xi_r \in [10^o, 60^o]$, where the absolute maximum Angle of Contact ξ was assumed to be $\xi = 60^o$. The graph shows the decrease of lateral stress dependent on the reduction of the limiting Angle of Contact ξ_r, calculated by the simulation software which was described in chapter 11.2. *Statistical approach: Less organised granular material, Monte Carlo Modelling* f.f.
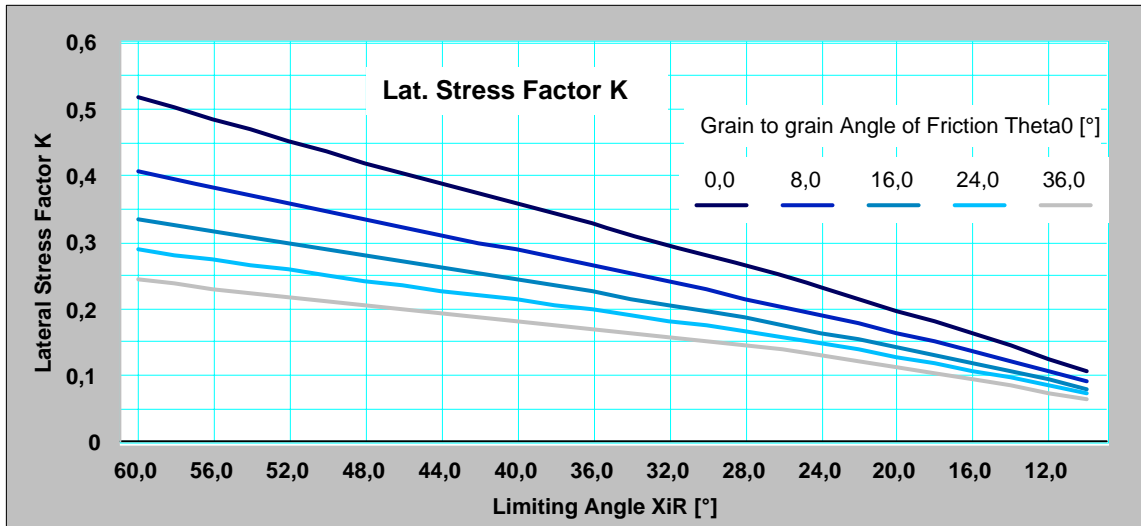
FIG. 146. Lateral stress factor under limited range of contact angles (File: StifferLines.123)

Then, calculating the ratio $m = \dfrac{\overline{K}(\xi, \vartheta_0)}{\overline{K}(\xi_r, \vartheta_0)}$ yields the following dependencies of the average distance of bearing chains *vs.* the microscopic angle of friction ϑ_0 and the reduced limiting angle of contact ξ_r, assuming $\xi = 60^o$:
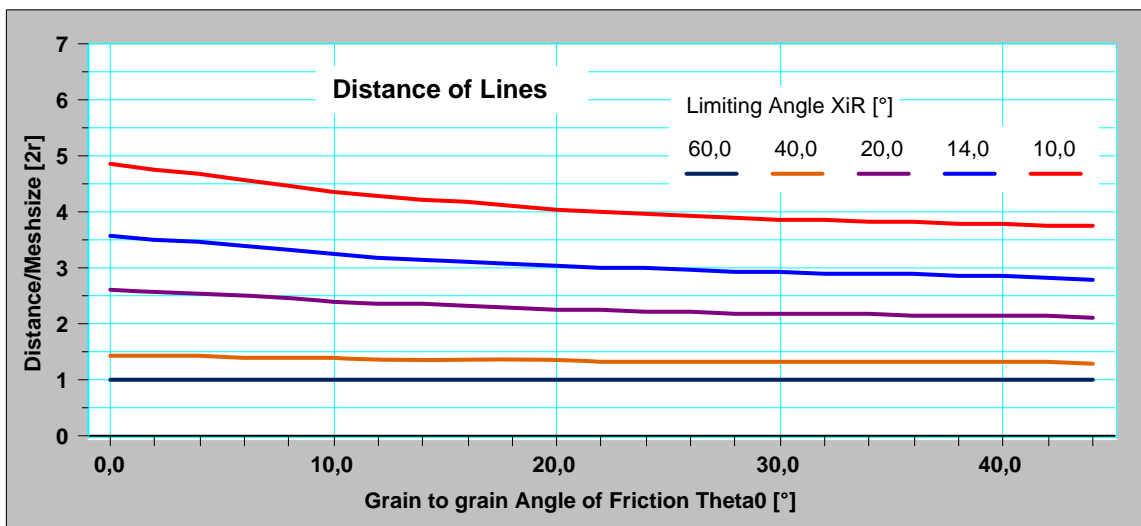

FIG. 147. Required distance of force chains resulting from limited range of contact angles (File: StifferLines.123)

Dependency on the Angle of Friction ϑ_0 is obviously weak as corresponds to an intuitive view on the structures which were made visible by the polariscope. Therefore, only the average meshsize value is used in further considerations:
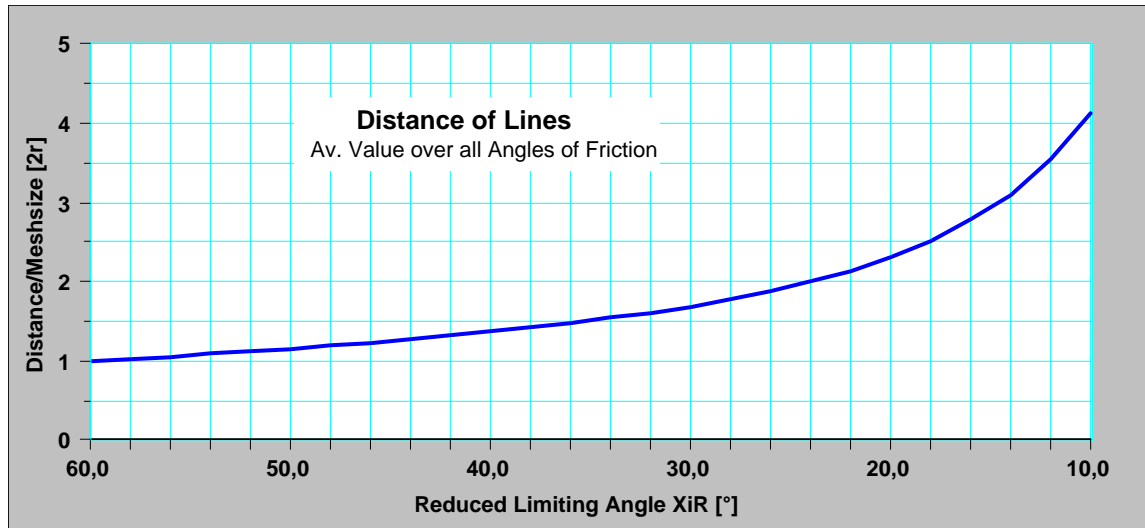
FIG. 148. Required distance of force chains resulting from limited range of contact angles (File: StifferLines.123)

13. 3. 3. 3 Isotropy

Since the shown graph does not provide concrete information about the resulting average mesh size, another argument needs to be brought into discussion:

As discussed before, the probability of a chain of a certain length can be estimated by exponentiating the probability of a single contact which is determined by the reduced range of possible contacts.

Preconditioning the existence of small scale structures which reduce the available range of contact angles already to $\xi' \simeq 36^o$, the probability of contact within a further reduced range of angles is:

$$P(\xi_r) = \frac{\xi_r}{\xi'}$$

This determines directly the probability of a chain of length n comprising only contact angles in the range $[-\xi_r, \xi_r]$:

$$P(\xi_r, n) = \left(\frac{\xi_r}{\xi'}\right)^{n-1}$$

Alternatively, the reciprocal provides the average distance at which such chains are to be expected:

$$M(\xi_r, n) = \left(\frac{\xi'}{\xi_r}\right)^{n-1}$$

Based on fundamental isotropy of a granular medium building small scale structures, there is no reason why the length of a stable force chain should differ a lot from the distance of such lines derived e.g. by the argument of equilibrium discussed before.
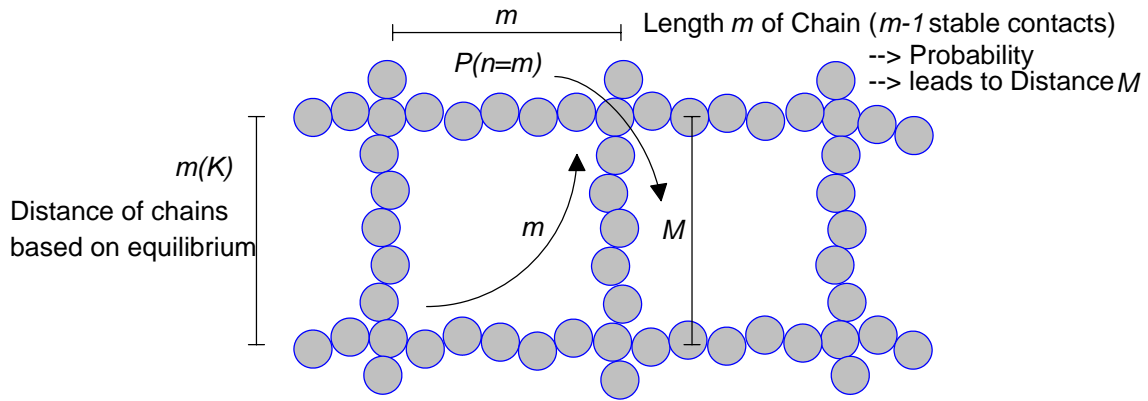
FIG. 149. Correlation of longitudinal and transversal chain distances and -lengths

Admittedly, this is not a very strong argument leading to exact results, but serves fairly well in order to justify a maximum extent of such structures. Then, the length of a chain *n* can be determined by the distance of force chains extracted by the equilibrium argument as

$$n = m = \frac{\overline{K}(\xi, \vartheta_0)}{\overline{K}(\xi_r, \vartheta_0)}, \text{ and therefore } M(\xi_r, n) = \left(\frac{\xi'}{\xi_r}\right)^{\frac{\overline{K}(\xi, \vartheta_0)}{\overline{K}(\xi_r, \vartheta_0)} - 1}.$$
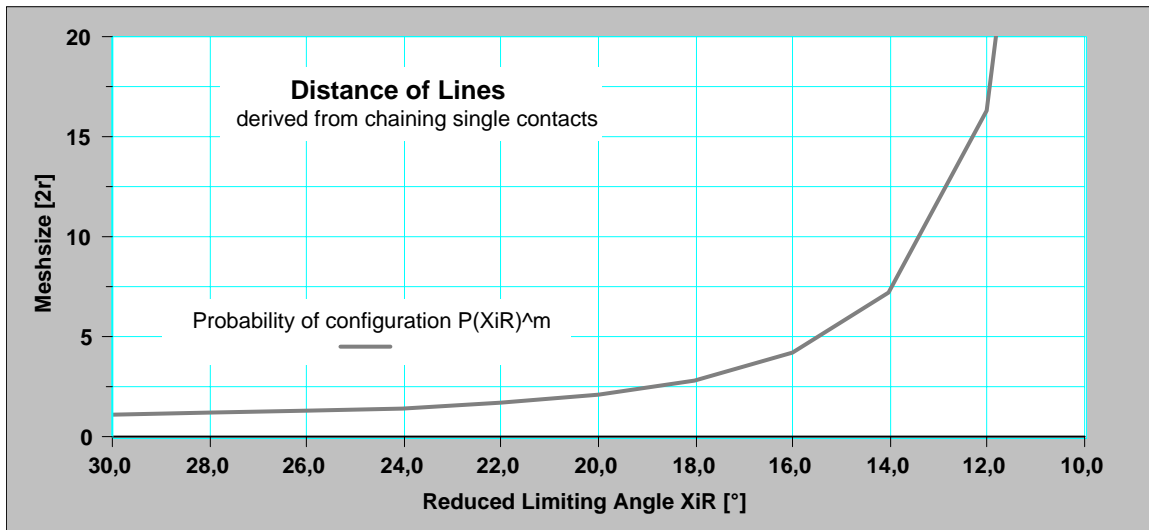
FIG. 150. Required distance of force chains resulting from chaining single contacts (File: StifferLines.123)

If both considerations hold true and as long as the isotropy argument is valid, the resulting chain distances *m* and *M* are expected to match.
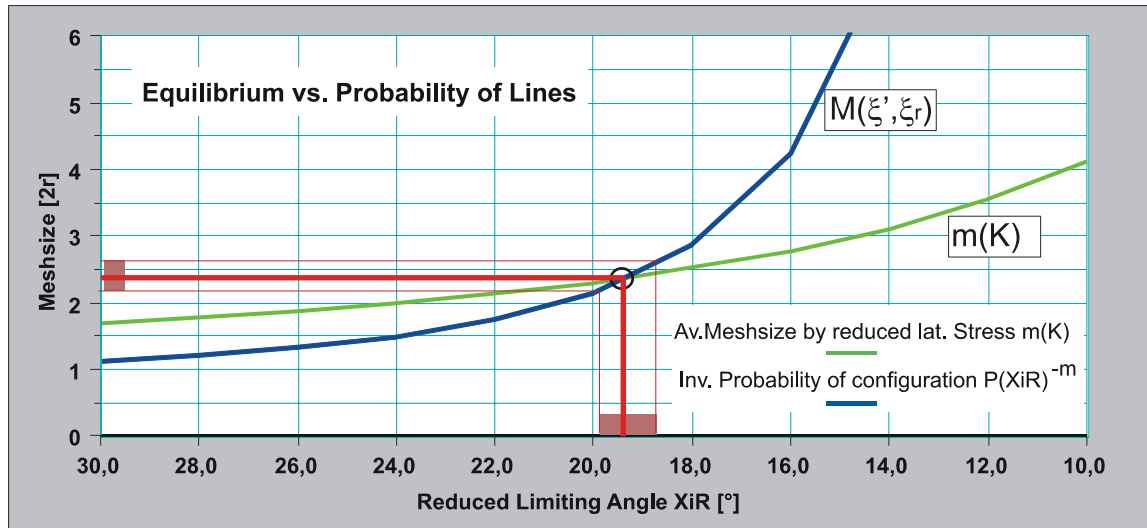
FIG. 151. Required distance of force chains, both approaches (File: StifferLines.123)

In fact, the building of meshes is possible without violation of the equilibrium. The real limiting angles of contact ξ_r seem to be located closely around 19°-20°. The resulting meshsize of about $2.4^{\pm 0.2}$ diameters of cylinders matches observations from photo elastic recordings very well (See next chapter for details). This value presents itself widely independent of the angle of friction involved, which confirms the commonly practised use of averaged values ignoring the network structure for volumes greater than several diameters of cylinders.

The observed intersection point is clearly positioned, yet due to the qualitative character of the used arguments, it can be taken only for a very rough estimation. Nevertheless, the diverging curves in the graph shown above justify definitely, that not much larger mesh sizes can be expected.

13. 3. 4 Exponential Prediction

The results of the previous section can be used to predict the distribution of mesh size much better. Here, only the obtained value of the mean meshsize and the exponential characteristic are taken in using the normalised exponential distribution:

$$P_z = \frac{1}{z_0} \exp - \frac{z}{z_0}.$$

In the present case it needs to be adapted, since the mesh size at least is $m = 1$, lower values do not make sense. This can easily be introduced by substituting $m := z + 1$ and leads to

$$P_z(m) = \frac{1}{m_0 - 1} \exp\left(-\frac{m-1}{m_0-1}\right)$$

Normalising:
$$\frac{1}{m_0 - 1} \int_1^\infty \exp\left(-\frac{m-1}{m_0-1}\right) dm = \frac{1}{z_0} \int_0^\infty \exp\left(-\frac{z}{z_0}\right) dz = 1$$

Mean value:
$$\overline{m} = \frac{1}{m_0 - 1} \int_1^\infty m \exp\left(-\frac{m-1}{m_0-1}\right) dm = \frac{1}{z_0} \int_0^\infty (z+1) \exp\left(-\frac{z}{z_0}\right) dz$$

$$\overline{m} = z_0 + \frac{1}{z_0}\left[-z_0 \exp\left(-\frac{z}{z_0}\right)\right]_0^\infty = z_0 + \frac{1}{z_0} z_0 = z_0 + 1 = m_0$$

This finally describes the distribution of mesh sizes

$$P_z(m) = \frac{1}{m_0 - 1} \exp\left(-\frac{m-1}{m_0-1}\right)$$

with $m_0 \simeq 2.4^{\pm 0.2}$ as the average mesh size and its deviation accordingly:
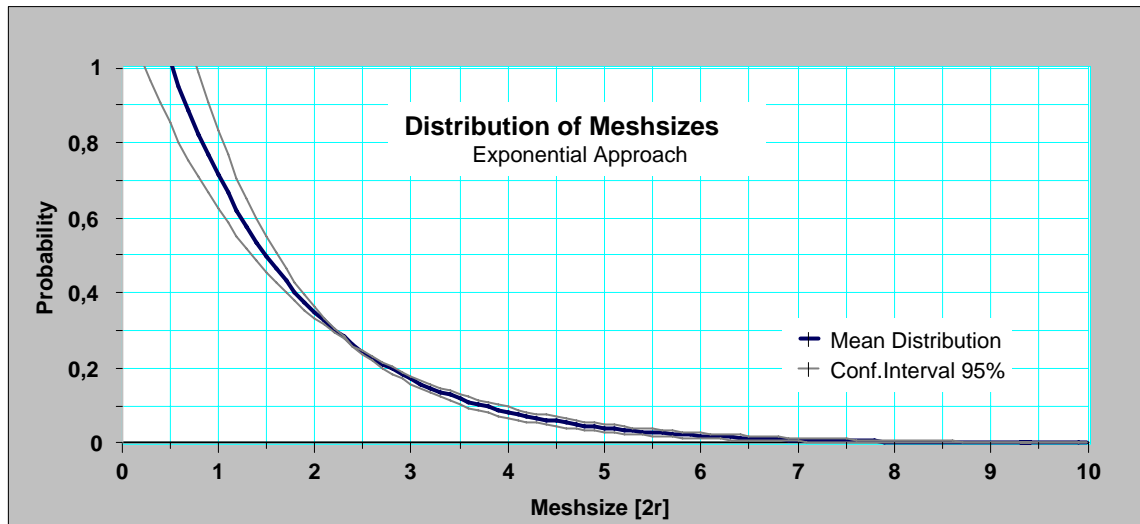
FIG. 152. Predicted exponential distribution of mesh sizes resp. chain lengths (File: DistribOf MeshSize.123)

13. 4 Validation by Measurement

The theoretical estimations made here need to be tested for correspondence with the experimental data obtained from the polariscope pictures in the measurement section. This concerns both, the average mesh size itself as well as the exponential characteristic of the distribution.

At first, the exponential distribution of intensity classes which equals the distribution of contact forces can easily be approved from the experimental observations made above. After eliminating typical acquisition artefacts like the noise of the camera, distributing some illuminated pixels to every class, we obtain a fairly good approximation of the experimental data writing the frequency of occurrence $W(\omega)$ as:

$$W(\omega) = a \cdot \exp - \frac{\omega}{\beta}.$$

In this case we set the constants $a = 0.07$ and $\beta = 12$, while ω represents the illumination respectively the force class.
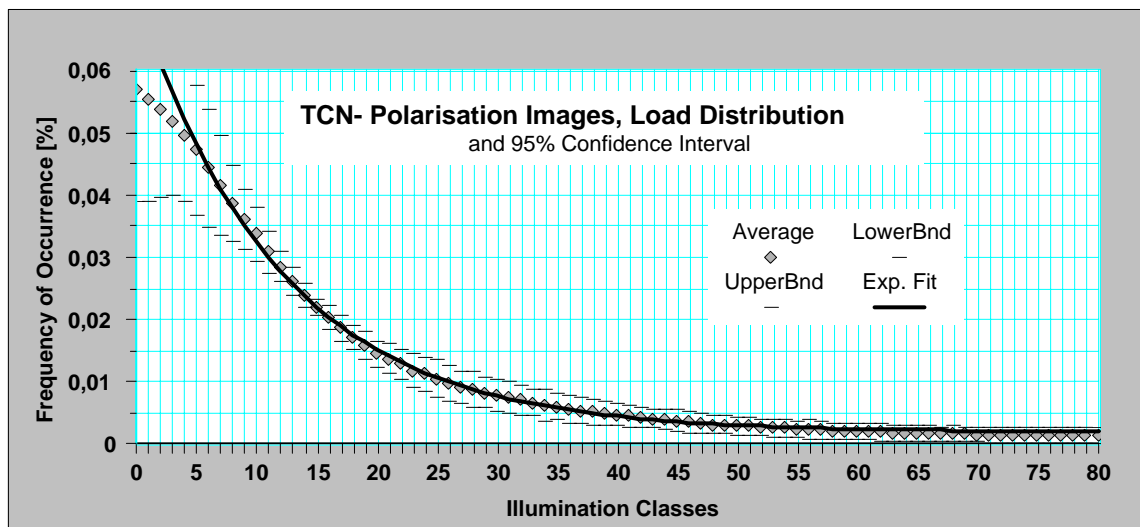
FIG. 153. Typical analysis of light intensities of several images, obtained from Polyester cylinders (File: TCN-Distrib.123)

The high quality of the general accordance of the measurement results with an exponential function is confirmed by the coefficients of regression:

	HLO-Readings			**LLO-Readings**		
Surfacematerial	Polyester	Polyolefin	Teflon	Polyester	Polyolefin	Teflon
Coeff of Regr. R²	0,993	0,992	0,995	0,995	0,994	0,996

Such a distribution of contact forces corresponds very well to the characteristics obtained by Mueth et al.[20]. In contrast to their findings, the constant part of the distribution is cut off by recomputing the original distribution with reference to the unloaded distribution.

This exponential characteristic can be mapped to the meshsize distribution described above since every single mesh concentrating forces on the border chains inevitably causes forces proportional to its size. Thus, an exponential meshsize distribution is confirmed by the obtained force distribution as well.

Besides the exponential characteristic of the Frequency of Occurrence, the mean values describing the distance between force bearing chains have been derived from the images for some surface materials.

Plotting them to the next graph together with the results of the theoretical estimation, we conclude fairly good correspondence:
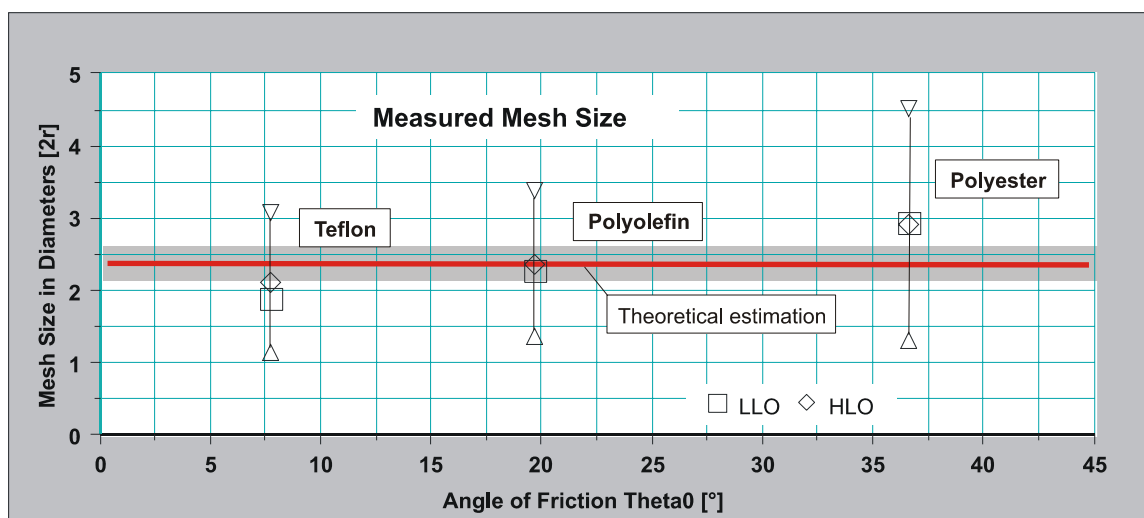
FIG. 154. Comparison of theoretical meshsizes vs. experimentally obtained values (File: MeshSizeInterpr.123)

- The range of mesh size values is met well varying from 2 to 3 diameters as predicated

- The error margins are rather high, but include the theoretical values.

- The measurement indicates slightly increasing mesh size with rising angle of friction, which corresponds to our intuition but is not covered by the theoretical estimation. Furthermore, this property cannot be confirmed due to the large error bars.

- Apparently there is no significant difference between HLO- and LLO-readings, where one would expect self organisational mechanisms to have greater impact.

13. 5 Definition of Scaling Units

Obviously a granular medium develops inhomogeneous stress distributions due to its inherently structured character which is confirmed in detail in the polariscope images.

However reviewing this chapter, we found several points of evidence for a restricted scope of influence of these inhomogenities:

- The estimation of scope based on an expanded frictional approach in granular systems with low level of organisation (LLO) yields an average range of 3-4 grain diameters.

- The same approach applied to granular media with a high level of organisation (HLO) leads in dependence of the direction to a scope of 3-7 grain diameters.

- The more complex estimation of the average mesh width in a force network results in values between two and three grain diameters which match the readings from the polarisation images very well.

These limited values raise the question of how far a granular medium can be treated by continuous approaches as has been successfully done throughout the history of soil mechanics.

On the other hand we are dealing with material of extremely nonlinear and discontinuous character, i.e. smallest variations of forces, positions or deformations have unlimited consequences. Therefore, simply averaging microscopic states can lead only to solutions ignoring any macroscopic building of structures.

This may motivate to make use of the tools of nonlinear dynamics and take over results from chaos theory, which traditionally deals with such behaviour. Yet a very fundamental discrepancy needs to be kept in mind:

The Theory of Chaos is based on the unpredictable behaviour of a well determined problem, like coupled pendulums, presenting chaotic characteristics under certain sets of parameters. The case of granular material is different from that. Here, the problem itself is defined only very diffusely: Some 10^6 particles, each with 6 degrees of freedom and all of unknown values, are interacting. Due to the nonlinear character of the contacting mechanisms, they are building macroscopic structures from their microscopic non linearity, reaching far beyond the extent of single particles. But these structures are limited in size and extent as shown above by the exponential decay of impact. Not exceeding about ten times the diameter of a single particle, these structures cannot have any effect in bigger scales and are expected to be describable by average values.

Notabene, the mean values need to be computed covering the structures, not only the single particles. Yet, accepting the considerations about equilibrium, accomplished in this chapter, the discrepancy is not very large, as long as small deformations and thus few organising mechanisms are working.

Under this consideration a set of scales volunteers to be defined (cp. Oger and Jernot in [56] Chapter 6):

The smallest scale is the one of a single particle. Named $R^{(1)}$, it is defined by the mean radius $2\bar{r}$ of a cylinder. Since the variance of radii is predetermined as low, mechanisms active in this range can be computed by averaging positions and angles of contact and will deviate little within the range.

Interaction of particles in the direct neighbourhood builds the observed macroscopic structures. As can be taken from the measurements as well as from the calculations of range, mean line lengths and average mesh sizes, the limit of extent will not exceed about ten times the diameter of a single particle. Thus we determine the scale for structures to $10 \cdot 2\bar{r}$ and call it $R^{(10)}$.

Beyond this size the behaviour of the material is ruled no more by single particles or the structures built by their nonlinear interaction, but can be described through average values. The scale characterised by stochastic values can therefore be called $R^{(100)}$, extending over some hundred diameters of a single particle.
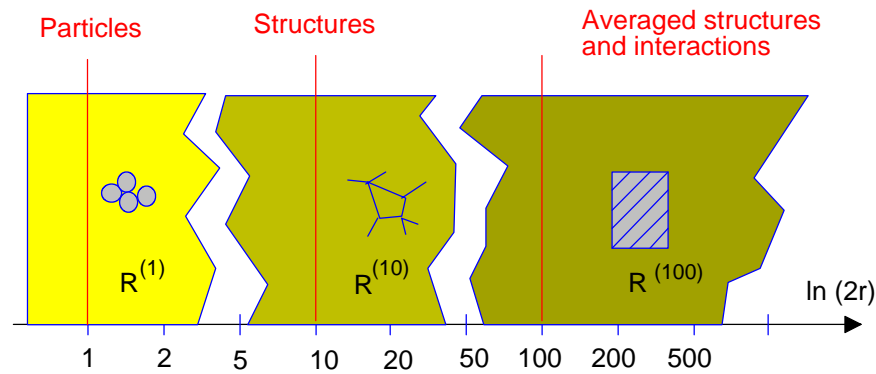
FIG. 155. General definition of scales for granular material

Remarks:

Some phenomena are not discussed in this paper but need to be mentioned here:

- *In dealing with granular media, e.g. in a silo, the effect of building 'arches' with a scope much larger than several grain diameters is observed. Such strong long-range structures can be hazardous since the range of selforganised high stability is potentially very narrow and may cause a dramatic breakdown if disturbed. Yet, with dry granular media the probability of building such a large structure is very low but not zero as indicated by the exponential characteristic of line lengths. Clearly, this is no more valid if cohesion of some strength is taken into account which is not pursued in this paper. Furthermore, the introduction of non cylindrical but sharply angled grains may increase the probability of larger structures.*

- *All arguments concerning scales refer to the average diameter $2\bar{r}$ of the grains. This presupposes a narrow distribution of radii since otherwise an average diameter has no meaning. Thus, granular materials comprising grains with widely varying diameters are not covered by such a concept. In chapter 2: Granular Parameters in Soil Mechanics we pointed out that the grading curves of naturally grown soil in general fail to meet this idealisation. Both the computational model as well as the physical model used for measurement purposes rather correspond to uniform gravel (Uniformity $U \simeq 1.6$). In natural soil, we assume the mechanics to be dominated by the granularity of the small grains as long as their fraction is sufficient to completely embed the large elements. Thus, we consider natural soil to be positioned primarily in the range $R^{(100)}$, where averaging is permissible.*

14 Conclusions

The major aim of this research was to investigate the distinctive influence of friction and structure on the behaviour of dry granular material, as evidenced by the redirection of stress applied in one direction to the transversal direction. Since many aspects of structural impact have been previously studied both theoretically and numerically on frictionless media or experimentally on a medium with fixed coefficients of friction, we adopted the opposite approach:

We measured the lateral stress response to a longitudinally applied stress on a granular medium with fixed structural parameters of grain size and shape, but using different coefficients of friction. Hence, the modification of the frictional parameters made by the structure was determined and discussed by appropriate plausibility computations.

The results presented are, like all experimental measurements, subject to reasonable interpretation, which can and need to be discussed further.

However, concerning two dimensional circular cylinder granules with diameters sharply distributed around a central value, the following conclusions can be drawn:

- Evaluating the packing fraction while exposing the system to deformation suggests to assume constant density with a weak inverse dependency on the Angle of Friction. The fact that the packing fraction value does not significantly vary with the level of organisation matches the known behaviour of coarse uniform gravel which cannot be compacted. Besides this, the similarity of the gradation curve of the model and the one of uniform gravel confirms its appropriate representation by the model. Furthermore, the measured packing fraction values match very well the recomputed void ratios known from natural uniform gravel or round sand.

- Such granular material, exposed to uniaxial shear deformation of about 20 % or more which is equivalent to a displacement of a few grain diameters, can be well described using the model of Rankine or the later derivatives of it, as long as a well-defined structural correction is applied to the microscopic grain to grain coefficient of friction.

- The structural correction contains terms derived from the broadness of the distribution of diameters and the degree of deformation. Existing local irregularities of the surface seem

not to play a significant role. Obviously their impact is averaged by the stochastically distributed slopes at the contact points.

- The dominant effect is the shifting of stable collectives against each other, where action takes place mainly in the shearing joint, allowing for a statistical approach based on the circular shape of the cylinders and the straightness of the joint.

- If the deformation remains below this limit, reaching 5 % to 10 %, which corresponds to a displacement of about one grain diameter, but is not zero, the behaviour is dominated by effects of single cylinders, moving, rolling or gliding according to the local properties of contacts.

- Under these circumstances local unevenness of the circumference of the cylinders is determined to be a most significant effect. Depending on the geometrical height and sharpness of irregularities, it adds a relevant term to the mean angle of friction, due to the breaking of symmetries.

- After correcting for the influence of local unevenness, the resulting lateral force response factor can be approximated as an exponentially decreasing function of the angle of friction. Being dominated by stochastical microstructures, the results cannot be described by approaches considering sliding joints like that of Rankine.

- However, such a state can be well described on the basis of a statistical approach, where positions and angles of contact are subject to known elementary distributions. The main parameter besides the microscopical angle of friction turned out to be the average maximum possible angle of contact, determined by the distribution of diameters. A minor additional correction proportional to the angle of friction needs to be made to include the impact of small locally stable configurations of cylinders which are created by self organising mechanisms triggered by the even small deformation of some percent.

- As the inherent structure of granular material can be taken in by modifying the effective Angle of Friction, the building of a macroscopic network of force bearing chains is of different character.

- The meshsize of such a network was determined to be of 2-3 average grain diameters and presents itself as the image of the fine level spatial distribution of forces. It could be

shown, that the influence of such inhomogeneities is limited to a range of about 10 diameters.

- Referring to the average size of the cylinders, we can define a scale, where microscopic behaviour dominates, where macroscopic structures play a role and where structural impact can be neglected. Such a limited scope corresponds to the well-proven approach of classical soil mechanics as effects of granular media are of minor influence on this scale. Yet, it must be kept in mind, that extensions of the model like the consideration of more angular grains or non zero cohesion will certainly enlarge significantly the range of impact. Furthermore, we naturally consider as very basic the narrow distribution of grain diameters around a nominal value for such a conclusion.

In order to apply these findings to more complex granular media and to finally meet the description of a wider range of natural soil, the model needs to be extended to three dimensions, different shapes of the grains need to be taken into account and last but not least it becomes necessary to consider different distributions of grain diameters.

Acknowledgements

First of all I would like to thank Prof. Dr.-Ing. N. Vogt, Zentrum Geotechnik, Techn. Univ. München for the supervision of this dissertation, particularly for his readiness to adopt this dissertation during the final period as first referee.

Further I am very much obliged to Prof. Dr. rer. nat. H.-J. Herrmann, ICP, Universität Stuttgart, who not only was kind enough to take the task of the second referee but also supported me time and again with his valuable annotations and remarks.

For many constructive and encouraging discussions during the finalisation of this dissertation I am deeply indebted to Prof. Dr.-Ing. J. Zimmermann, Technische Universität München.

Next I wish to express my thanks to Prof. Dr.-Ing. H.-J. Bösch, who largely supported this research work and to the *Dr.-Ing. Leonard-Lorentz-Stiftung*, who has made a major contribution to the experimental setup.

Furthermore I appreciate so much the many valuable and encouraging discussions with my father, O. Prof. Reg.Bmstr. A. Eber who unfortunately died during the finalisation of the dissertation and just missed the opportunity to see it finished.

My very special thanks go in particular to Dr.-Ing. W. Berry, European Space Agency, Netherlands who patiently reflected all my considerations and didn't get tired proof-reading this paper again and again.

Also deserving my thanks, Prof. Dr.-Ing. R. Floss, Zentrum Geotechnik, Techn. Univ. München has always been ready to review the topics of this paper in careful detail and full comprehensiveness.

Many other people, colleagues and friends have contributed their part to this paper in uncountable helpful conversations, thank you all!

Beyond all, I am very grateful to my wife for her patience during the time I elaborated this dissertation.

15 References

[1] H. M. Jaeger and S. R. Nagel, *Science* **255** (1992), 1523.

[2] S. R. Nagel, *Rev. Modern Phys.* **64** (1992), 1523.

[3] Ch. A. Coulomb, *Essai sur une application des règles de maximis es minimis à quelques problèmes de statique relatifs à l'architecture, - Mèmoires Acadèmie Royale des Sciences*, vol VII, Annèe 1773 - Paris, 1776

[4] C. A. Coulomb, *Acad. Roy. Sci. Mem. Phys. Diverse Savants* **7** (1773), 9.

[5] W. J. W. Rankine, *Philos. Trans. Roy. Soc. London* **147** (1857), 9.

[6] W.J.M. Rankine. *Handbuch der Bauingenieurkunst nach der 12. Auflage deutsch bearbeitet von F. Kreuter*, 1880, Wien (Lehmann & Wentzel)

[7] O. Reynolds, *On the dilatancy of media composed of rigid particles in contact*, Phil. Mag. Sehr. 5 **50** (1885)469

[8] I. Jaky: Die klassische Erddrucktheorie mit besonderer Rücksicht auf die Stützwandbewegung, Abhandlung IVBH. Int. Ver. für Brückenbau und Hochbau I (1938), Band 5.

[9] D. Mohr: Beiträge zur Theorie des Erddrucks, Zeitschrift des Architekten- und Ingenieurvereins zu Hannover, 1871/72, Hannover

[10] R. A. Bagnold, Proc. R. Soc. London, Ser. A. 225(1954) 49-63

[11] B. Francoise, F. Lacombe, H. J. Herrmann, *Phys. Rev. E* **65** (2002), 031311.

[12] J. W. Rudnicki and J. R. Rice, J. Mech. Phys. Solids 23, 371 (1975).

[13] D. M. Mueth, G.F. Debregeas, G.S. Karzmar, P.J. Eng, S.R. Nagel and H.M. Jaeger, *cond-mat 0003433*

[14] J. Astrom, H.J. Herrman and J. Timonen, Granular Packings and Fault Zones,*Phys.Rev. Lett* **84**, 638 (2000)

[15] S. Schollman, Phys. Rev. E 59,889 (1999)

[16] J.C. Geminard, W. Losert, J.P.Gollub, *Phys. Rev. E.* **59**,739, (1999)

[17] F. Radjai, D. E. Wolf, M. Jean and J.J. Moreau, *Phys. Rev. Lett.* **80**,61 (1998)

[18] S. N. Coppersmith, C.-h. Liu, S. Majumdar, O. Narayan and T.A. Witten, Model for force fluctuations in bead packs, *Phys. Rev. E,* **53** (1996) 4673

[19] C.-h. Liu, S.R. Nagel, D. A. Schecter, S. N. Coppersmith, S. Majumdar, O. Narayan and T. A. Witten, Force fluctuations in bead packs, *science,* **269** (1995) 513

[20] D. M. Mueth, H.M. Jaeger and S.R. Nagel, Force Distribution in an Granular Medium *Phys. Rev. E,* **57** (1998) 3164

[21] E. Bruce Pitman, Forces on bins: The effect of random friction *Phys. Rev. E,* **57** (1998) 3170

[22] E. Bruce Pitman, Average stresses and force fluctuations in noncohesive granular material *Phys. Rev. E,* **57** (1998) 3204

[23] P. A. Thompson and G. S. Grest, Granular Flow: Friction and Dilatancy Transition *Phys. Rev. Lett,* **67** (1991) 1751

[24] T. Pöschel and V. Buchholtz, Static Friction Phenomena in Granular Materials: Coulomb Law versus Particle Geometry *Phys. Rev. Lett,* **71** (1993) 3963

[25] J. Duran, E. Kolb and L. Vanel, Static friction and arch formation in granular material *Phys. Rev. E,* **58** (1998) 805

[26] D. Howell and R. P. Behringer, Fluctuations in a 2D Granular Couette Experiment: A Continuous Transition, *Phys Rev. Lett*. **82** (1999), 5241

[27] C. T. Veje, D. Howell and R. P. Behringer, Kinematics of a 2D Granular Couette Experiment at the transition to shearing, *Phys Rev.* E. **59** (1999), 739

[28] G. Gudehus: Erddruckermittlung, in Grundbau Taschenbuch 5. Auflage, Teil 1, 1996, Berlin (W. Ernst & Sohn)

[29] G. Gudehus: A comprehensive constitution equation for granular materials, Soils and Foundations 36, (1996), S.1-12

[30] I. Herle: Hypoplastizität und Granulometrie von Korngerüsten. Veröffentlichungen des Instituts für Bodenmechanik und Felsmechanik der Universität Karlsruhe, Heft 142 (1997)

[31] D. Kolymbas: Ein nichtlineares viskoplastisches Stoffgesetz für Böden. Veröffentlichungen des Instituts für Bodenmechanik und Felsmechanik der Universität Karlsruhe, Heft 77 (1977)

[32] P. v. Soos, Eigenschaften von Boden und Fels; ihre Ermittlung im Labor. In Grundbau Taschenbuch 5. Auflage, Teil 1, 1996, Berlin (W. Ernst & Sohn)

[33] W. Wu: Hypoplastizität als mathematisches Modell zum mechanischen Verhalten granularer Stoffe. Veröffentlichungen des Instituts für Bodenmechanik und Felsmechanik der Universität Karlsruhe, Heft 129 (1992)

[34] C. Marone, *Annu.Rev. Earth Planet.Sci.* **26**, 643 (1998)

[35] P. Segall, J.R. Rice, *J. Geophys. Res*. **100**, 22155 (1995)

[36] J.H. Dietrich, *Pageoph.* **116**, 790, (1978)

[37] J.R.Rice, *Pageoph.* **121**, 443, (1983)

[38] J.-C.Gu, J.R.Rice, A.L. Ruina, S.T.Tse, *J. Mech. Phys. Solids* **32**, 167 (1984)

[39] J.R.Rice, A.L. Ruina, *J. Appl. Mech.* **50**, 343 (1983)

[40] A.Ruina, *J. Geophys. Res.* **88**, 10359 (1983)

[41] E. Franke, Ruhedruck in kohäsionslosen Böden im ebenen Fall, Die Bautechnik 44 (1967) Heft 2

[42] E. Franke, Ruhedruck in kohäsionslosen Böden, Die Bautechnik 51 (1974) Heft 1

[43] J.P.Bardetand, J.Proubet, *J.Eng.Mech* **118**,397 (1992)

[44] H.-J.Tillemans, H.J.Herrman, *Physica A* **217**,261 (1995)

[45] S: Nasuno, A. Kudrolly, J.P.Gollub, *Phys.Rev.Lett*. **79**, 949 (1997)

  S: Nasuno, A. Kudrolly, A. Bak, J.P.Gollub, *Phys.Rev.Lett*. 58, 2161 (1998)

[46] P. Dantu, *Ann. Ponts Chauss. IV* 193 (1967)

[47] Linnenbrock, K.; Ferber, F.; Herrmann, K.P.: Numerical analysis of 3-D crack growth in thermally loaded two-phase compounds, 11 International Conference on Experimental Mechanics, 24 - 28.August 1998, Oxford

[48] M. Lätzel, S. Luding, H. J. Herrman, D. W. Howell and R. P. Behringer, Kinematics of a 2D Granular Couette Experiment, *Granular Matter*. **2** (2000), 123

[49] J. Geng, E.Longhi, R. P. Behringer and D. W. Howell, Phy. Rev. E, 64 (2001), 060301(R)

[50] A. Gervois and D. Bideau, Some geometrical properties of two dimensional hard disk packings, *Disorder and Granular Media*, D. Bideau and A. Hansen (editors) 1993 North Holland Amsterdam

[51] H.-J. Hein, Ein Stoffgesetz zur Beschreibung des thermomechanischen Verhaltens von Salzgranulat, Dissertation, Fakultät für Maschinenwesen, RWTH Aachen (1991)

[52] Jacques Duran, *Sands, Powders and Grains* 2000 Springer-Verlag New York Inc.

[53] G. Gudehus: Bodenmechanik, 1981 Stuttgart (Enke)

[54]   A. Kèzdi, Fragen der Bodenphysik, 1976 Budapest (Akad. Kiadò) Düsseldorf (VDI-Verlag)

[55] K. Terzaghi. Theoretische Bodenmechanik, 5.Auflage, ins Deutsche übertragen von R. Jelinek, 1954, Berlin (Springer)

[56] D. Bideau and A. Hansen (editors) *Disorder and Granular Media*, 1993 North Holland Amsterdam

[57] R. Jellinek: Eigenschaften des Bodens, in Grundbau Taschenbuch 1. Auflage, Teil 1, 1955, Berlin (W. Ernst & Sohn)

[58] P.v. Soos: Eigenschaften von Boden und Fels, in Grundbau Taschenbuch 3. Auflage, Teil 1, 1980, Berlin (W. Ernst & Sohn)

[59] J. R. Rice and A. L. Ruina, *J. Appl. Mech.* **105**, 343 (1983)

[60] T. Baumberger, P. Berthoud and C. Caroli, *Phys. Rev. B* **60** (1999), 3928.

[61] D.C. Drucker, H.J. Greenberg, W.Prager, *J. Appl. Mech - * Trans. ASME **73** (1951), 371.

[62] D. C. Drucker, W. Prager, H. J. Greenberg,, *Quart. Appl. Math* **9** (1952), 381.

[63] P. A. Vermeer, R. de Borst, *Heron* **29** (1984), 1-64.

[64] S. P. Timoshenko, J. N. Goodier, *Theory of Elasticity* , McGraw-Hill (1982).

[65] R. de Borst , *A reappraisal of the Cosserat continuum*, *Engng. Comp.* **8** (1991), 317-332.

[66] H. -B. Mühlhaus , Berücksichtigung von Inhomogenitäten im Gebirge im Rahmen einer Kontinuumstheorie, Veröffentlichungen des Instituts für Bodenmechanik und Felsmechanik der Universität Karlsruhe, Heft 106 (1987) .

[67] W. Eber, *Friction Measurements in Granular Media, Phys. Rev. E* **69** (2004), 021303.

[68] J. D. Goddard , *Continuum Modeling of Granular Assembies*, excerpt from *Physics of Dry Granular Media*, Proc. NATO ASI, Cargèse (1997), H. Herrmann et. al. (eds.), Kluwer (1998) .

[69] J. D. Goddard, A. K. Didwania, *Computations of dilatancy and yield surfaces for assemblies of rigid frictional spheres*, Quart. J. Mech. Appl. Math., **51** (1998), 15.

[70] W. F. Chen, D. J. Han, *Plasticity for Structural Engineers*, Springer (1988).

16 Appendix: Symbols and Abbreviations

16. 1 Chapter 1: Introduction

$\overline{K}$	Ratio of lateral stress in response to transversal stress
σ_1, σ_3	Stress, applied(1) or responding (2)
φ, c	Macroscopic, conventional Angle of Friction and cohesion, defined according to RANKINE

16. 2 Chapter 2: Granular Parameters in Soil Mechanics

ε_k	Strain in direction k, where $k \in [1,2,3]$
σ_k	Stress in direction k, where $k \in [1,2,3]$
γ_{kj}	Shearstrain in direction k, j, where $k, j \in [1,2,3]$
τ_{kj}	Shearstress in direction k, j, where $k, j \in [1,2,3]$
v	Coefficient of Poisson
E	Modulus of Young
σ_V	Yield stress due to different hypothesis
φ	Macroscopic, conventional Angle of Friction, defined according to RANKINE
c	Cohesion
ψ_D	Angle of Dilatancy
κ	Packing fraction
V	Volume
n	Porosity
e, e_i, e_d, e_c	Void ratio
$n^{(3d)}, n^{(2d)}$	Packing fraction, calculated for three rsp. two dimensions
$S(r)$	Grading curve of natural soil

U	Uniformity ($\simeq$ gradient of the graph characterising the granularity of a medium)

16. 3 Chapter 3: Experimental Setup

PET	Polyester
PTFE	Teflon
POC	Polyolefin
PVC	Polyvinylchloride

16. 4 Chapter 4: Measurement of Av. Forces

μ_0	Coefficient of Friction between single grains in granular material
$\vartheta_0 = \arctan\mu_0$	Grain to grain Angle of Friction, derived from μ_0
LLO	State of granular material at low level of organisation, i.e. no deformation history.
HLO	State of granular material at high level of organisation, after deformation, building smooth sliding joints.
$\overline{K}$	Ratio of lateral stress in response to transversal stress
$\overline{K^{total}}$	Measured averaged ratio of $\overline{K}$, including some sideeffects
F_x, F_y	Forces, used locally in direction x/y
$\overline{K^{frict}}, \overline{K^{elast}}$	Measured components of $\overline{K}$
$F^{load}, F^{response}$	Locally used forces
μ_w	Coefficient of Friction between the grains and the limiting wall
$\overline{K_a^{frict}}, \overline{K_p^{frict}}$	Measured $\overline{K}$, where the granular system is definitely in an active(a) state, where friction helps keeping the shape or in a passive (p) state, where friction withstands the stress shearing the system. This value is in both cases corrected for the frictional contribution
K_a^R	Theoretical definition of K_a according to RANKINE under the assumption $\varphi = \vartheta_0$

16. 5 Chapter 5: Measurement of Porosity rsp. Packing Fraction

n Porosity

κ Packing fraction

ε Horizontal deformation of granular sample

16. 6 Chapter 6: Surveyance of the Macroscopic Structure

ω Stress induced illumination of a cylinder in the polariscope

$W(\omega), W_0(\omega)$ Frequency of occurrence of a class of illumination, loaded resp. unloaded

λ Ratio of fully illuminated pixels with respect to all pixels in a polariscope image.

n Sidelength of the considered granular volume in units of diameters

d^{cw} meshsize in units of the average chainwidth

k number of meshes considered

16. 7 Chapter 7: Discussion of Results: Overview

ε Horizontal deformation of granular sample

16. 8 Chapter 8: Discussion of Porosity Measurements

κ_{rnd} Packing Fraction for Random Close Packing

$\kappa_{hc}, \kappa_{sqr}, \kappa_{opt.}$ Packing Fraction of honeycomb, square and triangular (opt.) lattice

z Coordination number, i.e. number of contacts

$\kappa_{\max}$ Maximum possible Packing Fraction by repeated manual deformation

κ_t Transition Packing Fraction

16. 9 Chapter 9: Discussion of Results: Well Organised Granular Material

α, β Geometrical angles, used locally

σ, τ Normal and tangential stress in the sliding joint

χ Angle to correct ϑ_0 in order to match φ_0

F_N, F_T Locally used Forces, normal (N) and transversal (T) to the surface of a grain

δ Limit of Angle of Contact within a sliding joint

ε Relative deformation of a system

δ_0 Maximum limit to δ, determined by deformation ε

16. 10 Chapter 10: Discussion of Results: Less Organised Granular Material

u Height of a surface irregularity with respect to the grain radius

χ_u Angle to correct ϑ_0 for local irregularities.

16. 11 Chapter 11: Statistical Approach

F_T, F_N Forces tangential rsp. normal to cylinder surface

$\overline{K}$ Average lateral Stress Factor

ξ Maximum Angle of Contact due to geometrical restrictions

ψ, ψ_1, ψ_2 Local angles

r Radius of concerned cylinder

Q_1, Q_2, Q_3 Enumerated contacts

$\widehat{K^{stoch}}$ Lateral force factor without frictional impact

γ_1, γ_2 Local angles

δF Variation of force

$P(\psi)$ Probability density of a configuration

g Formfactor, transforming force factors to stress factors

g^e Formfactor g using even distribution

g^c Formfactor g using COS distribution

$\kappa^{stoch,e}, \kappa^{stoch,c}$ Packing fraction for evenly/COS-shaped distribution of contact angles

16. 12 Chapter 12: Review on Measurements

                   All symbols explained in text

16. 13 Chapter 13: Structures in Granular Material

$\bar{\delta}$	Averaged angle of contact in a sliding joint
ε	relative longitudinal deformation of a granular system
ψ	Locally used angle
F_x, F_y	Forces acting in direction x, y
F_{Long}, F_{Lat}	Forces acting in longitudinal and lateral direction
$\widehat{K_a}, K_a$	Lateral force/stress factor in active state
L_0	Length of a force chain
L	Extent of a macroscopic granular system
ε	Relative Compression
F_{lat}, F_{long}	General lateral and longitudinal forces
m	Average distance of parallel force bearing chains in units of diameters $2\bar{r}$, based on equilibrium considerations
g^e	Formfactor using even distribution of contact angles
F_R	Retaining frictional force
μ^{av}	Average effective Coefficient of Friction in a slide joint
$\overline{W}$	Average scope in units of diameters $2\bar{r}$
$\bar{\chi}$	Average angle representing lateral contacts of a force chain
δ	Angle of contact within the sliding joint of a Rankine-like system
$\overline{N}$	Average length of a stable chain
ξ	Maximum Angle of Contact due to geometrical restrictions
$\Delta\xi$	Mean deviation of ξ
ξ'	Maximum Angle of Contact due to local ordered structures
ψ_m	Av. angular distance of adjacent contacts on a cylinder when completely packed.
ξ_r	Reduced max. Angle of Contact, acquired accidentally.

F_{chain} Longitudinal force within a force chain

M Distance between force bearing chains, based on the probability of a chain as a series of appropriate contacts.

ω Stress induced illumination of a cylinder in the polariscope

$W(\omega)$ Frequency of occurrence of a class of illumination, loaded state

$R^{(1)}, R^{(10)}, R^{(100)}$ Scales for single grain consideration, for macroscopical structures and for averaged treatment

17 Appendix: Measurement Data

17. 1 Coefficient of Friction
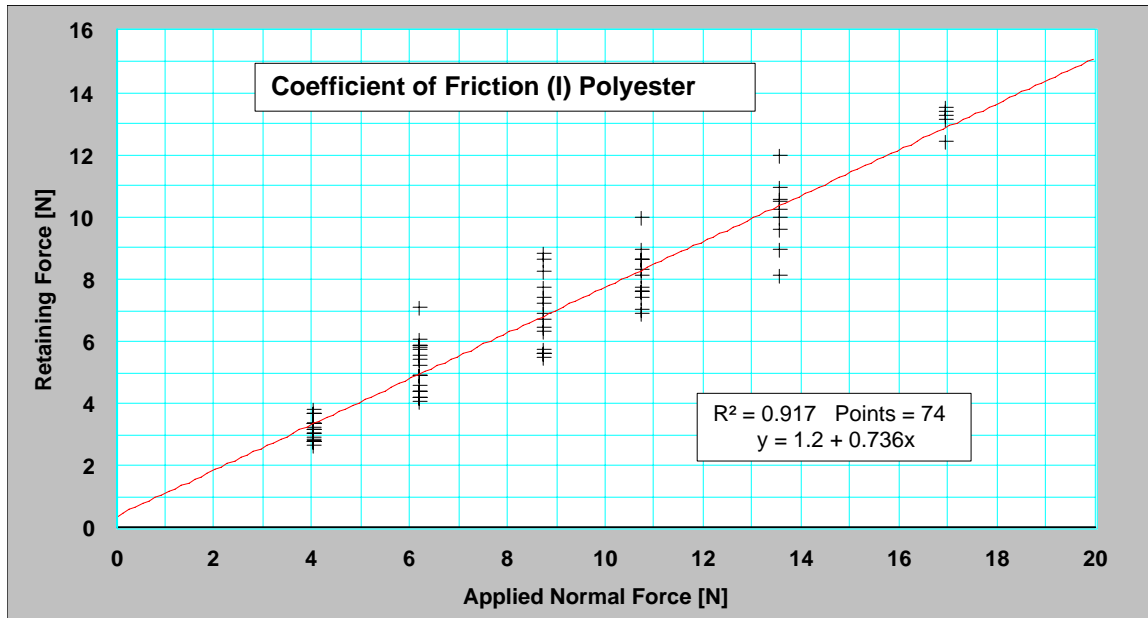
File: ReibungsmessungenI.123
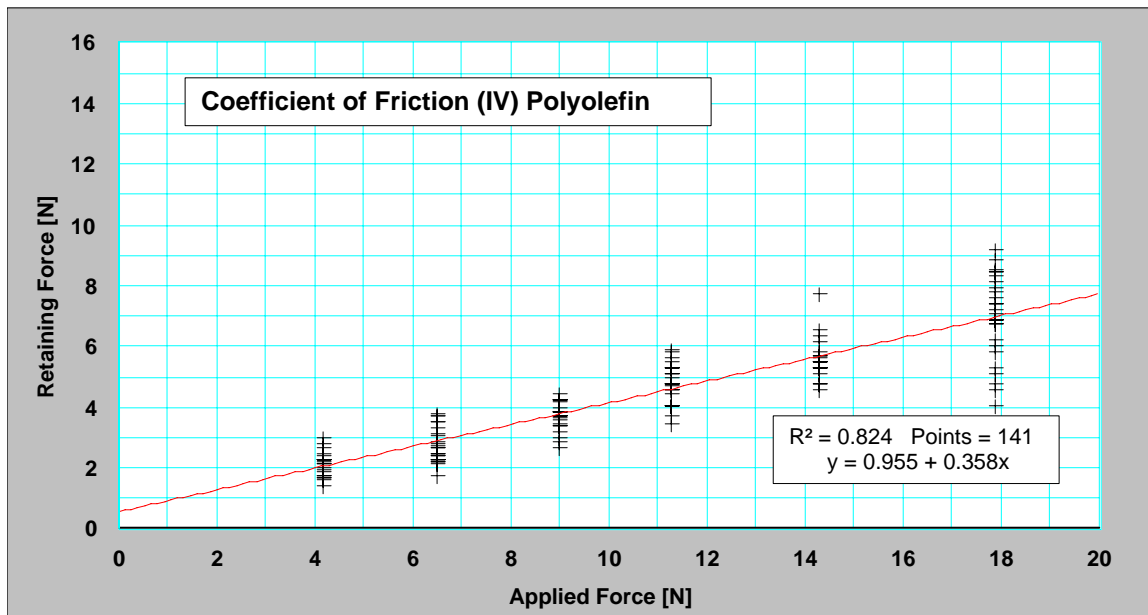
File: ReibungsmessungenIV.123
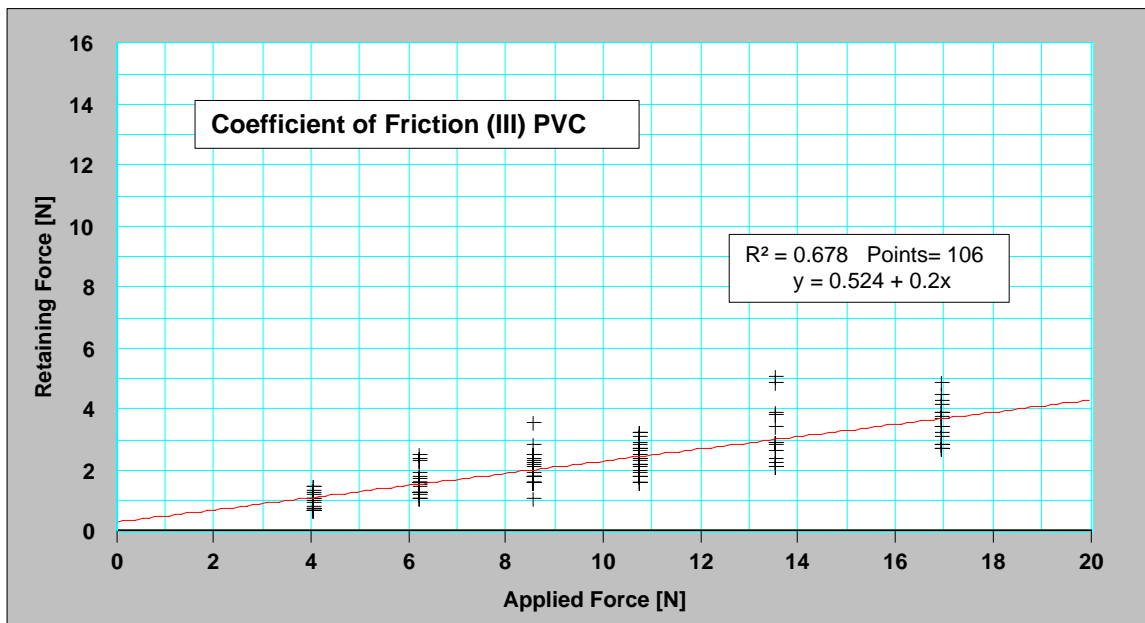
File: ReibungsmessungenIII.123
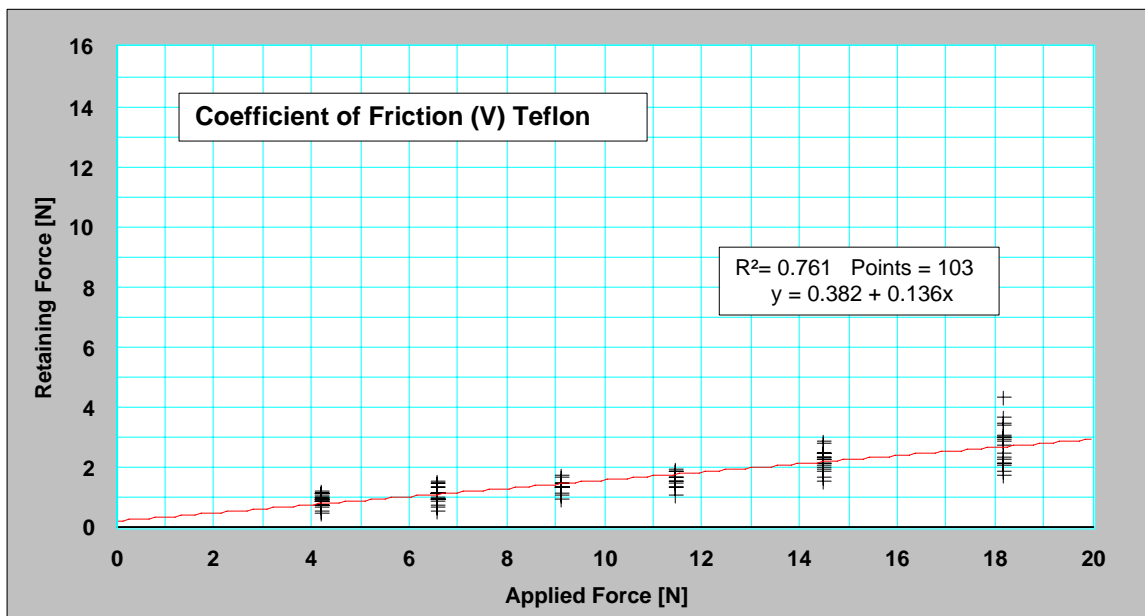
File: ReibungsmessungenV.123

17. 2 Elastic Contribution
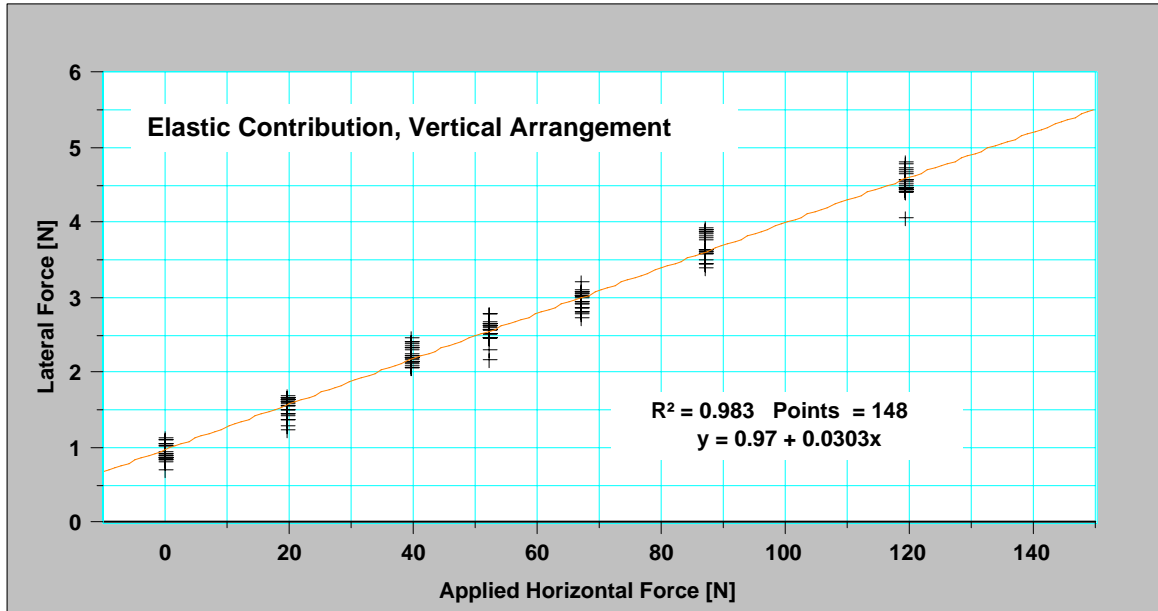
File: Messungen Poissonfaktor Vertical.123
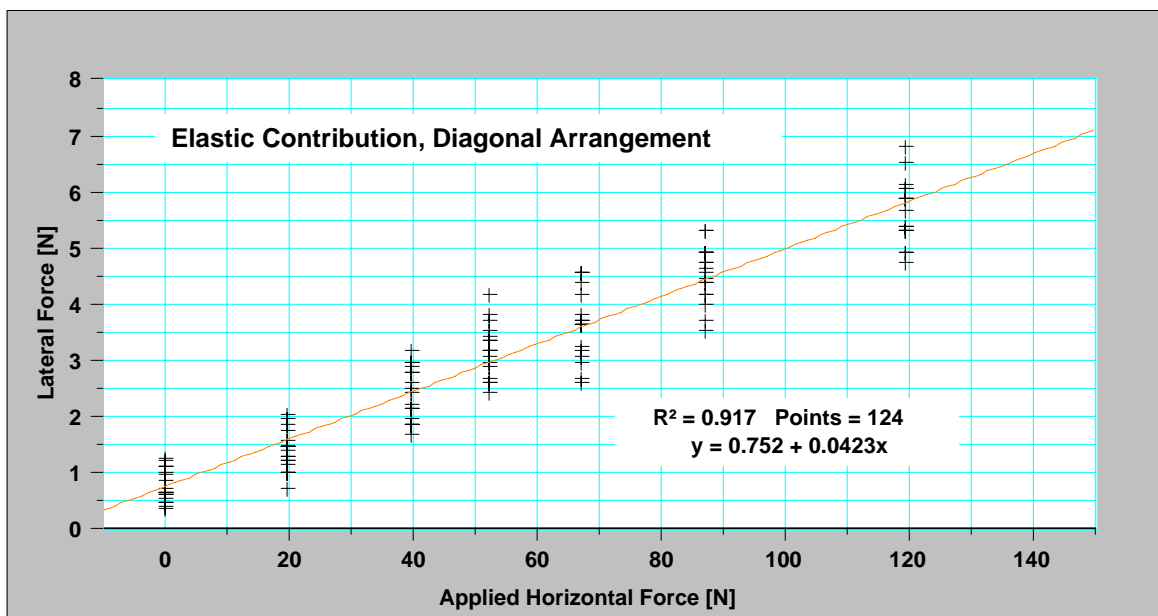
File: Messungen Poissonfaktor Diagonal.123

17. 3 Measurement of Lateral Force Factors

Horizontal fed stress *vs.* vertical corresponding stress after performing activating movement history of the granular material.

17. 3. 1 Covering material: Polyolefin
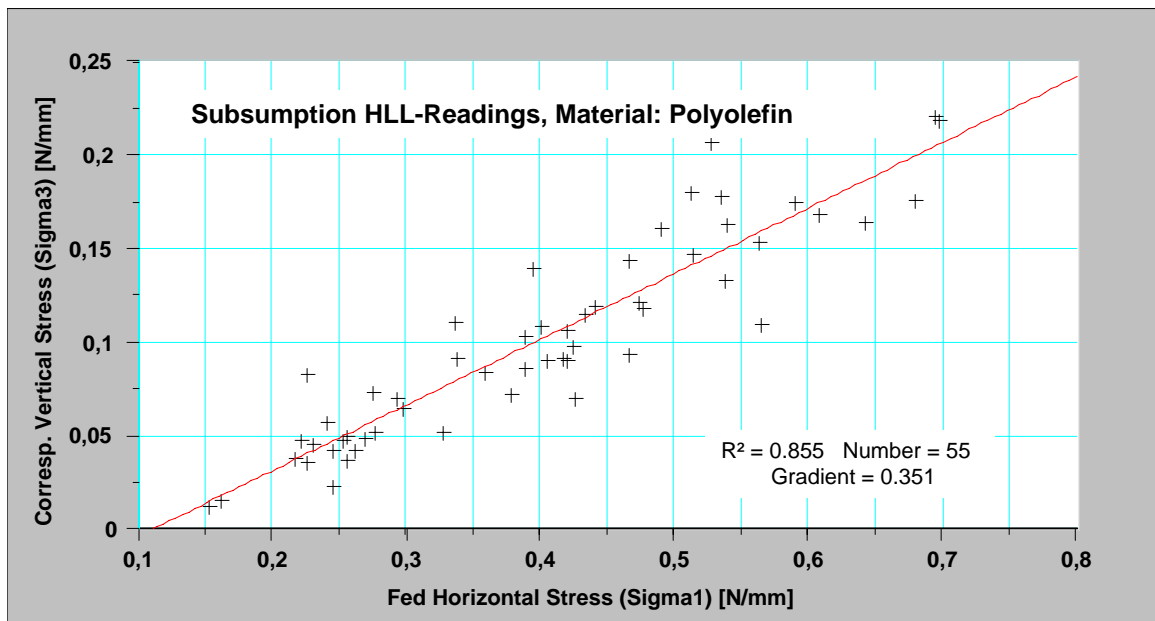
File: Sammelauswertung TCP.123
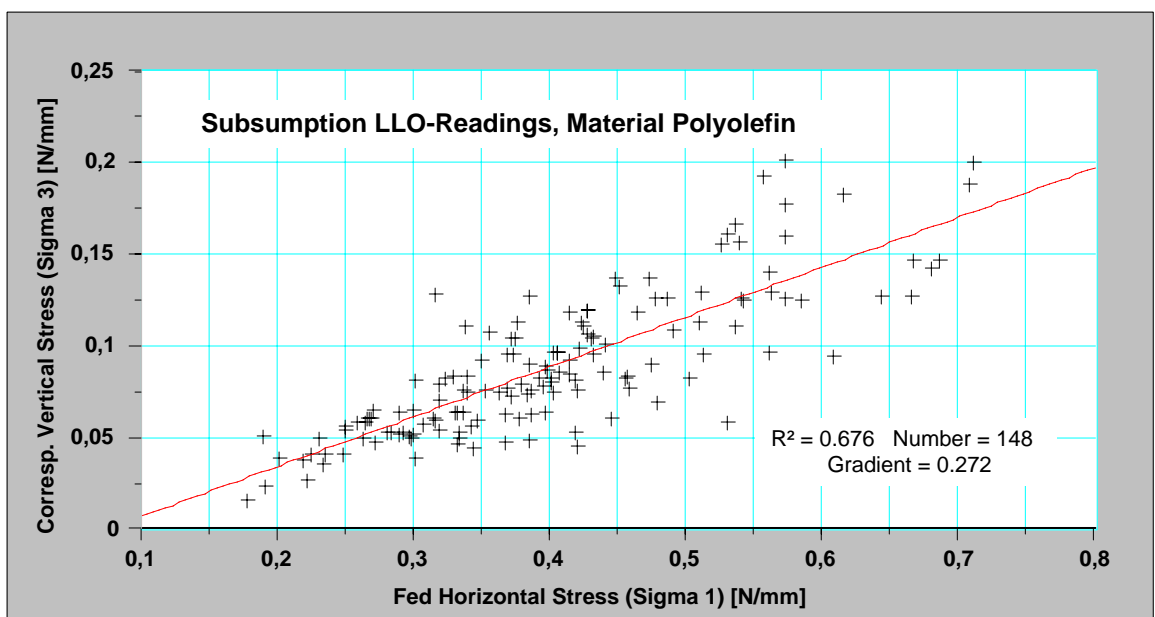
File: Sammelauswertung UCP.123

17. 3. 2 Covering Material: Polyester
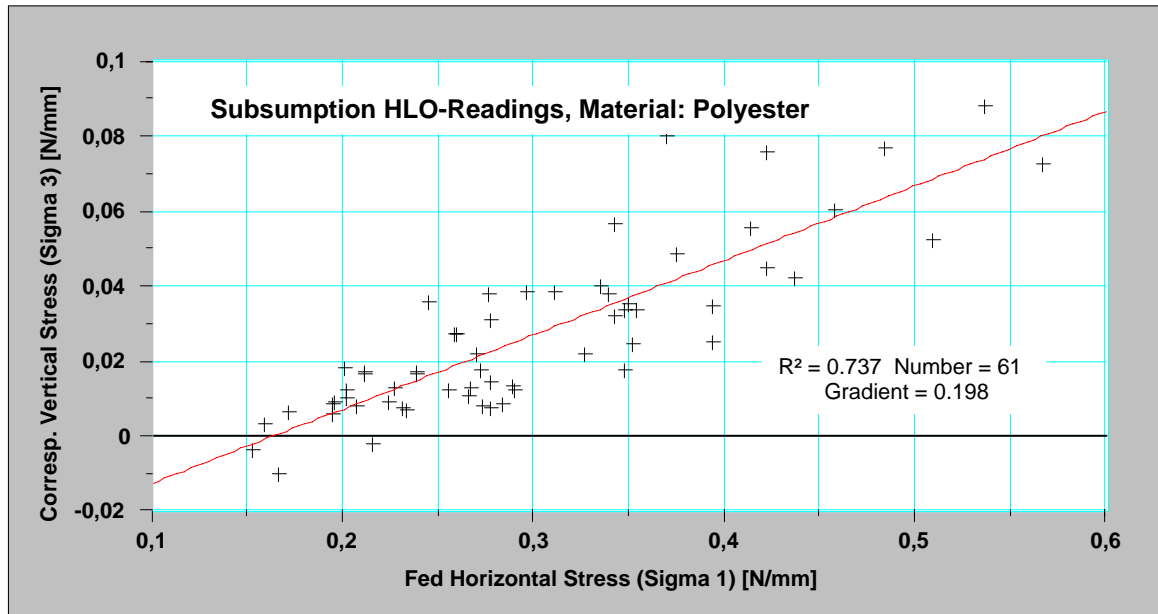
File: Sammelauswertung TCN.123
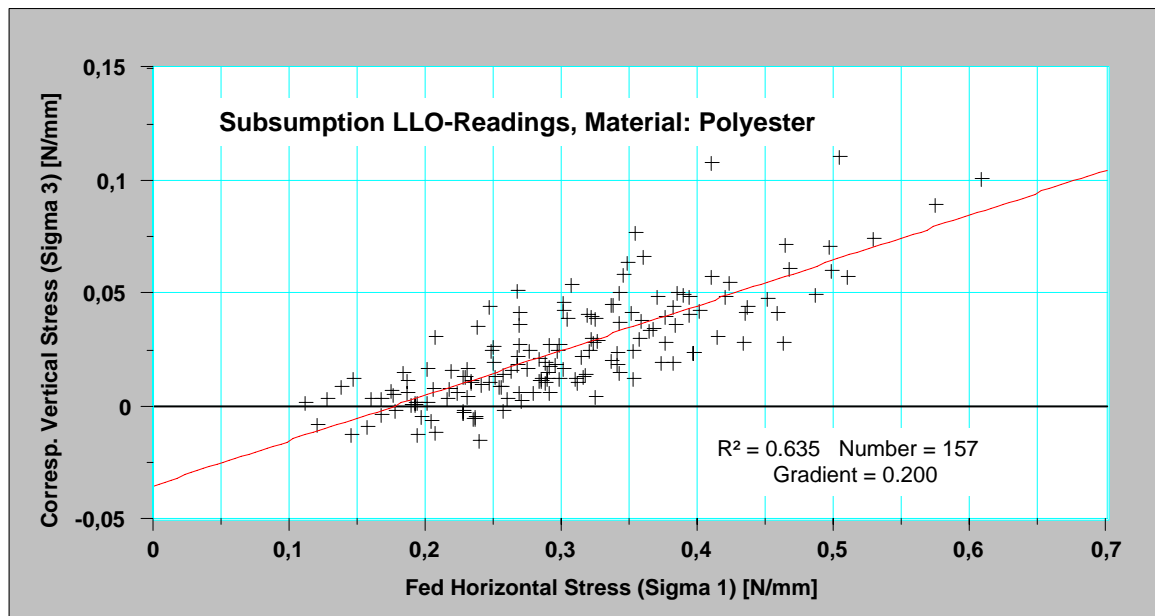
File: Sammelauswertung TCN.123

17. 3. 3 Covering Material: Polyvinylchloride
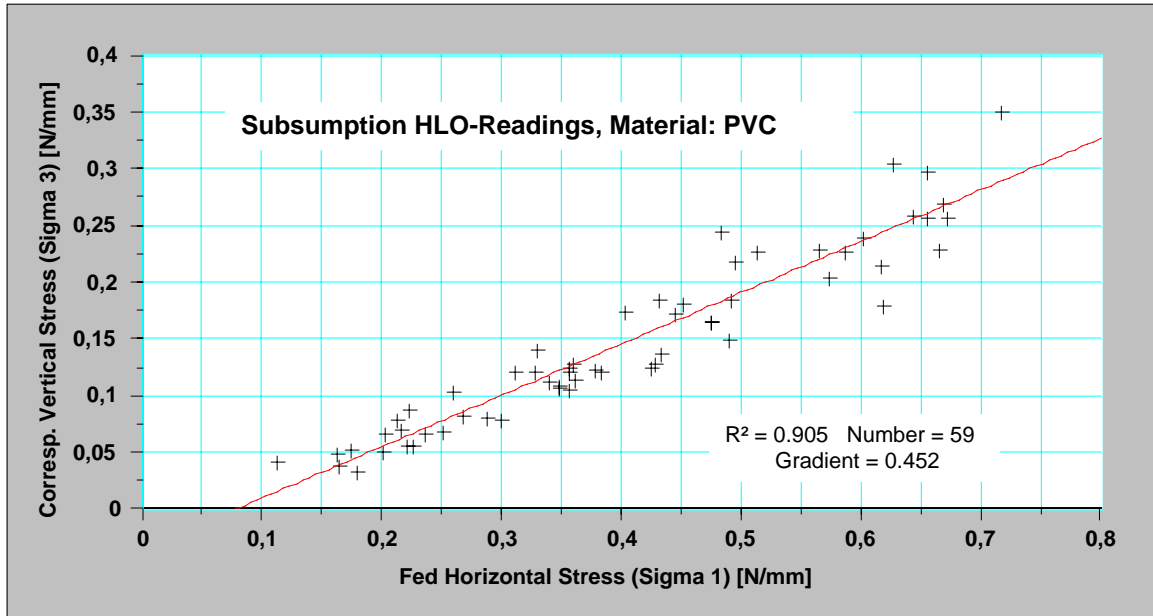
File: Sammelauswertung TCV.123
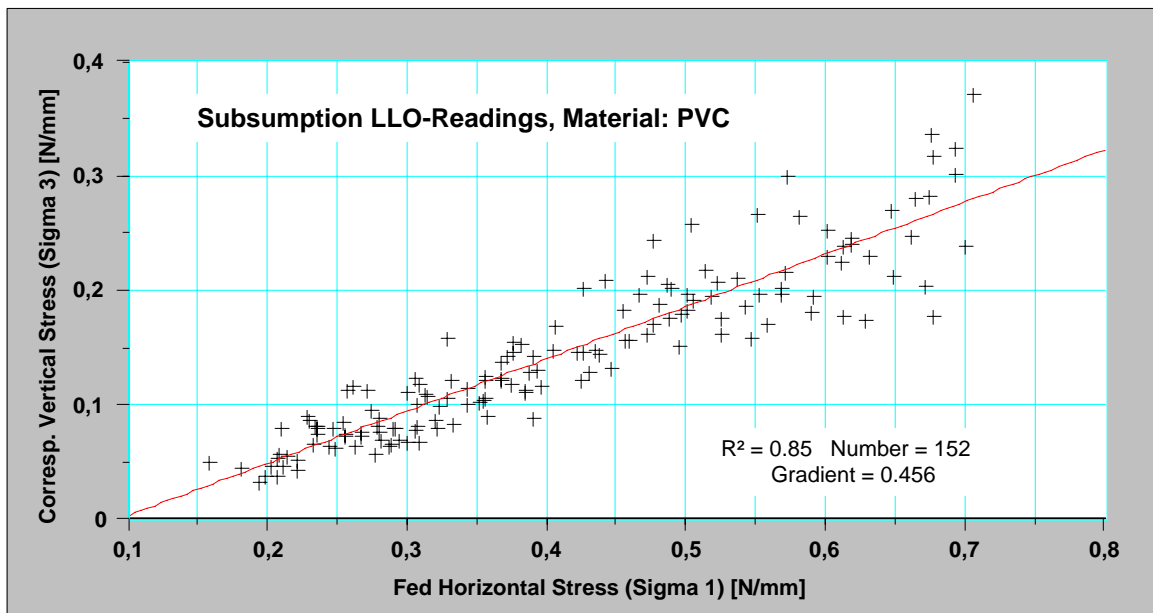
File: Sammelauswertung UCV.123

17. 3. 4 Covering Material: Teflon
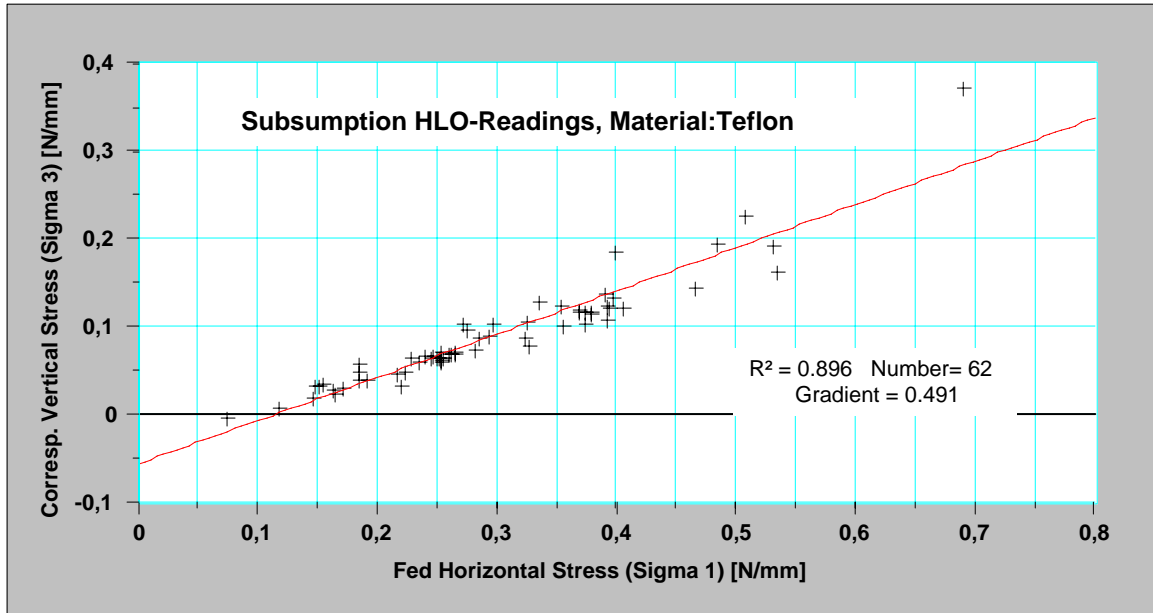
File: Sammelauswertung TCT.123
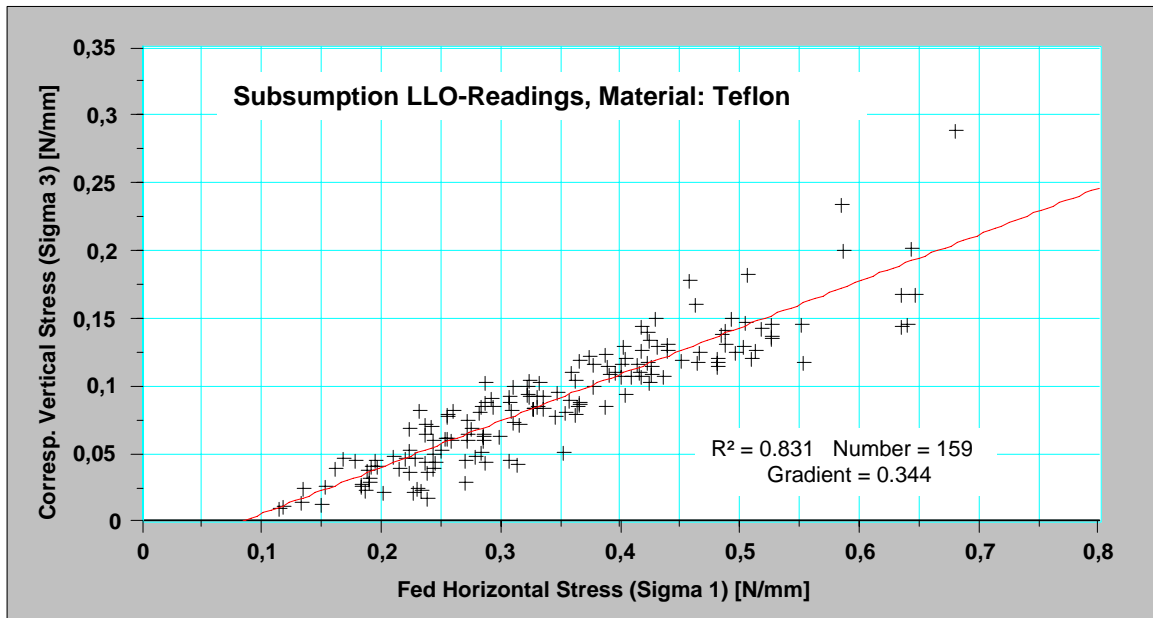
File: Sammelauswertung UCT.123

17. 4 Polarisation Images

17. 4. 1 Polyester Cylinders, High Level Of Organisation (TCN)
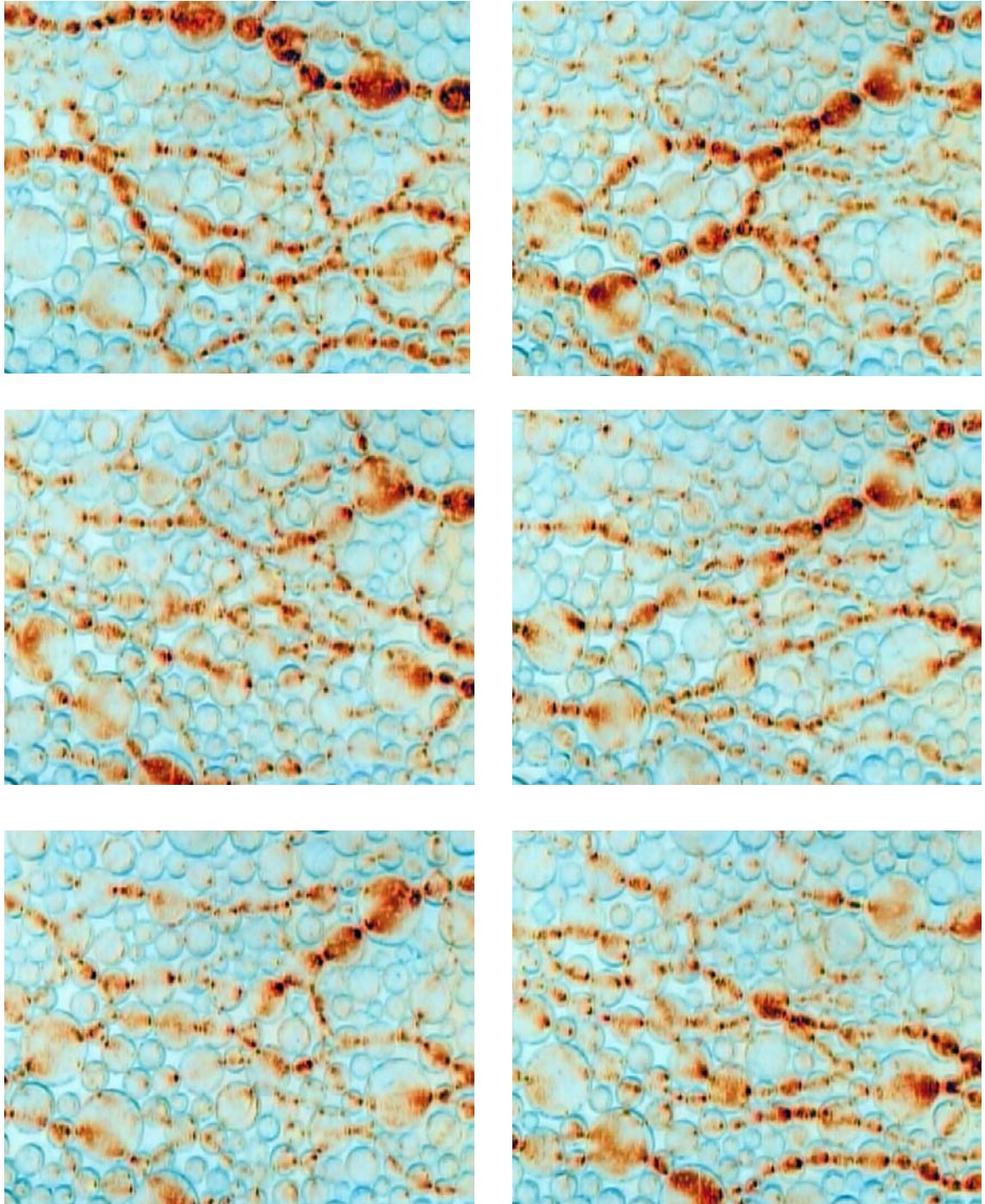
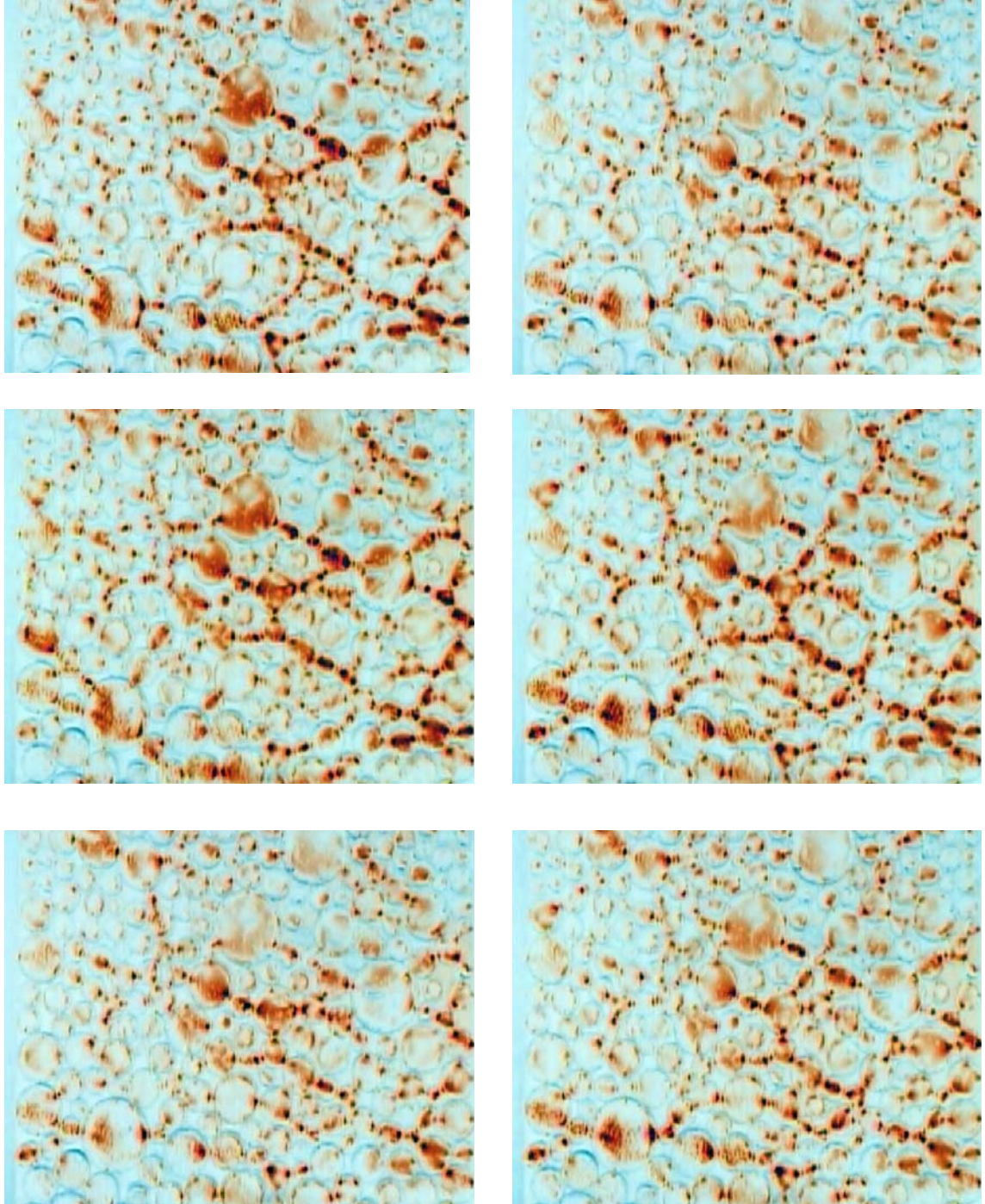## 17. 4. 2 Polyolefin Covered Cylinders, High Level Of Organisation (TCP)
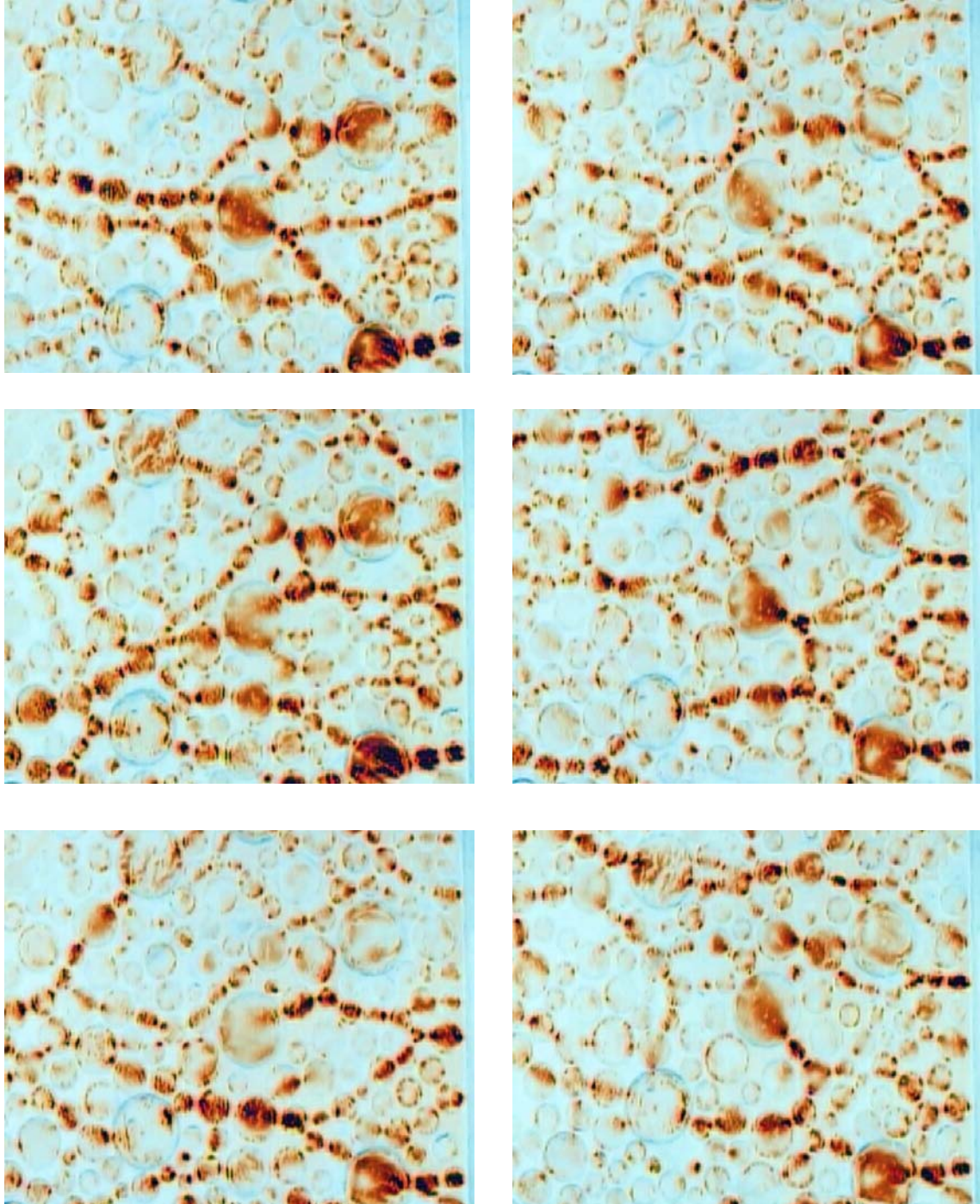
17. 4. 3 Teflon Covered Cylinders, High Level Of Organisation
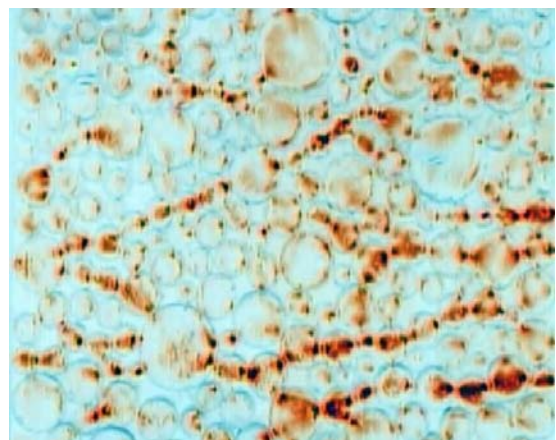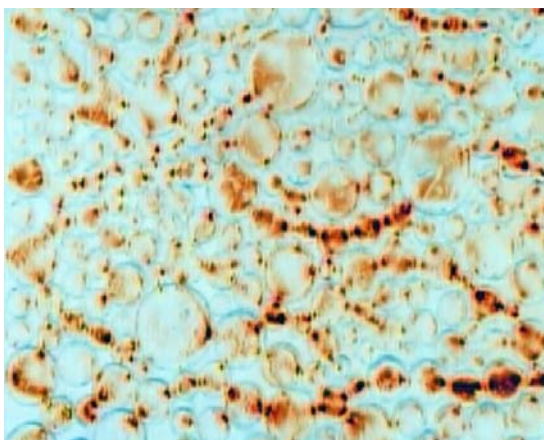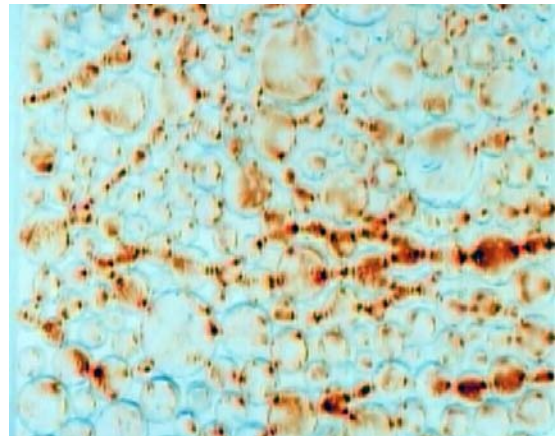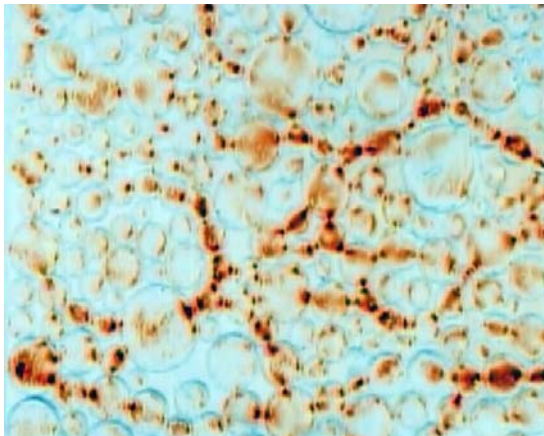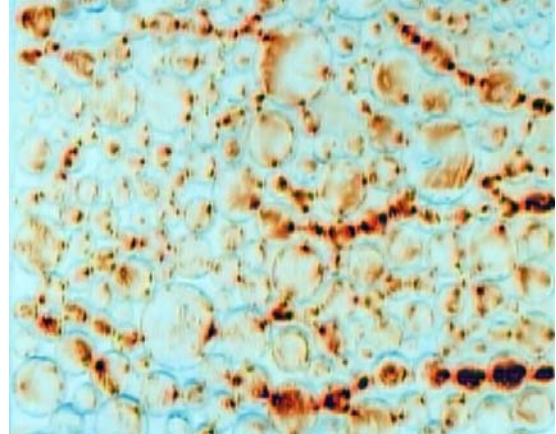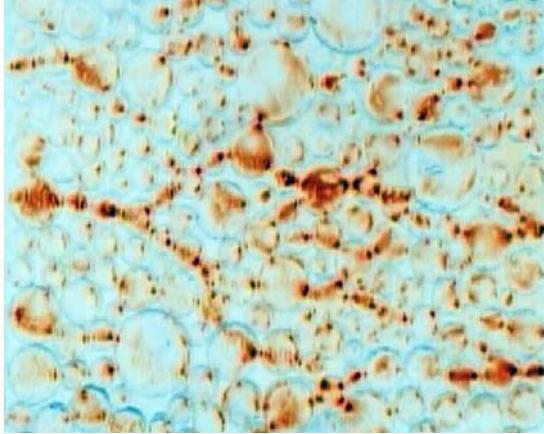
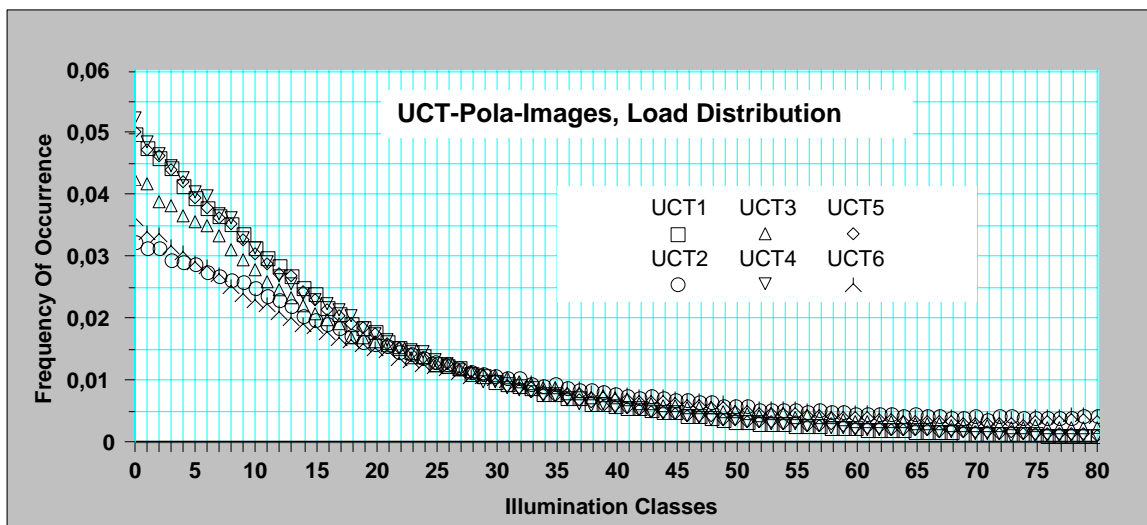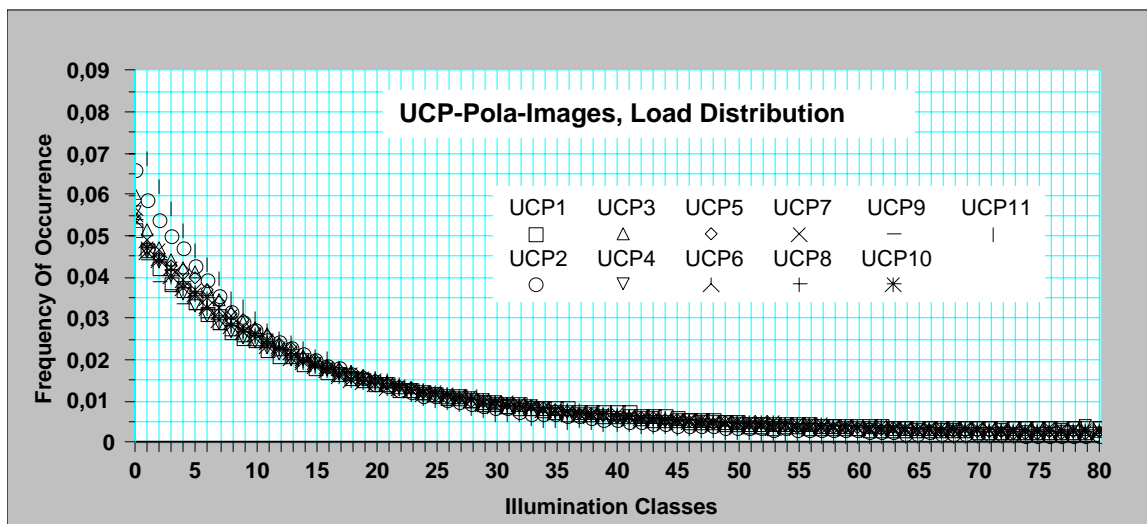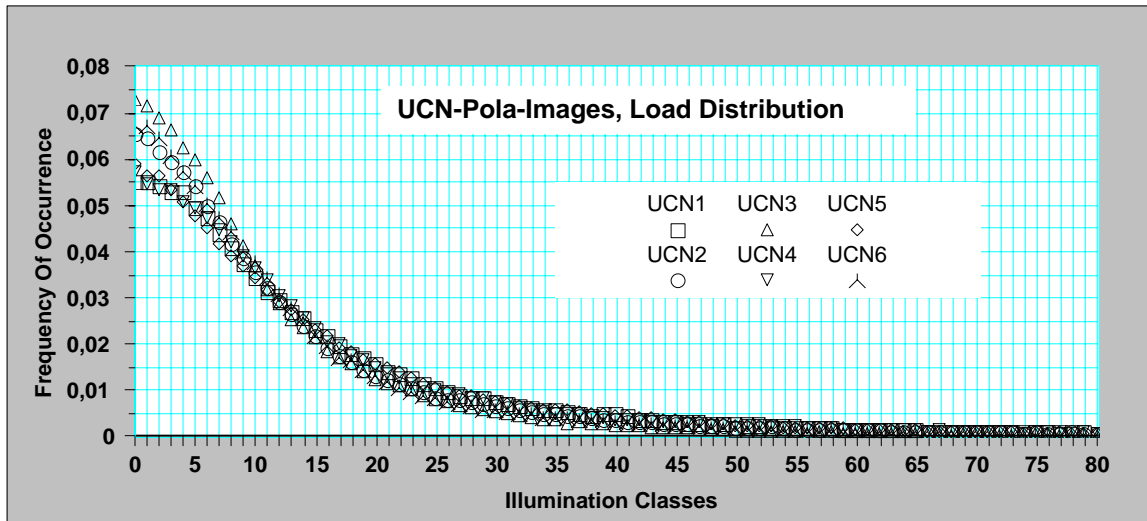## 17. 4. 4 Polyester Cylinders, Low Level Of Organisation
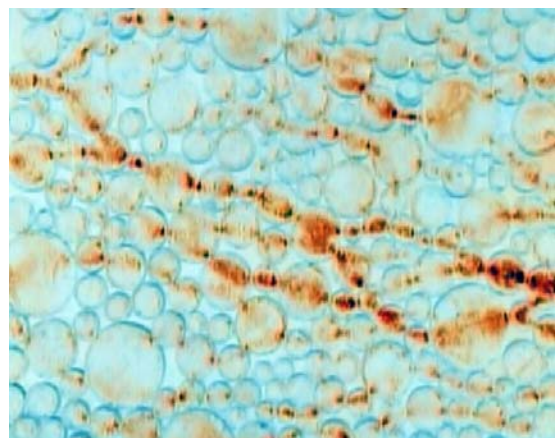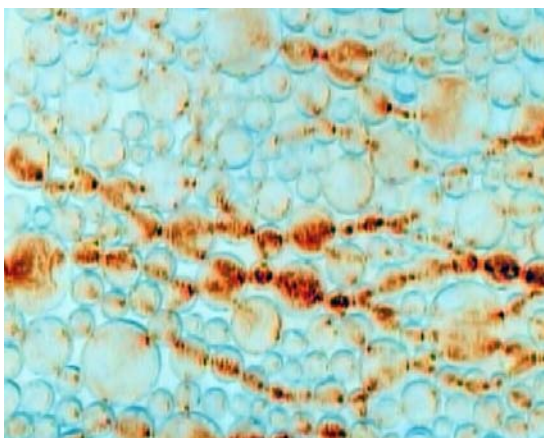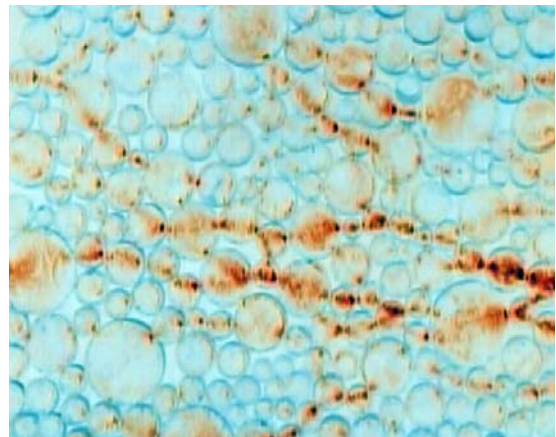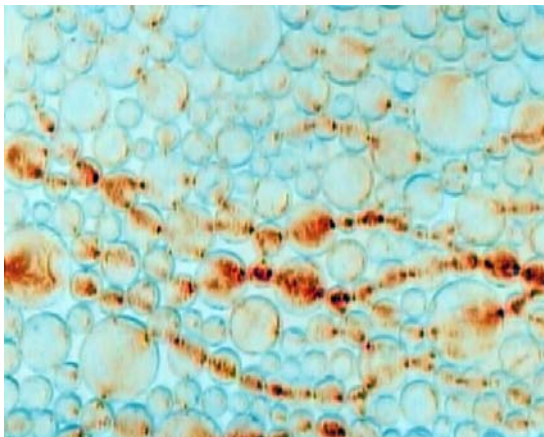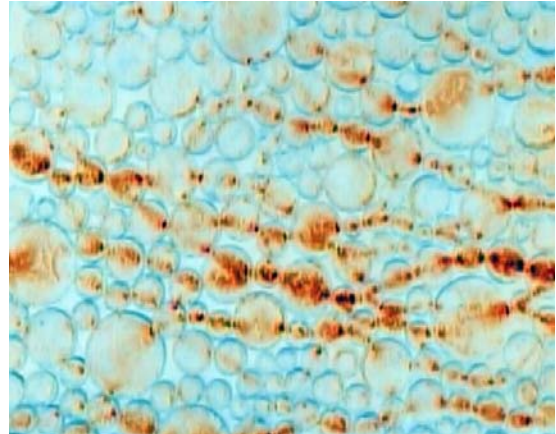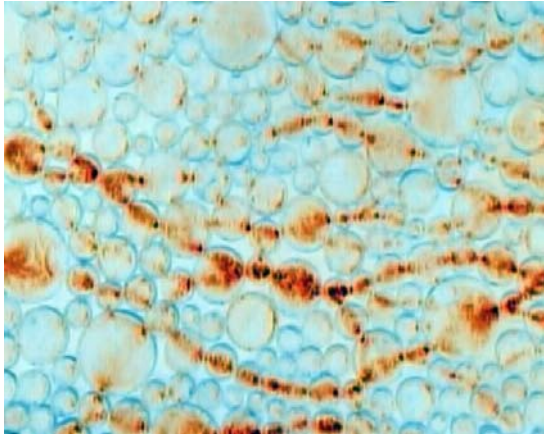
17. 4. 5 Polyolefin Covered Cylinders, Low Level Of Organisation
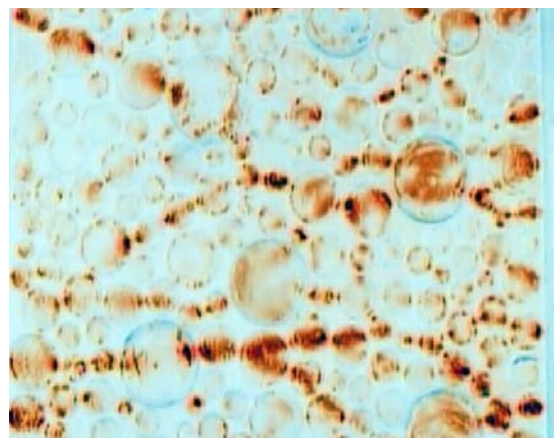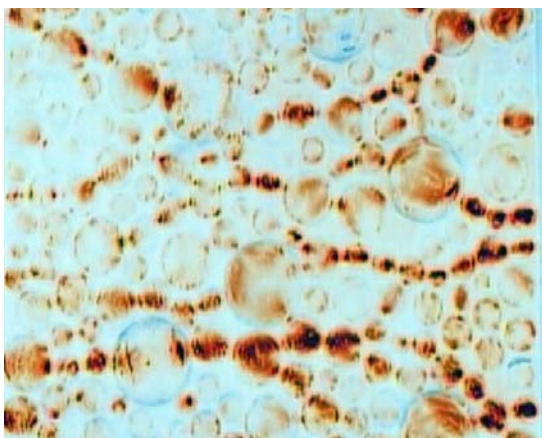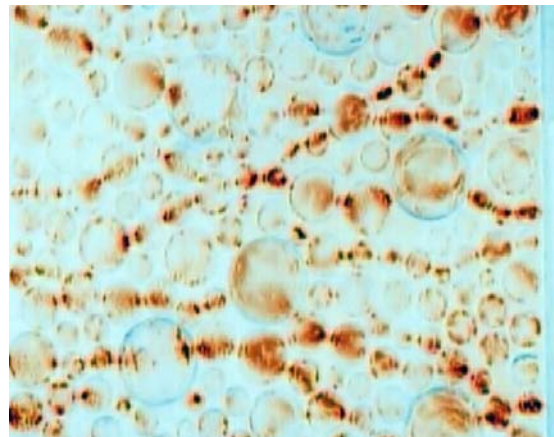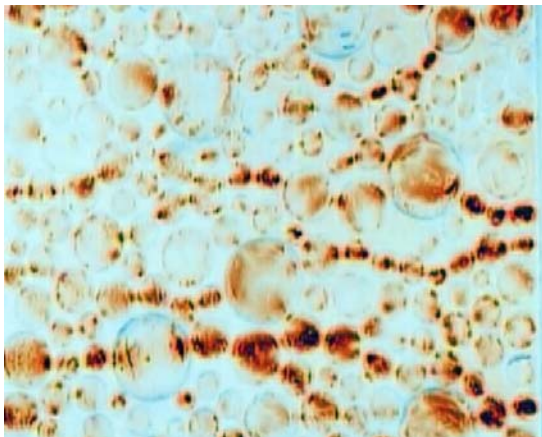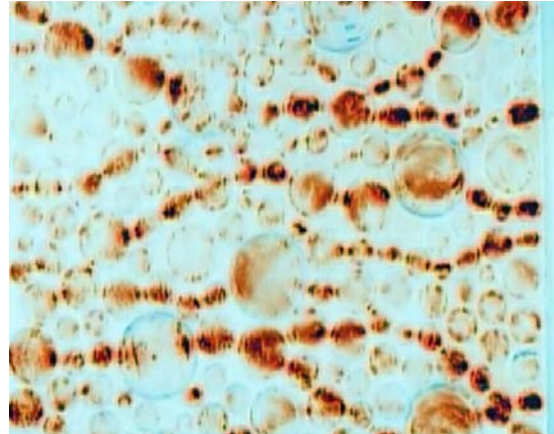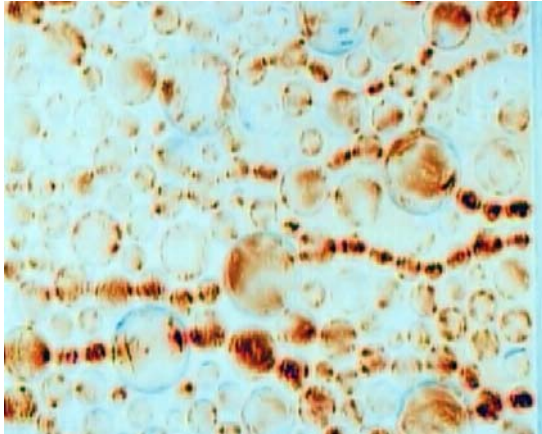
17. 4. 6 Teflon Covered Cylinders, Low Level Of Organisation

17. 5 Load Distributions, Low Level of Organisation

17. 6 Load Distributions, High Level of Organisation